

THE BELL SYSTEM TECHNICAL JOURNAL

VOLUME XL

JULY 1961

NUMBER 4

This issue of The Bell System Technical Journal is devoted to extensive discussion of Project Echo, an experiment in satellite communication conducted by Bell Telephone Laboratories in cooperation with the National Aeronautics and Space Administration, Jet Propulsion Laboratories, the Naval Research Laboratory, and others. The first paper describes the experiment and the results obtained. It is followed by eleven more detailed papers, each describing one of the parts of the Project Echo system.

Participation of Bell Telephone Laboratories in Project Echo and Experimental Results

By WILLIAM C. JAKES, JR.

(Manuscript received April 4, 1961)

On August 12, 1960, a 100-foot-diameter spherical balloon was placed in orbit around the earth by the National Aeronautics and Space Administration. The objective was to demonstrate the feasibility of long distance communication by means of reflection of microwaves from a satellite. It was intended that a two-way coast-to-coast voice circuit be established between the Jet Propulsion Laboratories facility at Goldstone, California, and a station provided for this purpose by Bell Telephone Laboratories at Holmdel, New Jersey. Similar tests were also planned with the Naval Research Laboratory and other stations.

Construction of the Holmdel station was begun early in 1959. This paper describes the general organization and operation of the station, and discusses the results of the Project Echo experiments that took place between the launching of the balloon and March 1, 1961. Successful voice communi-

tion was achieved a number of times using a variety of modulation methods, including frequency modulation with feedback, amplitude modulation, single-sideband modulation, and narrow-band phase modulation. Careful measurements were also made of the loss in the transmission path.

TABLE OF CONTENTS

	<i>Page</i>
I. Introduction	976
1.1 Purposes of the Project Echo Experiment	976
1.2 Description of the Experiment	977
1.3 Preliminary Tests	980
II. System Description	982
2.1 Transmitting System	983
2.2 Receiving System	986
2.3 Tracking	988
2.4 Communications	992
III. Experimental Results	995
3.1 Audio Tests	995
3.2 Balloon Scattering Cross Section	996
3.3 Detailed Study of Selected Passes	1000
3.4 Scintillations of Received Signals	1021
3.5 FM with Feedback Performance	1023
3.6 Tracking Performance	1025
3.7 Operation with Other Stations	1026
IV. Acknowledgments	1027

I. INTRODUCTION

1.1 *Purposes of the Project Echo Experiments*

Several years ago Bell Telephone Laboratories became interested in studying the feasibility of providing long distance communication facilities by means of reflection from orbiting earth satellites. Participation in NASA's Project Echo was undertaken as a first active step in this program, and it was hoped that the following objectives would be achieved:

- i. To demonstrate two-way voice communication between the east and west coasts.
- ii. To study the propagation properties of the medium, including the effects of the atmosphere, the ionosphere, and the balloon.
- iii. To determine the usefulness of various kinds of satellite tracking procedures.
- iv. To determine the usefulness of a passive communications satellite of the Echo I type.

It was anticipated that these objectives would be achieved primarily by conducting operations with the balloon launched by the National Aeronautics and Space Administration and the satellite-tracking facility of the Jet Propulsion Laboratories (JPL) located at Goldstone, California, about one hundred miles northeast of Los Angeles. The Bell

Telephone Laboratories (BTL) station is located at Holmdel, New Jersey. In addition, tests were planned in cooperation with the Naval Research Laboratory (NRL), facility at Stump Neck, Maryland; General Electric, Schenectady, New York; and stations in Europe.

1.2 *Description of the Experiment*

The diagram of Fig. 1 illustrates the general features of the experiment. An east-west channel was provided by transmission from a 60-foot paraboloid antenna at BTL to an 85-foot paraboloid at JPL via reflection from the balloon, using a frequency of 960.05 mc. The west-east channel utilized transmission from another 85-foot dish at JPL to a specially constructed horn-reflector antenna at BTL having a 20- by 20-foot aperture. The radiation in each channel was circularly polarized in order to avoid the necessity of tracking polarization during the satellite pass, and was transmitted in a clockwise sense from the JPL antenna and counter-clockwise from the BTL antenna. Reflection from the balloon reversed the sense of rotation of the field, so that the major share of the field received by the BTL horn was expected to be polarized counter-clockwise and that at the JPL receiving dish to be clockwise. In addition, the BTL horn was equipped with a second receiver arranged to respond to the clockwise component of the incoming signal, in order to obtain more information concerning the transmission properties of the medium.

The balloon was placed in an almost exactly circular orbit with an inclination of 47.3° , which provided periods of mutual visibility up to about 15 minutes for BTL and JPL and 25 minutes for BTL and NRL. The slant range from Holmdel to the balloon varied between 3000 and 1000 miles during a typical pass.

The facility at NRL consisted of a single 60-foot paraboloid equipped to either transmit or receive at 2390 mc. Ordinarily, both BTL and NRL received from JPL during the first part of a satellite pass while there was mutual visibility between JPL and BTL. After the balloon had "set" for JPL, NRL then transmitted to BTL, using counter-clockwise polarization. On a few passes JPL and NRL simultaneously transmitted to BTL and the two signals were separately recorded on the two BTL receivers, taking advantage of the oppositely polarized radiation from NRL and JPL and a slight difference in transmitted frequency of 0.4 mc to insure isolation of the two signals.

Additional tests were conducted on 961.05 mc at Holmdel, using a local receiver and an 18-foot paraboloid in a radar type of operation.

The communication tests were carried out primarily using frequency

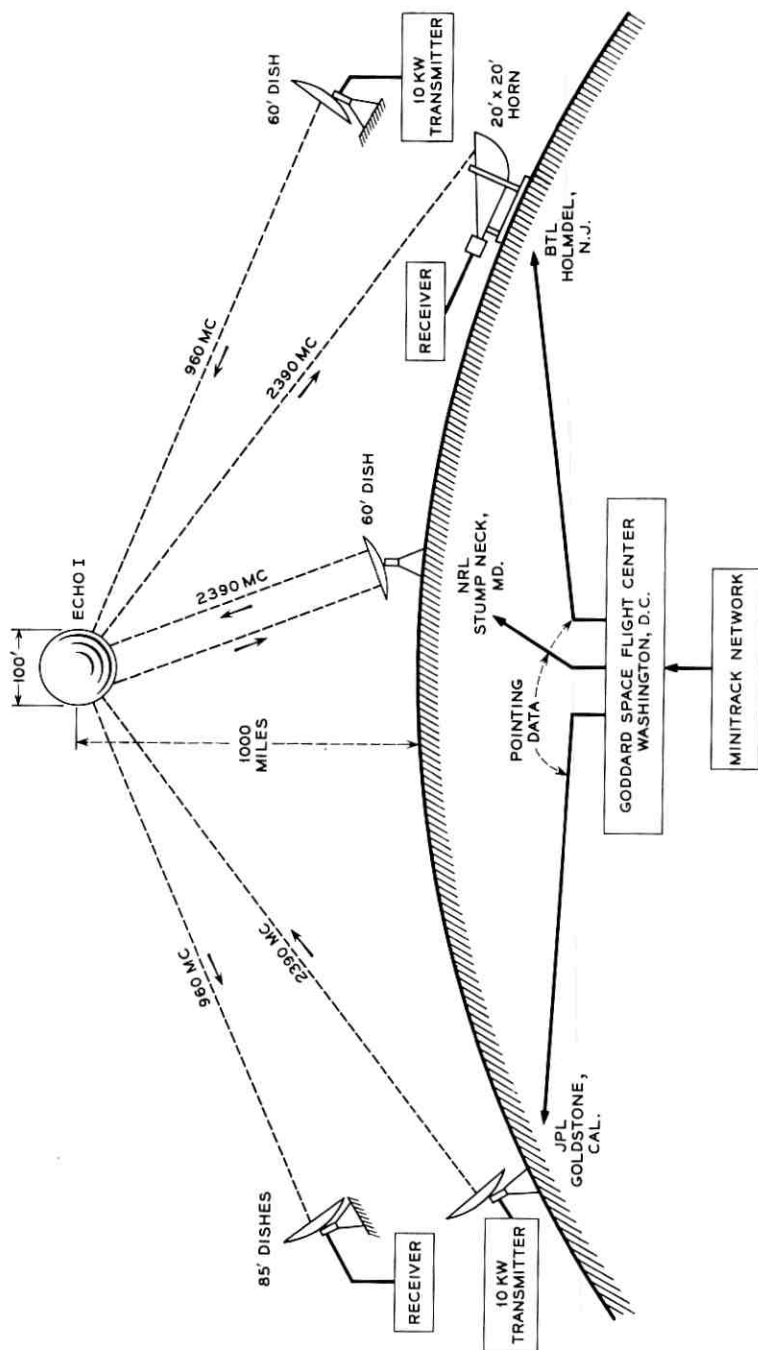


Fig. 1 — General features of the Project Echo experiment.

modulation with a peak index of 10, corresponding to ± 30 kc deviation. This results in an FM improvement factor of about 25 db, provided the carrier-to-noise ratio (C/N) is above the FM threshold. The threshold in the Echo demodulators has been improved relative to that of conventional frequency modulation by the application of negative feedback to the FM demodulator.¹ The threshold improvement for a modulation index of 10 and for 20 db of feedback is about 9 db, and occurs at an RF carrier-to-noise power ratio of about 14 db measured in a 6-kc bandwidth. Provision was also made for other types of modulation, including single sideband and frequency or phase modulation of low index. It was expected that the maximum carrier levels would be about -113 dbm for reception from JPL and BTL and -108 dbm from NRL. Taking the expected system noise temperatures into account, this would provide maximum baseband rms S/N ratios as follows, assuming the use of a modulation index of 10:

JPL to BTL at 2390 mc:	$S/N = 57$ db,
BTL to JPL at 960 mc:	$S/N = 49$ db,
NRL to BTL at 2390 mc:	$S/N > 57$ db.

The signal-to-noise (S/N) ratio depends on the satellite position, since this determines the free-space path loss, atmospheric attenuation, and receiver noise temperature. Over most of the region of mutual visibility, however, the baseband S/N ratio was expected to be at least 45 db.²

The threshold sensitivity of the BTL receivers is approximately -150 dbm, which corresponds to an effective system temperature of 23°K and a noise bandwidth of 6 kc, with a signal detection level 3 db below the average noise power. Under these conditions the maximum carrier-to-noise ratio was expected to be 34 db at 2390 mc at BTL, which would permit making meaningful measurements of both the direct- and cross-polarized components of the incoming signal. Means for carefully recording and calibrating these signals were thus provided.

It was anticipated that tracking the satellite accurately enough to achieve the hoped-for signal levels would be a difficult problem; therefore a number of different tracking modes were provided at BTL. Primarily, the entire system was slaved to a teletypewriter tape containing predicted look angles for a given satellite pass. This tape was based on orbit-reduction calculations performed at the Goddard Space Flight Center (GSFC), Greenbelt, Maryland, utilizing observations obtained from the Minitrack network. During the actual pass any differences between the position called for by the tape and the actual satellite posi-

tion were then corrected by means of information derived from optics, radar, or maximization of the 2390-mc received signal — whichever seemed best to use under the conditions of the moment. Alternatively, if no drive tape was available and if the satellite was visible, the system could be slaved to the optical system, which was then manually operated to track the satellite. All of the above methods were successfully used at one time or another; in fact, had they not all been provided, valuable data would have been lost.

1.3 Preliminary Tests

In order to gain experience and check the capabilities of the equipment, a number of preliminary experiments were performed with JPL, NRL, Lincoln Laboratories, General Electric, and others. A brief chronological summary of these tests is given in Table I.

TABLE I — SUMMARY OF PRELIMINARY EXPERIMENTS

Date	Test
Moonbounce	
11/23/59	960 mc FM to JPL
11/25/59	960 mc FM to JPL
12/23/59	960 mc NBPM to JPL
1/6/60	960 mc NBPM and FM to JPL
2/9/60	960 mc NBPM and FM to JPL
4/28/60	960 mc SSB to JPL
5/4/60	2390 mc FM JPL to BTL
5/10/60	Two-way FM tests with JPL
5/12/60	960 mc to Jodrell Bank
7/19/60	Two-way SSB tests with JPL
7/22/60	Two-way NBPM tests with JPL
7/27/60	First two-way live voice, SSB, with JPL
7/28/60	2390 mc from NRL using FM and NBPM
8/1/60	Two-way SSB tests with JPL
8/3/60	Two-way SSB tests with JPL
8/4/60	Two-way FM tests with JPL
8/7/60	First BTL radar track of the moon
Tiros	
4/28/60	960 mc to JPL, no acquisition
5/5/60	960 mc to JPL, signal received
5/11/60	960 mc to JPL, signal received
7/29/60	2390 mc from NRL, contact throughout two passes
Shotput	
10/28/59	Optical track only
1/16/60	960 mc carrier to Round Hill
2/27/60	Voice to Round Hill using FM

1.3.1 *Moonbounce Tests*

On November 23, 1959, shortly after the installation of the BTL 60-foot dish and the 10-kw, 960-mc transmitter, the first operation was held with JPL. Successful contact was made and some live voice was transmitted until a coaxial line broke down at BTL and operations were terminated. This was the first of a series of 17 such tests utilizing the moon as a reflector, continuing to the days immediately preceding the successful launching of Echo I on August 12, 1960.

As the tests progressed, more equipment was added at both terminals, until finally, on July 27, 1960, a two-way live voice communications circuit was established via the moon for the first time in history using single-sideband modulation (SSB). Valuable information concerning system operation and calibration was obtained on all the tests and, incidentally, some interesting data on the characteristics of the moon as a reflector, which are summarized below:

1. Effective scattering cross section is 9×10^{11} square meters, corresponding to a perfectly conducting sphere 670 miles in diameter. This is comparable to values obtained by other workers.

2. Speech as transmitted by SSB with reduced carrier is of fairly good quality, is perfectly understandable, and usually permits identification of the speaker. The quality of music is much like that received on short wave from overseas.

3. Use of broad bandwidth modulation systems will degrade the quality. For example, FM of such index that only the first sidebands are present provides voice transmission of considerably reduced intelligibility compared to SSB. Wide-deviation FM (as used in the Echo experiments) renders speech virtually unintelligible.

1.3.2 *Shotput Tests*

Five suborbital ballistic tests on the balloon payload were made prior to the final Echo launch. These launchings took place at Wallops Island, Virginia, and the trajectories were visible from Holmdel. Bell Telephone Laboratories participated in the first three, as follows:

Shotput 1: Optically tracked the balloon to gain tracking experience and compare predicted with observed trajectory.

Shotput 2: Successfully transmitted a 960-mc carrier to the Lincoln Laboratories station at Round Hill, Massachusetts, via the balloon.

Shotput 3: Demonstrated transmission of voice via the balloon using FM with feedback (FMFB) at 960 mc, again to Round Hill. The threshold improvement of the FMFB demodulators was verified.

Tracking was again optical on the latter tests.

1.3.3 *Tiros Tests*

In order to check the feasibility of satellite tracking by means of orbit predictions from Goddard Space Flight Center, and to make sure that BTL, JPL, and NRL indeed possessed stations in proper operating condition, a number of carrier transmission tests using reflection from *Tiros I* were scheduled. The small size and low orbit of this satellite made it a much more difficult target; nevertheless, two successful contacts with JPL and two with NRL were achieved. On two passes, *Tiros* was briefly observed optically, and its position noted to be within 0.1° of that predicted.

With the successful termination of these preliminary experiments, it was felt that the BTL station was in readiness for the Project Echo satellite experiment.

II. SYSTEM DESCRIPTION

Most of the BTL facilities for Project Echo are located on top of Crawford Hill, New Jersey, approximately 30 miles south-southwest of New York City, at 40.392° north latitude and 74.187° west longitude. An 18-foot paraboloid and other equipment used in the tracking radar are situated off the hill about one and a half miles away, in order to increase the isolation between the transmitted signals from the 60-foot dish and the radar receiver. Fig. 2 is a general view of the hilltop, and a simplified block diagram is shown in Fig. 3. The small buildings visible in the photograph house the various pieces of system equipment, as follows:

<i>Building</i>	<i>Location</i>	<i>Contents</i>
1	Next to 60-foot dish	960-mc transmitter, monitors
2	Between dish and horn	System controls, digital-to-analog converter, FMFB demodulators, TWX terminals, audio and signal level recorders
3	Next to horn	Horn servo drive, helium recovery plant
4*	At end of hilltop	Data storage and reduction equipment
Trailer*	Next to Building 2	Plotting board, telescope, angular offset controls

* Not visible in photograph

The system is briefly summarized in the following four sections, cover-



Fig. 2 — Bell Telephone Laboratories Echo station facilities on Crawford Hill, Holmdel, New Jersey.

ing the functions of transmitting, receiving, tracking, and communications. For more detailed descriptions of certain components the reader is referred to the companion papers in this issue.^{2-5, 7-13}

2.1 *Transmitting System*

2.1.1 *960-mc Transmitter*³

The BTL transmitter is a commercially available item which was purchased from a division of the International Telephone and Telegraph Company, and provides a 10-kw output with an exciter capable of FM with deviations up to ± 300 kc. In order to satisfy the various requirements for Project Echo, it has also been equipped with additional exciters and monitoring facilities.

Basically, the transmitter provides two output signals. One is centered at 960.05 mc and is designated the *communications* channel, and may be modulated with FM of indices from 1 to 10, phase modulation (PM) with 0.5 radian index, single-sideband modulation (SSB), double-sideband modulation (DSB), or AM. The modulation bandwidth extends

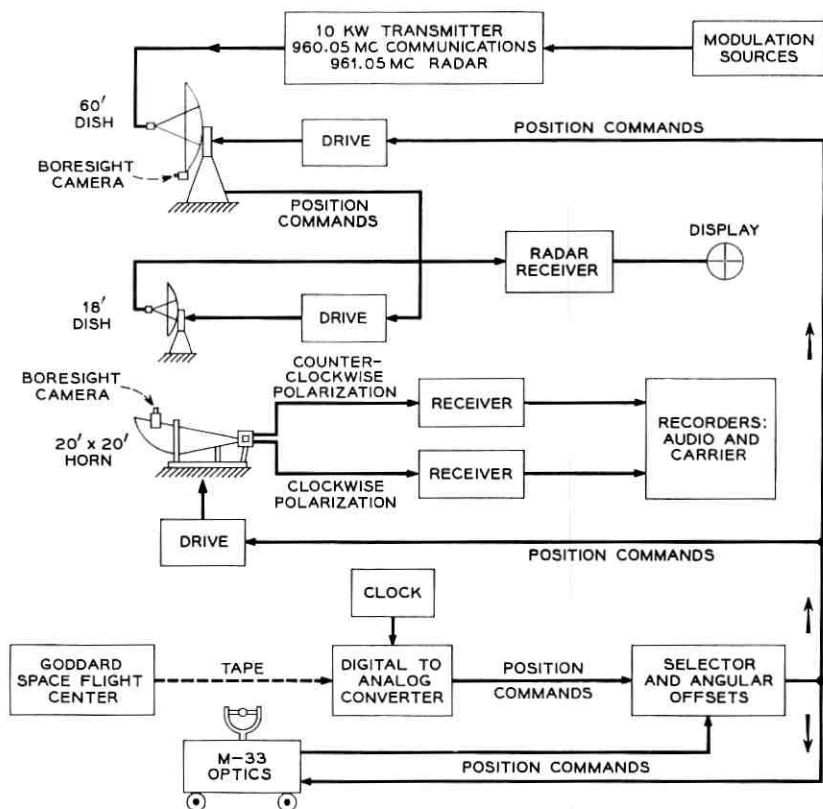


Fig. 3 — Block diagram of the BTL facilities.

from 200 to 3000 cps, corresponding to a satisfactory telephone circuit. The other output is centered at 961.05 mc, and is only used for the BTL radar. It is amplitude-modulated by a square wave whose frequency may be varied from 15 to 100 cps, depending on the range of the object being tracked. The power outputs in each channel may be independently varied from 0 to 10 kw, subject to the restriction that their sum cannot exceed 10 kw. Normally the communications channel is set at 7.5 kw and the radar channel at 2.5 kw. The simultaneous use of these two channels is made possible by the final amplifier in the transmitter. This employs a klystron with four external cavities arranged to give an overall passband of 3.5 mc. A gain of more than 40 db is available, so that only a watt or less of excitation is necessary. The klystron has a fairly linear amplification characteristic, and thus can handle the various excitations listed without appreciable distortion or cross modulation.

Means for monitoring the various transmitter characteristics were provided, including frequency print-out accurate to ± 30 cps, power recording accurate to ± 0.1 db, and receivers for recovering and recording the transmitted modulation. All monitor records were time-tagged with Greenwich Mean Time (GMT).

The over-all frequency stability of the transmitter depends on the particular exciter being used, and considerable effort was spent in making this as good as possible, with the following results:

<i>Exciter</i>	<i>Stability at 960 mc</i>
Wide-band FM	± 150 cps
Narrow-band FM or PM	± 50 cps
Radar	± 50 cps
SSB, DSB, or AM	± 20 cps

2.1.2 60-Foot Paraboloid

This antenna is a standard item and was purchased complete with pedestal and servo drive from the D. S. Kennedy Company. The servo drive uses 20-hp dc motors in each axis and is capable of positioning the antenna to an accuracy of $\pm 0.05^\circ$ in winds up to 35 mph at angular rates more than adequate for satellite tracking. Maximum slew speed is 10 degrees per second. The antenna will withstand winds up to 70 mph in the stow position and will survive 110 mph winds when locked in place. The Kennedy Company also supplied and installed the complete feed system, including the microwave plumbing down to the transmitter. This feed was designed so that any polarization whatever could be transmitted, whether linear of any orientation, circular of right- or left-handed sense, or even elliptical. As mentioned before, counter-clockwise circular polarization was always radiated for the Echo tests. On a few occasions it was reversed during a Moonbounce test with JPL to check the cross-polarization characteristics of the moon. The transmission line from the feed horn to the transmitter output is waveguide, except for a short section of coaxial cable required for the two rotating joints. Total transmission-line loss was measured to be 0.5 db.

After the antenna was installed in August 1959, several months of testing and alignment by Bell Telephone Laboratories personnel followed. The gain, cross polarization, and radiation patterns were all carefully measured, using a 960-mc source on a hilltop about 12,000 feet away. This distance is large enough so that the field produced by this source at the antenna is essentially flat (as was verified by direct measurement). The results of the tests were as follows:

Gain	43.1 \pm 0.1 db,
3-db beamwidth	1.2 degrees,
First sidelobes	-20 db,
Axial ratio	1 db,
Return loss	20 db.

2.2 Receiving System⁴

2.2.1 Antenna⁵ and Waveguide

A horn-reflector antenna (see Fig. 2) was used for 2390-mc reception at Holmdel because of its demonstrated low-noise properties⁶ and other features. The aperture of the antenna is approximately 20 by 20 feet; the over-all length of the antenna is about 50 feet. Careful measurements were made of the gain and radiation patterns before the Echo launch with entirely satisfactory results, as listed below:

Gain	43.3 db
3-db beamwidth	1.2 degrees
Axial ratio	1.2 db
Projected area	380 square feet
Effective area	288 square feet

The drive for the horn is very similar to that for the 60-foot paraboloid. A 10-horsepower dc motor is used for positioning in each axis, making possible maximum slew speeds of 5 degrees per second and accurate tracking in winds up to about 30 miles per hour.

The horn throat tapered down to round waveguide inside the antenna cab. A rotating joint having very low loss coupled the horn to the waveguide system, which contained the 90° phase-shift section for converting the two orthogonal circularly polarized waves to orthogonal linear waves, polarization takeoffs, and transducers to the coaxial lines leading down into the maser. Means were also provided for injecting a known amount of noise or 2390-mc reference signal into the waveguide for calibration purposes.

2.2.2 Low-Noise Amplifiers

Two masers were provided,⁷ both located in one dewar in the field of a single magnet, and were used for the two polarizations of the incoming signal. The maser gains were sufficient so that the noise figure of the following crystal converter did not appreciably affect the over-all sys-

tem noise temperature. Liquid helium was used to cool the masers to operating temperature. A dual 2390-mc parametric amplifier was also provided,⁸ and, in the event of maser failure, could be switched into the system in place of the maser in a few minutes. The C/N ratio is degraded by about 10 db when a parametric amplifier is used.

2.2.3 IF Preamplifiers and Demodulators

The crystal mixers or parametric amplifier down-converters were followed by 70-mc IF preamplifiers, which raised the signals to levels suitable for transmission to the control building via slip rings in the horn and coaxial cable. The remainder of the receiving system was located in the control building, including the FMFB demodulators, Sanborn pen recorder, frequency monitor, and audio recording and distribution equipment. The FMFB demodulators also included an AGC circuit which was used for signal-level recording. On occasions when SSB or NBPM was used, an SSB receiver was substituted for the FMFB demodulators,⁹ and in this case phase lock was used to remove the Doppler shift. A second conventional SSB receiver then recovered the modulation.

2.2.4 Recording

Since the voltage-controlled beating oscillator in the feedback demodulator automatically tracked the incoming signal frequency, its frequency was directly proportional to the Doppler shift. Its output at $68.8 \text{ mc} \pm f$, where f was the Doppler shift, was measured by a frequency counter and displayed by Nixie* lamps for photographic recording once every second.

A four-channel Sanborn recorder was used for recording the signal levels of the clockwise and counter-clockwise circularly polarized components. The system noise temperature was also continuously recorded during each pass.

The audio output of the system was recorded on magnetic tape, and also was available for local or outside telephone lines, or for the station public address system.

2.2.5 System Sensitivity

Measurements show that the over-all system noise temperature, including sky noise, was about 45°K or less throughout the significant

* Nixie lamps are number-indicating lamps that are often used in frequency-counting circuits.

part of the Project Echo experiments, with the minimum value ever observed being about 21.5°K . The sky noise is a function of antenna elevation, as pointed out elsewhere, so that the system temperature varies during a satellite pass.

2.3 Tracking

2.3.1 General

As mentioned in the Introduction, several means were provided for tracking the balloon. From Fig. 4 it is evident that the antennas were pointed principally by information from a predicted drive tape, with corrections being inserted manually using current data yielded by optics, radar, or carrier peaking. This was the usual mode of operation. An alternative mode was available in which the system antennas could be slaved to the positional read-outs of the optical tracker, which was then operated manually to track the satellite. Positional commands were all of the analog type obtained from synchro control transmitters. A two-

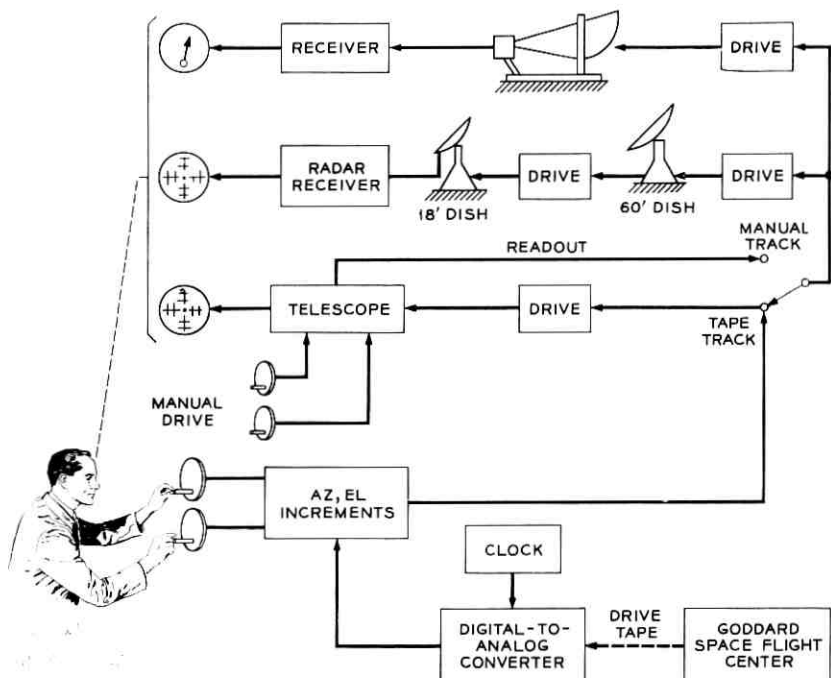


Fig. 4 — Block diagram of BTL tracking modes.

speed, 36:1 system was used in each coordinate. The device for manually inserting angular offsets, or corrections, utilized synchro differential generators and was located in the trailer which carried the optical tracking telescope. Displays from the optics, radar, and carrier-level indicators were located adjacent to the differential control unit so that one operator could select the most suitable display and insert the corrections accordingly. Angular offsets up to 360° in azimuth and 90° in elevation could be used.

Drive units for the 60-foot dish and horn are similar, consisting basically of Ward-Leonard-type systems using dc motors.

2.3.2 *Digital-to-Analog Converter (DAC)*¹⁰

This unit serves to convert the digital information contained in the drive tape to the analog (synchro) positional commands for controlling the antennas and optics. The drive tape supplies a block of five separate quantities, called a data point, every four seconds. This gives time, azimuth, elevation, azimuth rate, and elevation rate of the satellite, with these quantities appearing on the tape in binary-coded decimal form, using four bits for the digit and one for a parity error check. The decoding equipment in the DAC utilizes the rate information to provide positional commands in between the four-second data points, so that the antennas will move smoothly.

Using commercial 60-word-per-minute facilities, it takes 20 to 30 minutes to transmit the usual drive information for Echo I. For the first several months after launching, the computer at the Goddard Space Flight Center supplied the drive tapes. Since the beginning of 1961 the tapes have been obtained from a computer at Bell Telephone Laboratories, and are based on orbital elements supplied by the Smithsonian Astrophysical Observatory in Cambridge, Massachusetts.

The drive tapes are read photoelectrically at a time corresponding to the time of the data point. As the tape advances from one point to the next, the angular quantities are read into transistorized logic circuits, where they are sorted and decoded. The decoding process results in a rectangular pulse output whose duration corresponds to the input quantity, causing a motor to turn a gear train to the appropriate angular position with an accuracy of $\pm 0.02^\circ$. To the gear train are fastened a number of synchro transmitters, which supply positional command signals to the dish, horn, and optical drives.

The DAC also includes a very stable clock which is used as the station master clock, as well as for the time comparison involved in reading the drive tapes.

2.3.3 *Optical Tracker*

A component of a surplus M-33 fire-control radar system was obtained on loan for use as the tracking telescope. It consists of a large trailer carrying a periscope-type optical train leading down to convenient operator positions inside the trailer. The field of view is about 6° , with a magnification of $8\times$ and an objective lens about 2 inches in diameter. Stars down to a magnitude of about +8 can be seen on a clear night. Modifications were made to the angular data-takeoff units so that the telescope could be (a) slaved to the command signals originating from the DAC and (b) manually controlled to follow an object and provide suitable positioning signals to the antennas. Both complete manual and aided manual modes were available. Star sights were used to check alignment, and in general showed residual errors of $\pm 0.02^\circ$. In normal use the operator watched through the telescope while it moved in accordance with the commands derived from the drive tape, then, if errors were detected, the appropriate angular offsets were inserted, causing all the system antennas and the telescope to track the target accurately.

Several plotting boards were included in the M-33 trailer as part of the normal fire-control equipment. One of these was modified so that a plot of azimuth versus elevation of the telescope could be obtained during a satellite pass. Timing marks spaced 30 seconds apart were also provided, and a plotting accuracy of about $\pm 0.5^\circ$ was obtained. These plots were quite useful in making rapid examinations of tracking, and showed bad data points graphically.

2.3.4 *Tracking Radar*¹¹

A separate 18-foot paraboloid is used to receive the 961.05-mc signal reflected from the satellite. It is equipped with a rotating feed which produces a conically scanned beam for obtaining angular error information. The radar antenna is slaved to the angular read-out synchros associated with the 60-foot dish, and follows to an accuracy of $\pm 0.05^\circ$.

Since the radar transmitter and receiver are fairly close together, gating had to be used to prevent masking of the signal from the satellite by the transmitter. As mentioned before, the radar carrier is at 961.05 mc, 1.0 mc away from the communications frequency of 960.05 mc, and is 100 per cent square-wave modulated. There is a 3-db loss in average signal level due to the square-wave modulation. The lowest pulse repetition frequency is 15 cps, corresponding to a range of 3,000 miles. This means that the reflected signal arrives just after the end of the transmitted pulse. As the range decreases, the pulse repetition frequency is

increased correspondingly to compensate for the decrease in the width of the received pulse.

The radar receiver is equipped with a 961-mc parametric amplifier¹² which is followed by appropriate IF and detection circuits for obtaining the azimuth and elevation errors. These were derived by two phase detectors, fed in parallel by the input signal and separately by reference square waves 90° apart produced by cam-operated switches at the antenna feed. The dc error signals were then brought to the M-33 trailer, where they positioned the spot on a cathode ray tube, thus showing the position of the satellite with respect to the system pointing axis to the operator in much the same manner as that given by the tracking telescope. The operator then manually inserted the proper angular offsets to center the spot.

The over-all system sensitivity is about -150 dbm, and good pointing information was obtained for levels of -145 dbm and higher. Pre-detection bandwidth is 500 cps. Since the incoming signal frequency is Doppler-shifted by ± 35 kc during a typical pass, a very good automatic frequency control circuit is necessary. A postdetection filter with about a one-second time constant was used to increase the tracking signal-to-noise ratio.

In addition to angular error data, the radar receiver was used to measure the scattering cross section of the satellite by recording the automatic gain control voltage. A distant test source was used for calibration purposes, but this part of the system was not put into operation until about October 1960.

2.3.5 Alignment

In order to conduct meaningful communication and transmission tests, it was felt that the system antennas should be able to track the balloon to an accuracy of $\pm 0.1^\circ$. Part of this error would inevitably be due to antenna misalignment or bore-sighting errors; hence, some time was spent in measuring and adjusting to keep these errors within at most $\pm 0.05^\circ$. Since the predicted look angles for the satellite would always be referred to the assumed local geocentric coordinate system, it was first necessary to establish that the mechanical axes of the antennas and tracking telescope were properly aligned with respect to these coordinates. To do this, an initial alignment was made using surveying methods, and then this was checked by mounting a telescope on the unit under test and taking star sights for a number of stars over the entire sky hemisphere. Analysis of these data then revealed any sys-

tematic errors, such as tilt of the azimuth axis, and these were then corrected and checked by more star sights.

The next step was to adjust the electrical axes of the antennas to coincide with the mechanical axes. This was done, in the case of the 60- and 18-foot dishes, by aiming the antenna at a distant microwave source whose position was accurately known, and adjusting the feed until the peak signal occurred at the proper position. Time limitations prevented carrying out a similar procedure for the horn. In this case, mechanical and optical methods were used to align the reflector. Subsequent electrical checks showed a residual error of less than 0.1° .

Finally, the data comparison units used in the servo drive follow-ups had to be aligned so that all units pointed in the same direction for a given positional command signal. No allowance for parallax was made for any units, since the largest separation (between the radar receiving antenna and the rest of the system) only corresponded to an error of 0.08° for the Echo satellite at closest approach.

The results of these tests were generally satisfactory, and indicated that the desired objectives had been achieved.

2.3.6 *Tracking Data Recording*

In order to have a record of the positions of the various moving elements of the system during a satellite pass, each element was provided with synchro read-outs which were periodically photographed. Pictures were taken at one-second intervals of a panel carrying the two-speed azimuth and elevation position dials for the DAC, M-33 (optics), 60-foot dish, and horn antenna. A Greenwich Mean Time clock also appeared in the photographs. Position angles could be read to $\pm 0.01^\circ$, and time to 0.5 second. An enlargement of one frame of such a record is shown in Fig. 5. Also shown are a set of Nixie lamps for recording the 2390-mc received signal frequency.

The 60-foot dish and horn antennas were each equipped with a bore-sight camera¹³ that could be started at will whenever the satellite was visible. Pictures were taken at four frames per second, and included a reticle for indicating angular offsets to an accuracy of $\pm 0.01^\circ$ and a time-coded counter.

2.4 *Communications*

2.4.1 *Telephone*

A variety of telephone services were provided for both local and long distance communications. Each of the four buildings on Crawford Hill

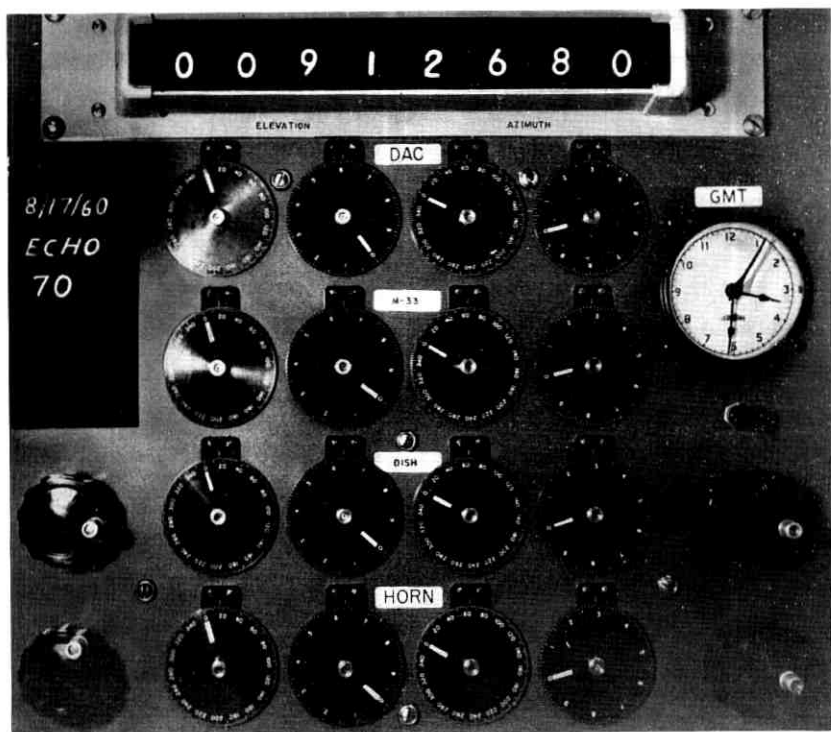


Fig. 5 — Reproduction of one frame of the data-recording camera film.

was tied in with the Holmdel PBX for routine internal calls. Three direct lines were also provided to the Middletown central office: one serving all four buildings in parallel and a second going to the transmitter and control buildings (1 and 2). The third went to the control building, and was used only for calls to facilities other than JPL for consultation during an actual operation. Finally, a private four-wire line was established to the Goldstone site with provision at each end for switching the instrument between the land line and the satellite facility for any of four modes of operation:

1. Two-way conversation by land line;
2. East-to-west by satellite, west-to-east by land line;
3. West-to-east by satellite, east-to-west by land line;
4. Two-way by satellite.

2.4.2 Teletypewriter

Two teletypewriter lines were brought into the control building. One was a private full-time service to the space control (SPACON) of the God-

dard Space Flight Center. This was used to maintain contact with SPACON and other stations tied into this net, and also for the transmission of drive tapes from the GSFC computer to BTL.

The other line provided a general utility TWX service, and included a tape puncher for receiving drive tapes from other sources.

2.4.3 *Intercommunications*

During operational activities all station personnel concerned were in touch with each other by a headset-type intercommunication system. Conversation on this loop was also recorded on magnetic tape as a matter of record.

A public address system was provided which served as a general announcing system for all locations, both indoors and outdoors. When appropriate, the signals being carried by the satellite circuit could be connected to the public address system for the benefit of all station personnel.

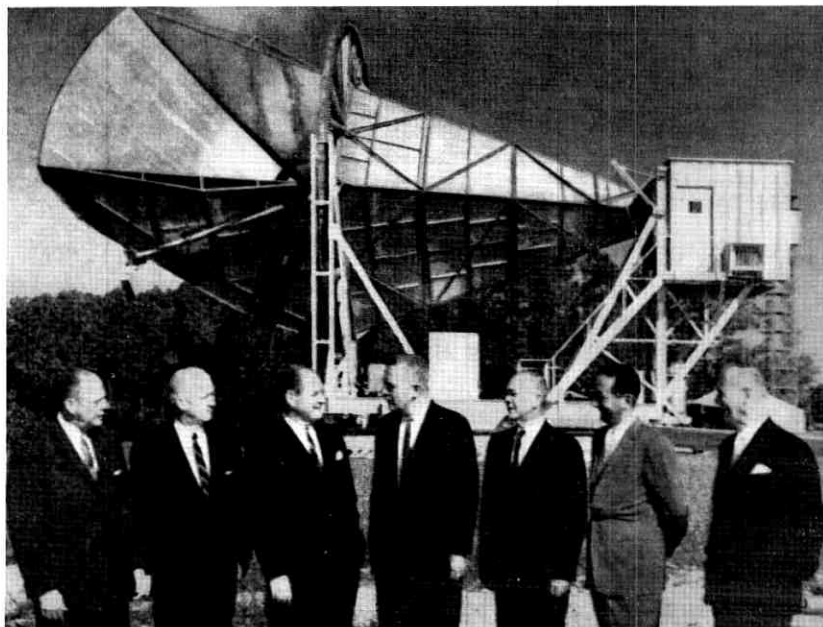


Fig. 6 — Reproduction of the actual facsimile sent from NRL to BTL on September 22, 1960. Shown, left to right, are Commissioners John S. Cross and Rosel H. Hyde of the Federal Communications Commission; T. Keith Glennan of the National Aeronautics and Space Administration; Frederick W. Ford, FCC Chairman; and Commissioners Robert T. Bartley, Robert E. Lee, and T. A. M. Craven.

III. EXPERIMENTAL RESULTS

Since the successful launching of the Echo I balloon on August 12, 1960, operations were carried on by the BTL station for about 120 passes up to March 1, 1961. Of these, four were with JPL only, 50 were with NRL only, 27 were with both JPL and NRL during the same pass, and 39 were with the BTL radar only. Tests with other stations were carried on during 29 of the 120 passes. In general, the objectives of the experiment have been achieved, as will be discussed in detail in the following sections.

3.1 *Audio Tests*

Modulation tests of various kinds were performed on a total of 51 passes with JPL and NRL. Breaking this down further: voice and music transmission were tried using FMFB on 16 passes with JPL and 15 with NRL, using SSB on two passes with JPL, using NBPM on one pass each with JPL and NRL, and using AM once with NRL. Data-type transmission either of facsimile or frequency-shift keying was tried on 15 passes with NRL using FMFB. A sample of facsimile transmission is shown in Fig. 6. Listed below are some of the more significant tests performed in 1960:

<i>Pass No.</i>	<i>Date</i>	<i>GMT</i>	<i>Event</i>
1	8/12	1140	First demonstration of transmission via the balloon: President Eisenhower's message sent from JPL to BTL.
11	8/13	0705	First two-way audio transmission between JPL and BTL: prerecorded messages of President Eisenhower and Senator L. B. Johnson.
12	8/13	0911	First two-way live voice: W. C. Jakes of BTL and P. Tardani of JPL talked briefly.
21	8/14	0233	R. M. Page's message received with excellent quality from NRL.
23	8/14	0644	Music sent from BTL to JPL.
24	8/14	0850	Double bounce of live voice: NRL to BTL to JPL.
33	8/15	0212	Two-way live voice with JPL using standard outside telephone lines connected to the satellite circuit.
35	8/15	0623	SSB with JPL.
60	8/17	0744	NBPM with JPL.

70	8/18	0311	F. R. Kappel, L. DuBridge, and J. B. Fisk talked between California and the East Coast via the satellite.
503	9/22	1541	Demonstration of facsimile picture transmission from NRL.
1097	11/10	0703	Reception of speed mail from NRL by facsimile.

Measurements of the signal-to-noise ratio in the audio band were made during many of the passes. After accounting for some residual noise in the audio output circuits, good agreement was obtained with the predicted values for all types of modulation used. The superiority of the FM over SSB or NBPM was clearly evident. The quality of voice or music using FM was excellent, and indistinguishable from that of a land-line circuit. With the successful demonstration of facsimile on later passes, it was concluded that the balloon in conjunction with the existing terminal equipment at BTL and JPL provided an excellent circuit with the designed bandwidth of 200 to 3000 cps, and that any service that could be transmitted in this bandwidth could equally well be handled by the satellite circuit.

3.2 *Balloon Scattering Cross Section*

Measurements of the actual received power from the balloon were made during all passes worked, and data are available for at least one or more of the following four modes of transmission on each pass:

- JPL to BTL at 2390 mc,
- BTL to JPL at 960 mc,
- NRL to BTL at 2390 mc,
- BTL to BTL at 961 mc (BTL radar).

By comparing these measurements with theoretical values an estimate may be made of the average scattering cross section of the balloon and its variation with time. The received power may be calculated from the usual free-space transmission formulas,² provided that the system parameters, such as transmitted power, antenna gain, slant range to the balloon, frequency, and effective scattering cross section of the balloon, are known.

There are a few additional factors that must be taken into account before comparison can be made with the observed data. Obviously, if either of the two antennas involved in a transmission path is not aimed at the satellite properly, the full antenna gain will not be realized. In this case it must be determined where the antenna actually was aimed,

using boresight camera data or a comparison of positional recordings with predictions, and allowance made in accordance with the antenna patterns.

A factor which becomes important at low elevation angles is power absorption by the atmosphere. This effect has been calculated,¹⁴ and the curves of Fig. 7 show the variation in one-way loss with elevation angle and frequency. Since the antenna elevation angle at each end of the path is known, the loss can be evaluated and included.

Normally, the effects of atmospheric refraction would not be involved, since the antennas either were tracked by optics or radar, in which case refraction would be automatically compensated, or by predictions that would include this effect. Through a programming error, however, the drive tapes up to October 6, 1960, included the refraction correction in the wrong sense. The error was rectified and proper corrections made after that date. The only antenna appreciably affected was the NRL 60-foot dish, since the BTL antennas had comparatively wide beams, and the JPL antennas were almost always tracked by radar or optics. Assuming a reasonable pattern for the NRL 60-foot dish at 2390 mc (no

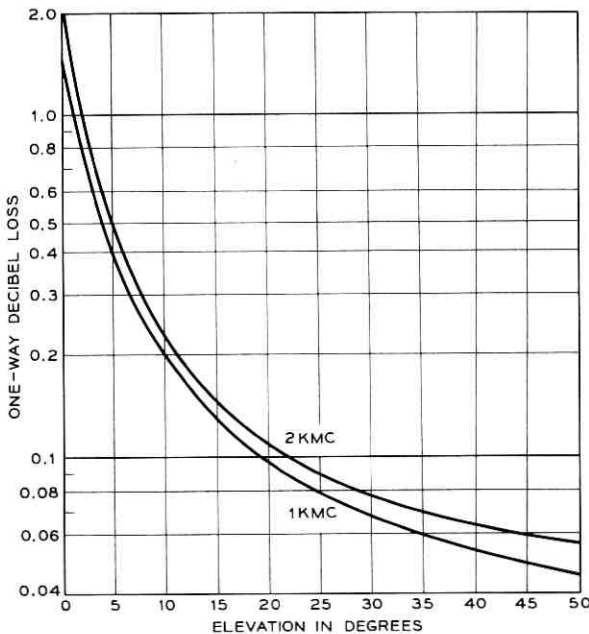


Fig. 7 — Absorption due to atmospheric oxygen and water vapor.

measured patterns were available) and a standard atmosphere, the calculated received power levels were appropriately modified using the correction curves shown in Fig. 8, providing optical corrections were not being used by NRL at the time.

Records of transmitted power were kept at all stations, and were reasonably complete over all passes worked. Nominally JPL radiated 9 kw at 2390 mc, NRL radiated 9 kw, and BTL radiated a total of 10 kw at 960 mc, the power being split between the communications channel and the radar channel, as described earlier. All of these records were made available so that the appropriate corrections could be made.

3.2.1 Results

Comparison of actual received power with that predicted has been made on 96 passes. For each pass studied, the predicted received power was computed for one-minute intervals in time and plotted on the actual records. In general, it was found that the observed values differed from the predicted values by an approximately constant factor during the significant part of each pass, so that a single number expressed in db served to characterize the difference between the observed and predicted received power. Fig. 9 contains the plots of these points as a function of time from launch and transmission mode, each point representing one

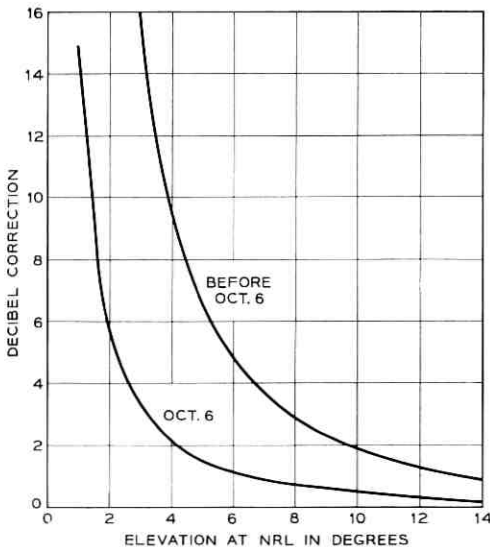


Fig. 8 — Correction curves for refraction at NRL.

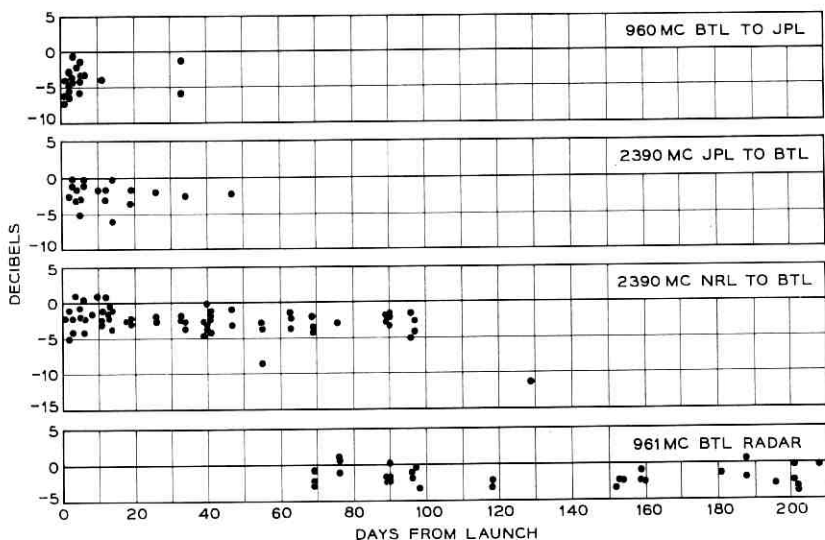


Fig. 9 — Difference in decibels between predicted and observed received signal power.

pass. In all cases, attempts were made to correct for atmospheric loss, transmitter power, and atmospheric refraction, where necessary. However, errors in pointing were not accounted for in all cases.

The JPL antennas were almost always pointed very accurately at the balloon by their radar or optics, as evidenced by boresight camera pictures and examination of a few angular read-outs. Occasional pointing errors were mostly due to momentary loss of radar lock and could be identified as such and subsequently ignored.

Pointing of the BTL antennas was good for the same reasons as for JPL; again, the occasional errors in pointing were obvious and could be ignored.

No pointing data were available from the NRL antenna, so it had to be assumed that the drive tapes were accurate, or that optical corrections were being used.

It is felt that the most significant data were obtained from the JPL-BTL transmissions at 2390 mc. This path involved the fewest unknowns and had the most accurately calibrated receiver. From the plot in Fig. 9, it can be seen that on several passes the received signal power was equal to that predicted for reflection from a perfectly conducting 100-foot sphere. On the basis of these data alone, it can be assumed that a successful inflation was achieved.

The data for the 960-mc BTL-JPL transmissions show a much greater spread between predicted and observed values. This may be in large part attributed to the fact that the JPL 960-mc receiver was usually calibrated only once before a series of passes which might take four hours or more, and during this time calibration drifts were inevitable. The BTL 2390-mc receiver was completely calibrated before and after every pass. There is also some uncertainty about the gain of the JPL receiving dish at 960 mc, since it was equipped with a rather complicated dual-frequency feed and there was not enough time to measure the gain accurately.

Although there was no time before launch of Echo I to determine accurately the antenna gain or transmission-line loss for the NRL transmitting dish, the use of the estimated values showed good agreement with theory on a number of passes. The spread of values of the difference between observed and predicted received power was essentially the same over both 2390-mc paths.

The BTL radar did not become useful for scattering cross section measurements until about two months after the launch. Since January 1, 1961, it has been the only source of such data, and is probably accurate to about ± 1.5 db. These data indicate that, as of March 1, 1961, Echo I was probably an approximately spherical object with a diameter no less than 70 feet and a somewhat wrinkled skin. There may be a few flattened areas, as indicated by a rare deep fade in the BTL radar signal, but it is evident that it could still be used for voice communication.

3.3 *Detailed Study of Selected Passes*

3.3.1 *Transmission at 2390 mc*

A four-pen Sanborn recorder was used at BTL during the Echo experiment to record the incoming signals and the system noise temperature, as described earlier. Samples of these records, taken during certain passes of particular interest, are shown in Figs. 10 through 22 and described in the following sections.

Pass 1 (Fig. 10):

This was the first passage of the balloon over the United States following its launch from Cape Canaveral, Florida. As shown by the record, a signal was received from JPL for three periods of one to three minutes' duration. The gaps in reception were due to incorrect data points on the drive tape, which caused the antennas to slew away from the satellite track and drop out of servo lock. There was no optical visibility at BTL

during this pass, and, since the BTL radar was still unproven, tracking was accomplished by inserting angular offsets to maximize the output meter of the 2390-mc receiver. The drive tape used was supplied prior to the launch and corresponded to one of the nominal trajectories, with reference time appropriately adjusted to correspond to that of the launch. It is obvious that, had the launching not been virtually perfect, there would have been no reception at all on the first pass because of the severe acquisition problem. The upper record in Fig. 10 shows the variation of the direct polarization component (counter-clockwise) with time, and the third record shows that of the cross-polarized (clockwise) component. Also plotted are the computed values of received power assuming perfect pointing and a fully inflated, perfectly reflecting balloon. The cross-polarized component was calculated assuming only the ellipticities of the JPL dish and BTL horn to be effective in producing this component, i.e., no allowance was made for Faraday rotation or any other possible effects in the transmission path, such as a distorted balloon. These ellipticities are known to be about 1.2 db for each antenna (although there is some evidence that the BTL horn ellipticity may be less), or a maximum/minimum axial ratio $e = 1.155$. The maximum value of the cross-polarized component is then

$$E = \frac{e^2 - 1}{e^2 + 1} = 0.142,$$

or 17 db less than the direct component.

The differences between the observed and calculated signal level of the direct component may be entirely accounted for during the second and third periods of reception by the errors in pointing of the BTL horn. These were established by comparison of the horn angular recordings with the predicted values obtained from a later, more accurate determination of the orbit. The JPL antenna was in smooth, accurate track during these two periods, according to a similar comparison. The corrected values of calculated level, taking these pointing errors into account, are shown as small circles, and the excellent agreement is obvious. Accurate read-out data for the BTL horn were only available for the last minute of the first period, due to a momentary failure of the data-recording camera; hence no corrected values are shown for the first period. There are indications, however, that pointing inaccuracies of both the BTL horn and the JPL dish were responsible for the difference between calculated and observed level during this time.

About one minute after first reception, word was passed to JPL to start modulation, and President Eisenhower's message was then success-

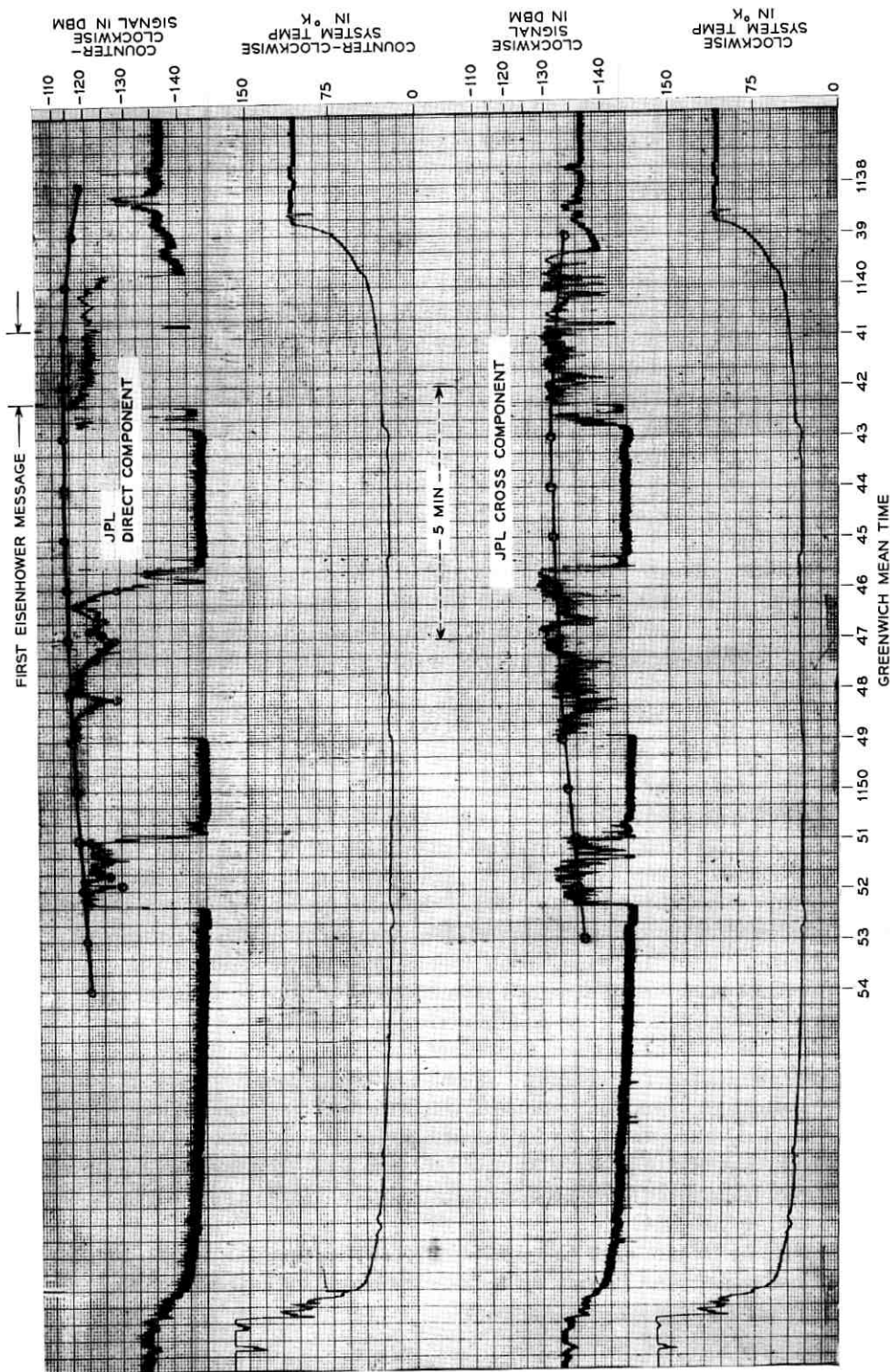


Fig. 10 — First pass (August 12, 1960).

fully transmitted in its entirety, and was repeated during the second and third periods. Modulation shows up on the record as small, dense scintillations superimposed on the larger average variations.

During the 12 minutes of the pass the drive tape predictions were found to be in error by an amount varying progressively from $+1^\circ$ to -1° in elevation and from -1° to -3° in azimuth. These errors were compensated for by the insertion of angular offsets, as mentioned earlier.

The second and fourth tracks in Fig. 10 show the variation in system noise temperature for each of the two receiving channels. Before the pass the noise was fairly high, since the horn was pointing almost at the horizon and received a large amount of thermal radiation from the ground and atmosphere. As the antenna moved up to follow the balloon, the temperature rapidly dropped, so that at 2.5° elevation the temperature was down to 75°K . At 5° it was 50°K , then it slowly decreased to its minimum value of about 25°K near the middle of the pass. The small irregularities in temperature during the pass correspond to the slewing of the antenna caused by bad data points.

Note that there are indications of signal reception starting shortly after 1138 GMT, before the antennas actually started tracking. This proved later to be a very common occurrence and is caused by atmospheric refraction.

Pass 70 (Fig. 11):

This is probably the best example of a completely successful pass with both JPL and NRL. By this time the drive tape predictions were accurate to within a few tenths of a degree and personnel at all locations had become more proficient in tracking and station operation. The level of received signal from both JPL (upper record) and NRL (lower record) was in excellent agreement with theory almost throughout the pass. An interesting event occurred at 0319 GMT, when the direct signal component from JPL showed a few fades while the character of the cross-polarized signal changed appreciably, resulting in increases at the exact times when the direct component was decreasing. Inspection of bore-sight camera data at BTL and pointing readout at JPL showed that this could not be accounted for by pointing errors. System errors, such as momentary changes in transmitted power or receiver gain also were ruled out, since the same effect was observed at 960 mc on the east-west path. It was not observed on the JPL 2388-mc radar, however, leading to the conclusion that either an airplane flew in between the BTL site and the balloon, or the balloon had a large section of surface with anomalous curvature which was common to the BTL-JPL path but not effec-

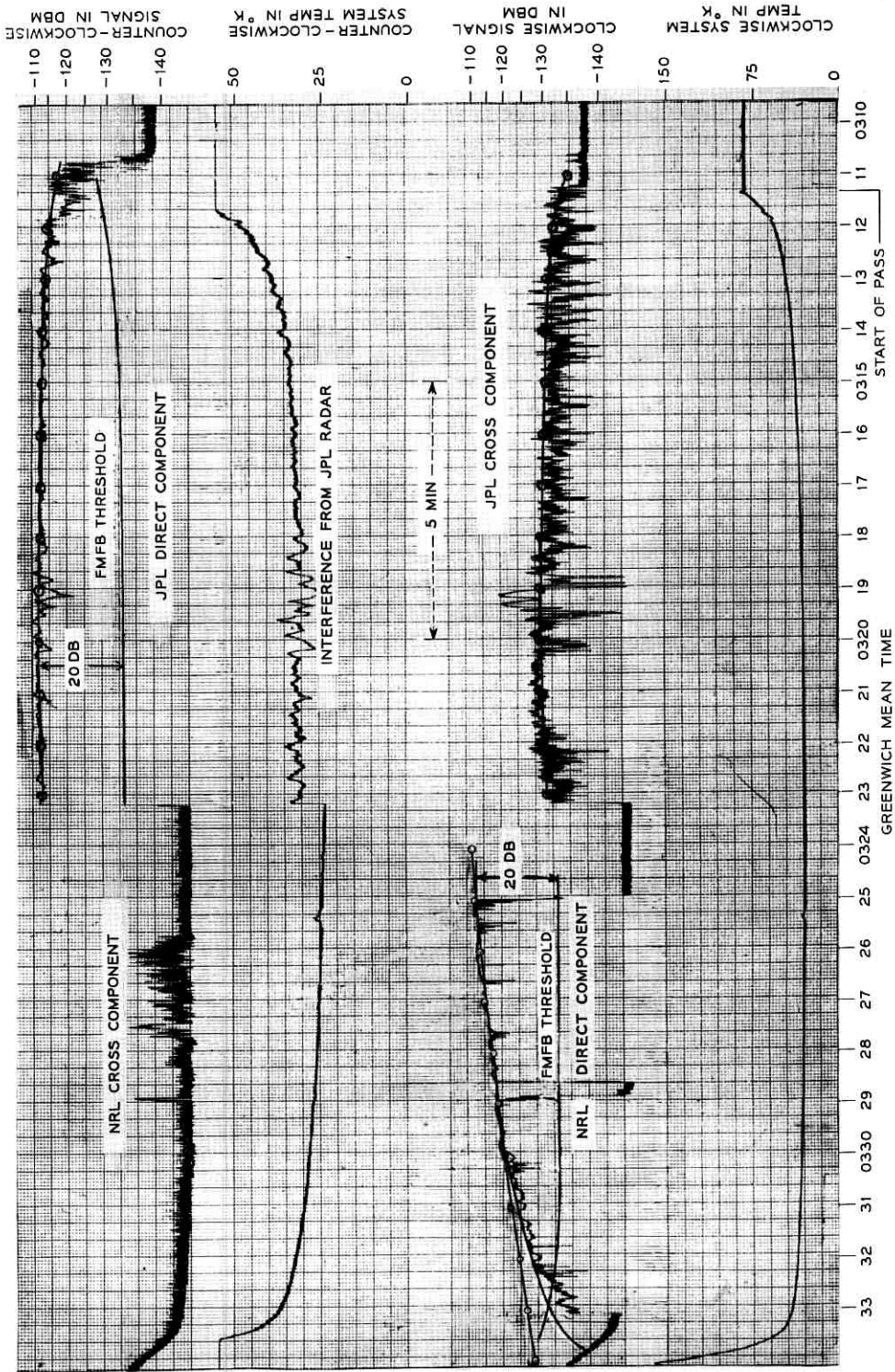


Fig. 11 — Pass 70 — alternate reception (August 18, 1960).

tive in the JPL-JPL radar path. The included angle at the balloon between JPL and BTL at that time was very nearly 90° ; thus, geometrically at least, the latter conclusion is tenable. It seems unlikely that an airplane could have been responsible, since the effect lasted about 45 seconds and the BTL antenna beam was at an elevation angle of 38° at the time. It is difficult to imagine a possible airplane trajectory that would keep it in the beam for this long. In addition, one would expect to see the lights on the airplane in the boresight camera film, and no such evidence was observed. The conclusion, then, is that the balloon very likely had a deformity at this time.

The theoretical curve for NRL at the end of the pass (circled points) assumes that refraction corrections were properly inserted. Assuming that the pointing data provided to NRL had corrections put in with the wrong sign, the smooth curve below was obtained using the corrections from Fig. 8, which obviously is in better agreement with the observations.

The apparent agreement of the cross-polarized signal with theory tends to support the conclusion that there is no strong mechanism in the transmission path to produce birefringence at this frequency. No curve is plotted for the NRL cross component, since no data were available for the ellipticity of the NRL dish. It appears to be of a lower value than JPL, however.

The odd appearance of the counter-clockwise system temperature record was traced to a spurious harmonic from the JPL radar transmitter produced by slight nonlinearity effects.

The value of the incoming carrier level corresponding to the break point of the FM system is also shown on the records as "FM threshold." Note that good voice communication was possible during almost the entire pass.

Pass 119 (Fig. 12):

The helium transfer process at BTL failed shortly before the pass, preventing operation with the maser. The standby parametric amplifiers were connected in place of the maser, allowing operation with about 10 db less signal-to-noise ratio. This can be clearly seen from the record, although the signal was still above the FM threshold for a good portion of the pass. JPL was received briefly, and then NRL. Note again the good agreement between calculated and observed signal levels, including also the refraction correction at the end of the pass.

Pass 156 (Fig. 13):

Only NRL was received on this pass. It is noteworthy because this was the first time that an eclipse of the balloon occurred during a pass,

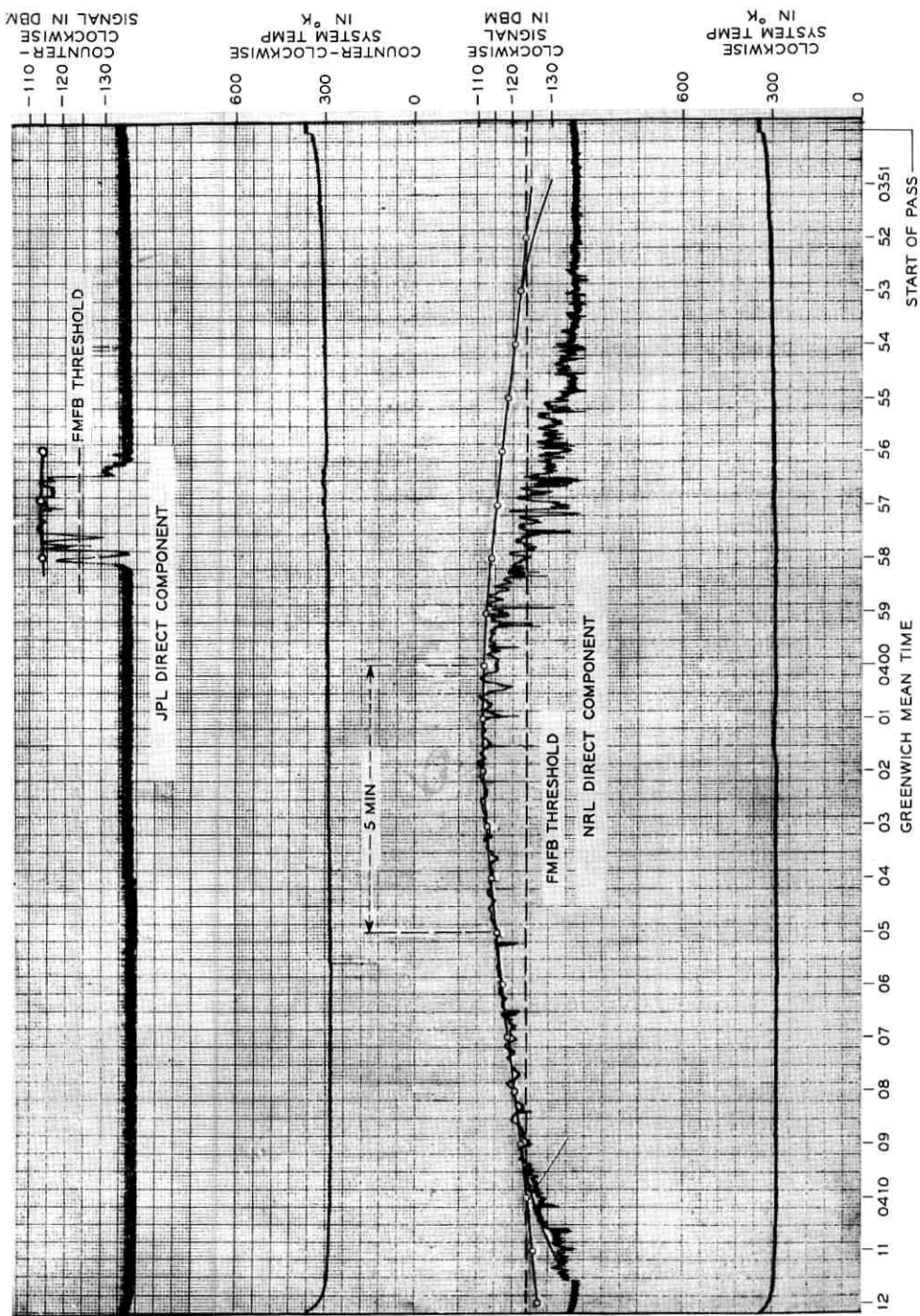


Fig. 12 — Pass 119 — parametric amplifiers (August 22, 1960).

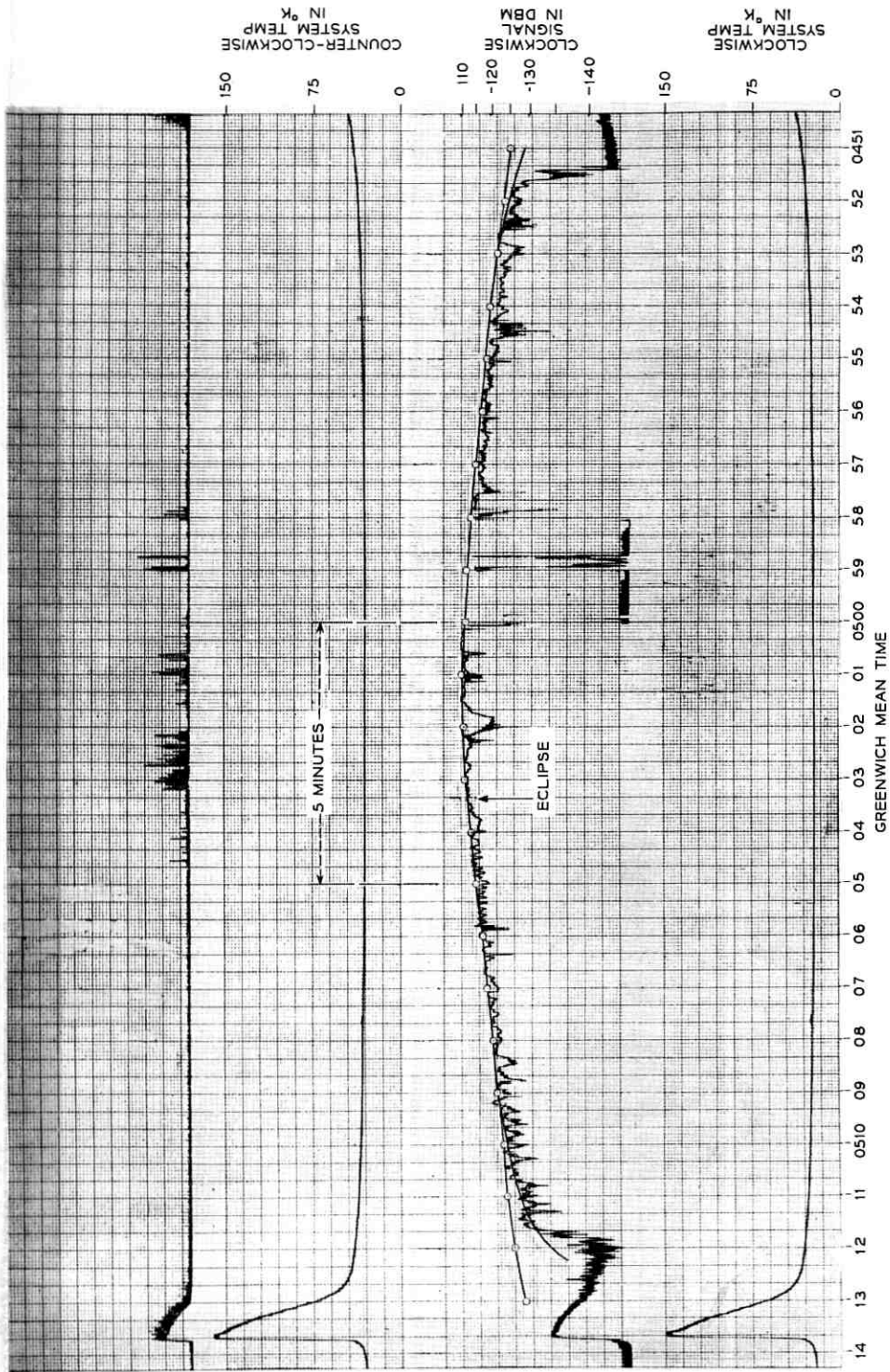


Fig. 13 — Pass 156 — tenth eclipse (August 25, 1960).

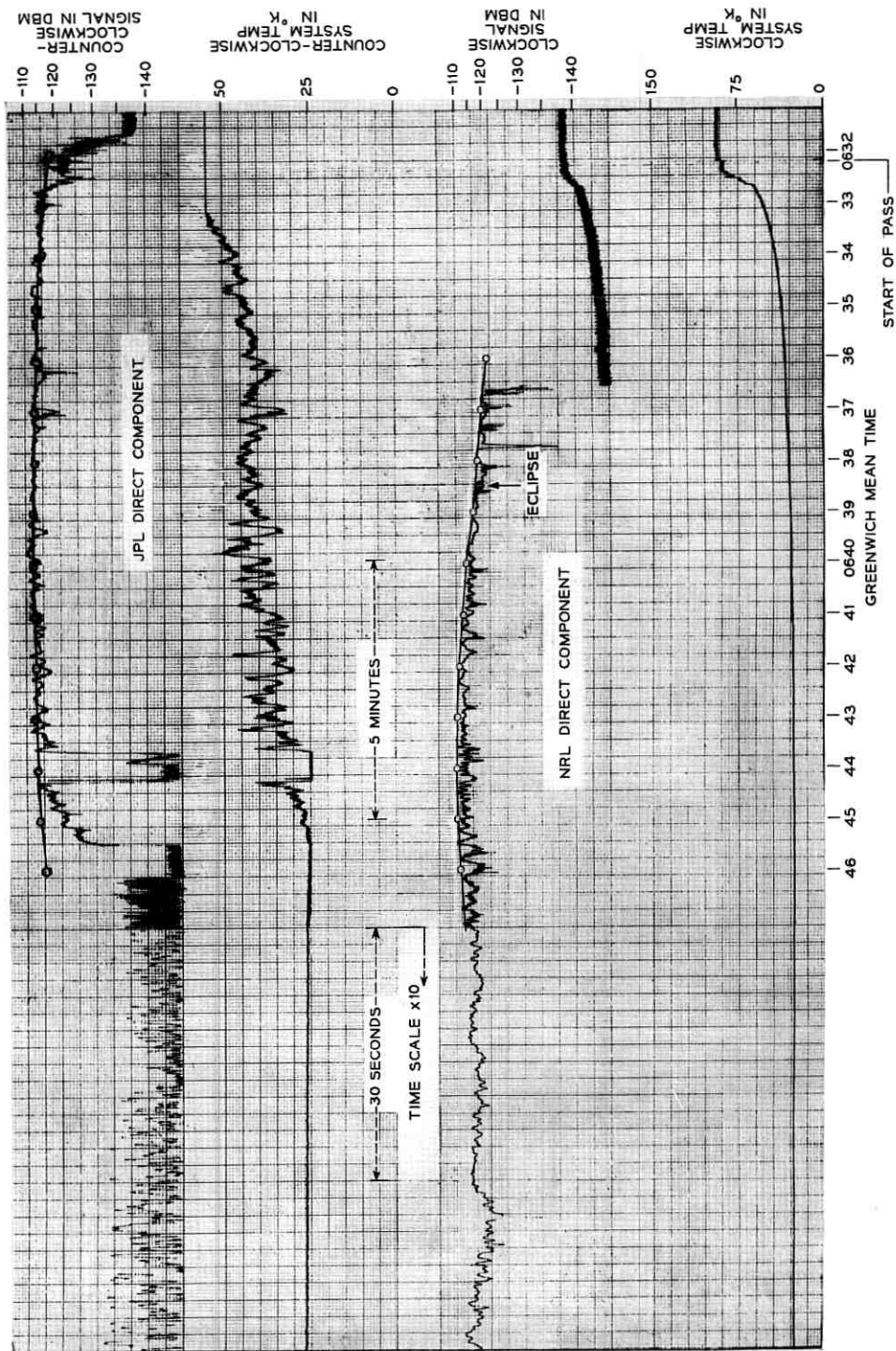


Fig. 14 — Pass 169 — simultaneous reception (August 26, 1960).

as noted at 0503:20 GMT. This was actually the tenth eclipse of the balloon. About 40 seconds later, at 0504, the signal began a strikingly periodic variation of ± 2 db amplitude and 6 seconds period, which disappeared at 0506. This had never been seen before and at the time was attributed to changes in environment associated with the eclipse. These periodic scintillations have since been observed from time to time, but there has not been any observable correlation between their onset and eclipses. Many hypotheses have been advanced to account for them, but as yet no data exist to determine the mechanism.

Comparison of signal level with the calculated curve shows that the average cross section is apparently less than nominal. Occasional signal peaks rise slightly above the theoretical curve. This is significant, and is consistent with a hypothesis of a balloon not fully distended, so that areas of much greater radius of curvature may develop. It should be noted in passing that the balloon was predicted to lose positive gas pressure around this time.

Pass 169 (Fig. 14):

On this pass JPL and NRL were simultaneously received for about eight minutes in an attempt to determine whether the different geometry involved in the transmission paths would have any bearing on the received signal levels. The results are consistent with a balloon that is more or less randomly deformed from its original spherical shape. Note that the JPL signal was in better agreement with the calculated values than was that from NRL, since the satellite eclipsed, and optical tracking could not be maintained by NRL throughout the pass.

Pass 229 (Fig. 15):

The operations on this pass were similar to those on pass 70. The average balloon cross section is still apparently within a few db of theoretical, although the effects of shrinking have become more pronounced, as shown by the increased scintillations of the received signal.

An eclipse occurred at 0450:30 with no observable effect, except that the JPL signal gradually decreased. It was later discovered that JPL lost radar track at 0448 and reverted to the drive tape at that time. The small error in the tape then must have slowly moved the JPL antenna away from the balloon, causing the loss in signal strength.

The cross-polarized signal level from JPL was still no higher than the nominal computed value.

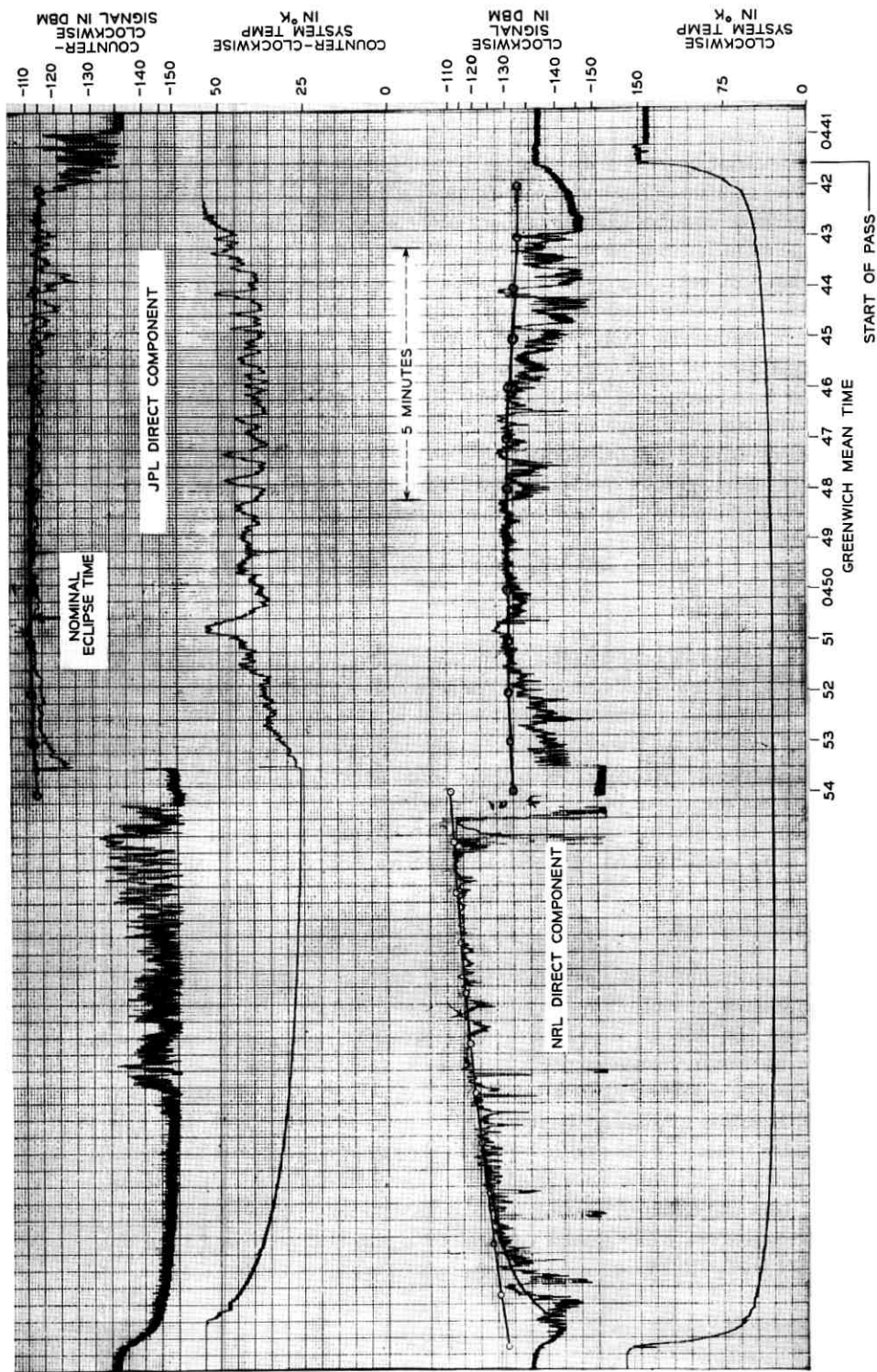


Fig. 15 — Pass 229 — typical scintillations (August 31, 1960).

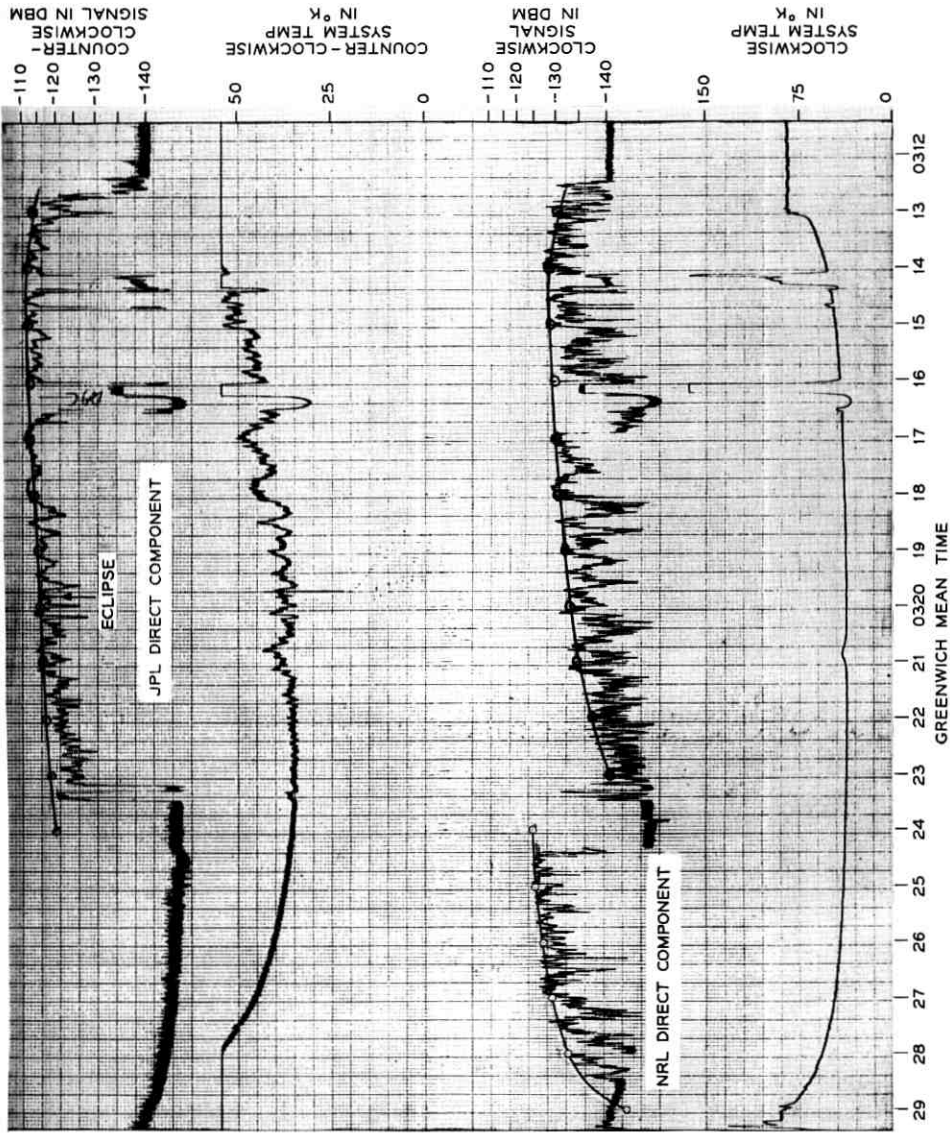


Fig. 16 — Pass 411 — last operation with JPL (September 15, 1960).

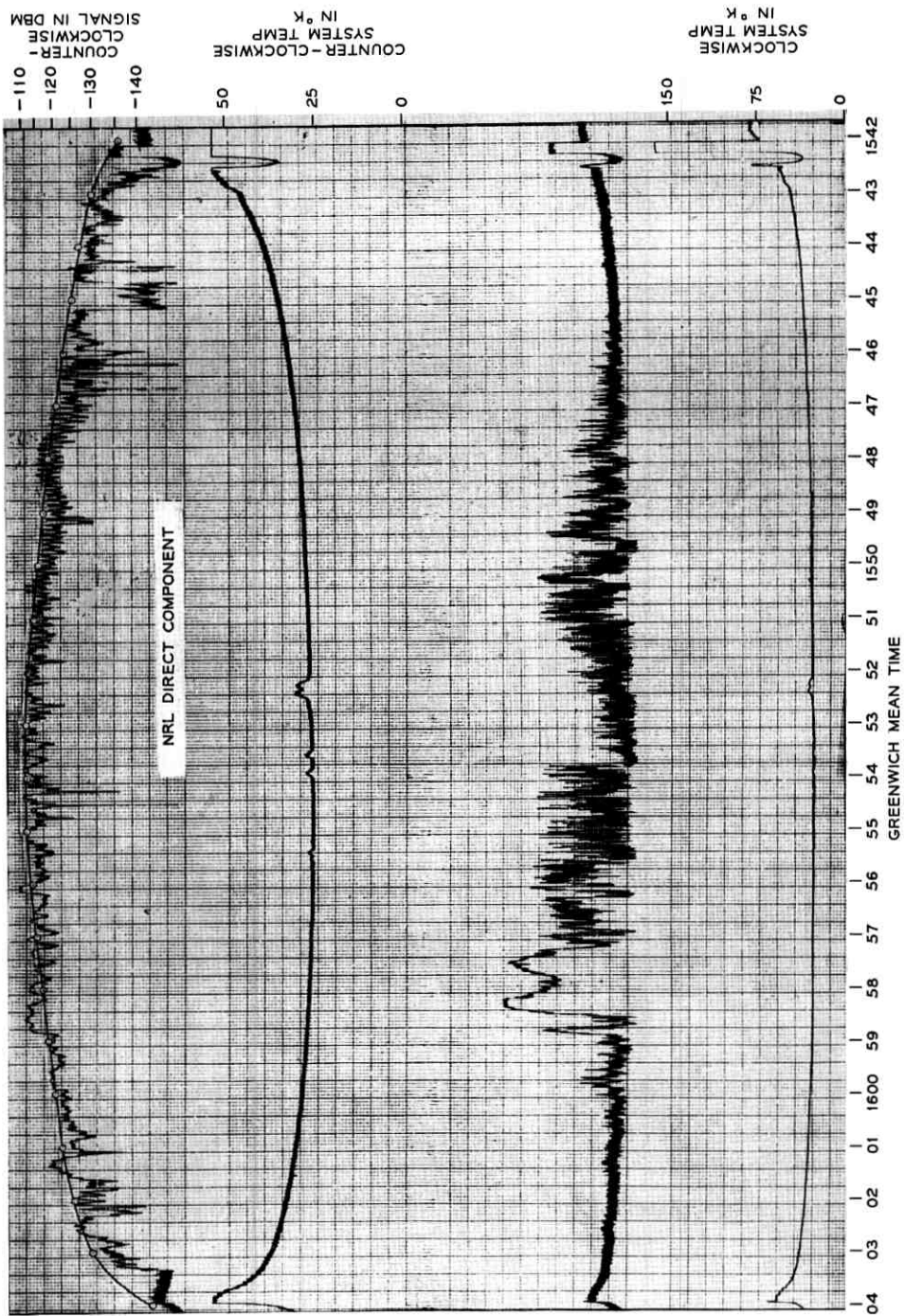


Fig. 17 — Pass 503 — facsimile reception from NRL (September 22, 1960).

Pass 411 (Fig. 16):

This was the last pass during which JPL was received. Note the increased scintillations of both the JPL and NRL signals, and also the apparent loss in average cross section. The cross-polarized component is again close to theoretical, although it is somewhat lower, on the average, than earlier passes.

Pass 503 (Fig. 17):

During this pass NRL signal was switched to the upper record when facsimile transmission was demonstrated from NRL to BTL (see Fig. 6) with excellent results. Special care was taken at GSFC with the drive tapes for this event, and optical checks at BTL showed the predictions to be accurate within $\pm 0.1^\circ$. Incidentally, this was one of the first passes during which it was discovered that the balloon could be seen in broad daylight using the M-33 optics. The air was exceptionally clear, however.

In spite of the good tracking at both stations, the signals still showed appreciable scintillations, and especially noteworthy are the strikingly periodic variations from 1546 to 1551 GMT. Also significant is the fact that the signal exceeded the theoretical value many times, sometimes by as much as 5 db. The only explanation for this that has been advanced requires the balloon surface to have one or more large flat areas.

The several small humps in the two system temperature records between 1552 and 1556 GMT were probably due to the side lobes of the horn looking at the sun.

Pass 674 (Fig. 18):

This is another example of the periodic scintillations observed before. The general character of the signal is very similar to that of pass 503, although the fading range seems to have increased.

Pass 842 (Fig. 19):

It was apparent that the drive tapes for this pass were somewhat in error. The satellite was obscured at NRL, preventing optical tracking, and thus, in an effort to improve the pointing there, NRL was requested to insert small angular offsets from time to time. The rather deep fading that is shown by the graph is probably due more to the tracking difficulties than to effects from the satellite itself.

The balloon was in complete sunlight throughout both pass 674 and

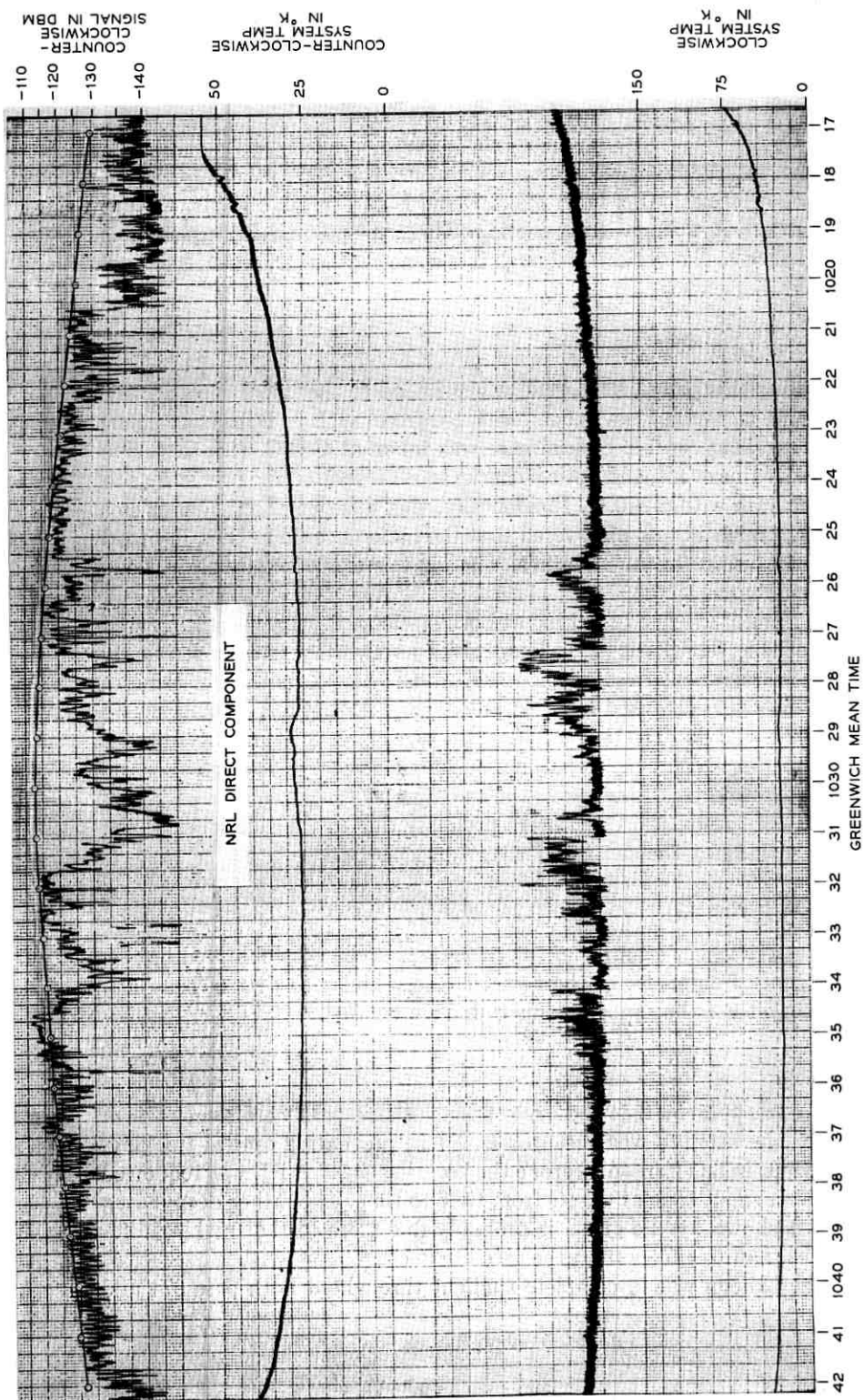
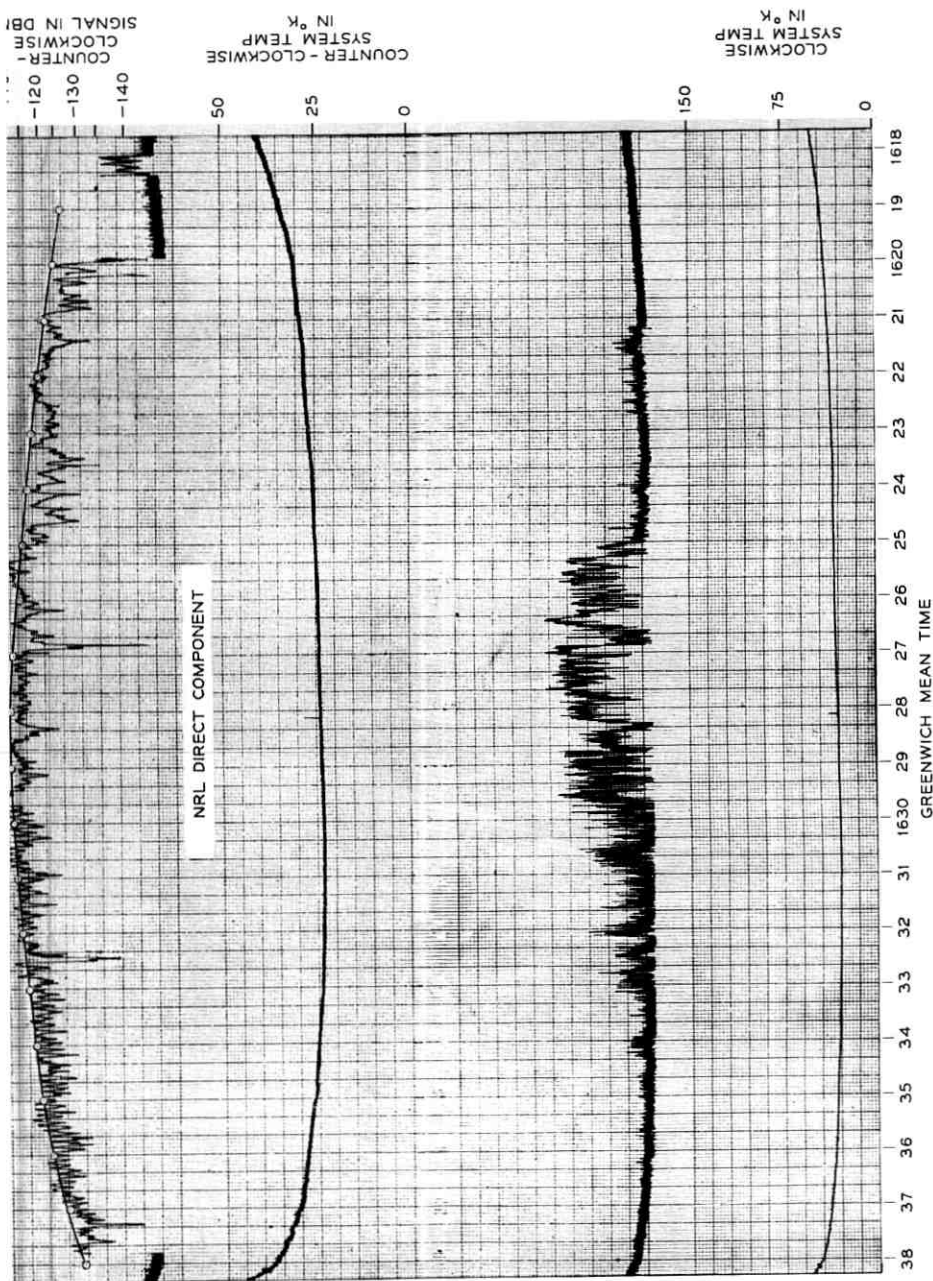


Fig. 18 — Pass 674 — periodic scintillations (October 6, 1960).



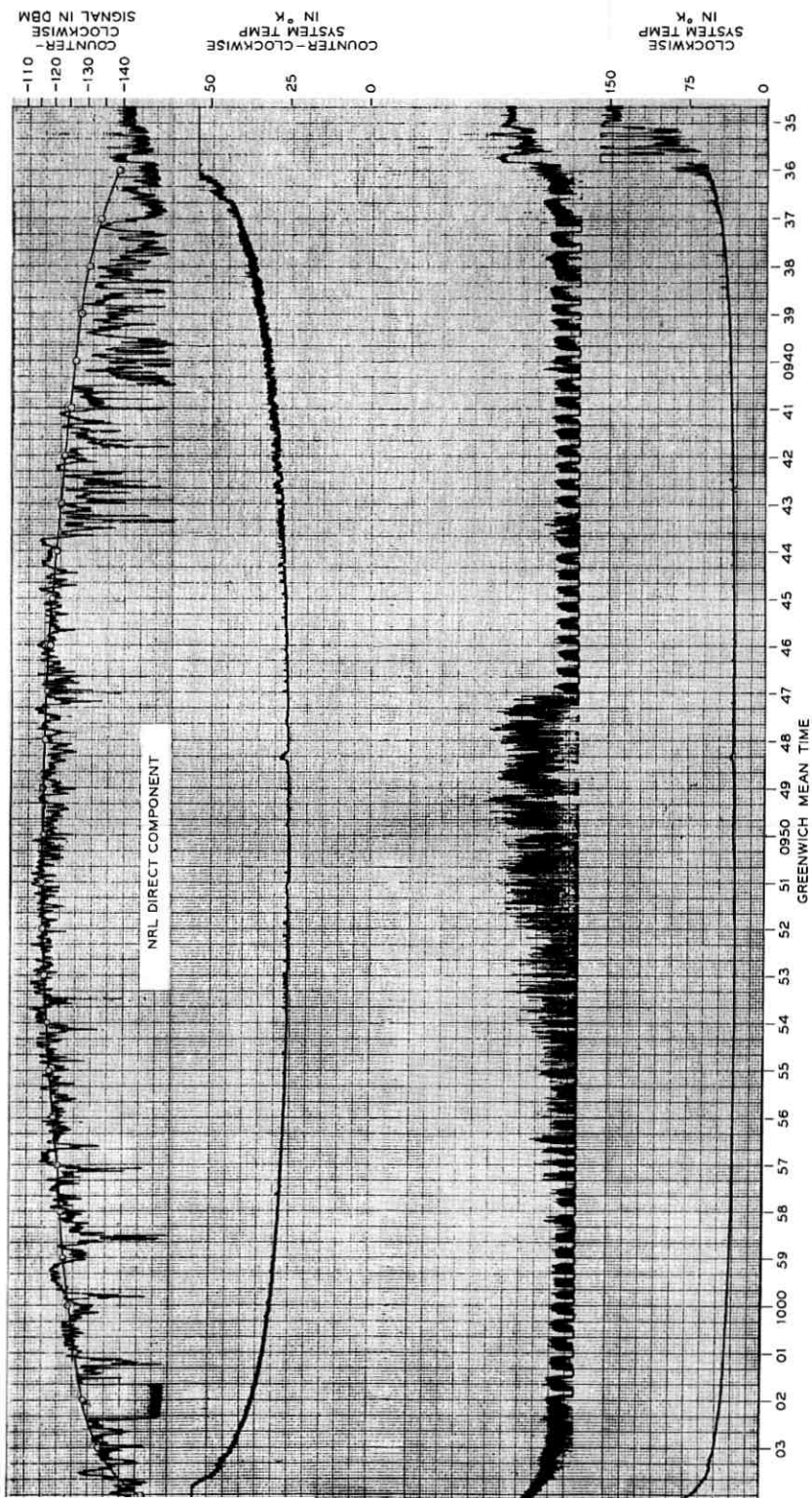


Fig. 20 — Pass 1086 (November 9, 1960).

842, so that again there is no apparent correlation between eclipse and the onset of the periodic scintillations.

Pass 1086 (Fig. 20):

The balloon was in eclipse until 0943:40, when the signal reception from NRL improved immediately, since optical tracking aids could then be employed. Scintillations were still heavy, however, although the general character of the signal was not as bad as on some previous passes.

The odd performance of the cross-polarized signal record was due to BTL equipment troubles in that channel.

Pass 1192 (Fig. 21):

On this pass, BTL and NRL used optical offsets to the drive tape from 0107 to 0116 GMT, at which time the balloon eclipsed and there was virtually no reception from then on. Scintillations were not too severe, and were of a somewhat different periodic nature than before.

3.3.2 *Transmission at 960 mc*

Transmission to JPL was attempted on the first pass of Echo, but results were marginal and no modulation was received. Apparently a combination of bad data points on the drive tape caused the BTL dish to slew off course, and low gain in one of the dish servo control amplifiers resulted in a sluggish return to the track after the bad data point had passed. The low gain evidently developed shortly before the pass, as earlier checks had shown normal performance. The net result was that the dish was in smooth track only at the following times (GMT) for the brief durations indicated, as determined by later comparison of the dish read-out records with the true orbit:

<i>Time of Start</i>	<i>Duration (seconds)</i>
1142:29	15
1145:04	32
1145:44	30
1146:46	126
1150:00	16
1151:40	70

During these periods the BTL dish pointing accuracy was no better than that of the horn, since both were receiving the same angular offsets. The 2390-mc received signal record shows that the average level was down some 8 to 10 db, and approximately the same numbers would then

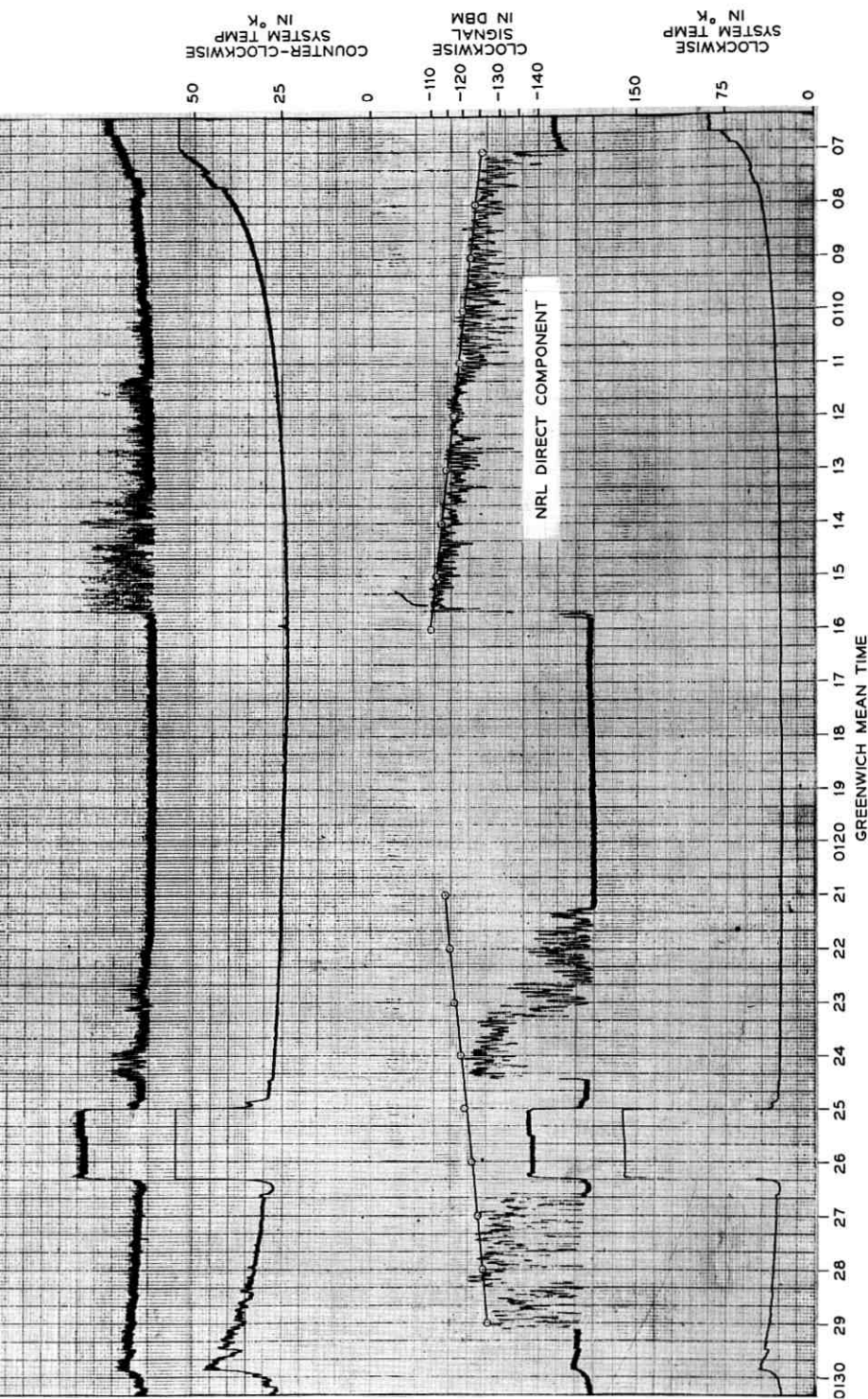


Fig. 21 — Pass 1192 (November 18, 1960).

apply to the dish. This means that the level of the available signal at JPL was probably no better than -123 dbm, which is significantly below the FM threshold, and therefore accounts for the poor results.

Out of 27 remaining passes when successful transmission took place from BTL to JPL at 960 mc, a total of 18 resulted in usable signal recordings at JPL. Fifteen of these have been copied and are shown in Figs. 22 and 23, along with the theoretically computed values. This series of passes covers the first 11 days after launch, and it is quite evident from the steady signals that tracking was generally excellent and the balloon had a fairly smooth surface. As mentioned before, the apparent discrepancy between the observed and calculated levels of signal strength may have been caused by the uncertainties in receiver calibration and antenna gain.

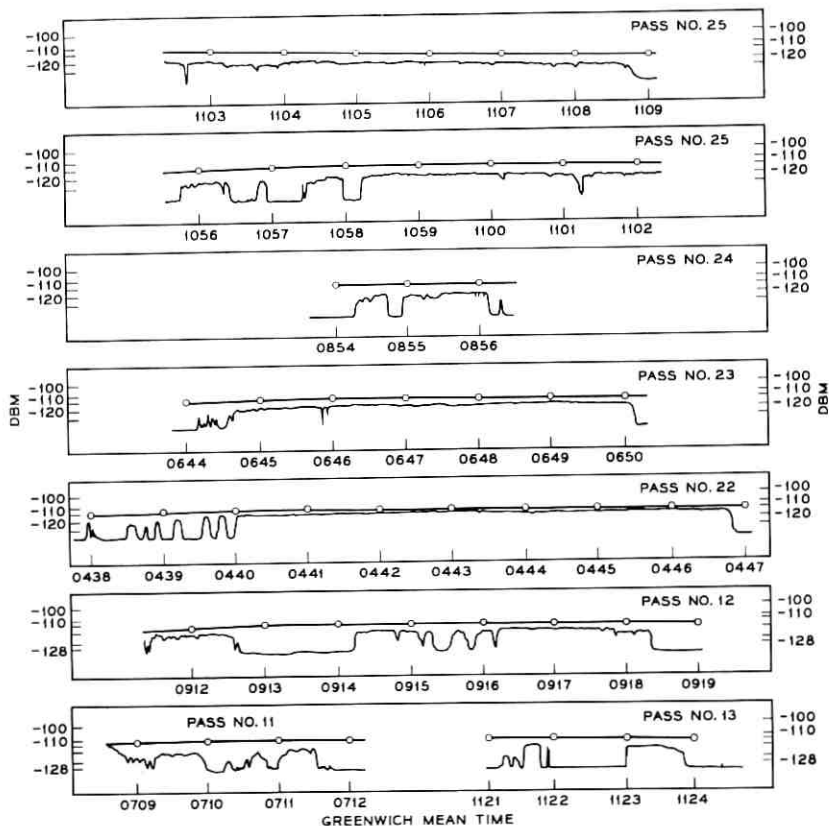


Fig. 22 — Variation of power received by JPL for various passes at 960 mc.

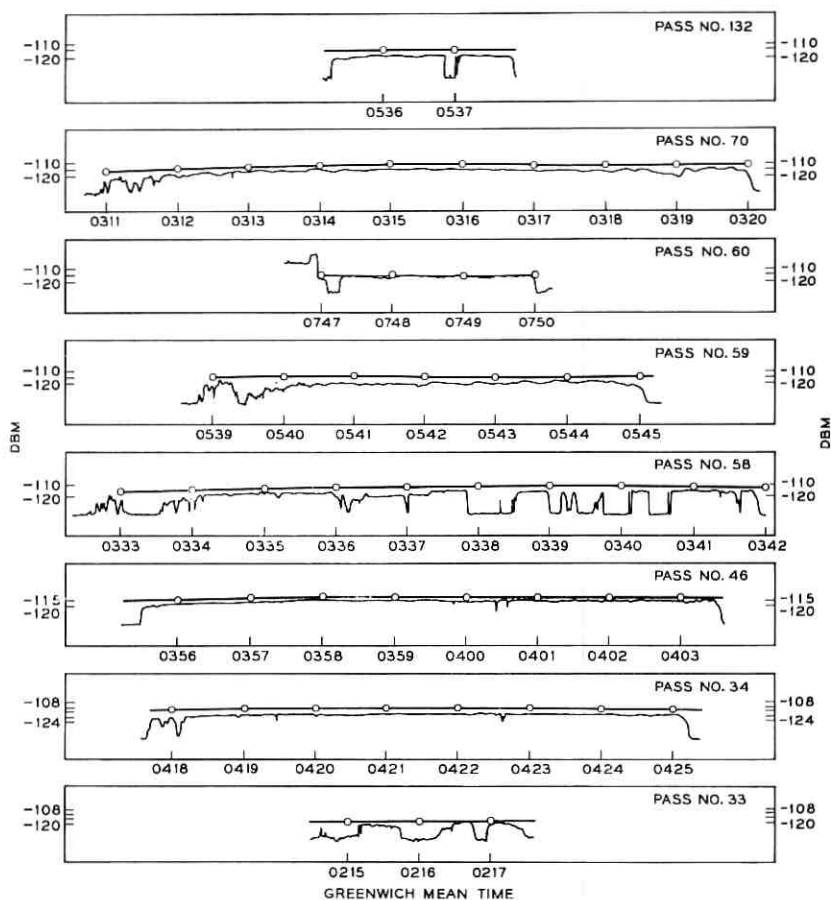


Fig. 23 — Variation of power received by JPL for various passes at 960 mc.

Note the dip in level of 0319 GMT on pass 70; this corresponds to the dip noticed at the same time on the 2390 mc records.

3.3.3 Doppler Shift

The variation of received frequency with time observed on a few selected passes has been plotted in Figs. 24 and 25, together with the computed curves. These were all taken at 2390 mc, where the Doppler shift is given by

$$\Delta f = -7.97 (v_1 + v_2) \text{ cps,}$$

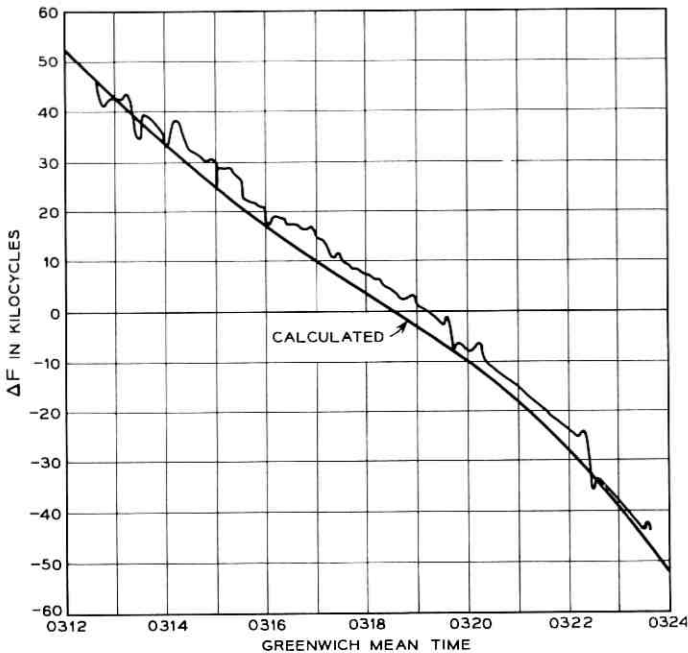


Fig. 24 — Observed Doppler shift on pass 70, JPL to BTL at 2390 mc.

with v_1 and v_2 being the range rates to each station expressed in meters per second. The range rates for these passes were supplied by the GSFC computer.

The agreement between calculated and observed values is fairly good. The average difference is probably due to uncertainty as to the exact frequency of the first beating oscillator in the BTL receiver, nominally 2320 mc; transient differences from the average are generally due to momentary manual adjustments in tuning.

3.4 Scintillations of Received Signals

For all passes worked, an estimate was made of the average signal excursions above and below the median level. The data for each pass were obtained by first drawing in the computed received power and the median signal (estimating an average by eye). Those portions of each pass containing obvious systematic errors, such as transmitter failure or pointing difficulties, were excluded. Then an average curve was drawn through the maximum values of the signal, and the same was done for the minimum values. The difference between each of these two curves

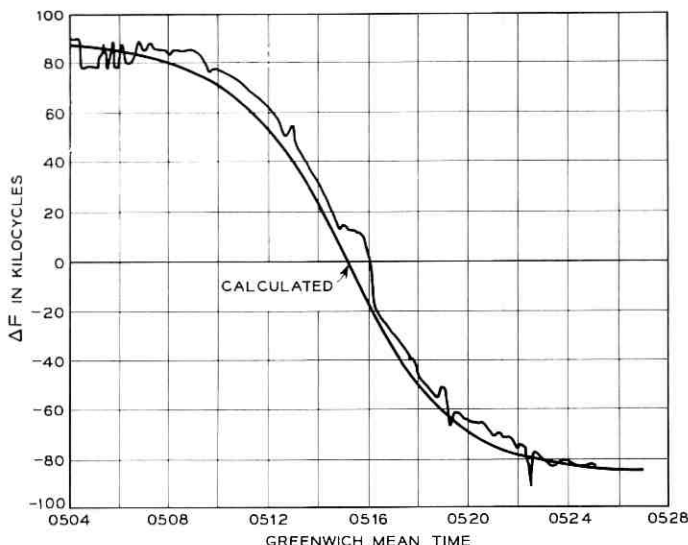


Fig. 25 — Observed Doppler shift on pass 217, NRL to BTL at 2390 mc.

and the median was then recorded. These data were further condensed by plotting only the maximum departures from nominal scattering cross section for all the passes occurring on each day. These plots are shown in Fig. 26, and include results from the JPL and NRL 2390-mc transmissions to BTL, and the BTL 961-mc radar.

Both the JPL and NRL transmissions show about the same scintillation range during the first few days after launching, approximately +2 to -8 db. After 20 days, the scintillations of the NRL signal were somewhat greater than those from JPL. As noted earlier, the scintillations were generally random, except for the occasional occurrence of some having a strongly periodic characteristic of 4 to 8 seconds. These periodic scintillations were observed only on the NRL transmissions.

The BTL radar records show considerably smaller scintillations than those for NRL or JPL, as shown by the plot in Fig. 26. From October 20 to December 20, a total of 14 passes occurred when the radar was in operation and records were available at the same time that a signal was being received from NRL. These records were carefully examined, but very little correlation was found between the fine structure of the scintillations of the two records. According to the radar records, the scintillations did not change appreciably from October 1960 to March 1961.

The occurrence of occasional signal peaks greater than theoretical,

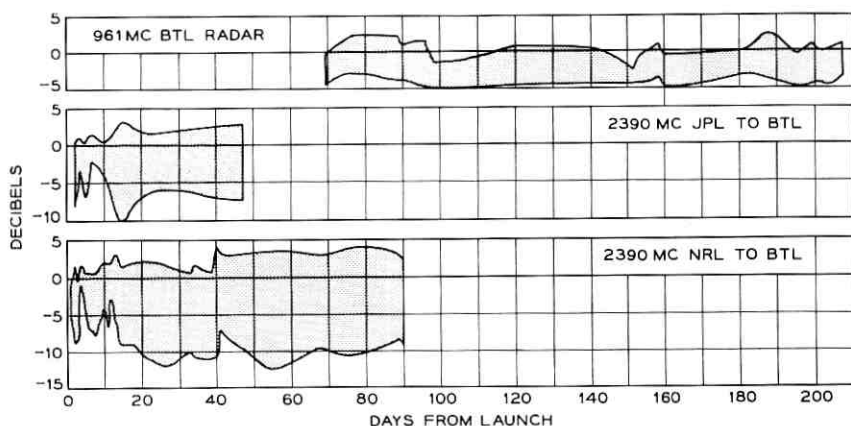


Fig. 26 — Variation of peak-to-peak signal levels with time.

assuming a 100-foot balloon, is consistent with the hypothesis of a slightly distorted balloon surface. There may be one or more flattened areas, any one of which could return more signal than a round balloon. On the other hand, it is possible that several signals reflected from these separate areas could add in phase, thus producing a signal stronger than that possible from an isotropic scatterer. Similarly, these various components could interfere destructively, and it is probably this mechanism that produces an occasional deep fade in the signal.

It should be noted in passing that, although direct transmission between NRL and BTL has been observed by means of tropospheric scattering, such transmission could not interfere with reception during a satellite pass since the frequencies are considerably different due to the appreciable Doppler shift.

Greater scintillations were observed on all passes for low satellite elevations, regardless of whether operation was with NRL, JPL, or the BTL radar. These can be explained to some extent by operational effects, such as difficulty in acquiring and tracking the balloon at long range, but it is also possible that anomalous propagation through the earth's atmosphere contributed to the fading. This effect has been experienced by others, and has been found to be quite severe, on occasion, for elevation angles below about 10° .

3.5 FM with Feedback Performance

On August 16 a series of tests was made on one of the FM demodulators at BTL while signals were being received at 2390 mc. The noise

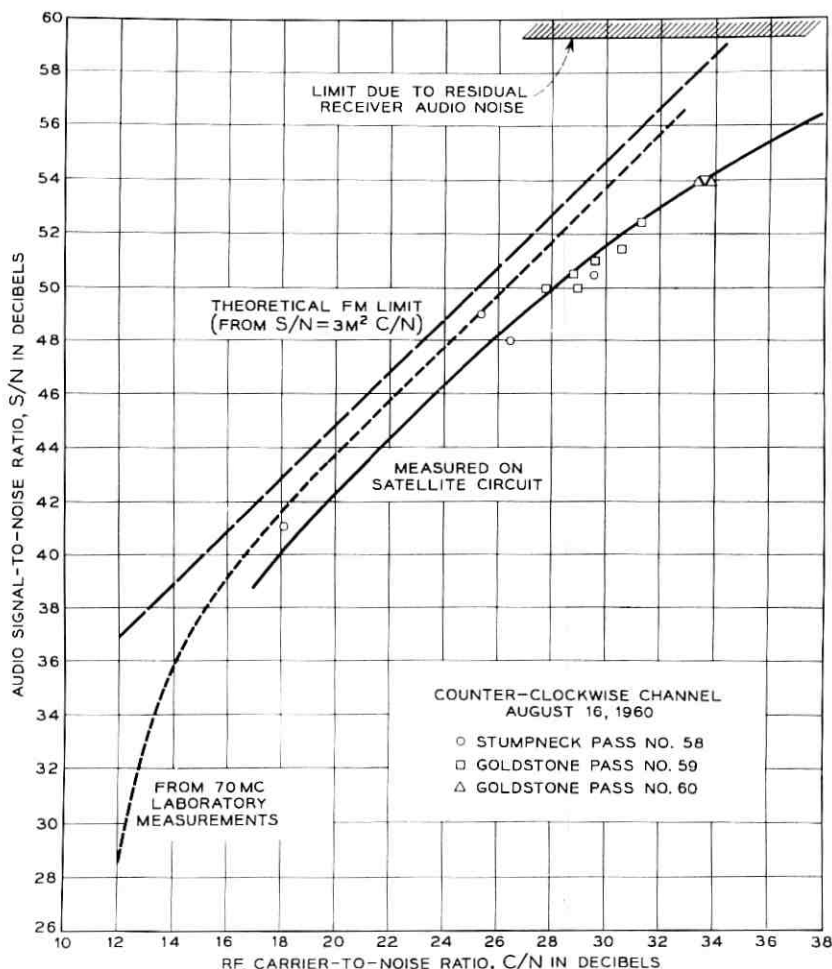


Fig. 27 — Measurements of FM with feedback.

power in the audio baseband, as a function of the input power and feedback factor, was determined using a Western Electric 2B noise measuring set. The results are shown in Fig. 27, together with the results of similar measurements made in the laboratory on another receiver of this type. The signal was measured above the threshold. Also plotted is the theoretical value based on simple FM theory, which holds above the threshold:

$$S/N = 3m^2(C/N),$$

where

S/N = rms signal-to-noise ratio in audio band,
 C/N = carrier-to-noise power ratio measured in a 6-ke bandwidth,
 m = modulation index.

With due regard to measurement difficulties during a pass, good agreement with the simple theory and laboratory measurements was observed.

3.6 *Tracking Performance*

3.6.1 *DAC Operation and Orbit Predictions*

The digital-to-analog converter (DAC) proved to be very reliable, and has required only minor repairs and adjustments since installation early in 1960. Occasional errors in pointing while it was slaved to the drive tape were usually due to errors in the tape itself arising from such causes as faulty operation of tape perforators, transmission anomalies in the TWX circuit between Holmdel and Washington, or a misplaced card in the deck used to generate the tape at the GSFC computer. The parity error-checking circuit in the DAC logic prevented about 90 per cent of these errors from appearing in the output positioning signals.

During each pass of the satellite an effort was made to assess the prediction accuracy of the drive tapes by a rough appraisal of the angular offsets* required to track the balloon. The results show that, on the average, the tapes from GSFC progressively deteriorated with time, with errors increasing from about 0.2° in August 1960, to about 1° in December 1960. Occasional tapes were much better — pass 503 on September 22 being a notable example with 0.1° errors — and a few were much worse. Several factors were responsible for these errors:

1. Anomalies in upper air density occurred due to solar activity. This effect became more pronounced as radiation pressure increased the orbit eccentricity, and the balloon traveled through denser air during part of each orbit.
2. The Minitrack beacons on the balloon gradually grew weaker, until the signals were virtually useless for accurate orbit determination by the end of December.
3. On January 1, 1961, the steady increase in eccentricity reversed. This made it difficult to establish the proper values for the time rate of change of the orbital elements. After January 1961, the drive tapes were

* The possibility of manually inserting corrections (offsets) proved to be extremely valuable. Without this feature, it is believed that at least half the passes would have been missed completely, and the rest would have been of doubtful value.

based on orbital elements supplied by the Smithsonian Astrophysical Observatory, as mentioned earlier, and the errors were on the order of 0.2° .

3.6.2 *Optical Tracking*

Operation with optics when the balloon was visible was superior to any other tracking method. The errors could be kept within $\pm 0.05^\circ$ either by complete manual control or inserting angular offsets using a drive tape.

3.6.3 *Radar Tracking*

On occasion, the satellite was visible while the radar was in operation, and these opportunities were seized to make boresight comparisons between optics and radar. The results generally showed that the radar was accurate to the design objective, $\pm 0.1^\circ$.

3.7 *Operation with Other Stations*

During the course of the Echo experiments, occasional tests were carried out with stations other than the principal participants (JPL and NRL).

3.7.1 *Jodrell Bank, England*

Transmissions were attempted to Jodrell Bank on passes 141 and 142, August 24, using AM with voice and music modulation. Reception was reported, but the S/N ratio was very poor, rendering the voice barely intelligible. This was probably due to the following factors:

1. Using AM lost 9 db compared to SSB;
2. Tracking accuracy was marginal at the Jodrell station, since its dish was not designed to track fast-moving satellites and no means were available for correcting the prediction.

3.7.2 *Centre Nationale d'Etudes des Télécommunications, France*

Reception was reported on pass 70, August 18, at 960 mc, using a fixed 10-foot dish and 20 cps bandwidth. On two later passes, 1447 and 1448 on December 8, reception was again reported using a 30-foot dish which tracked the satellite optically. A S/N ratio of 12 db in a very narrow bandwidth was achieved.

3.7.3 *Stanford Research Institute, Scotland*

At the request of NASA and the Stanford Research Institute, transmissions were attempted at 960.05 mc to the 140-foot dish at the Stanford facility in Scotland on passes 118, 119, 130 on August 22, and again during pass 142 on August 24. Weak reception was reported.

3.7.4 *Malvern, England*

Successful transmissions of carrier to Malvern occurred on passes 213, 214, and 215 on August 29 at 960 mc. The receiver used a 20-foot dish and a parametric amplifier with a 5 db noise figure.

3.7.5 *General Electric Laboratories, Schenectady, New York*

BTL transmissions were heard in Schenectady at 960 mc during 11 passes in August. The receiver used a 28-foot paraboloid tracked by predicted orbit and a parametric amplifier with 4 db noise figure. Later on, a number of two-frequency transmissions were made for the purpose of studying the amplitude and phase correlation of the signals, as follows:

<i>Passes</i>	<i>Date</i>	<i>Frequency Separation</i>
1584	12/20/60	10 kc
1874, 1875, 1876	1/12/61	10 kc
1946, 1947	1/18/61	10 kc
1958, 1959	1/19/61	10 kc
2118, 2119	2/1/61	1 mc
2131	2/2/61	1 mc

The analysis of the results is being done by General Electric; a computer is being used to calculate the correlations.

IV. ACKNOWLEDGMENTS

Project Echo could not have succeeded without a high degree of cooperation among the several organizations involved, and in particular the efforts of a great many people at the National Aeronautics and Space Administration, Jet Propulsion Laboratories, Naval Research Laboratories, and Bell Telephone Laboratories deserve recognition in bringing about the results described here.

For Bell Telephone Laboratories, the contributions of many individuals concerned with particular components of the project are acknowledged in the 11 companion papers that follow. Others who were active

in the over-all preparation and operation of the experiment include L. R. Lowry, E. L. Frantsvog, W. E. Legg, R. A. Desmond, G. J. Stiles, and J. N. Hines. The first four named above also carried out the task of data reduction. The project was under the active leadership of J. R. Pierce, R. Kompfner, and C. C. Cutler, whose guidance and continuing interest are gratefully acknowledged.

The operational phases of the project were supported under contract NASW-110 with NASA.

REFERENCES

1. Chaffee, J. G., The Application of Negative Feedback to Frequency-Modulation Systems, *Proc. I.R.E.*, **27**, 1939, p. 317.
2. Ruthroff, C. L., and Jakes, W. C., Jr., this issue, p. 1029.
3. Schafer, J. P., and Brandt, E. A., this issue, p. 1041.
4. Ohm, E. A., this issue, p. 1065.
5. Crawford, A. B., Hogg, D. C., and Hunt, L. E., this issue, p. 1095.
6. DeGrasse, R. W., Hogg, D. C., Ohm, E. A., and Scovil, H. E. D., Ultra-Low-Noise Antenna and Receiver Combination for Satellite or Space Communication, *Proc. Nat. Elect. Conf.*, **15**, 1959, p. 370.
7. DeGrasse, R. W., Kostelnick, J. J., and Scovil, H. E. D., this issue, p. 1117.
8. Kibler, L. U., this issue, p. 1129.
9. Ruthroff, C. L., this issue, p. 1149.
10. Klahn, R., Norton, J. A., and Githens, J. A., this issue, p. 1207.
11. DeLange, O. E., this issue, p. 1157.
12. Uenohara, M., and Seidel, H., this issue, p. 1183.
13. Warthman, K. L., this issue, p. 1227.
14. Hogg, D. C., Effective Antenna Temperatures Due to Oxygen and Water Vapor in the Atmosphere, *J. Appl. Phys.*, **30**, 1959, p. 1417.

PROJECT ECHO

System Calculations

By CLYDE L. RUTHROFF and WILLIAM C. JAKES, JR.

(Manuscript received March 22, 1961)

*This paper describes system calculations made in preparation for the Project Echo communication experiment and their adaptation to the problem of interpreting the results of the experiment.**

I. INTRODUCTION

Many factors, such as power output, frequency, antenna gain, free-space path loss, receiver noise temperature, and method of modulation, influence the performance of a satellite communication system such as the Project Echo experiment. In addition to those mentioned, which are also common to point-to-point microwave systems, three other factors must be considered in the design of satellite communication systems. All three are functions of satellite position in the region of mutual visibility. They are:

- (a) variations in free-space path loss,
- (b) variations in sky noise temperature,
- (c) loss in the earth's atmosphere.

In this paper these system parameters are used to predict the performance of the voice circuits that constitute the Echo communications experiment. The performance is discussed for the case of normal propagation conditions, and does not take into account attenuation due to rainfall or multipath fading. These are statistical occurrences, and are beyond the scope of this paper.

II. FREE-SPACE PATH LOSS FORMULA

Assume a transmitting antenna of actual gain G_1 radiating power of P_T watts. The power density at a distance d_1 will then be

* As discussed elsewhere in this issue, the Project Echo communication experiment was a joint operation of the National Aeronautics and Space Administration, Jet Propulsion Laboratories, Naval Research Laboratory, and Bell Telephone Laboratories.

$$\Phi_1 = G_1 \frac{P_T}{4\pi d_1^2}.$$

The amount of power intercepted by an object of projected area σ will then be

$$P_1 = \Phi_1 \sigma.$$

A sphere, in effect, radiates this energy isotropically; hence the power density a distance d_2 from the sphere will be

$$\Phi_2 = \frac{P_1}{4\pi d_2^2}.$$

The amount of power received by an antenna having effective aperture area A_2 from this field is

$$P_R = \Phi_2 A_2 = \Phi_2 \frac{\lambda^2 G_2}{4\pi},$$

where

$$G_2 = \frac{4\pi A_2}{\lambda^2}.$$

After suitable substitutions the received power is:

$$P_R = G_1 G_2 \frac{\lambda^2 \sigma P_T}{(4\pi)^3 d_1^2 d_2^2}. \quad (1)$$

Rearranging (1) gives the free-space path loss, L :

$$L = \frac{P_T}{P_R} = \frac{(4\pi)^3 d_1^2 d_2^2}{G_1 G_2 \lambda^2 \sigma}. \quad (2)$$

This expression serves to calculate the expected free-space path loss, providing the various parameters can be determined to sufficient accuracy. The path loss is a function of satellite position as indicated by the presence of $d_1^2 d_2^2$ in (2).

III. SYSTEM PARAMETERS

In order to compute the free-space path loss, antenna gains and frequencies of operation are required. These constants are detailed below:

<i>Antenna</i>	<i>Gain, db</i>	<i>Line loss, db</i>	<i>Net gain, db</i>
BTL 2390 mc horn	43.3 ± 0.16	0	43.3 ± 0.16
BTL 960 mc dish	43.1 ± 0.1	0.5	42.6 ± 0.1
BTL 961 mc dish	32.6 ± 0.2	0	32.6 ± 0.2
JPL 2390 mc dish	53.7*	0.4	53.3
JPL 960 mc dish	45.8 ± 0.6	0.2	45.6 ± 0.6
NRL 2390 mc dish	50.2*	1.6*	48.6

* Estimated values, not measured.

IV. FREE-SPACE PATH LOSS COMPUTATIONS

The free-space path loss has been computed for the Echo balloon as a function of position for the two-way path between Goldstone and Holmdel. The balloon scattering cross section, σ , was assumed to be that of a 100-foot-diameter sphere, perfectly conducting and many wavelengths in diameter, so that

$$\sigma = \frac{\pi(100)^2}{4} = 7854 \text{ square feet.}$$

The frequency in the east-west direction was 960 mc; in the west-east direction it was 2390 mc. Equation (2) was used to compute path loss; the results are presented in Figs. 1 and 2. Fig. 1 is a plot of path loss versus satellite altitude when the balloon was midway between the terminals. Fig. 2 shows contours of constant free-space path loss relative to the loss at midpath for a satellite height of 1000 miles and assuming the radius of the earth to be 3950 miles. The contours are in steps of 1 db, and are plotted on a stereographic projection. The inclination of the orbit of Echo I is 47.27° , which limits the northern extent of mutual visibility. The necessary equations for these computations are derived in Appendix A.

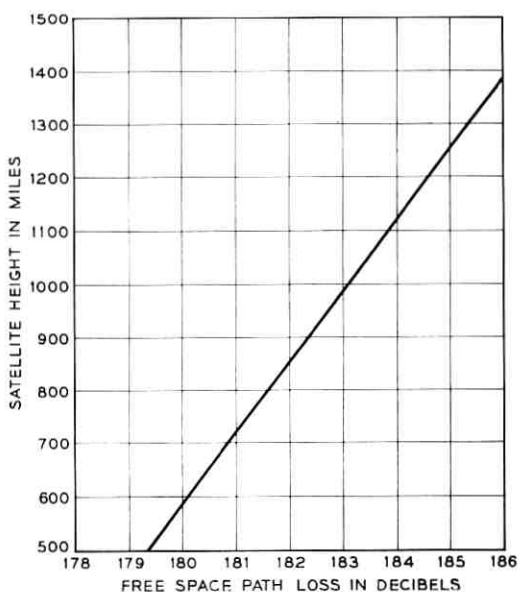


Fig. 1 — Path lost in east-west direction, Holmdel to Goldstone; for west-east direction, subtract 0.5 db.

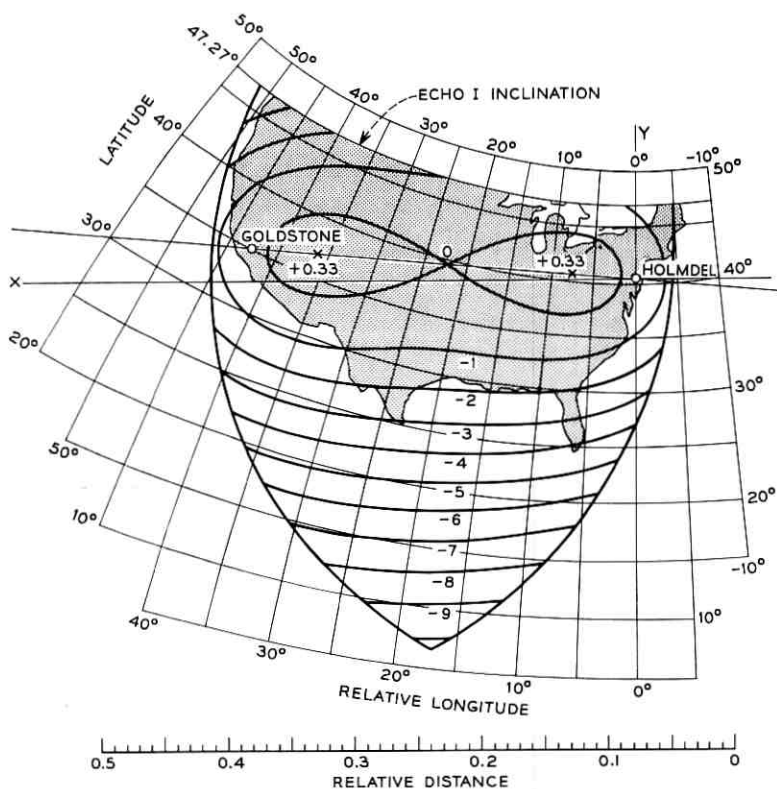


Fig. 2 — Contours of constant free-space path loss, Holmdel to Goldstone.

Stump Neck is only 200 miles from Holmdel, so the path loss from NRL-BTL can be computed as the round-trip loss from either terminal to the balloon. The error in this assumption is less than 0.6 db (Appendix B) for any position in the area of mutual visibility. The contours of constant path loss for this case are circles centered on Holmdel; they are shown in Fig. 3. The path loss at 2390 mc and a satellite altitude of 1000 miles is 178.7 db.

It can be seen from Figs. 2 and 3 that the difference between maximum and minimum path loss on the JPL-BTL path is about 10 db, while for the NRL-BTL path this difference is 19 db. It should also be noted that between NRL and BTL this maximum difference is encountered twice on every pass, while the maximum difference almost never occurs on the JPL-BTL path.

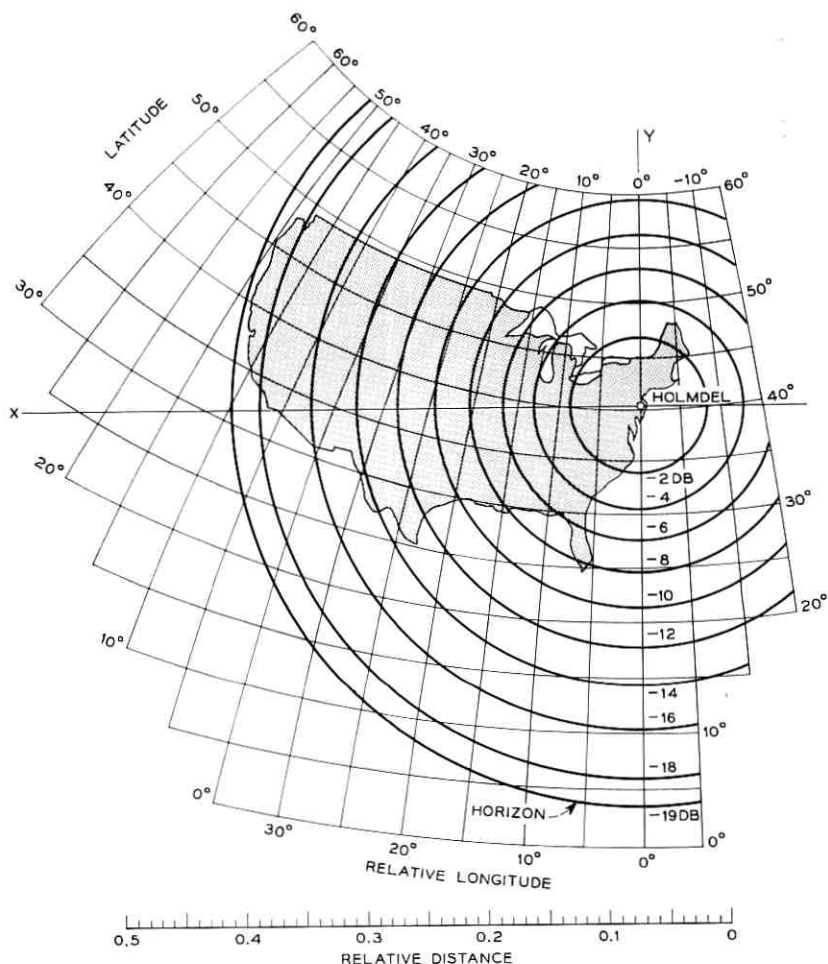


Fig. 3 — Contours of constant free-space path loss, Stump Neck to Holmdel.

V. EXPECTED SIGNAL-TO-NOISE RATIOS IN VOICE CIRCUITS

The signal-to-noise power ratios to be expected depend upon the type of modulation technique that is employed, as well as upon the received carrier-to-noise power ratio. The first step is to compute the carrier-to-noise ratio at the receiver for suitable conditions, and then to discuss the modulation methods and voice band signal-to-noise performance. This has been done for the two-way voice path between JPL and BTL, and

TABLE I — SATELLITE MIDWAY BETWEEN TERMINALS

Parameter	East-to-West	West-to-East
Transmitted power:	+70 dbm (10 kw)	+70 dbm (10 kw)
Frequency:	960.05 mc	2390 mc
Transmitting antenna net gain:	42.6 db	53.3 db
Receiving antenna net gain:	45.6 db	43.3 db
Free-space path loss:	183.1 db	182.6 db
Loss through atmosphere:	0 db	0 db
Received carrier power:	-113.1 dbm	-112.6 dbm
Receiver system noise temperature:	350° K	25° K
Receiver noise power in 6-ke band:	-135.4 dbm	-146.8 dbm
Carrier-to-noise ratio at receiver (C/N):	22.3 db	34.2 db

the results are tabulated in Table I. The satellite is assumed to be midway between the terminals.

For other positions of the balloon in the region of mutual visibility, the C/N ratio is modified by three effects:

- (a) variations in free-space path loss;
- (b) variations in sky noise temperature;
- (c) loss in the earth's atmosphere.

The first item has been discussed in Section IV, and the correction for position can be made for any satellite position from Fig. 2. The remaining two items have been discussed by Hogg¹ and by DeGrasse, Hogg, Ohm, and Scovil.² For example, the sky noise temperature and atmospheric loss can be calculated when the antennas are pointed at the horizon. The loss through the atmosphere and system noise temperature are then 3.2 db and 435°K for the east-west circuit, and 4.2 db and 110°K for the west-east circuit. This would be the worst case. For elevation angles above 10°, however, these effects are essentially negligible.

The audio signal-to-noise ratio depends to a considerable extent on the modulation technique. Three techniques, single-sideband (SSB), FM, and FM with feedback (FMFB), are considered here. The transmitters are assumed to be peak-power-limited and the audio signal to be the maximum rms sine wave obtainable. The audio bandwidth is 3 kc, and the noise bandwidth is assumed to be 6 kc.

5.1 Single-Sideband (SSB)

The maximum transmitted rms sine wave power is 3 db less than the transmitter peak, C . However, for SSB the noise bandwidth may be reduced to 3 kc, resulting in an audio signal-to-noise ratio of

$$S/N = C/N.$$

5.2 Frequency Modulation (FM)

The audio signal-to-noise ratio for this case is given by the standard FM formula, which applies when the receiver input is above the threshold:

$$S/N = 3M^2C/N,$$

where M is the index of modulation.

The index for the Echo experiment was 10, so when the receiver is operated above the threshold the signal-to-noise ratio is 25 db better than that of SSB. However, the threshold for this receiver occurs at a C/N of approximately 22 db, because the noise bandwidth required to accommodate this signal is about 66 kc.

5.3 Frequency Modulation with Feedback (FMFB)

The audio signal-to-noise ratio for this receiver is the same as that for FM when the C/N is above the threshold. However, this receiver has a threshold near $C/N = 13$ db.³ At any C/N equal to or greater than 13 db, the audio S/N exceeds that of SSB by 25 db.

When the balloon is midway between the terminals the expected S/N , based on the formulae above, would be as follows:

	<i>Audio S/N for SSB</i>	<i>Audio S/N for FM, FMFB</i>
East-to-west:	22.3 db	47.3 db
West-to-east:	34.2 db	59.2 db (57 db measured*)

The same general comments apply to the NRL-BTL circuit; the path loss being modified according to the free-space path loss differences shown in Fig. 3 and the difference in free-space path loss when the balloon is directly above the terminals. When the balloon is directly overhead the audio S/N would be

	<i>Audio S/N for SSB</i>	<i>Audio S/N for FM, FMFB</i>
NRL-BTL	38.6 db	63.6 db (>57 db measured*)

VI. RECEIVED SIGNAL STRENGTH USING ORBITAL PARAMETERS

The foregoing material was based on the assumption that the satellite orbit was circular and the altitude was 1000 miles. After the experiment was underway it was necessary to compute the loss for the known posi-

* The maximum S/N obtainable in this receiver is limited by the audio amplifier noise. This begins to be significant at a S/N of about 50 db and accounts for the difference between the computed and measured signal-to-noise ratios.

tion of the balloon in order to compare the measured and theoretical received signal amplitudes.

For this purpose a program was written for the IBM 7090 computer for calculation of a path-loss parameter, L , for two given stations using Echo I at the same time:

$$L(t) = 10 \log \left[(4\pi)^3 \frac{d_1^2(t)d_2^2(t)}{\lambda^2\sigma} \right],$$

where t refers to time. The inputs to this program are the orbital elements, station coordinates, frequency, and balloon cross section. The received power in decibels is then:

$$(P_R)_{db} = 10 \log (G_1 G_2 P_T) - L(t).$$

To save computer time, $L(t)$ was only calculated for one frequency, 2390 mc, since the values only differed by a constant from those of another frequency. Calling this value $L_0(t)$, and using the antenna gains from the table, the following expressions for received power in dbm were derived:

BTL to JPL at 960 mc:	$P_R = 166.1 - L_0 \pm 0.7,$
JPL to BTL at 2390 mc:	$P_R = 166.6 - L_0,$
NRL to BTL at 2390 mc:	$P_R = 162.9 - L_0,$
BTL to BTL at 961 mc:	$P_R = -122.0 - 40 \log d.$

The last line refers to the BTL radar, and the slant range d is in kilometers. These numbers must be corrected by any variation in transmitted power from 10 kw.

APPENDIX A

The variation in free-space path loss as a function of the position of the satellite in the region of mutual visibility can be understood by examining the behavior of $d_1^2 d_2^2$ in (2).

The geometry is shown in Fig. 4. The distances from the satellite to terminals H and G are d_1 and d_2 respectively. The path loss is proportional to $d_1^2 d_2^2$. Using the law of cosines,

$$\begin{aligned} d_1^2 &= R^2 + (R + h)^2 - 2R(R + h) \cos \alpha = A - B \cos \alpha, \\ d_2^2 &= R^2 + (R + h)^2 - 2R(R + h) \cos \gamma = A - B \cos \gamma, \end{aligned} \quad (3)$$

where $\cos \gamma = \cos \varphi \sin \alpha \sin \beta + \cos \alpha \cos \beta$.

Now let $M = B/A$ and normalize to A :

$$\frac{d_1^2 d_2^2}{A^2} = (1 - M \cos \alpha)(1 - M \cos \varphi \sin \alpha \sin \beta - M \cos \alpha \cos \beta). \quad (4)$$

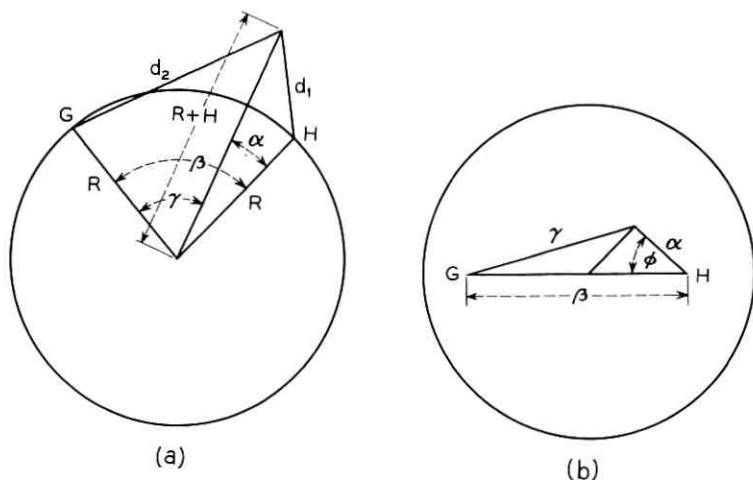


Fig. 4 — Satellite geometry for path-loss calculations.

Solving for $\cos \varphi$ results in

$$\cos \varphi = \frac{(1 - M \cos \alpha)(1 - M \cos \alpha \cos \beta) - \left(\frac{d_1^2 d_2^2}{A^2}\right)}{M(1 - M \cos \alpha)(\sin \alpha \sin \beta)}, \quad (5)$$

with

$$M = \frac{2R(R + h)}{R^2 + (R + h)^2},$$

β = central angle between terminals H, G,

$\frac{d_1^2 d_2^2}{A^2}$ = normalized path-loss parameter.

We are interested only in points which do not fall below the horizon. Thus, α has a maximum determined by

$$\cos \alpha_{\max} = \frac{R}{R + h}. \quad (6)$$

The normalized path-loss parameter when the satellite is midway between the terminals is found by noting that $\varphi = 0$ and $\alpha = \gamma = \beta/2$. Thus

$$\left(\frac{d_1^2 d_2^2}{A^2}\right)_0 = (1 - M \cos \beta/2)^2. \quad (7)$$

The maximum value of this parameter occurs when the satellite ap-

pears on the horizon to both terminals. For this case, $\gamma = \alpha_{\max}$ and

$$\left(\frac{d_1^2 d_2^2}{A^2}\right)_{\max} = \left(1 - \frac{MR}{R+h}\right)^2. \quad (8)$$

When the satellite is at midpath for an altitude of 1000 miles the values of these parameters are as follows:

$$\begin{aligned} R &= 3950 \text{ miles,} \\ \alpha &= \beta/2 = 16.89^\circ, \\ A &= 4.01 \times 10^7 \text{ miles}^2, \\ B &= 3.91 \times 10^7 \text{ miles}^2, \\ M &= 0.975, \\ d_1^2 d_2^2 &= 7.2 \times 10^{12} \text{ miles}^4. \end{aligned}$$

A program has been prepared for the IBM 704 computer using expressions (5) through (8), and the path-loss contours of Figs. 2 and 3 were plotted from these data. Negative signs indicate increasing loss.

The points of minimum path loss are found by setting $\varphi = 0$ in (4) and differentiating with respect to α :

$$\begin{aligned} \frac{d}{d\alpha} \left(\frac{d_1^2 d_2^2}{A^2}\right) &= M \sin \alpha [1 - M \cos(\beta - \alpha)] \\ &\quad - (1 - M \cos \alpha) M \sin(\beta - \alpha). \end{aligned} \quad (9)$$

The desired points will be solutions of the equation obtained by setting (9) equal to zero; $\alpha = \beta/2$ is a solution, but it is not necessarily a point of minimum loss. By the usual tests we have the following: the midpath point is a maximum loss point if $\cos \beta/2 - M$ is negative. Conversely, if $\cos \beta/2 - M$ is positive, the midpath is a minimum loss point.

APPENDIX B

When the terminals are close together, as are Stump Neck and Holmdel, their central angle β is small, and the path-loss computations are simplified, because $d_1^2 d_2^2 \approx d_1^4$. The purpose of this appendix is to derive the maximum error incurred by using this approximation. From (3),

$$d_2^2 = d_1^2 + 2R(R+h)(\cos \alpha - \cos \gamma), \quad (10)$$

where $\cos \gamma = \cos \varphi \sin \alpha \sin \beta + \cos \alpha \cos \beta$.

Substituting for $\cos \gamma$ in (10) results in

$$d_2^2 = d_1^2 + 2R(R+h)[\cos \alpha (1 - \cos \beta) - \cos \varphi \sin \alpha \sin \beta]. \quad (11)$$

If $\beta \ll \pi/2$, this reduces to

$$d_2^2 = d_1^2 - 2R(R + h)\beta \sin \alpha \cos \varphi. \quad (12)$$

The ratio of the two sides of the approximation is

$$\frac{d_1^2 d_2^2}{d_1^4} = \frac{d_2^2}{d_1^2} = 1 - \frac{2\beta R(R + h) \cos \varphi \sin \alpha}{R^2 + (R + h)^2 - 2R(R + h) \cos \alpha}. \quad (13)$$

The path-loss error in decibels is given by $10 \log$ [equation (13)]. The error will be maximum when $\cos \varphi = \pm 1$ and $\alpha = \alpha_{\max}$. Assuming that $R = 3950$ miles, $h = 1000$ miles, and $\cos \varphi = -1$, then $\alpha_{\max} = 37.1^\circ$, and

$$\frac{d_2^2}{d_1^2} = 1 + 2.65\beta, \quad \beta \ll \pi/2. \quad (14)$$

For the NRL-BTL path, $\beta \approx 200/3950 = 0.0506$ radian, and $d_2^2/d_1^2 = 1.134$. The maximum error is $10 \log 1.134 = 0.546$ db.

REFERENCES

1. Hogg, D. C., Effective Antenna Temperatures Due to Oxygen and Water Vapor in the Atmosphere, *J. Appl. Phys.*, **30**, 1959, p. 1417.
2. DeGrasse, R. W., Hogg, D. C., Ohm, E. A., and Scovil, H. E. D., Ultra-Low-Noise Antenna and Receiver Combination for Satellite or Space Communication, *Proc. Nat. Elect. Conf.*, **15**, 1959, p. 370.
3. Ruthroff, C. L., FM Demodulators with Negative Feedback, this issue, p. 1149.

PROJECT ECHO

960-mc, 10-kw Transmitter

By J. P. SCHAFER and R. H. BRANDT

(Manuscript received April 6, 1961)

The 10-kw transmitter operating at 960 to 961 mc which was used at the eastern terminus of Project Echo is described. This transmitter is located on Crawford Hill near Holmdel, New Jersey. The 10-kw output feeds into a waveguide line leading to a 60-foot dish antenna. Exciter-driver units are available to drive the power amplifier with various modulations, such as wide-deviation FM, low-index phase modulation, single-sideband or double-sideband modulation with or without carrier, 960.05 or 961.05 mc constant-frequency cw and radar on-off pulses at 961.05 mc. The main output amplifier consists primarily of a four-stage, externally-tuned-cavity, water-cooled klystron operating at a beam voltage of 16 to 18 kv.

The transmitter has been operated during many Moonbounce, tropospheric scatter, and Echo I tests with very satisfactory results.

I. GENERAL INTRODUCTION

This paper describes the 960 mc, 10-kw output radio transmitter used in Project Echo.* The main transmitter unit and its input stage driver unit are standard commercial equipments supplied by the Federal Telecommunication Laboratory.† These units were selected from a number of those available, since they came closest to our particular requirements for wideband FM transmission.

These general requirements were that the transmitter could (a) deliver 10 kw of RF power into a 50-ohm load at a frequency of about 960 ± 2 mc; (b) be frequency-modulated over the audio frequency band with deviations of ± 200 to 300 kc; and (c) be used with other types of modulation such as single-sideband (SSB), double-sideband (DSB), interrup-

* Although this equipment was designed by the Bell System as part of its research and development program, it was operated in connection with Project Echo under Contract NASW-110 for the National Aeronautics and Space Administration.

† Division of International Telephone and Telegraph Corporation.

ted continuous wave (ICW), etc. The transmitter has performed satisfactorily for all required tests.

The main radio amplifier consists of a four-stage klystron (Eimac 4K-50,000 LQ) having external tunable cavities and operates at beam voltages of 16 to 18 kv. The necessary power supplies, cooling system, and control units are also incorporated as part of the transmitter.

The driving stage amplifier is capable of delivering up to 10 watts, but for normal 10-kw klystron output less than one-half watt is required; i.e., the klystron has a power gain of 40 to 50 db.

The modulating units have an output of about one watt at a frequency of 70 mc and feed into a mixer which is also driven by an 890.05-mc cw signal of the proper level. This latter frequency originates in a crystal controlled oscillator at 49+ mc and is stepped up to the desired value by an 18-times frequency multiplier. The final output frequency is the sum of the 890.05 and the 70-mc modulated frequencies, or 960.05 mc.

The transmitter with all the necessary controls, power supplies, cooling system, driver units, measuring equipment, and recorders is housed in a metal building that has 16 by 26 feet of floor space and a 10-foot ceiling. This building is located at the base of the 60-foot-diameter Kennedy dish antenna (see Fig. 1). A control panel for manual operation and orientation of the dish antenna is also included in this building.

II. THE POWER AMPLIFIER

The 10-kw power amplifier, as previously mentioned, consists primarily of the water- and air-cooled klystron. With its control circuits and power supplies it is contained in a three-compartment metal cabinet 152 inches long, 37 inches deep, and 85 inches tall. The heat exchanger, used for klystron cooling, is about the same height and depth and is 56 inches long; this is placed along the rear wall of the building and not in line with the transmitter proper. Figs. 2 and 3 show the general arrangement of equipment.

A liquid-cooled dummy load consisting of a 6-foot length of $3\frac{1}{8}$ -inch 50-ohm coaxial line is provided for output power calibration and measurement. The RF power is dissipated directly in the coolant liquid, and by calorimetric measurement of temperature rise and flow rate, the power may be calculated. The coolant liquid used is a 50 per cent water and ethylene-glycol mixture for protection from freezing when the transmitter is not in use. The same coolant liquid and heat exchanger is used for both the dummy load and klystron closed circulation system.

The power amplifier output terminates in a $3\frac{1}{8}$ -inch coaxial line, coupled to the fourth-stage cavity of the klystron. The klystron output

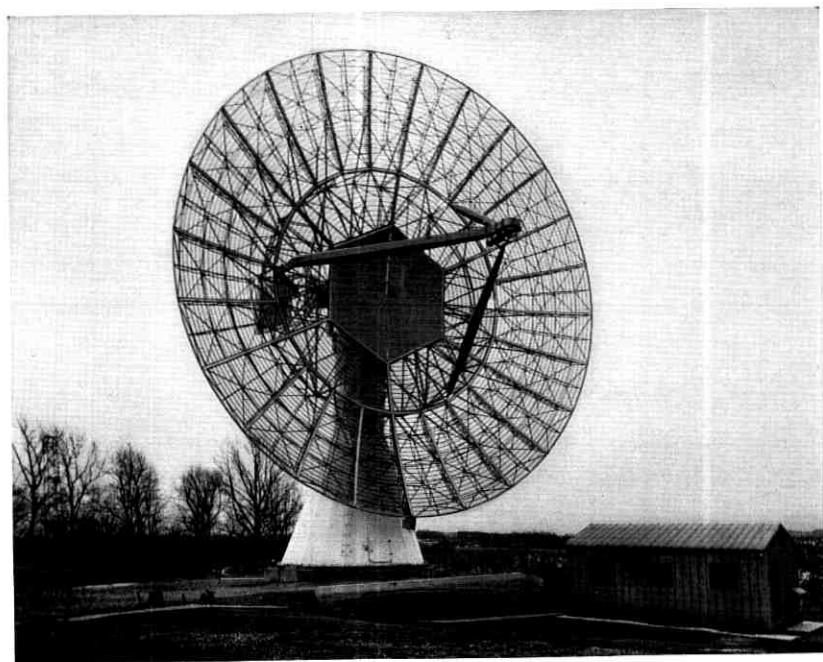


Fig. 1 — Transmitter building and Kennedy dish antenna at Crawford Hill.

may be connected either to the dummy load or to the line feeding the antenna. A coaxial-to-waveguide transducer with pressure seal is used to convert from the coaxial output to the $4\frac{7}{8}$ - by $9\frac{3}{4}$ -inch rectangular waveguide going to the 60-foot dish antenna. The waveguide line is kept under about one-half pound pressure of dry nitrogen to prevent moisture leakage.

Circuits and meters are provided for continuously monitoring the incident and reflected RF power at both input and output of the power amplifier. The actual transmitted power is continuously recorded with an Esterline-Angus pen recorder.

The high-power klystron is capable of dissipating the total beam power in its collector (about 35 kw), and can therefore be safely operated without RF power drive. This makes it feasible to gate the driver stage, as is done for radar pulse or SSB transmission. Two high-voltage rectifiers are provided. One supplies 2000 volts at 0.7 ampere for the klystron bombarder and the other supplies 18 kv at 2.0 amperes for the klystron beam circuit. The beam voltage may be continuously varied from 12 to 18 kv. The primary power requirement of the transmitter, including

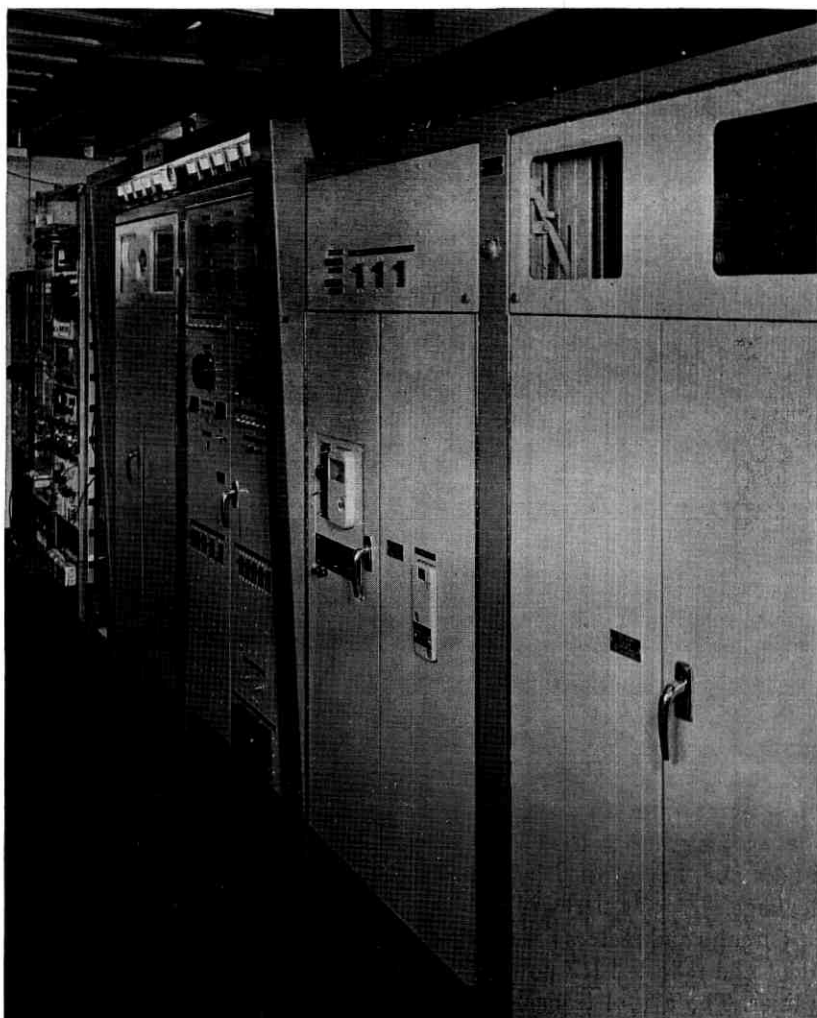


Fig. 2 — Front view of complete transmitter, showing FM driver unit, control and monitor panel, measuring equipment, and antenna manual control.

the heat exchanger, is about 50 kw maximum, three-phase, four-wire, 208 volts.

III. DRIVER MODULATION UNITS

Various types of exciter-modulator units have been provided to drive the power amplifier, as is shown in Fig. 4. They all generate a signal at

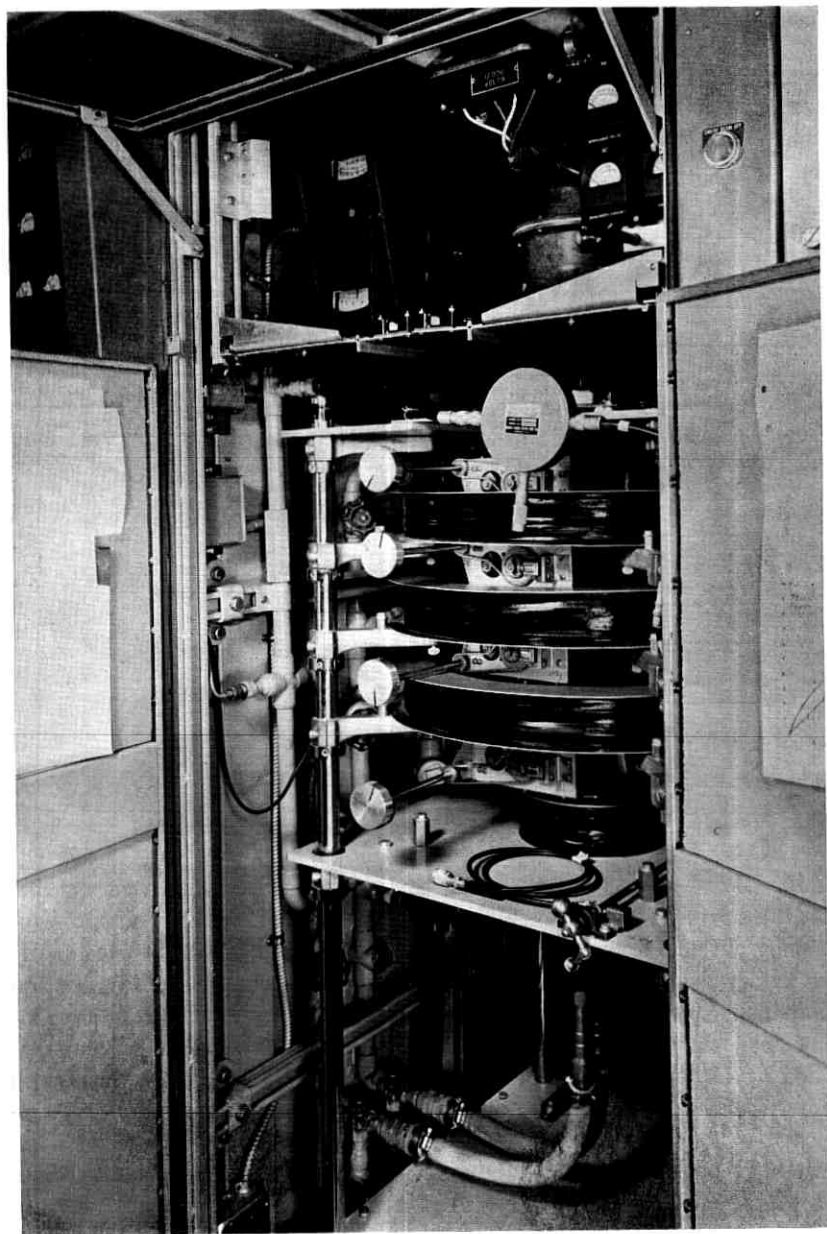


Fig. 3 — 10-kw klystron in cabinet.

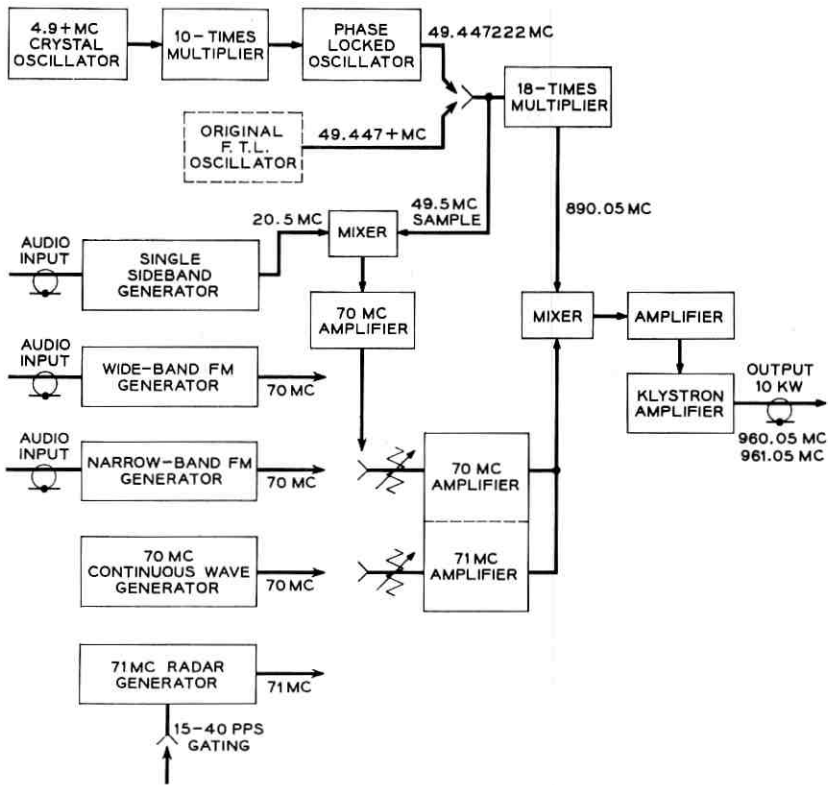


Fig. 4 — Over-all block diagram of transmitter.

about 70 mc, either cw or modulated, which is mixed with a very stable and accurate frequency of 890.05 mc to produce the final output frequency of 960.05 mc (961.05 for radar). Fig. 5 is a block diagram of the frequency generation and mixer-amplifier arrangement; it may be seen that the frequency stability of the output frequency is primarily dependent upon the crystal supplying the 49.44+ mc output, which is multiplied by 18 to give the 890.05-mc mixer signal. The crystal and oven in the original equipment did not meet our requirement, and they were replaced by a high-stability Western Electric crystal oscillator and oven assembly operating at 4.944+ mc. This was followed by a ten-times multiplier arrangement to give the desired 49.44+ mc frequency. In order to remove residual FM noise from the oscillator-multiplier output frequency, a phase-lock oscillator was interposed between the ten-times multiplier and the driving point of the three-times multiplier. W. W.

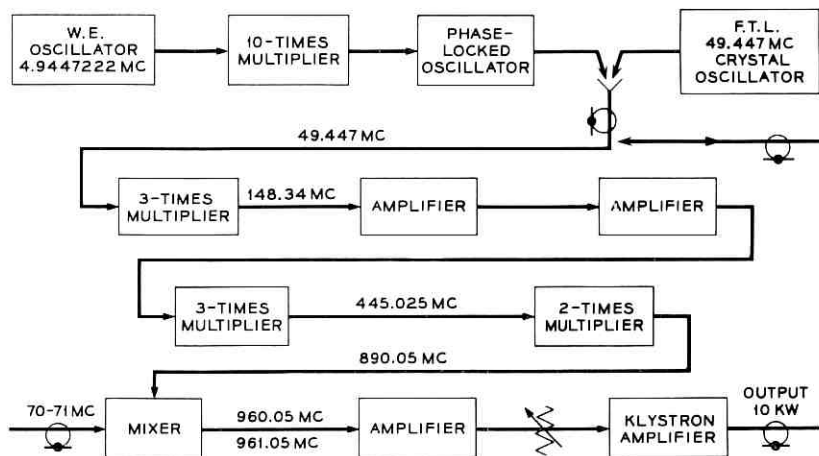


Fig. 5 — Block diagram of crystal generator and multiplier, showing mixer-amplifier arrangement.

Rigrod and A. J. Rustako of Bell Laboratories were responsible for the design and procurement of the improved crystal control system as well as for the addition of the SSB exciter equipment described below. The 890.05 mc frequency is now stable to about two parts in 10^9 . This new arrangement is an integral part of the driver circuit for all types of modulation, which are all added to the mixer at the 70-mc frequency level.

3.1 Wide-Deviation FM Modulator

This is an FM modulator-exciter provided by Federal Telecommunication Laboratory (Model NUS 3315.3) and is the basic one for the Echo tests. This unit is capable of producing an FM driving signal with deviations of ± 300 kc, for baseband frequencies from zero to 500 kc. Fig. 6 is a block diagram showing the arrangement of the FM generator circuits.

The wide-deviation FM exciter has operated satisfactorily in conjunction with the FM with feedback (FMFB) method of reception during the Echo tests. The actual deviation used was ± 30 kc, as was determined by quality overload tests with the FMFB receiver,¹ using audio and voice frequency modulation.

3.2 SSB Exciter

This is also a commercial unit, Technical Materiel Corporation, Model SBE-3, referred to previously. Fig. 7 is a block diagram showing the

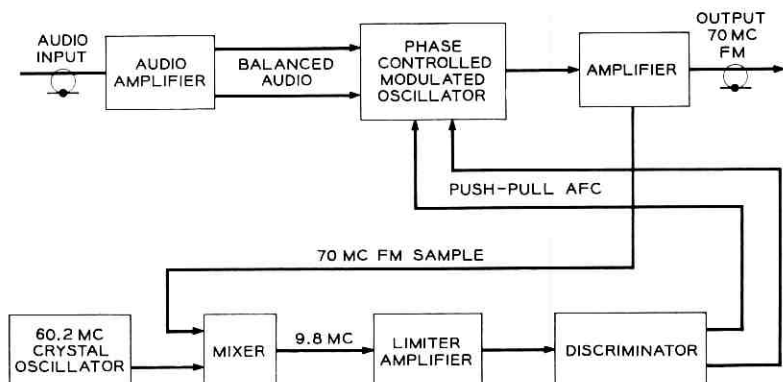


Fig. 6 — Block diagram of wide-deviation FM modulator.

general method of signal generation, and Fig. 8 is a photograph of the equipment. This unit can produce single- or double-sideband modulation with controlled amounts of carrier and has an audio bandwidth of 350 to 7500 cycles. Its output at a frequency of $20.55 + mc$ is mixed with a sample of the $49.447 + mc$ crystal-controlled output to give the $70 mc$ desired for introduction to the F.T.L. driver.

3.3 Low-Index Phase Modulator

This unit was built to use during comparison tests of various types of transmission and replaced one that was furnished for the original Moon-bounce tests by the Jet Propulsion Laboratories. This new unit is much smaller and more compact than the JPL unit and, like all the driver units, has an output frequency of $70 mc$. It is capable of producing phase modulation of at least one-half radian over the audio frequency voice band. It is crystal-controlled with a $35-mc$ crystal, and this frequency is doubled and phase-modulated in a buffer stage. Fig. 9 gives the principal circuit details.

3.4 70- and 71-mc CW Units

The crystal-controlled oscillators for these units were made by Bulova Watch Company. A buffer stage and amplifier were added to each oscillator output and provision made for controlling the pulse-gating of the $71-mc$ unit. These units were provided to produce a very stable frequency with a minimum of residual FM modulation, when used to drive the F.T.L. mixer, again producing 960.05 or $961.05 mc$ antenna power. The former frequency is used for constant frequency transmission during

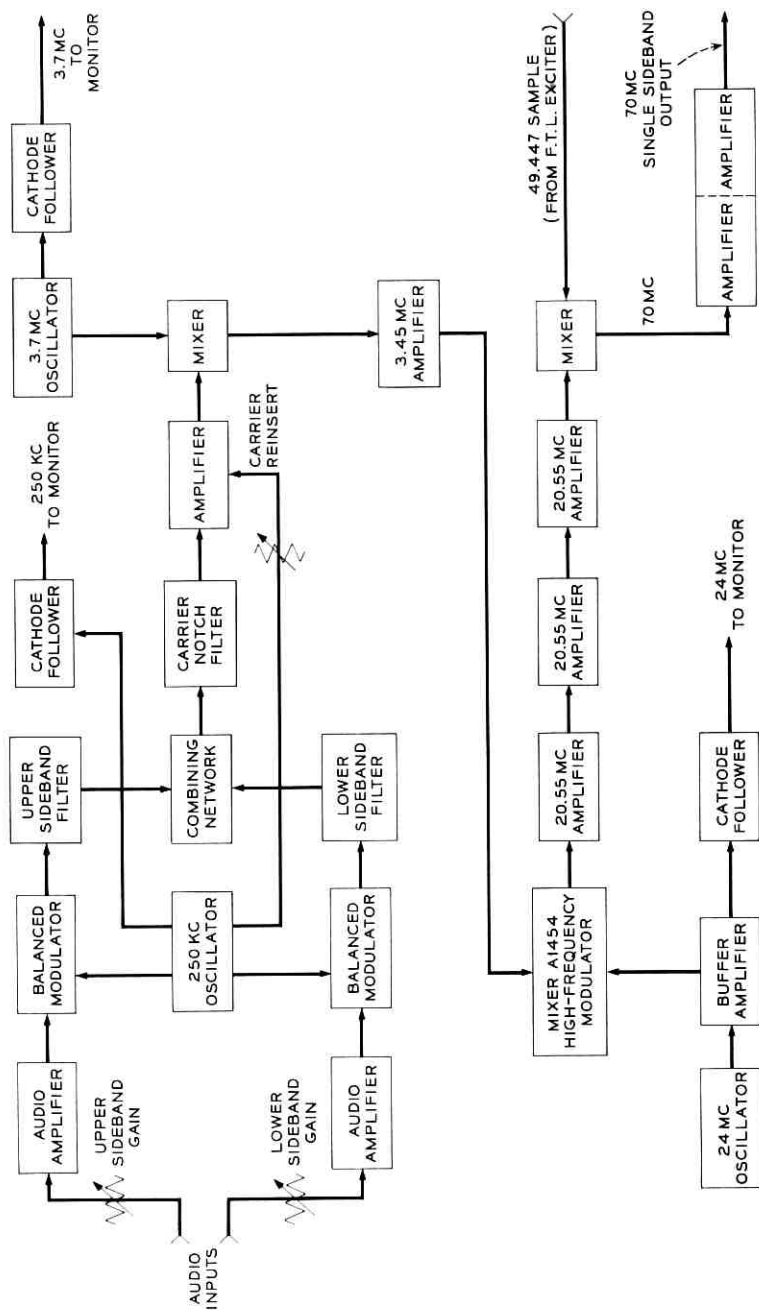


Fig. 7 — Block diagram of single-sideband modulator.

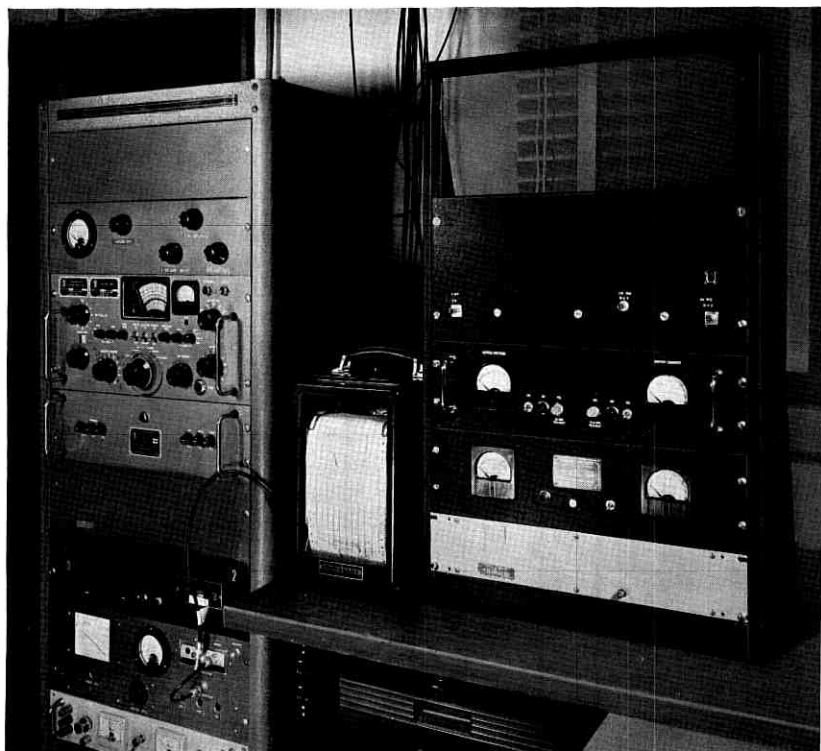


Fig. 8 — Left, single-sideband generator and monitor; center, RF power-level recorder; right, double-sideband generator.

doppler measurements and the latter for radar pulse tests. Fig. 10 is a block diagram of these exciters.

3.5 Radar 71-mc Unit

A separate 71-mc crystal-controlled oscillator was built to replace the Bulova unit described in Section 3.4 because of some difficulties encountered when the latter was pulse gated for radar transmission. The principal trouble was that the duty cycle of the on-and-off pulses changed as much as 3 to 1 when the keying frequency was changed from 15 to 45 cycles. This has been corrected in the new unit. Fig. 11 shows a block diagram of the present arrangement.

A twin 70- and 71-mc amplifier is provided so that the transmitter can be excited with either or both a 70-mc modulated signal (for FM, PM, SSB, etc.) and the on-off 71-mc radar pulses. The two signals are

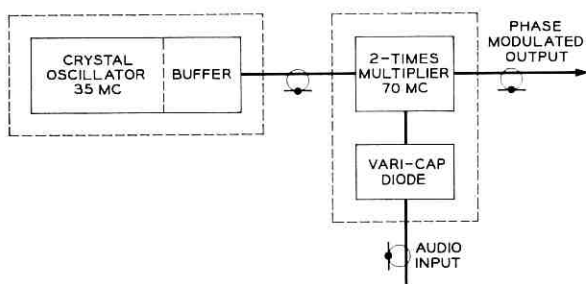


Fig. 9 — Block diagram of low-index phase modulator.

fed in separately through attenuator controls so that any desired level is introduced (see Fig. 4). The combined sum of the two signals then drives the regular F.T.L. mixer. The total output antenna peak power is kept to 10 kw.

The radar gating is done by a relay controlled from the radar receiver location and is described in more detail in a companion paper.²

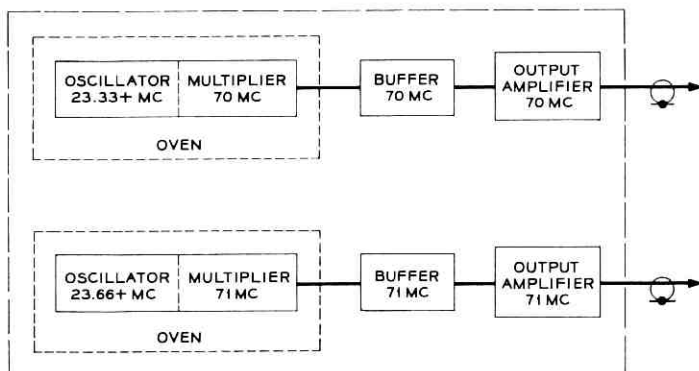


Fig. 10 — Block diagram of 70- and 71-mc crystal oscillators and amplifiers.

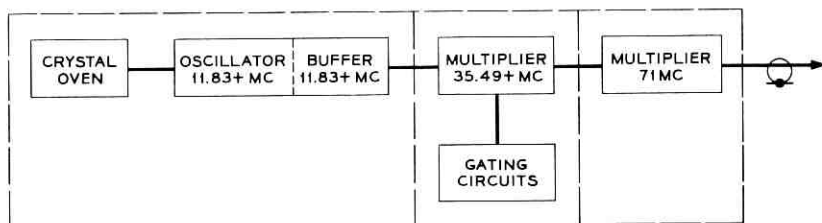


Fig. 11 — Block diagram of 71-mc radar oscillator.

IV. MONITORING EQUIPMENT AND CONTROL PANELS

During normal operations it is necessary to monitor or record such characteristics of the transmitter as (a) transmitted frequency, (b) transmitted power, (c) modulation quality, and (d) time.

Since there are many different modes and conditions of transmission the monitoring apparatus becomes relatively complex, as is shown by the block diagram, Fig. 12, and the photograph, Fig. 13. If the functions are examined according to the four categories listed above, operation should be readily understood.

4.1 Transmitted Frequency

Frequency counters to operate at 960.05 mc were not available, so a sample of the transmitted signal (obtained from a probe in the output

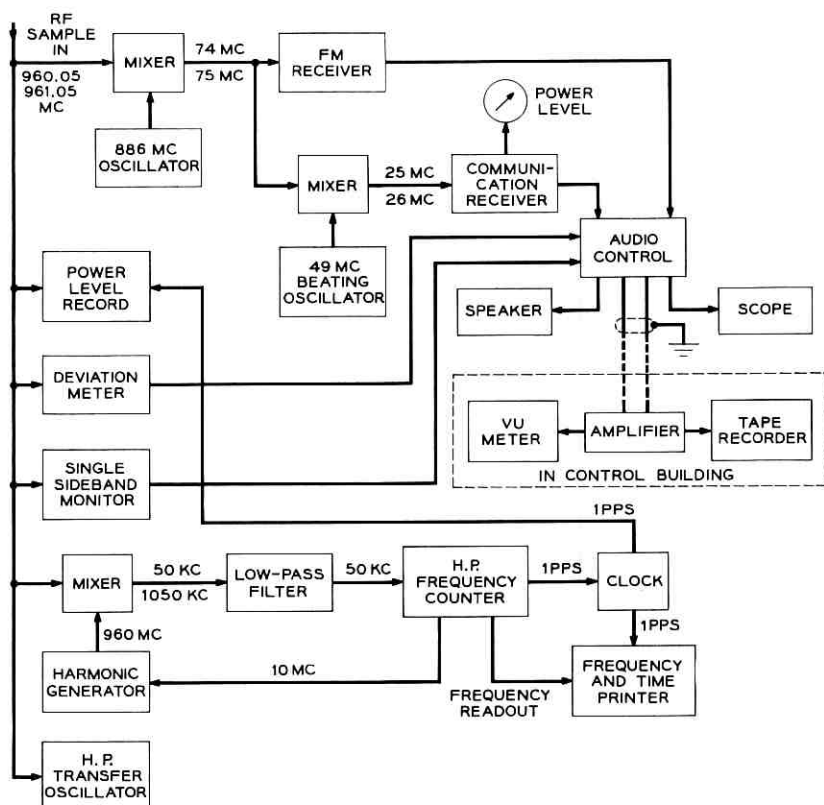


Fig. 12 — Block diagram of RF monitoring equipment.

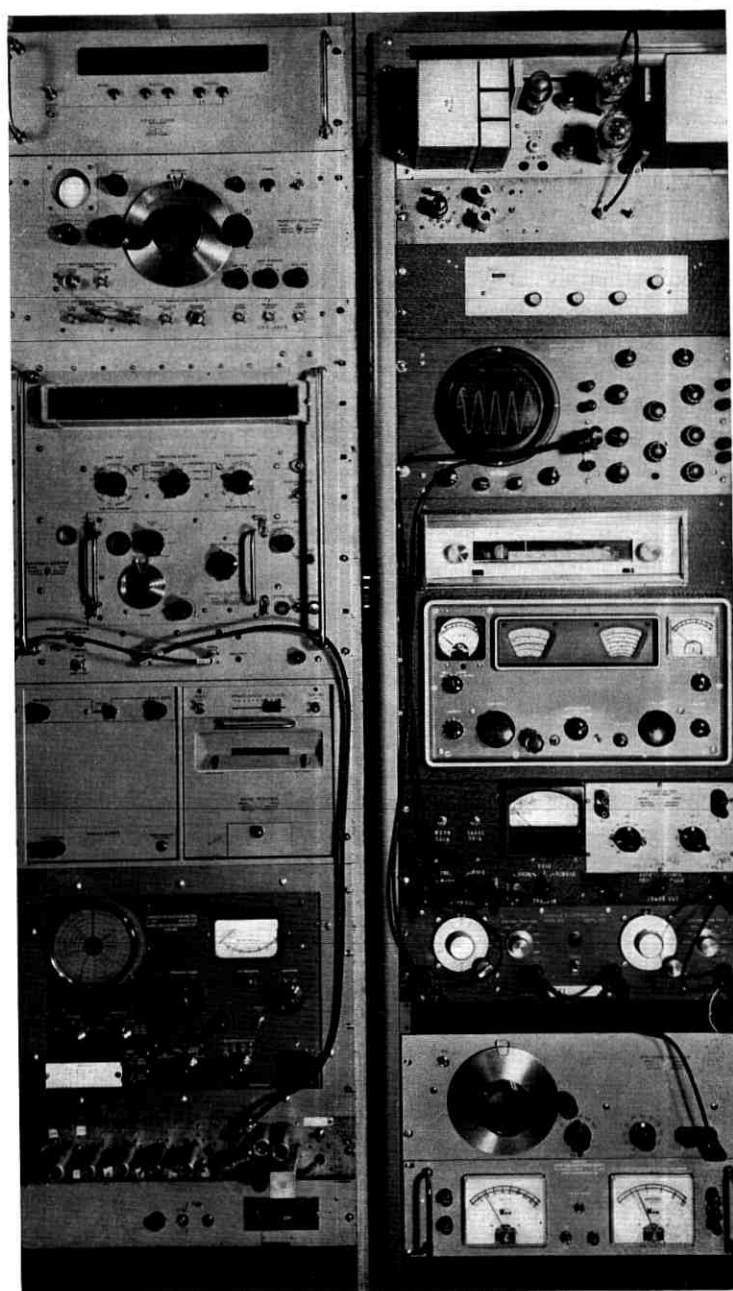


Fig. 13 — Monitoring and measuring equipment.

coaxial line and fed to all monitoring equipment) is mixed with a 960.00-mc signal, and the difference frequency of 50 kc is read by a Hewlett-Packard 524C frequency counter and also printed out on a paper tape by a Dymec 560A digital recorder. A 10-mc signal available from the frequency counter is multiplied by the harmonic generator to 960 mc and provides a beating oscillator with a stability and accuracy equal to that of the frequency control crystal oscillator in the counter. The manufacturer's specifications indicate a short term stability of three parts in 10^8 or approximately 30 cycles at 960 mc. The counter cannot determine whether the signal is above or below 960 mc, but this is done by means of a Hewlett-Packard type 540B transfer oscillator.

When both radar and communication channels are being transmitted, there are two frequencies, of approximately 50 kc and 1050 kc, out of the mixer. The frequency counter is unable to distinguish between these two, so a low-pass filter with a cut off frequency of 80 kc is inserted between the mixer and counter in order to eliminate the 1050 kc and measure the 50 kc. Similarly, a high-pass filter could be used to eliminate the 50 kc and measure the high frequency.

4.2 *Transmitted Power*

Two different methods of monitoring output power are employed. In the first, a probe in the output coaxial line powers a diode rectifier. The crystal current drives an Esterline-Angus strip recorder and provides a continuous ink record of the average power output. A second probe and diode powers the regular output power meter. When only one carrier is transmitted this is quite satisfactory. However, when more than one carrier is being transmitted (especially when one of them is a pulsed carrier) the indicated powers are meaningless. Measurement under these conditions requires a selective system which will accept one carrier frequency and reject all others.

In the second method of monitoring power, a sample is taken from the RF monitoring line and heterodyned to 74 mc. (This frequency is also used for the FM monitoring to be described later.) A second converter reduces the frequency to 26 mc. A Hammarlund HQ 110 communications receiver is then used as a variable-frequency IF amplifier with a bandwidth adjustable between about 3 kc and 500 cycles. An additional detector was installed to drive a microammeter which has been calibrated to read directly from 0 to 12 kw.

With this system it is possible to adjust and monitor each carrier to a specific power level, including each sideband of double-sideband transmission.

4.3 Modulation Quality

Three different methods are employed in the measurement and monitoring of wide-band frequency modulation, narrow-band FM or phase modulation, and amplitude modulation.

For wide-band FM a sample of the signal is heterodyned to 74 mc (as discussed previously) and received on a Sherwood S-30000 II FM tuner whose input circuits were modified to cover a range of 70 to 80 mc. The detected output is amplified in the audio control unit to be described later, and may be monitored visually on an oscilloscope or audibly on a loudspeaker. Spurious noise and hum are measurable down to about -70 db below the normal signal deviation of ± 30 kc. Frequency deviation is measured by a Marconi TF-791D deviation monitor. The actual signal-to-noise ratio for normal FM operation is about 45 to 50 db.

Deviation of narrow-band FM or phase modulation is also measured by the Marconi deviation meter. Audio output available from this instrument is monitored through the audio control.

Amplitude-modulated signals are received on the same communications receiver and detector described under power monitoring. Audible and visible presentations are available through the audio control.

The single-sideband monitor, which was also designed and engineered by W. W. Rigrod and A. J. Rustako, is shown in block form in Fig. 14. Its operation, in brief, is as follows: A sample of the 960.05 mc SSB output signal is mixed with a sample of the 890-mc exciter drive to produce a

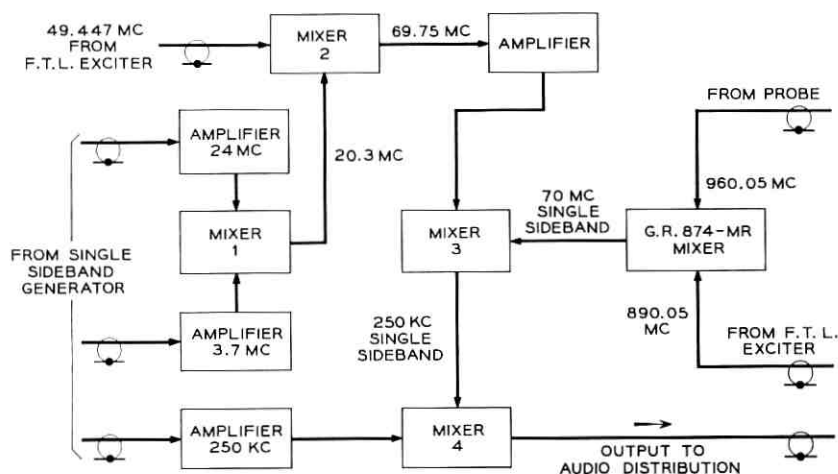


Fig. 14 — Block diagram of single-sideband monitor.

modulated 70-mc output in a General Radio 874-MR mixer. Frequencies of 3.7 and 24 mc, available from the SSB generator, are combined to produce 20.3 mc in mixer 1. In mixer 2 this frequency is added to a sample of the 49.45 mc driving the F.T.L. exciter to produce 69.75 mc, which is subtracted from the 70 mc out of the G.R. mixer to produce a modulated 250-kc signal in mixer 3. By beating this with a sample of the 250-kc oscillator in the SSB generator, audio output is recovered in mixer 4 and routed to the audio distribution control. By utilizing the same oscillators for both transmitting and monitoring, small frequency variations are cancelled out and complete synchronization is assured.

4.4 Time

Comparison of frequency or signal-level recordings of a received reflected signal with the corresponding frequency and power-output recordings at the transmitter requires that there must be a time reference permanently impressed on each recording.

The Hewlett-Packard frequency counter will furnish highly accurate one-per-second pulses. These trigger a Dymec DY 2508A clock which indicates hours, minutes, and seconds on a Nixie tube readout, and can also furnish time data to a Dymec 560A digital recorder. Frequency count data from the 524C counter are also fed into the printer, and the result is a paper tape printed record containing the last five digits of the frequency and six digits indicating time. Rate of printout may be varied from one each 20 seconds to five per second.

The Esterline-Angus power-level recorder charts are printed with a time scale of three inches per hour, and this is generally of sufficient accuracy. When a short transmission with a higher resolution is required the tape may be speeded up to three inches per minute and a second recording pen, driven by the one-per-second pulses from the digital clock, will record one-second intervals along the chart. Thus, by accurately setting the digital clock to a known time standard such as WWV or CHU, both the frequency and power recordings are accurately indexed in time. Samples of the frequency counter printout and the high-speed operation of the E-A power level recorder are shown in Fig. 15.*

V. AUDIO DISTRIBUTION

All audio circuits required for transmission or monitoring are routed to an audio control panel, shown in block form in Fig. 16.

* Data records shown in Figs. 15, 18, and 19 were taken in connection with National Aeronautics and Space Administration Contract NASW-110.

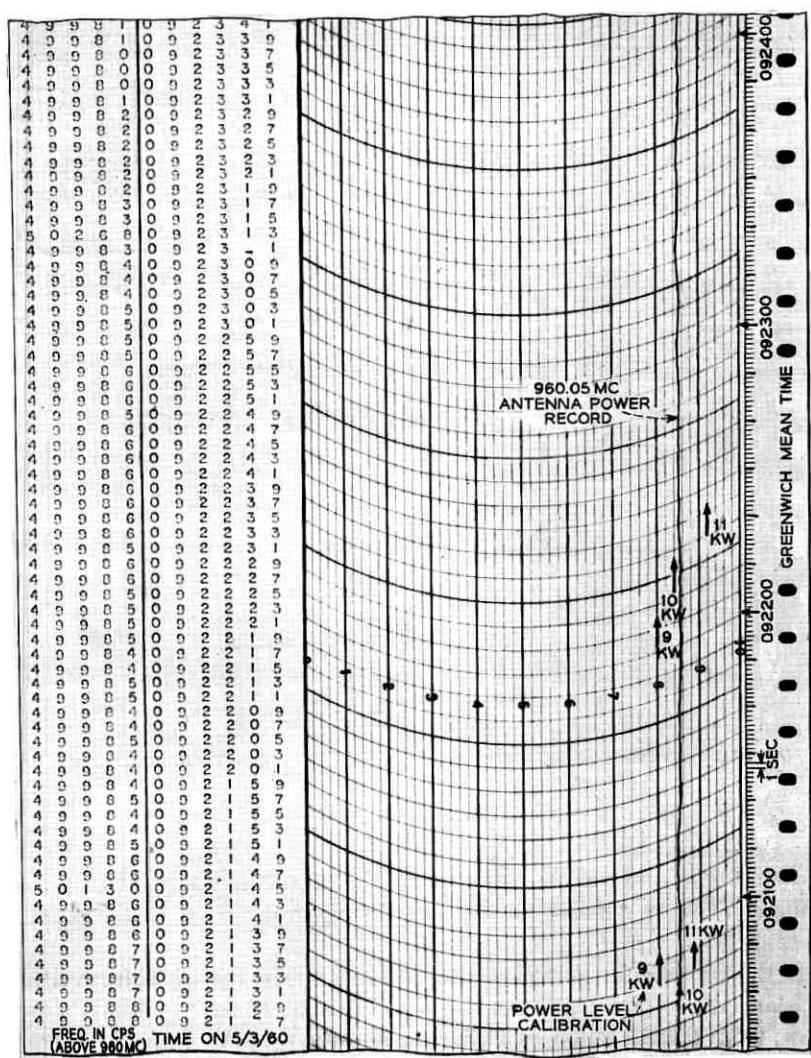


Fig. 15 — Typical frequency counter printout (left) and high-speed RF power-level recording (for Tiros pass of May 3, 1960).

In the monitor control section, outputs from the various detectors are selected and amplified by a one-stage amplifier having a 600-ohm output impedance and variable gain. A balanced 600-ohm line transmits the signal to the main console in the station control building. An oscilloscope and high-impedance input audio amplifier driving a monitor loudspeaker

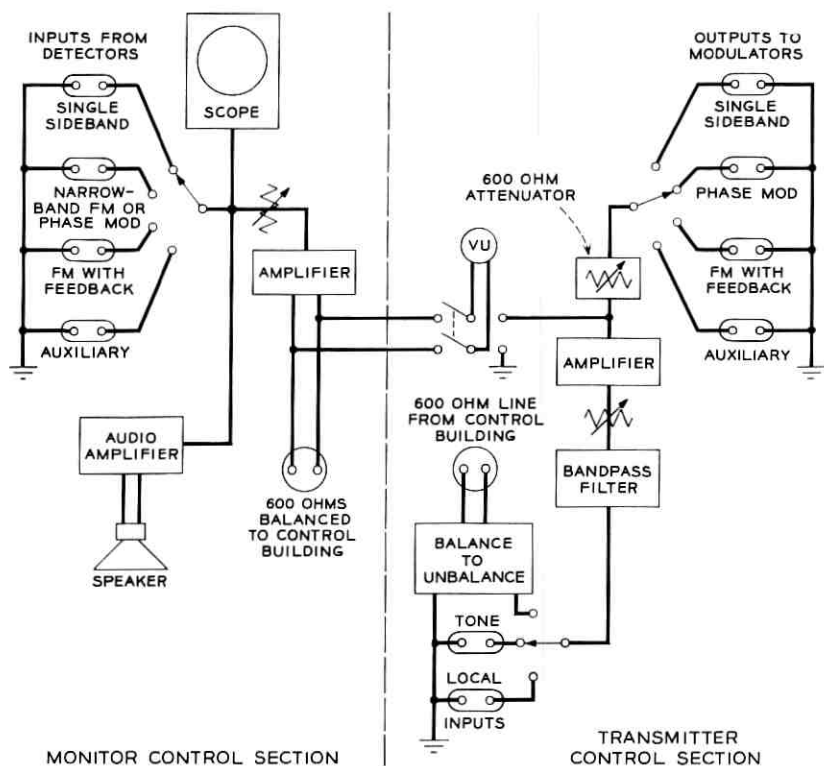


Fig. 16 — Block diagram of audio control panel.

allow audible and visible checking of the inputs to the control panel, while a VU-meter measures the level being transmitted to the control building.

In the transmitter control section a switch selects the signal from either a balanced 600-ohm line from the console in the control building, a sine wave from a local audio oscillator, or an audio signal of any type from a local source. An amplifier similar to the one in the monitor section amplifies the selected signal and transforms it to 600 ohms unbalanced. A second switch routes this output to the desired modulator. A VU-meter and a Hewlett-Packard 350A attenuator allow the measurement and adjustment of level into the modulator.

The frequency response of the audio distribution system is ± 1 db from 30 to 12,000 cps, and it is linear up to 1.8 volts rms into 600 ohms. However, any desired restricted audio bandwidth at the transmitter

input may be provided by means of a Spencer-Kennedy 302 variable electronic filter. This versatile unit consists of two filters, each of which is adjustable for cut-off frequencies from 20 cps to 200 kc, and may function as either a high-pass or low-pass unit, or as a combination band-pass. Rate of cut-off is 18 db per octave, and the two sections may be operated in series to provide a slope of 36 db per octave.

VI. MEASUREMENTS AND CHARACTERISTICS

A number of the over-all transmission characteristics of the transmitter are of interest. One of particular concern for various types of transmission is the input-output overload characteristic, in terms of 70-mc drive to the F.T.L. mixer and the 960-mc (or 961-mc) power in the antenna. For straight FM modulation, the linearity of this characteristic is not important; this is, of course, the type of transmission for which the set was designed. However, for SSB or any type of amplitude modulation, particularly when radar transmission is added, a departure from linearity will introduce some distortion, and this makes difficult the determination of the division between the 960- and 961-mc power output.

Most of the non-linearity occurs in the power klystron. The higher the beam voltage used, the straighter the characteristic and the lower the distortion. Fig. 17 shows some typical characteristics of the relationship between the 70-mc input and the 960-mc output. It will be seen that there is no departure from linearity for the low-power driver stage over the range required to drive the klystron to full power (one-half watt). The klystron characteristic at 17 kv shows a curvature above about 3 or 4 kw output and is about 3 kw down from the ideal at 10 kw. The characteristic at 18 kv is somewhat better than the one at 17 kv, and this is the one used during tests when linearity is of any importance (18 kv is the maximum voltage available with the present equipment). These load characteristics have also been checked at 961 mc and are essentially identical with those at 960 mc.

The over-all frequency characteristic of the transmitter is determined by various parameters, such as the tuning and adjustment of the mixer-amplifier of the exciter, the tuning of the klystron cavities, and the coupling adjustments to the load. The band can be adjusted to about 4 mc at the 3 db points and 2 mc at the 0.5 db points. For the particular application in which it is being used for Echo tests in which only relatively narrow frequency bands are used, the main concern is that nearly equal outputs at 960 and 961 mc are obtained for equal 70- and 71-mc drive amplitudes. This is easy to accomplish.

The transmitter output circuit operates into a fairly well matched load

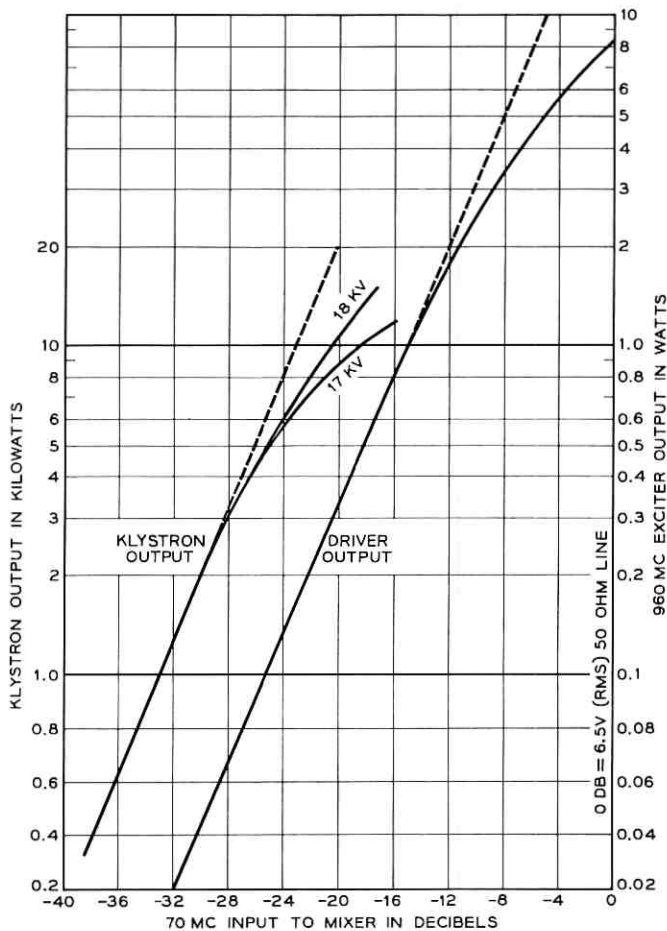


Fig. 17 — Input-output characteristics of 960-mc driver and 10-kw klystron amplifier.

with either the dummy water load or the 60-foot dish antenna. The actual reflected power with 10 kw output is about 100 watts for the antenna and about 30 watts with the dummy load, corresponding to return losses of 20 and 25 db respectively.

The calibration of the antenna output power meter is checked occasionally by transferring the transmitter output to the dummy load, where coolant flow and temperature measurements give a measure of actual power. From these readings a calibration curve for the power meter is obtained. This meter is a special dc milliammeter calibrated in kilowatts,

which is coupled to the output RF line through a crystal diode. A similar arrangement is used to obtain a direct current to operate the Esterline-Angus recorder that gives a continuous record of output power when the transmitter is in operation. Figs. 18 and 19 are sample recordings showing the variations in power with time for various types of emission.

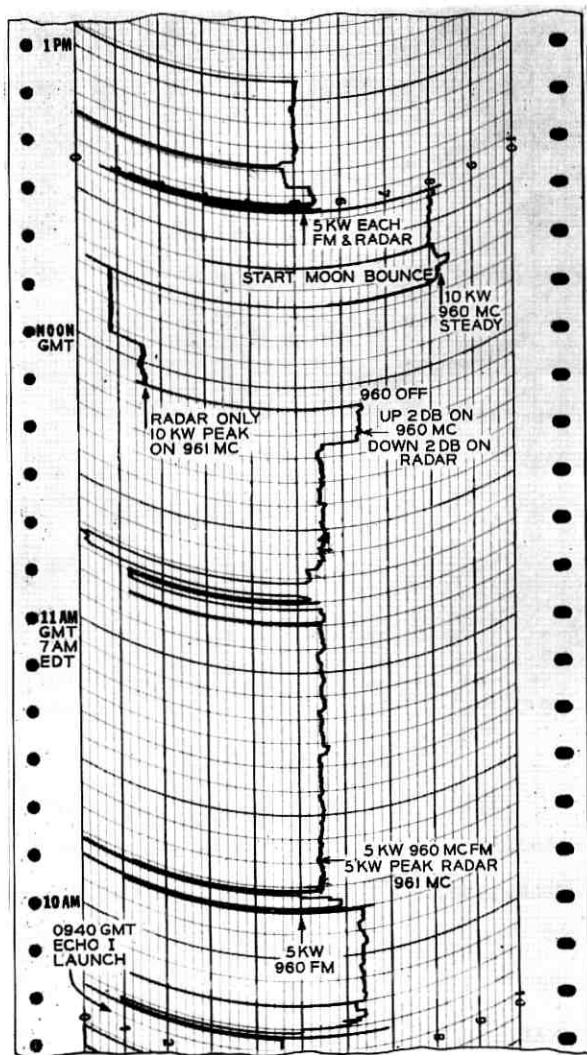


Fig. 18 — Antenna power-level recording for Echo pass 1 (August 12, 1960).

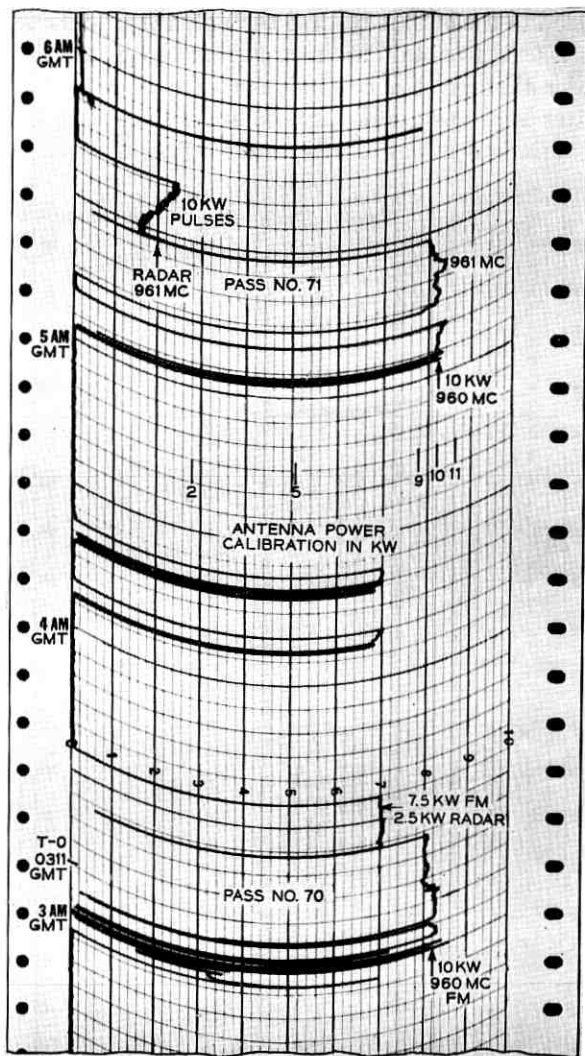


Fig. 19 — Antenna power-level recordings for Echo passes 70 (August 18, 1960).

It is believed that the power as read by the meter or registered on the recorder is accurate to about ± 0.1 db.

VII. OPERATIONAL RESULTS AND CONCLUSIONS

The operation of the 10-kw transmitter has been very satisfactory since it was placed in service in July 1959. There have been a few minor

equipment failures during this time, but fortunately they occurred at other than scheduled pass times. One interruption causing lost time in one of the early Moonbounce tests was due to arcing in some loose contacts near the rotary joints of the coaxial feed line to the dish antenna. This was corrected and no further trouble has been encountered from this source.

One annoying type of trouble which required considerable time to run down was what were termed "momentary interruptions." These would occur without regard to beam voltage or load and would only last for a second or two, which is the recycling time of the main high-voltage circuit breaker. Sometimes several interruptions would occur within a few minutes, and at other times they would be spaced several hours or days. These interruptions were finally traced to faulty vibration-sensitive relays in the beam current and body current overload circuit and to a faulty air-flow switch in the heat exchanger. They vibrated enough at certain times to open the relay contacts, which in turn opened the holding coil of the main circuit breaker. This breaker would reclose automatically and power would be reapplied without giving a positive indication or warning light. Since these relays and the air switch have been replaced, the momentary interruptions have apparently been eliminated.

There have been many long and extended transmission periods at full 10-kw output power with beam voltages up to 18 kv during Moonbounce, tropospheric scatter, Shotput, and Echo test transmissions. After the successful launching of Echo I there were transmissions during 124 different passes of the balloon from pass 1 on August 12, 1960, to pass 2407 on February 24, 1961. These tests are continuing.

Many different types of modulation have been used, such as wide-deviation FM, low-index phase modulation, constant-frequency cw, single-sideband and double-sideband with varying amounts of carrier, and on-off radar pulses.

Radar pulse signals are employed to aid in tracking the balloon and therefore are transmitted simultaneously with the communication channel modulated frequency. This requires a division of transmitted power between the two frequencies, the total not to exceed 10 kw. The power can be divided as desired, depending on the conditions of the particular test. Sometimes it is desirable to favor either the communication signal or the tracking radar. A nominal division frequently used has been 7.5 kw communication and 2.5 kw radar peak power.

The radar pulses are keyed at a low-frequency rate of 15 to 45 cycles, with a duty cycle nearly equal to 50 per cent time on and off. Due to compression nonlinearity of the high-power klystron input-output characteristic, it is difficult to control the division of power between the two

frequencies. If they are set separately to a given amount and then applied together, each signal and the sum will be lower than desired. They must therefore be adjusted when both are operating. The value of the power at each frequency is obtained by the use of the narrow-band frequency-selective amplitude-measuring receiver described in Section IV. There is a certain amount of amplitude modulation introduced into the communication channel by reason of the klystron compression when the radar pulses are added, but this has not caused any trouble or added any appreciable noise in the monitoring FM receiver output. There is some low-level pulse noise in the SSB receiver output, but this has not been considered harmful to good speech quality. Low-frequency high-pass filters help to eliminate the interference due to radar keying.

VIII. ACKNOWLEDGMENTS

The authors wish to recognize the helpful suggestions and cooperation of many people working on Project Echo, particularly O. E. DeLange, for his part in selecting the transmitter equipment and his close cooperation in the engineering necessary to provide radar pulse modulation; G. S. Axeling, F. E. Guilfoyle, and A. J. Rustako for operating assistance during some of the long night tests and for their parts, along with that of J. T. Ruscio, in building and providing necessary auxiliary equipment; L. R. Lowry, for his supervision in furnishing adequate housing, power and grounds facilities at the transmitter building; and, of course, to W. C. Jakes, Jr., for his general advice and encouragement as Project Echo engineer.

REFERENCES

1. Ruthroff, C. L., FM Demodulator with Negative Feedback, this issue, p. 1149.
2. DeLange, O. E., Satellite-Tracking Radar, this issue, p. 1157.

PROJECT ECHO

Receiving System

By E. A. OHM

(Manuscript received April 10, 1961)

A tracking horn-reflector antenna, a maser preamplifier (or standby parametric preamplifier), and a special FM demodulator were combined to form a low-noise receiving system which was used to achieve a high-quality voice circuit via the Echo I passive satellite. This paper describes the 2390-mc receiving system located at Holmdel, New Jersey.

I. INTRODUCTION

By using large antennas and a high-powered transmitter, it was calculated that a modest carrier could be received in New Jersey from California via the Echo I satellite.¹ In order to establish a good voice circuit with this carrier, it was clear that the effects of noise had to be reduced by using a very-low-noise receiver. It was also clear that a special demodulator, which featured FM with negative feedback,² could reduce the noise effects still further. Although a parametric amplifier in combination with this type of demodulator would yield a good voice circuit under near-ideal conditions, a maser would allow a circuit with a more practical carrier-to-noise margin.* In this regard, a previous experiment had demonstrated that an ultra-low-noise system temperature could be achieved in practice by using a low-noise horn-reflector antenna in combination with a traveling-wave solid state maser.³ In accordance with these preliminary results, a larger horn-reflector tracking antenna was combined with two traveling-wave masers or alternately two "standby" parametric amplifiers to provide two separate low-noise systems, one for each sense of circular polarization. Special FM demodulators were used to achieve voice circuits of excellent quality from the resulting modest

* It is important to maintain some margin; otherwise, at a critical carrier-to-noise ratio a small decrease in carrier or increase in noise will change the voice circuit from one that sounds good to one that is completely unintelligible. A discussion of this "threshold" effect is included in a companion paper by Ruthroff.² For the 3-kc audio circuit used here, the "threshold" ratio of carrier to noise power (referred to a 6-kc band) is 14 db.

carrier-to-noise ratios. In addition, AGC voltages from the FM demodulator were used to monitor the carrier levels, voltages proportional to the system temperatures but independent of incoming carrier levels were derived, and each of these voltages was recorded and calibrated. The discussion also points out how certain measuring and operating techniques were used to obtain the most accurate experimental results.

Section II describes how the receiver generated useful output information. It is followed by sections on the system noise temperature, the FM demodulator AGC characteristics, and the experimental results.

II. RECEIVER DESCRIPTION

A block diagram of the receiving system is shown in Fig. 1. Its operation will be explained by describing how each successive block acts on the carrier and/or noise as it passes through the receiver. (The italicized words in this section refer to blocks labeled in Fig. 1.)

Starting on the left it is assumed that both senses of circularly polarized carrier and noise powers are incident on the antenna. A special significance of the *sky* is that thermal radiation from the atmosphere increases the system noise temperature (as indicated in Fig. 2) as the antenna is lowered toward the horizon. The *horn antenna* focuses the circularly

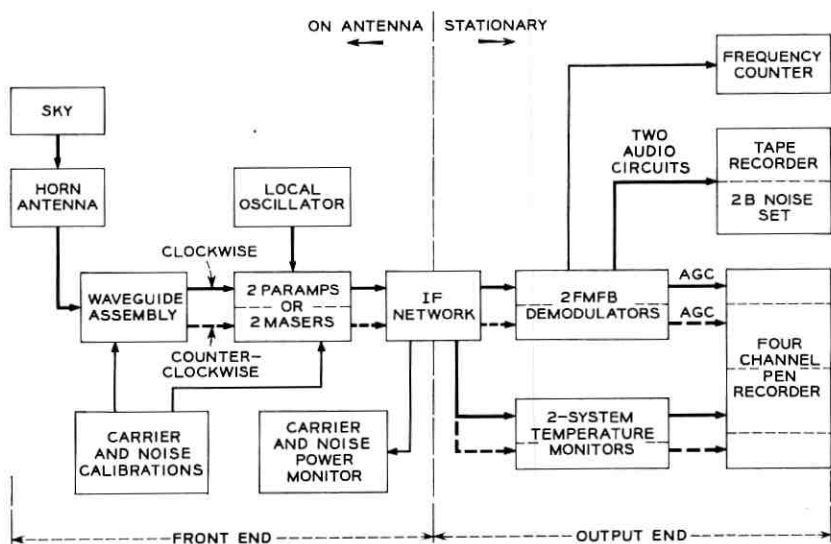


Fig. 1 — Block diagram of Holmdel receiver.

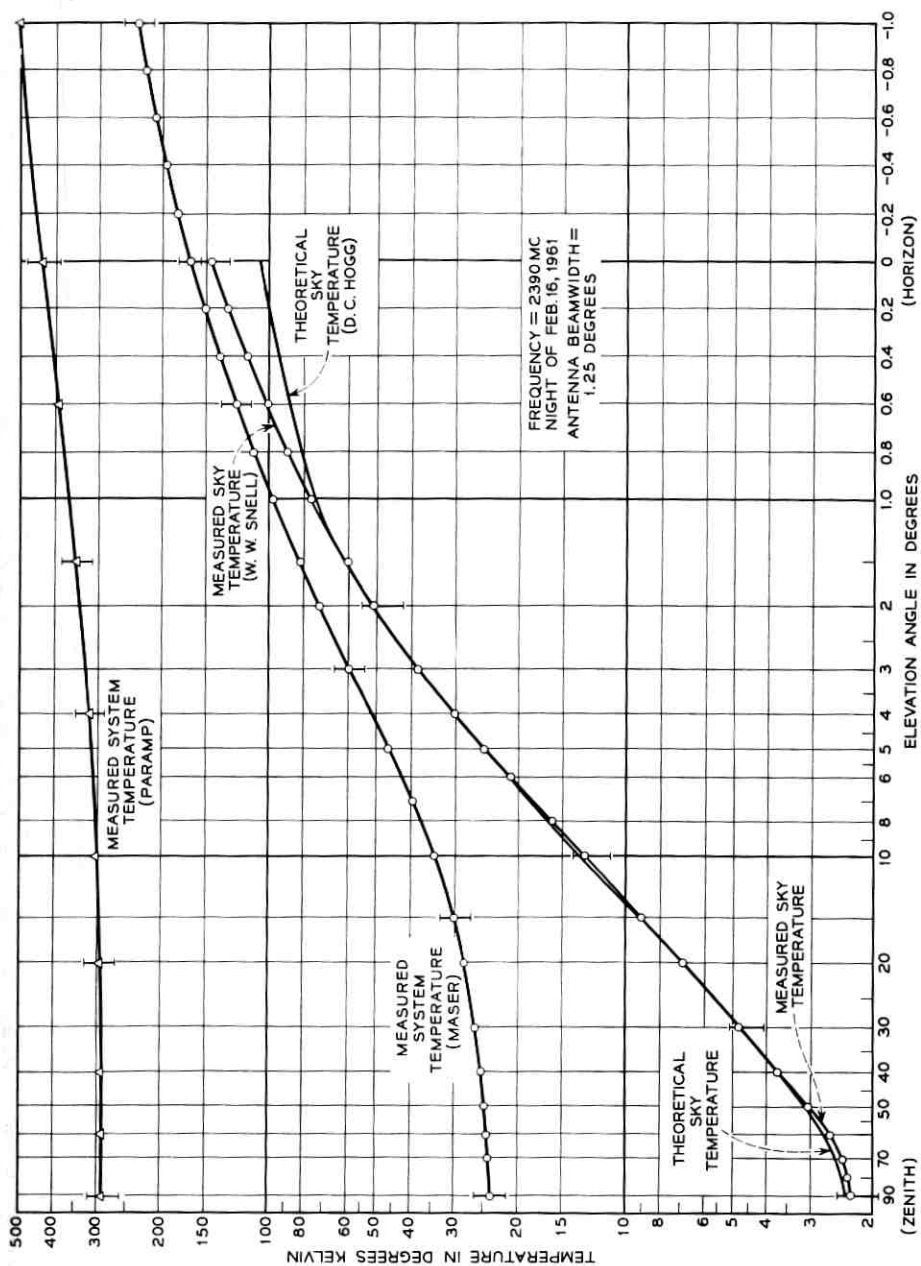


Fig. 2 — Measured sky and system temperatures.

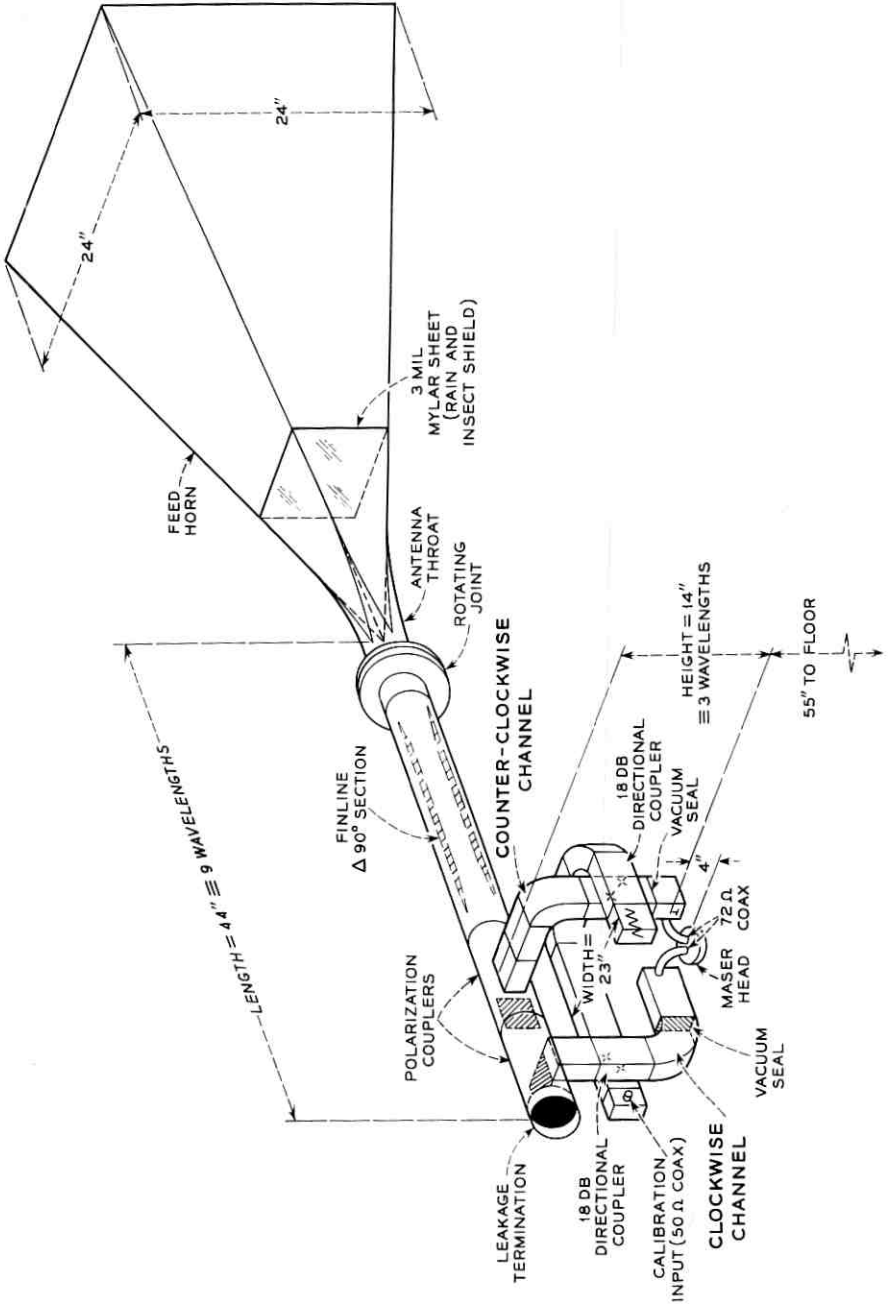


Fig. 3 — Waveguide assembly.

polarized carriers and noise into the *waveguide assembly*, which is shown in Fig. 3. There, after passage through a rotating joint, the finline $\Delta 90^\circ$ section converts the two senses of circular polarizations into orthogonal linear polarizations, and these are further separated by the polarization couplers into separate waveguide channels. These are indicated as the "clockwise" and "counter-clockwise" channels in Fig. 3. Two 18-db waveguide directional couplers are also provided in this region for the convenient insertion of *carrier and noise calibrations* into each channel. From here the two channels are connected via waveguide-to-coaxial transducers to two *maser preamplifiers* or alternatively to two *parametric preamplifiers*. From this point on the channels are completely alike and independent, and therefore only one of them will be discussed.

After sufficient preamplification to nearly eliminate the effects of the noise from the following stages, the carrier and noise powers are heterodyned with a *local oscillator* to an intermediate frequency. The *IF network* further amplifies the carrier and noise to reduce the effects of possible interference, and then transmits this information via the antenna slip ring assembly and long runs of coaxial cable to the "output end" of the receiver. A means for bridging the antenna end of either IF transmission line with a *carrier and noise power monitor* is also provided, so that the "front end" of each channel can be readily tuned and its system temperature measured from inside the antenna cab.

One output of each IF transmission line is connected to an *FM with negative feedback (FMFB) demodulator*. This unit recovers the audio modulation from the frequency modulated carrier with the usual FM advantage, but for a much smaller carrier-to-noise ratio than otherwise possible. For proper demodulation over a wide range of 70-mc carriers, the 1.2-mc input of the FM limiter is held constant with an AGC feedback loop, which is shown in Fig. 3 of Ref. 2. A sample of this AGC voltage is forwarded to the *recorder*, where a back bias is superimposed to display the voltage range of greatest interest. By adding known 2390-mc carrier powers to the RF input of each channel (via the 18-db waveguide directional couplers) it was practical to calibrate AGC carrier level voltages before and after every pass. Typical recorded AGC voltages are shown in Fig. 4, where they are labeled "counter-clockwise channel carrier" (top recording) and "clockwise channel carrier" (third from top).*

Thus far it has been tacitly assumed that the carrier and noise bandwidths are identical. Actually, the modulated carriers, including Doppler

* These experiments were performed under Contract NASW-110 for the National Aeronautics and Space Administration.

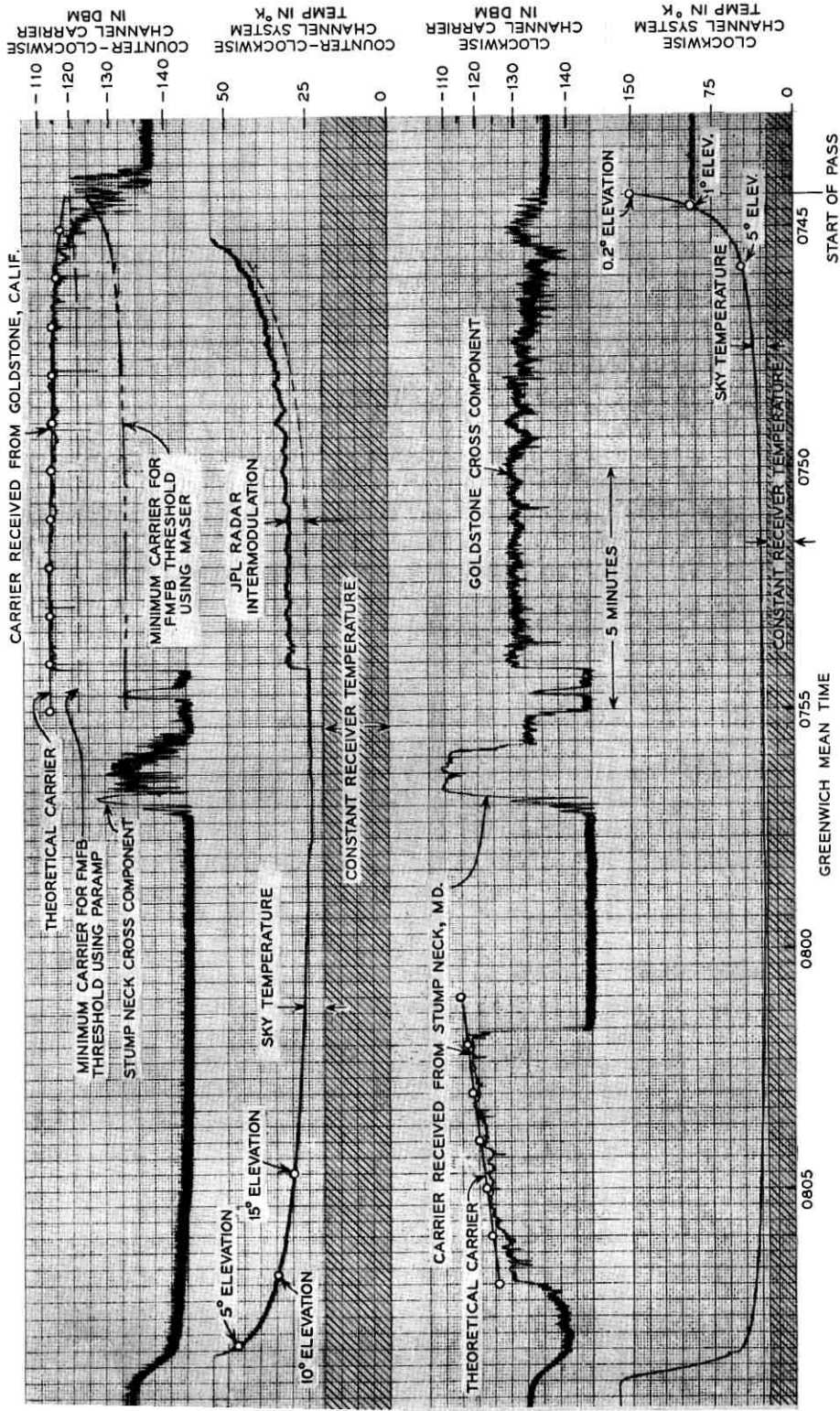


Fig. 4 — Typical receiver recordings (for Pass 60, August 17, 1960).

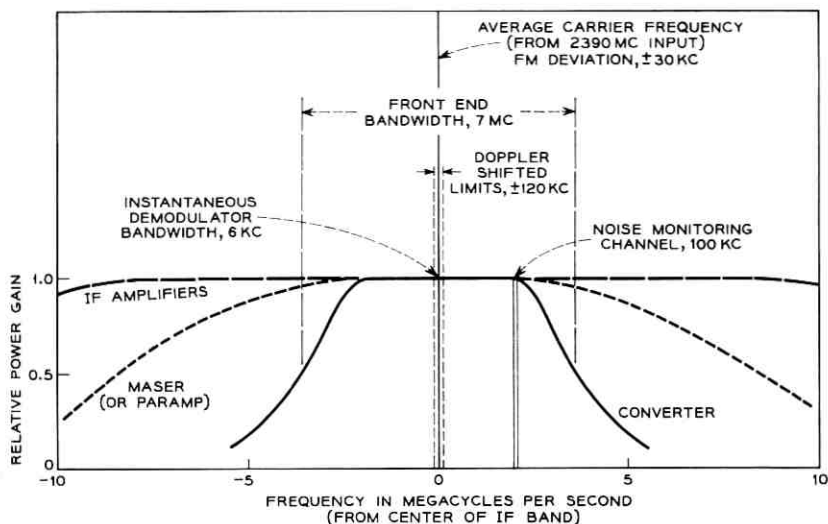


Fig. 5 — Receiver bandwidths.

shifts, occupy only a small portion of the “front-end” bandwidth, as shown in the center of Fig. 5; this permits the use of a simple circuit that can continuously monitor the system temperature while carriers are also being received. Assuming constant gain it can be shown that the output noise from any slice of the “front-end” bandwidth is proportional to the system temperature. In order to eliminate carrier interference, the noise temperature monitoring channel was chosen as far as practical from the carrier frequency, as is also shown in Fig. 5.

A second output of each IF transmission line is accordingly connected to a *system temperature monitor*, where the required selectivity is achieved with a very narrow-band IF amplifier. By following this with a precision square-law detector, a dc output voltage is obtained which is proportional to the system temperature. To calibrate this output voltage a known amount of excess noise from a standard noise lamp is added to the input waveguide via the 18-db directional couplers shown in Fig. 3. The resulting calibrated voltages, which indicate system temperature, are also shown in Fig. 4, where they are labeled “counter-clockwise channel system temperature” (second from top) and “clockwise channel system temperature” (bottom recording).

The *frequency counter* output was used to tune the FM demodulators in the presence of large Doppler shifts, and the *2B noise set* was used to verify the quality of the satellite system voice circuits.

Thus the useful receiver outputs are two audio circuits, one for each sense of circular polarization, and a set of four calibrated voltage records, which represent the received carrier powers and noise temperatures for each polarization. These recordings, also seen in Figs. 10 through 21 of Ref. 4, show how the west-to-east satellite system was operating at all times.

III. SYSTEM NOISE TEMPERATURE

The sky, antenna, waveguide, maser, and converter all made significant contributions to the system noise temperature. This section shows by the use of measurements, calculations, or reasonable estimates how much temperature was added by each of these sources. The sum of these temperatures is found to be in fair agreement with measurements of the over-all system temperature. Details of the over-all system measurements are given in Appendix B.

3.1 *Sky*

Since the background sky temperature, which varies with the antenna elevation angle, is always observed by a satellite-tracking antenna, it is necessary to include it as a part of the system noise temperature. As shown in the lower curve in Fig. 2, the sky temperature contribution (measured as shown in Appendix C) is only 2.3°K at the zenith but increases to 25°K when the antenna is lowered to a five-degree elevation. Thus, about 23°K must be added to the system temperature at the zenith in order to design a system which will work down to this elevation. Closer than this to the horizon the sky temperature increases even more rapidly, and as a result it becomes progressively more difficult to provide a system for satellite communications. Fortunately the higher temperatures are only present for a small portion of a pass as shown by the typical system temperature recordings of Fig. 4. Although communications cannot typically be maintained close to the horizon, this time can be well spent in acquiring the satellite and making preliminary carrier-level measurements.

Although there are additional isolated sources of sky temperature, they are not usually encountered during a satellite pass because they are few and far between. The sun, however, which has a temperature of 40,000°K at 3 kmc, can add about 4000°K via the main beam of the antenna. The added temperature is less than the sun temperature because the antenna beamwidth, about 1.25 degrees in this case, is greater than the angle subtended by the sun, which is 0.5 degree. The sun was also observed to add

from 5 to 20°K via various side lobes. Using the main beam, the hottest radio star, Cassiopeia A, was found to add 14.3°K, the moon about 16°K, and the center of the galaxy 4.5°K. Incidentally for a more uniform sky temperature reference, the antenna should be pointed about 14 degrees south of the zenith, a region traversed by fewer and cooler radio stars.

3.2 Antenna

The tracking horn antenna is described in a companion paper by Crawford, Hogg, and Hunt.⁵ It is similar to those used for microwave radio relay; its main advantage for a low-noise system is that the exceedingly low back and far side lobes* reduce interference, and are estimated to add only $2 \pm 1^\circ\text{K}$ to the system temperature. This estimate is based on the temperature "not otherwise accounted for" in a previous experiment;³ it is somewhat larger than the calculated temperature expected from back lobes measured on a similar antenna.

A second advantage is that a long waveguide run, which adds to the system temperature, is not required. A third advantage is that the way this antenna can be mounted⁵ makes it convenient to provide a shielded laboratory for the preamplifiers and associated receiving equipment.

3.3 Waveguide

The purpose of the waveguide assembly is to transmit the received circularly polarized energy from the antenna to the preamplifiers with the minimum amount of added noise. The waveguide assembly is shown in Fig. 3 and its general operation was described in Section II. Since each 0.1 db of insertion loss adds about 7°K to the system temperature, it was well worth while to minimize waveguide losses. Broadband components are used throughout in order to minimize the use of lossy tuning devices. The possibilities of significant resonance losses were eliminated by adjusting each component to have a return loss of 35 db or greater over a 100-mc bandwidth. In addition, all parts were made as short as practical. A summary of the loss of each waveguide component is given at the end of this subsection in terms of the equivalent increase in system temperature or "loss temperature." The particular source of this temperature, i.e., whether based on a measurement, calculation, or an

* Although the side lobes near the main beam are normal in size, they are usually pointed toward the cold sky, and therefore do not add much to system temperature. This is confirmed in Fig. 2 by the close agreement between the measured and theoretical sky temperatures. As can be seen the agreement is good from the zenith down to an elevation angle of only $1\frac{1}{2}$ degrees.

estimation of the insertion loss, is also indicated. The unique features of the waveguide assembly are discussed below.

3.3.1 Rotating Joint

The most important practical aspect of the waveguide assembly is the rotating joint, which allows the antenna to rotate in elevation while the rest of the receiver is connected solidly to the floor of the antenna cab. This, of course, eliminated the need for designing equipment to swing $\pm 45^\circ$ with the antenna elevation.

A cross section of the rotating joint is shown in Fig. 6. The purpose of the multiple chokes is to reduce the insertion loss and to drastically reduce leakage from the antenna cab calibration equipment into the receiver front end. Assuming a high (free-space) impedance at the outer edge, all lengths were adjusted to give the minimum impedance at the inner surface of the waveguide. L_1 , L_3 , and L_5 were found from Schelkunoff's analysis⁶ of cylindrical cavity resonators. As shown by Mum-

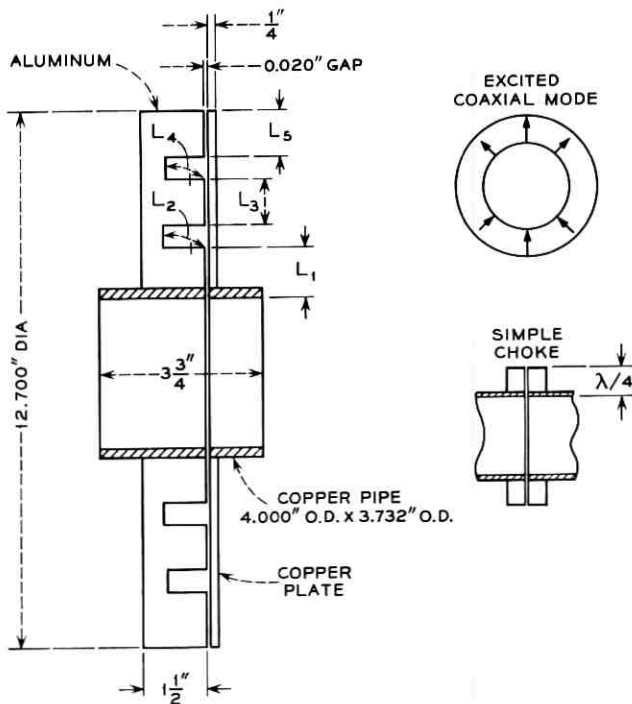


Fig. 6 — Rotating joint.

ford,⁷ the desired lengths are somewhat shorter than a quarter wavelength due to the greater capacitive loading at the smaller radii. L_2 and L_4 were adjusted to resonate with L_1 and L_3 assuming excitation of the TE_{01} coaxial mode,⁶ which is also shown in Fig. 6.

The total measured loss temperature of the rotating joint assembly is only $0.14 \pm 0.02^\circ\text{K}$, and the gap itself accounts for only about 0.05°K of this. For comparison purposes, the loss temperature of a simple choke, also shown in Fig. 6, is about 1°K using dominant-mode waveguide, and about 0.4°K using oversize waveguide which has a diameter of 1.4 wavelengths. It was also noted that the nominal 20-mil gap is adequate to allow for residual mechanical distortions of the supporting structure and that the loss temperature increased about 15 per cent due to 15-mil offsets of the rotating portion of the joint. These offsets are due to the slightly eccentric rotation of the antenna throat.

3.3.2 *Finline*

The waveguide assembly also acts as a circular polarization filter in that it separates the two senses of incident circular polarization. This action can be explained as follows. Any circularly polarized wave can be thought of as two linear waves at right angles in space and displaced 90° in time phase from each other, as shown at the top of Fig. 7. An observer at "A" would see a wave that rotates in the counter-clockwise direction. If wave #1 is retarded a quarter-wavelength or 90° with finline (or other) loading, a vertically polarized wave will result. Similarly, if #1 had been lagging #2, instead of leading, the observer at "A" would have seen a clockwise rotation. If #1 is now retarded 90° by the same finline, #2 and #1' will be lined up. The result is a horizontally polarized wave. Thus the counter-clockwise wave is transformed to vertical, and the clockwise wave to horizontal linear polarization by the 90° retardation of one linear component. This finline $\Delta 90^\circ$ component was designed with only a modest fin penetration, as shown at the bottom of Fig. 7, in order to keep the insertion loss low and to reduce the residual mismatch. The required match was achieved by dividing each fin taper length into three $\lambda_g/4$ segments and adjusting the slopes of these three consecutive segments to be in the ratio of $1:\sqrt{2}:1$ (this ratio was found empirically to give the best broadband match). The measured relative phase shift was 90 ± 1 degrees at 2390 mc. The power coupled from one channel to the other, due to the ± 1 degree tolerance, is down at least 40 db.

3.3.3 *Polarization Coupler*

The pertinent details are shown in Fig. 8. Because of the unique triangular plates the return loss of the "straight-through" polarization was

greater than 40 db over many octaves. There is some power cross coupled from one polarization to the other because of small mechanical asymmetries, but this is also down at least 40 db.

The polarization filter consists of the finline in combination with the adjacent polarization coupler oriented as shown in Fig. 3. After allowing for arbitrary phasing of the above couplings, and since the rotating joint and antenna throat are fairly symmetrical, it appears that the total power that can be coupled from one channel to the other (via the waveguide) must be down at least 34 db.

3.3.4 Antenna Throat

The cross sections of this taper were varied smoothly to give a "raised cosine" distribution of reflection coefficient per unit of waveguide wavelength. For the slopes of this antenna feed horn about three wavelengths

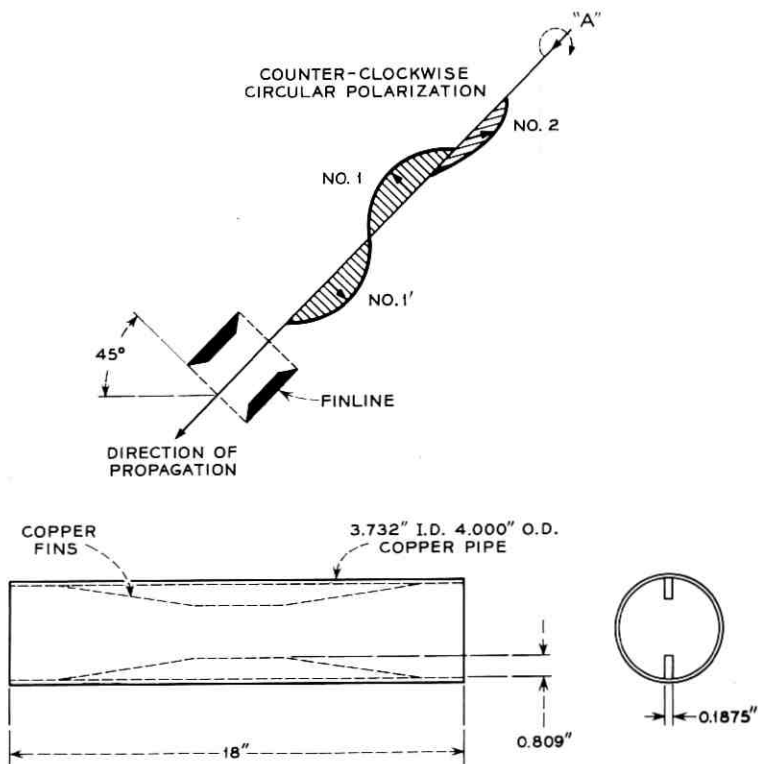


Fig. 7 — Finline 90° section.

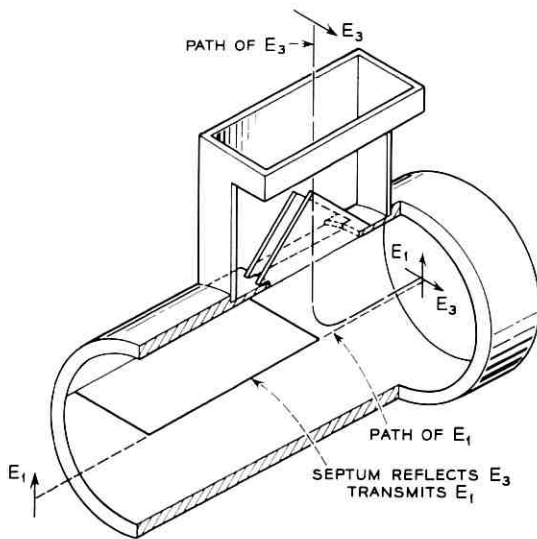


Fig. 8 — Polarization coupler.

are required to go from the constant impedance of free space to that of the dominant mode waveguide (a ratio of 1.7 to 1). Bolinder⁸ shows that the theoretical return loss for this length is a respectable 67 db. Therefore this well-matched electroformed throat turned out to have an excess length, i.e., beyond the apex of the antenna throat, of only one-half wavelength. Assuming an increased loss factor of 1.25 for surface roughness for electroformed copper,⁹ the temperature contribution of this component was calculated to be $0.33 \pm 0.05^\circ\text{K}$.

3.3.5 Waveguide-to-Coaxial Transducer

Because of its near-minimum attenuation constant, a 72-ohm characteristic impedance was chosen for the maser input coaxial line. The coaxial probe of this transducer was otherwise conventional, but it had to be carefully adjusted in length and location to achieve the lowest possible insertion loss. Another feature of this component is a new location for the maser vacuum seal. It was moved from a cold location in the coaxial line to the much warmer waveguide connecting flange in order to prevent increased loss from water condensation. The seal itself is an 11-mil sheet of Mylar cemented in a countersunk flange with a special adhesive. The outer wall of the coaxial line was connected to the transducer with a commercial flare fitting. This provided an excellent vacuum connection

when used with a thin soft-copper flared-washer seal and made it possible to disconnect the maser quickly for an emergency switch to the parametric amplifier.

3.3.6 Directional Coupler

The measured coupling of the conventional cross-guide coupler is 18.15 ± 0.15 db. It can be shown that the loss temperature, due to the insertion loss, can be calculated from

$$T^{\circ}\text{K} = \frac{290}{\log^{-1} \frac{\text{db}_{\text{coupling}}}{10}}$$

The loss temperature in this case is $4.45 \pm 0.15^{\circ}\text{K}$. When a parametric amplifier is used, an 18-db coupling is needed to add sufficient noise from an argon lamp for a system temperature measurement. Using a maser the coupling could be reduced to 27 db and the corresponding loss temperature would then be a less objectionable 0.7°K . For the Echo experiments it was decided to retain the 18 db-couplers in order to allow a faster switch to the standby parametric amplifiers.

The wall loss adds about $0.20 \pm 0.02^{\circ}\text{K}$ for a total loss temperature of $4.65 \pm 0.17^{\circ}\text{K}$.

3.3.7 Summary

The loss temperatures of many of the waveguide parts were calculated using the measured attenuation constants of the round and rectangular waveguides. These calculations include estimates, when necessary, for the somewhat higher insertion losses due to "greater than dominant mode" wall current densities. The loss temperatures of all the waveguide parts are summarized in Table I.

TABLE I — WAVEGUIDE SOURCES OF SYSTEM TEMPERATURE

Source	Counter-Clockwise Channel	Clockwise Channel	
Throat	$0.33 \pm 0.05^{\circ}\text{K}$	$0.33 \pm 0.05^{\circ}\text{K}$	calculated
Rotating joint	$0.14 \pm 0.02^{\circ}\text{K}$	$0.14 \pm 0.02^{\circ}\text{K}$	measured
Finline	$0.46 \pm 0.06^{\circ}\text{K}$	$0.46 \pm 0.06^{\circ}\text{K}$	calculated
Polarization coupler (bend)	$0.48 \pm 0.05^{\circ}\text{K}$	$0.48 \pm 0.05^{\circ}\text{K}$	measured
Polarization coupler (straight)	—	$0.23 \pm 0.04^{\circ}\text{K}$	calculated
Rectangular waveguide	$0.19 \pm 0.02^{\circ}\text{K}$	—	calculated
Directional couplers	$4.65 \pm 0.17^{\circ}\text{K}$	$4.65 \pm 0.17^{\circ}\text{K}$	calculated
E-plane bend	$0.25 \pm 0.03^{\circ}\text{K}$	—	calculated
H-plane bend	—	$0.27 \pm 0.03^{\circ}\text{K}$	measured
Waveguide-to-coaxial transducer	$0.50 \pm 0.25^{\circ}\text{K}$	$0.50 \pm 0.25^{\circ}\text{K}$	measured
Predicted total	$7.00 \pm 0.65^{\circ}\text{K}$	$7.06 \pm 0.67^{\circ}\text{K}$	

The total loss temperature of the waveguide could be reduced about 0.5°K by using higher conductivity copper (which is commercially available) in place of red brass (which was used for the rectangular parts) and impure copper (which was used for the round parts).

3.4 *Maser*

This low-noise preamplifier assembly is described in a companion paper by DeGrasse, Kostelnick, and Scovil.¹⁰ It had the ability to amplify the incoming carrier and noise more than 36 db without adding more than 8°K to the system temperature. The large gain was required in order to reduce greatly the system temperature contribution from the following converter. The gain was also very stable, an important factor in keeping the receiving system properly calibrated. The variation during a half-hour period, from the initial input carrier level calibration before a satellite pass until the recheck after the pass, was typically only a few tenths of a decibel.

3.5 *Converter*

Since the converter system temperature contribution (referred to the amplifier input) is the converter temperature reduced by the net gain from the input, a low noise figure was required. Since the maser saturation threshold occurs at an output level of -40 dbm, low leakage from the local oscillator was also desirable. To meet these requirements a balanced converter using 1N263 diodes was designed by R. H. Turrin. It had a noise figure of 7.5 db (1300°K) and local oscillator leakage power on the order of -20 dbm. The leakage power was further reduced to -47 dbm with a coaxial isolator. Since the additional loss between the maser and converter was 2.3 db (1.35 db for interconnecting coax, 0.75 db for the isolator, and 0.2 db for a monitoring directional coupler) and the maser gain was 36.3 db, the net gain from the input was reduced to 34 db. The converter system temperature contribution was therefore calculated to be $0.6 \pm 0.15^{\circ}\text{K}$. The limits are due mainly to measured day-to-day changes of the maser gain.

3.6 *Total System Temperature*

A rough idea of the total system temperature was found by adding together the contributions of all of the known sources, as shown in Table II.

The total system temperature was also measured by using the noise-lamp technique which is discussed in Appendix B. Using this method

TABLE II — SOURCES OF SYSTEM TEMPERATURE

Source	Temperature
Sky (at zenith)	$2.30 \pm 0.20^\circ\text{K}$
Horn antenna	$2.00 \pm 1.00^\circ\text{K}$
Waveguide (counter-clockwise channel)	$7.00 \pm 0.65^\circ\text{K}$
Maser assembly	$7.00 \pm 1.00^\circ\text{K}$
Converter	$0.60 \pm 0.15^\circ\text{K}$
Predicted total system temperature	$18.90 \pm 3.00^\circ\text{K}$

the temperature was found to vary a few degrees from day to day, but the lowest temperature was consistently $22.2 \pm 2.2^\circ\text{K}$. By realistically assuming that all sources were then contributing their fair share (as is also tacitly assumed in Table II) it is possible to improve the over-all accuracy. The actual system temperature must be in the overlap region of the measured results and the total results of Table II, namely between 20 and 21.9°K . The most likely minimum system temperature was therefore

$$T_{\text{system}} = 21 \pm 1^\circ\text{K}.*$$

The inference from this result is that the “+” temperature possibilities of Table II must predominate.

3.7 Parametric Amplifier

This fairly low noise “standby” preamplifier is described in a companion paper by Kibler.¹¹ The receiving system was designed so that the “paramp” could be switched into the system, tuned, and calibrated in about 15 minutes. The chief effect of using it in place of the maser was to increase the minimum system temperature to 290°K . The resulting temperatures for all angles of antenna beam elevation are shown by the upper curve in Fig. 2. The paramp gain usually decreased about a decibel during a pass, and this turned out to be a limiting factor in the received carrier calibration accuracy.

IV. FM DEMODULATOR AGC CHARACTERISTICS

The FM features of the demodulator are discussed by Ruthroff.² The purpose of this section is to show how the AGC voltage features were exploited in order to obtain accurate recordings of the 2390-mc received carrier power.

A simplified block diagram of the FM demodulator (Fig. 3 of Ref. 2) shows that there are two feedback loops, one for FM, and the other for

* $17.25 \pm 1^\circ\text{K}$ without the paramp standby provision, i.e., with a 27 db waveguide directional coupler in place of the 18 db coupler.

AGC. The purpose of the FM loop is to make the VCO frequency track the FM deviations of the input carrier. The primary purpose of the AGC loop is to keep the 1.2-mc carrier amplitude at the limiter input fairly constant over a wide range of input power. The secondary purpose is to calibrate the AGC voltage as a function of known 2390-mc input carriers and, conversely, deduce the input levels from AGC voltages generated by the actual received carriers.

Since the AGC voltage is derived from the amplitude of the carrier and/or AM noise in the path common to both feedback loops, it is also a function of the FM demodulation process. It turns out that the maximum AGC voltage is always obtained where the FM demodulator is "tuned" by properly adjusting the VCO frequency. For strong carriers it was found that the audio circuit quality was always improved by maximizing the AGC voltage; and for weak carriers, i.e., those below the FM threshold, it was found that erratic AGC voltages could be readily maximized by using audio quieting as a tuning aid.

A practical feature of the demodulator was that all tuning was readily accomplished with a single control. This made it possible to calibrate just before and after each pass to decrease long-term drift errors. Aided by the VCO frequency counter, this also made it possible to acquire readily and track accurately the received carriers despite Doppler shifts of ± 90 kc. The feeling from this experiment was that automatic frequency tracking could and should be provided for future satellite receivers.

A typical FM demodulator AGC characteristic is shown in the right-hand curve of Fig. 9. The known 2390-mc carriers were inserted via the waveguide couplers after the input noise was minimized by pointing the antenna toward the zenith. For reference, the curve on the left in Fig. 9 is an AGC characteristic which was obtained by using equivalent 70-mc carriers that were essentially noise-free. As can be seen, the net gain from the "front end" was adjusted to utilize the region of highest AGC voltage. This placed the AGC "voltage range of interest" in the most linear portion as shown on the right, and this also gave the most nearly constant amplitude at the limiter input. The 2390-mc AGC characteristic is identical to the noise-free reference for carrier levels well above the threshold. As the 2390-mc carrier is decreased below the threshold the AGC characteristics begin to diverge. The reason for this is the FM loop loses control, which intermittently detunes the receiver. For a correct average VCO tuning and an unmodulated received carrier the AM noise increases, and this in turn increases* the AGC from the "noise-free" case in a known reproducible way, as shown by the right-hand curve in Fig. 9. As the

* Modulated carriers will decrease the AGC voltage somewhat.

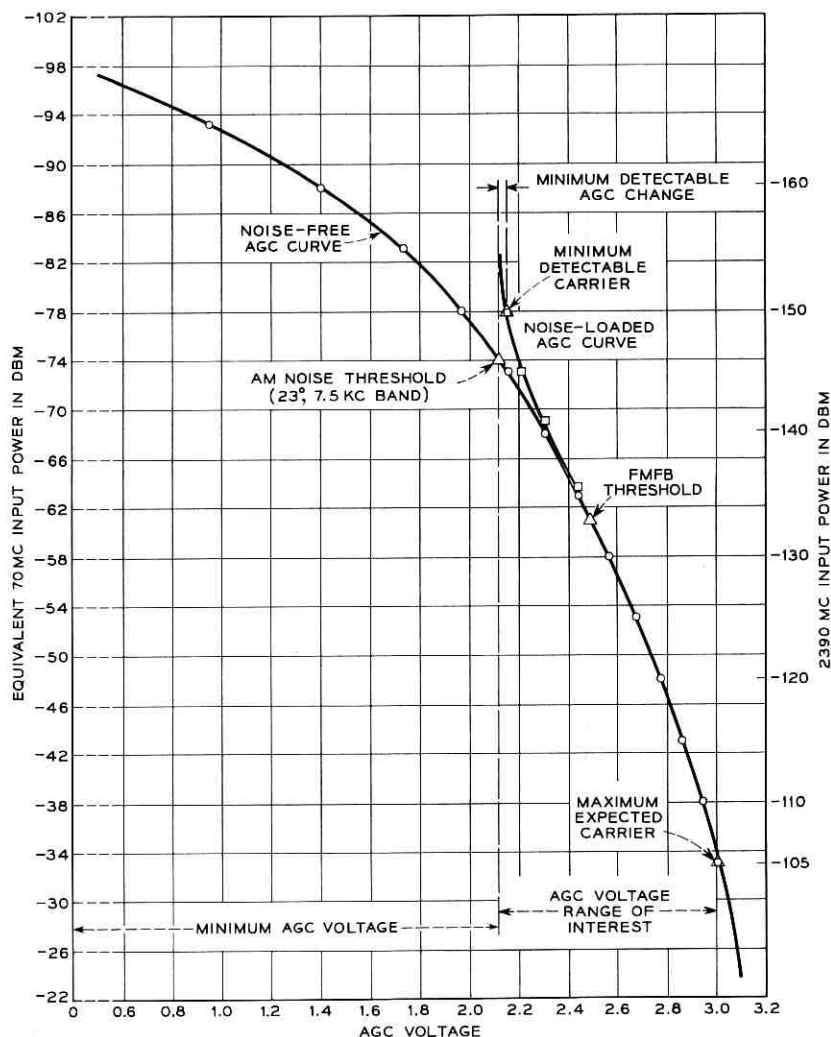


Fig. 9 — FMFB demodulator AGC characteristics.

2390-mc input is decreased well below the threshold a minimum AGC voltage is reached as shown by the sharp vertical rise of the right-hand curve in Fig. 9. This limit is due to noise power from the front end; it will now be calculated. Since the FM feedback is ineffective at these levels the demodulator acts like an AM detector. The noise bandwidth of the demodulator AGC circuit is given by the bandwidth when the FM loop

is open² and is only 7.5 kc. For a 23°K system temperature the limiting noise power is -146 dbm. As in other AM systems, a somewhat smaller carrier will cause an observable change in the AGC voltage and, as shown in Fig. 9, the minimum detectable carrier for this demodulator was -150 dbm. The significance of this was that the carrier could be detected and measured down to the horizon and the cross component could be readily monitored during most of each pass.

The AGC "voltage range of interest" of Fig. 9 was attenuated somewhat and back-biased in order to use the total recorder chart area as shown by the top recording of Fig. 4. The 2390-mc input carrier power calibrations are shown on the right-hand edge. The over-all calibration accuracy was limited mainly by uncertainties of the input carrier powers, and is estimated to be within 0.5 db of nominal. The time constant of the AGC circuit was about 0.02 second; since the typical fades were much slower, none of the fading rates shown on any of the AGC recordings was limited by the recording equipment.

In addition to the received carrier measurements some noise measurements were made with the over-all receiving system in order to verify the audio FM demodulator characteristics. Since the threshold carrier-to-noise power (referred to a 6-kc band) is 14 db and the average temperature at the zenith, 23°K, the minimum threshold carrier power was calculated to be -133 dbm. The actual threshold carrier was found by noting the minimum calibration power required to avoid "popping" in the audio circuit when the antenna was pointed toward the zenith. This turned out to be -133 dbm, as expected.

The quality of the audio circuit was verified as follows. Shortly *before* a pass a 70-mc FM test oscillator was temporarily connected to the demodulator input. The carrier level was set equal to that anticipated from the satellite system. The FM (sine wave) deviation was set at the maximum allowed by the demodulator, and the corresponding maximum audio power was measured at the output with a 2B noise set. The audio output noise from the received unmodulated carrier was then measured *during* the pass. These results were combined to give a reasonable indication of the signal-to-noise ratio. The carrier of the corresponding carrier-to-noise ratio was found from the calibrated AGC voltages, and the noise power (referred to a 6-kc band) was calculated from the observed system temperature. The resulting signal-to-noise ratio versus carrier-to-noise ratio was plotted and found in good agreement with previous laboratory results, as well as with the results predicted from FM theory, all shown in Fig. 27 of Ref. 4.

The main characteristics of the receiver are summarized in Table III.

TABLE III — OVER-ALL RECEIVER CHARACTERISTICS

Nominal frequency	2390 mc
Two channels	One for each sense of circular polarization
RF cross coupling (between channels)	-34 db
Audio bandwidth (each channel)	0.2 to 3 kc
Maximum FM deviation	± 30 kc
Minimum system temperature	$21 \pm 1^\circ\text{K}^*$
Minimum threshold carrier power	-133 dbm
Minimum detectable carrier power	-150 dbm
Carrier calibration range	-110 dbm to -150 dbm
Time constant of carrier recordings	0.02 second
Carrier calibration accuracy	From ± 0.5 db above threshold to ± 2 db well below threshold

* $17.25 \pm 1^\circ\text{K}$ without a paramp standby provision.

V. EXPERIMENTAL RESULTS

The main experimental results, which include complete data of the west-to-east satellite systems, are given by the four-channel pen recordings shown in Figs. 10 through 21 of Ref. 4. Two high-quality voice circuits, with signal-to-noise ratios greater than 36 db, were also available from the receiver whenever the resulting ratio of received carrier-to-noise power (referred to a 6-kc band) exceeded 14 db. These experimental results are shown in Fig. 27 of Ref. 4.

A locus of the minimum carrier level required during a typical pass (for the critical 14-db carrier-to-noise ratio) is shown in the top recording of Fig. 4. For convenience, this is superimposed on a recording of a carrier received from Goldstone under good tracking conditions. The minimum carrier level required using a paramp instead of a maser is also shown. These plots verified the fact that a good voice circuit could be achieved using the paramp under modest carrier fading conditions (which are shown) and that the fading margin for a good voice circuit using the maser was about 16 db over most of a pass. (This is significant, since the consistent maximum fading due to the balloon* turned out to be only 10 db.)

After accounting for some known transmitter, refraction, and tracking errors, the calibrated carrier level recordings verified that the entire communication system was working properly, and that the path losses were characterized by the propagation laws of free space. The recordings also measured the random variations that occurred during every operational pass and the random decreases in average level that occurred from pass to pass.

* Shown in Pass 1086, after 0944 GMT (Fig. 20 of Ref. 4).

Certain observed characteristics of the carrier level recordings were also used to identify some otherwise unknown transmitter tracking errors. The key characteristics were (a) a much more jagged than normal carrier level recording, especially in conjunction with a lower than normal average level;* (b) an anomalous increase in carrier level adjacent to a gross pointing error;† and (c) a period of decreased main carrier level, with simultaneous increase in the average cross-component level.‡ These additional clues made it possible to eliminate some questionable data in order to evaluate more accurately the reflection characteristics of the balloon.

The recorded system temperatures verified that the background sky temperature varied as anticipated, and that the isolated sources of large sky temperature were seldom encountered. The temperature recordings also showed that other sources, such as lightning, clouds, nearby radars, and radio stars occasionally added only a few degrees to the system temperature.

VI. ACKNOWLEDGMENTS

There were several people, in addition to those already mentioned, who made significant contributions to this receiver. The complex assembly and testing, in particular, could not have been accomplished on schedule without the timely and generous aid of W. W. Snell, who rendered alert, critical assistance, and H. A. Anderson, who ingeniously solved many of the complicated installation problems. Other timely aid was provided by H. E. Keller, who tuned the waveguide parts, F. A. Dunn, who constructed and tested the very-narrow-band IF amplifiers, R. A. Semplak, who provided the crystal-controlled local oscillator, R. H. Turrin, who designed the crystal converters and tuned the antenna slipping assembly, and W. E. Legg, who assembled the RF generator needed to "pump" the maser. The precision square-law detectors (with large output voltages), the precision system temperature measurements (needed to determine the sky temperature), and the automatic nitrogen transfer system are all due to W. W. Snell. Aid in operating the receiver was provided by E. L. Frantsvog (helium transfers), R. A. Desmond (calibration), and W. F. Bodtmann (FM demodulator tuning). After the Echo I experiments were concluded, the waveguide losses were precisely measured by G. S. Axeling.

Although this equipment was designed by the Bell System as part of

* Shown in Pass 1086, prior to 0944 GMT (Fig. 20 of Ref. 4).

† See Pass 229 at 0453:30 GMT (Fig. 15 of Ref. 4).

‡ See Pass 60 at 0756:50 GMT (Fig. 4 of this paper).

its research and development program, it was operated in connection with Project Echo under Contract NASW-110 for the National Aeronautics and Space Administration.

APPENDIX A

Front-End Tuning

In order to maintain the low inherent system temperature and calibrate the receiver before and after each satellite pass, a fast, easy-to-use measuring system was required. Such a system was interconnected to both channels of the receiver; the connections to a single channel are shown in Fig. 10. Front-end RF test signals were generated in the antenna cab and inserted into the receiver via an 18-db waveguide directional coupler. The IF results were then readily monitored and/or measured via a permanently installed IF coupling network.

All required signal levels were achieved by attenuating a known reference power with coaxial attenuators, as shown in the lower left of Fig. 10. Since the calibrated input carriers were as low as -150 dbm, shielding precautions were required to reduce RF leakage from the test equipment to the input waveguide. Some highly effective features were the multiple

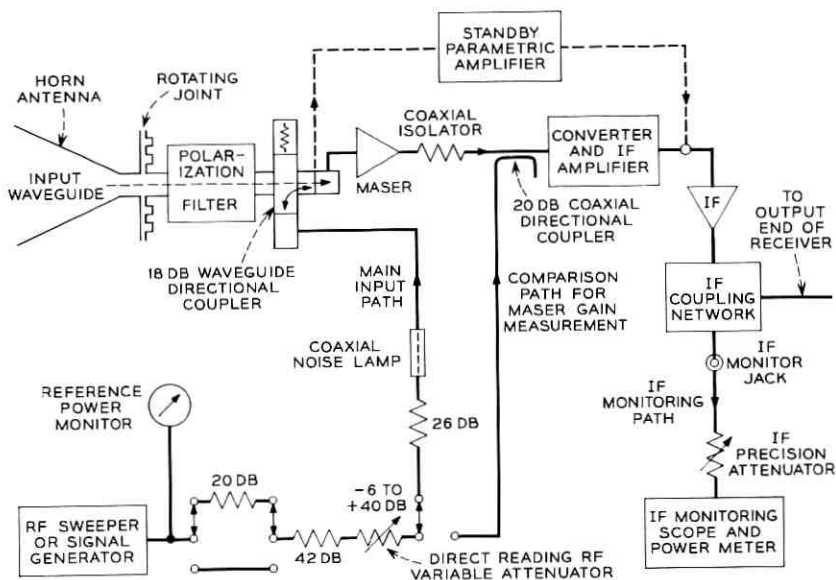


Fig. 10 — Front-end measuring system.

chokes used around the waveguide rotating joint and the well-shielded General Radio connectors used for coaxial attenuator switching. The attenuator values were selected to prevent (after proper switching) erroneous results due to saturation effects or poor carrier-to-noise ratios. The selected values also allowed the use of a direct-reading General Radio RF attenuator for the entire input carrier calibration range.

The first tuning step was to optimize the bandpass characteristic of the maser or the paramp, using a swept signal well above the noise. The maser gain was then found by comparing the known input carrier power with that required when it was inserted after the maser (via the permanently installed 20 db coaxial directional coupler). The monitored IF power was held constant for this measurement. Alternatively, the paramp gain was found by inserting a known input carrier and comparing this to the 70-mc power at the IF monitoring jack. After achieving the normal gain and frequency range the system temperature was checked as shown in Appendix B. The final step was to furnish known input carriers to calibrate the AGC voltages (about 10 minutes before each pass). As again can be seen in Fig. 10, this was done by simply adjusting the direct-reading RF attenuator when the fixed attenuators were connected as shown.

APPENDIX B

System Temperature Measurements

After the antenna had been pointed toward the zenith, data for the system temperature were found by coupling excess noise from an argon noise lamp into the input waveguide as shown in Fig. 10 and then measuring the increase in IF output power. The system temperature was then calculated from

$$T_{\text{system}} = \frac{T_H L_{\text{coax}} L_{\text{coupler}}}{Y - 1},$$

where T_H is the excess noise at the output terminal of the coaxial noise lamp, L_{coax} is the insertion loss between the noise lamp and the directional coupler, L_{coupler} is the coupling loss of the waveguide directional coupler, and Y is the ratio of lamp "on" to lamp "off" power at the IF monitor jack. T_H was calculated¹² using the measured³ electron temperature of a similar argon lamp ($10,500 \pm 265^\circ\text{K}$ at 6 kmc), and the measured insertion losses (15.5 db "on" and 2.4 db "off") for this particular coaxial noise lamp mount. The result was $T_H = 8360 \pm 225^\circ\text{K}$. The measured insertion loss of the coaxial line was 1.31 db and the measured coupling

of the directional coupler was 18.15 ± 0.15 db. Therefore the total excess temperature coupled into the waveguide, T_{coupled} , was $94.6 \pm 6^\circ\text{K}$, and

$$T_{\text{system}} = \left(\frac{94.6 \pm 6}{Y - 1} \right) ^\circ\text{K}.$$

Using a paramp, the observed values of Y varied from 1.30 to 1.35. The corresponding paramp system temperatures are 270 and 315°K . Using a maser, Y was typically about 5 and therefore the maser system temperature was about 23°K . A 27-db coupler could have been used instead of the 18-db coupler to reduce Y to a still acceptable value of 1.65. This would also have reduced the system temperature 3.75°K . For the paramp, however, Y would then have been too small for a meaningful measurement. The 18-db couplers were therefore retained in service to provide a standby measuring technique for the paramp system temperature. The resulting system temperatures for other antenna beam elevations are shown in Fig. 2.

APPENDIX C

Sky Temperature

Since the sky temperature seen by a narrow beam antenna is proportional to the length of antenna beam passing through each layer of atmosphere, the sky temperature at the zenith, whatever its value, will approximately double when the antenna beam is lowered to an elevation of 30 degrees. It will redouble at 14.5 degrees, quadruple at 7.2 degrees, etc., as given by

$$T_{\text{sky at } \theta} \cong \frac{T_{\text{sky at } \theta_z}}{\sin \theta} \quad \theta > 5^\circ, \quad (1)$$

where θ is the elevation of the antenna beam above the horizon and θ_z is an elevation of 90° . It turns out that only a narrow range of sky temperatures, when doubled, redoubled, etc. (and added to a constant), will match the observed maser system temperatures. Following this restraining principle, it can be shown that the sky temperature at the zenith can be determined from the maser system temperatures and the theoretical ratio, N , of $T_{\text{sky at } \theta}$ to $T_{\text{sky at } \theta_z}$. This result is given by

$$T_{\text{sky at } \theta_z} = \frac{T_{\text{system at } \theta} - T_{\text{system at } \theta_z}}{N - 1}, \quad (2)$$

where N , derived from (1), is given by

$$N = \frac{T_{\text{sky at } \theta}}{T_{\text{sky at } \theta_z}} \cong \frac{1}{\sin \theta}. \quad (3)$$

For improved accuracy, more exact values of N which take into account the curvature of the earth's atmosphere should be used (these ratios can be found from the results of a theoretical derivation of sky temperature¹³); random experimental limits should be allowed for; and the required use of zenith system data should be eliminated. A more general form of (2) was therefore derived which allows these advantages:

$$T_{\text{sky at } \theta_z} = \frac{\left(\frac{T_{\text{max at } \theta} + T_{\text{min at } \theta}}{2} \right) - \left(\frac{T_{\text{max at } \theta_0} + T_{\text{min at } \theta_0}}{2} \right)}{N_\theta - N_{\theta_0}}, \quad (4)$$

where T_{max} and T_{min} are the respective temperature limits (after allowing for random experimental errors) for two elevations, θ and θ_0 ; and N_θ and N_{θ_0} are the theoretical sky temperature ratios, defined in (3), for these two elevations. For greatest accuracy, many different combinations of θ_0 and θ (chosen to be widely separated) must be used and great care must be exercised to allow for random increases in system temperature due to the antenna side lobes.

It can also be shown that the limits of the sky temperature are given by

$$\Delta T_{\text{sky at } \theta_z} = \pm \frac{\left(\frac{T_{\text{max at } \theta} - T_{\text{min at } \theta}}{2} \right) + \left(\frac{T_{\text{max at } \theta_0} - T_{\text{min at } \theta_0}}{2} \right)}{N_\theta - N_{\theta_0}}.$$

By selecting measured maser system temperatures from Fig. 2 for many pairs of elevation angles down to 5° , the sky temperature at the zenith was found to be

$$T_{\text{sky}} = 2.30 \pm 0.2^\circ\text{K}.$$

This was in good agreement with the theory, which had predicted a value of 2.4°K .

APPENDIX D

Liquid Nitrogen

The outer dewar of the maser had to be kept cold with liquid nitrogen and, due to "boil-off," the liquid in the dewar had to be replenished

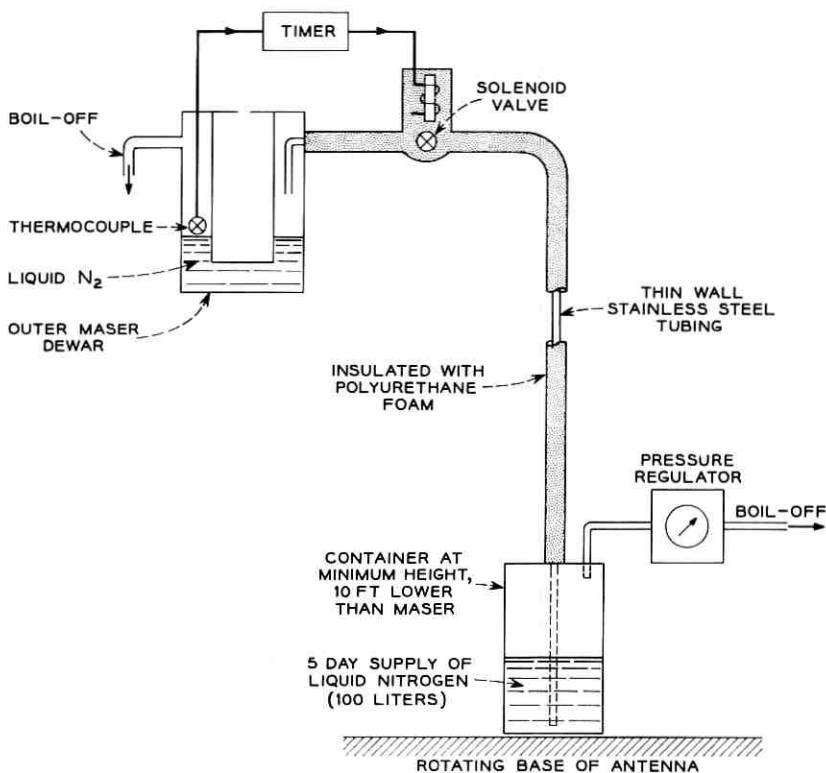


Fig. 11 — Automatic liquid nitrogen transfer system.

every 12 hours. Fig. 11 shows how batches of liquid were automatically supplied for periods of five days. Since it was too heavy and bulky to go into the antenna cab, the 100-liter supply container was located on the rotating base of the antenna. The boil-off losses of the resulting long transfer line were kept within reason by using thin wall stainless steel tubing surrounded by an insulating foam.

The sensing device of the system was a thermocouple furnished in the outer maser dewar which sent a signal to the timer when liquid was required. The timer kept the solenoid valve open just long enough to fill the dewar. The liquid was pumped through the open solenoid valve at a predictable rate by the storage container "back pressure." This was stabilized by the pressure regulator, which could also adjust the back pressure for different flow rates.

Although preliminary cooling of the line (and valve) during the trans-

fer process boiled off some nitrogen, changing of output flow from warm to cold gas and then increasing quantities of liquid greatly reduced the thermal shock on the dewar. This system, designed and built by W. W. Snell, is highly recommended for automatic nitrogen servicing.

APPENDIX E

Liquid Helium

In order to operate the maser, the inner maser dewar had to be cooled with liquid helium.

Because liquid helium has an extremely low temperature and a low specific heat, special vacuum-insulated storage and handling facilities were required to prevent excessive "boil-off" losses. The resulting storage containers were therefore quite heavy and the liquid had to be "transferred" (from storage to another dewar) in batches via vacuum-insulated transfer lines.

For daily maser operations large quantities of liquid were required, and these could not be supplied locally. The necessary amounts were accordingly shuttled every fourth day from Tonawanda, New York, in two special 100-liter containers. This type of "super-insulated" container was selected because it could conveniently supply the maser for four days from a platform on the rotating base of the antenna. This eliminated the need for daily heavy lifting, and indeed all lifting, since the platform could be easily reached by truck. Another convenient feature of this container was that liquid nitrogen servicing was not required. As a result, the container was relatively light (for its capacity) and one person could easily load it on the antenna.

The helium transfer system is shown in Fig. 12. The transfer line was flexible, so that it could be easily connected to the storage containers on the lower end (this starts the transfer) and easily inserted into the maser dewar on the other (after the line was very cold). The liquid was pumped by storage container back pressure. The rate of liquid flow into the line was monitored by watching the scale weight, and the boil-off rate was monitored by watching the flow meter. If these readings were abnormal the transfer was stopped (by disconnecting from the storage container) to find the source of trouble. Otherwise, the transfer was continued until the scale reached a predetermined cutoff weight.

The cutoff weight was a function of the initial weight of the container and the length of time it was desired to operate the maser. The operating times for different quantities of liquid (from the storage container) are

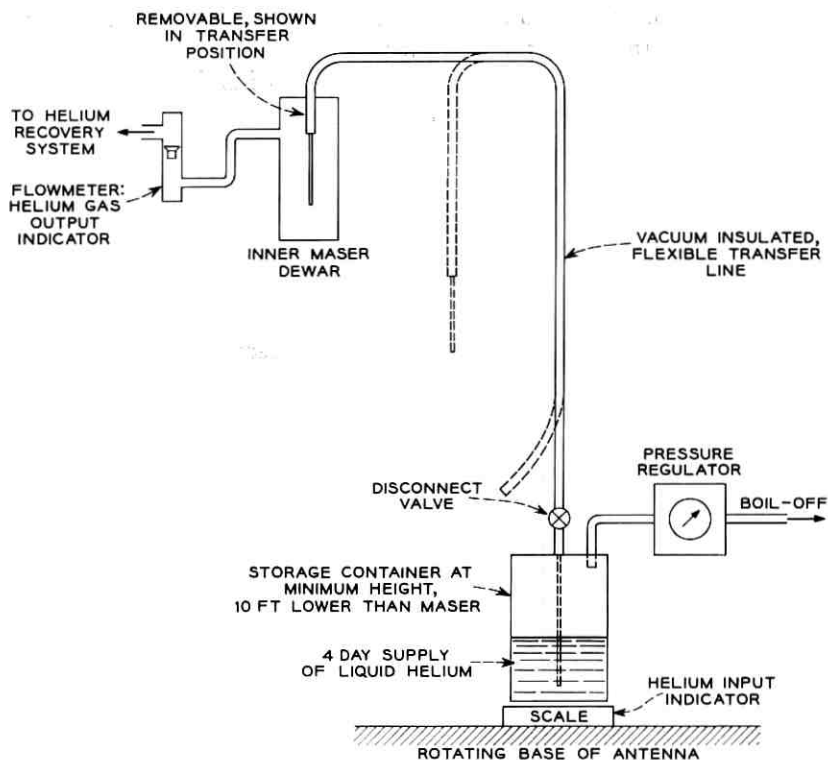


Fig. 12 — Liquid helium transfer system.

shown in Fig. 13. As can be seen, these are also a function of the initial temperature of the dewar. The maximum operating time was over 18 hours, well in excess of the 12 hours required for a series of Echo passes. For daily transfers 12 hours could be obtained using only 14 liters of liquid. The normal objective, which included a 1-liter safety factor, was 15 liters. Since the corresponding weight was $4\frac{1}{4}$ pounds, the normal cutoff weight of the storage container was selected to be about $4\frac{1}{4}$ pounds less than its initial weight.

After the transfer was completed the transfer tube was removed from the maser (to eliminate the tube as a heat leak), and the aperture was sealed with a stopper. The liquid helium in the maser dewar was then "pumped down" (with a vacuum pump) to reduce the maser temperature still further. The pressure declined smoothly until the "lambda" pressure was reached; it then declined at a much slower rate. By noting

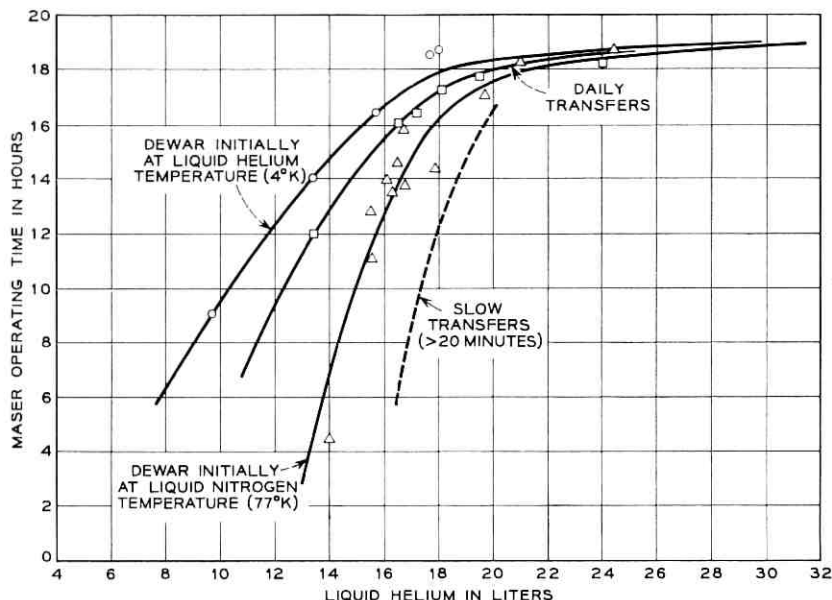


Fig. 13 — Liquid helium required vs. maser operating time.

the time from the start of the pump down to the lambda point and comparing this with previous data, the maser running time could be reliably predicted to within a half hour or so. The vacuum pump, incidentally, was located at the base of the antenna in order to rid the cab of its noise and vibration.

Since the receiver was planned during a period of helium shortage, a gas recovery system was included as a conservation measure. The boil-off from the helium transfer and the exhaust from the vacuum pump were piped to the recovery system (in a nearby building) via a rotating joint on the vertical axis of the antenna mount. Although the integrated boil-off rate exceeded the storage and compression capacity by a large factor, the excess time was short, and 75 per cent of the available gas could be recovered and purified.

REFERENCES

1. Ruthroff, C. L., and Jakes, W. C., Jr., System Calculations, this issue, p. 1029.
2. Ruthroff, C. L., FM Demodulator with Negative Feedback, this issue, p. 1149.
3. DeGrasse, R. W., Hogg, D. C., Ohm, E. A., and Scovil, H. E. D., Ultra-Low-Noise Antenna and Receiver Combination for Satellite or Space Communication, Proc. Nat. Elect. Conf., **15**, 1959, p. 370.

4. Jakes, W. C., Jr., Participation of Bell Telephone Laboratories in Project Echo and Experimental Results, this issue, p. 975.
5. Crawford, A. B., Hogg, D. C., and Hunt, L. E., A Horn-Reflector Antenna for Space Communication, this issue, p. 1095.
6. Schelkunoff, S. A., *Electromagnetic Waves*, D. Van Nostrand Co., New York, 1957, pp. 269, 260, 390, 327.
7. Mumford, W. W., unpublished manuscript.
8. Bolinder, E. F., Fourier Transforms in the Theory of Inhomogeneous Transmission Lines, Trans. Royal Inst. Tech., Stockholm, No. 48, 1948.
9. Beck, A. C., and Dawson, R. W., Conductivity Measurements at Microwave Frequencies, Proc. I.R.E., **38**, 1950, p. 1181.
10. DeGrasse, R. W., Kostelnick, J. J., and Scovil, H. E. D., 2390-mc Traveling-Wave Masers, this issue, p. 1117.
11. Kibler, L. U., Standby Receiver System, this issue, p. 1129.
12. White, W. D., and Greene, J. G., On the Effective Noise Temperature of Gas Discharge Noise Generators, Proc. I.R.E., **44**, 1956, p. 939.
13. Hogg, D. C., Effective Antenna Temperatures Due to Oxygen and Water Vapor in the Atmosphere, J. Appl. Phys., **30**, 1959, p. 1417.

PROJECT ECHO

A Horn-Reflector Antenna for Space Communication

By A. B. CRAWFORD, D. C. HOGG and L. E. HUNT

(Manuscript received April 7, 1961)

This paper describes the mechanical features of the horn-reflector antenna used for receiving signals reflected from the Project Echo balloon satellite and presents in some detail the electrical characteristics (radiation patterns and gain) measured at a frequency of 2390 mc. Theoretically derived characteristics which agree very well with the measurements are also presented; details of the calculations are given in the appendices.

I. INTRODUCTION

The horn-reflector type of antenna was originated at Bell Telephone Laboratories, Holmdel, New Jersey, in the early 1940's¹ and is now in extensive use in the Bell System's transcontinental microwave relay network.² It is a combination of a square electromagnetic horn and a reflector that is a sector of a paraboloid of revolution, as illustrated in Fig. 1. The apex of the horn coincides with the focus of the paraboloid. Since the antenna design is based on geometrical optics and has no frequency-sensitive elements, it is extremely broadband; it is not polarization-sensitive and can be used in any linear or circular polarization. The antenna is essentially an offset paraboloidal antenna, so that very little of the energy incident on the reflector is reflected back into the feed to produce an impedance mismatch. Due to the shielding effect of the horn, the far side and back lobes are very small.

These features, together with high aperture efficiency, make the horn-reflector attractive for use in satellite communication systems. In particular, the low side and back lobes insure that when the antenna beam is pointed to the sky very little noise power is received from the ground;* the antenna is thus a low-noise transducer which permits exploitation

* A discussion of the noise properties of antennas is given in Ref. 3.

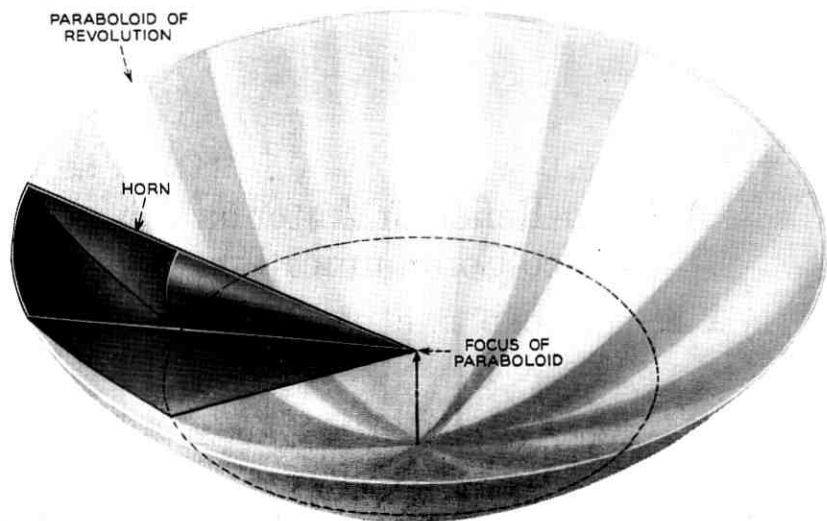


Fig. 1 — Sketch showing relationship of horn-reflector antenna to a paraboloid of revolution.

of the low-noise features of the maser amplifier. An effective noise temperature of about 2°K has been measured for the horn-reflector type of antenna.⁴

II. MECHANICAL DESCRIPTION OF THE ANTENNA

Fig. 2 is a photograph of the horn-reflector antenna erected on the Crawford Hill site of the Holmdel Laboratory and used in the Project Echo experiment.* To permit the antenna beam to be directed to any part of the sky, the antenna is mounted with the axis of the horn horizontal. Rotation about this axis affords tracking in elevation while the entire assembly is rotated about a vertical axis for tracking in azimuth. The antenna is about 50 feet in length, the radiating aperture is approximately 20 by 20 feet, and the weight is about 18 tons. The structure was designed to survive winds of 100 miles per hour.

The elevation structure, both horn and reflector, is constructed of aluminum. The elevation wheel, 30 feet in diameter, supports all radial loads and rotates on rollers mounted on the base frame. All axial or thrust loads are taken by a large ball bearing at the apex end of the

* Although this antenna was designed and constructed by the Bell System as part of its research and development program, it was operated in connection with Project Echo under Contract NASW-110 for the National Aeronautics and Space Administration.

horn. The horn proper continues through this bearing into the equipment cab. Here is located a tapered transition section from square to round waveguide, a rotating joint, and waveguide take-offs which provide for the simultaneous reception of either two orthogonal linearly polarized signals or two circularly polarized signals of opposite sense. The ability to locate the receiver equipment at the apex of the horn, thus eliminating the loss and noise contribution of a connecting line, is an important feature of this antenna.

The triangular base frame is constructed of structural steel shapes. It rotates on wheels about a center pintle ball bearing on a track 30 feet in diameter. The track consists of stress-relieved, planed steel plates which were individually adjusted to produce a track flat to about $\frac{1}{64}$ inch. The faces of the wheels are cone-shaped to minimize sliding friction. A tangential force of about 100 pounds is sufficient to start the antenna in motion.

The horn flares at an angle of 28° . As can be seen in Fig. 1, the antenna is generated by swinging the side projection through this angle. Thus the two sides of the horn are flat surfaces, while the front and back surfaces are sections of cones. There are several advantages to this type of construction: right-angle sections can be used for the corners of the horn; the reflector can be constructed of identical longitudinal sections;

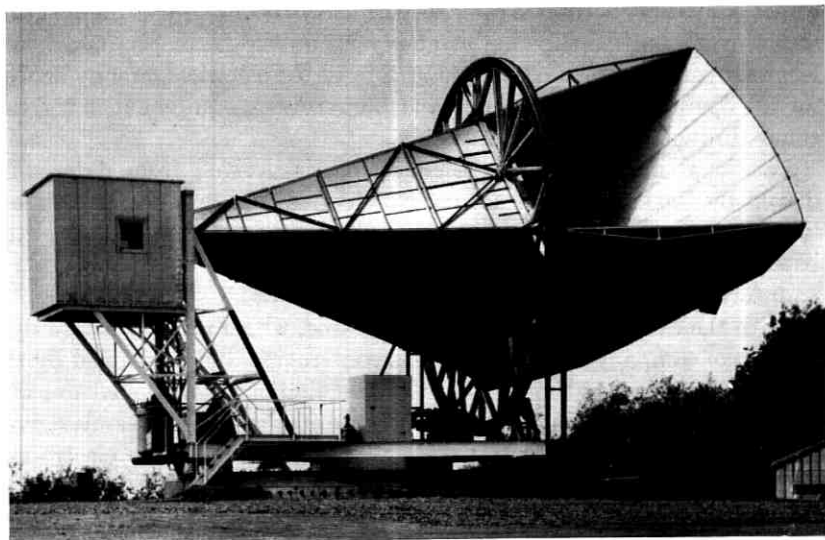


Fig. 2 — Horn-reflector antenna used in Project Echo experiment.

the intersections of the front and back conical surfaces with the paraboloid of revolution are circles in planes perpendicular to the axis of the paraboloid, thus providing accurate and readily available references for use in constructing the reflector. Nine accurately fabricated parabolic ribs were used for the reflector, one end of each being fastened to a curved (arc of a circle) beam at the wheel while the other end was fixed on a circle scribed on a temporary horizontal work table. The ribs were tied together by cross bracing and by a large triangular crossbeam, which in turn was tied by columns to the vertical wheel. The aluminum sheets that make up the reflecting surface were then fastened to the ribs; these have curved stiffeners to produce the small curvature required in the plane perpendicular to the ribs. It is believed that the reflector surface is accurately paraboloidal to $\pm \frac{1}{32}$ inch.

The antenna is driven in azimuth and elevation by 10 H.P. direct-current servo gear-motors.* Power is transmitted by sprockets (with teeth specially cut for rack operation) to roller chains which are fastened to the vertical wheel and to the plates forming the horizontal track. The roller chain proved to be a satisfactory substitute for a large bull gear; by the use of a radial arm and dial indicator, the rollers of the chains were adjusted to lie on 30-foot-diameter circles to an accuracy of about 0.005 inch. The maximum speed of rotation in both azimuth and elevation is 5° per second; the maximum acceleration for both axes is 5° per second per second. Power for the drives is brought to the rotating structure through a slip-ring assembly inside the small plywood house located over the center bearing (Fig. 2). All the electrical circuits needed for the operation of the antenna and the receiving equipment in the cab come through the slip-ring assembly.

Positional information for the antenna is derived from data units driven by large (48-inch) accurately cut and accurately aligned gears located on the bearings at the apex of the horn and at the center of the base frame. The data units contain synchro transmitters and control transformers operated in a two-speed, 1:1 and 36:1, system.

With the exception of the steel base frame, which was fabricated by a local steel company, the antenna was constructed and assembled by the Holmdel Laboratory shops under the direction of H. W. Anderson, who also collaborated in the design. Assistance in the design was also given by R. O'Regan, S. A. Darby and several members of the electro-mechanical development group at the Whippany Laboratory. The latter group also was instrumental in procuring special equipment such as data units, gears, and slip-ring assembly.

* This is more power than required, particularly for the elevation drive, but these motor and control packages were standard items and were readily available.

The antenna has performed well electrically and mechanically during the Project Echo experiment. It was subjected to winds of 80 mph during Hurricane Donna, September 12, 1960, without damage. It has been customary to disengage the azimuth sprocket drive when the antenna is not in use, thus permitting the structure to "weathervane" and seek a position of minimum wind resistance.

III. THEORETICAL DISCUSSION

The manner in which the spherical wave diverges from the apex of the horn is shown schematically in Fig. 3(a). This wave, for the greater

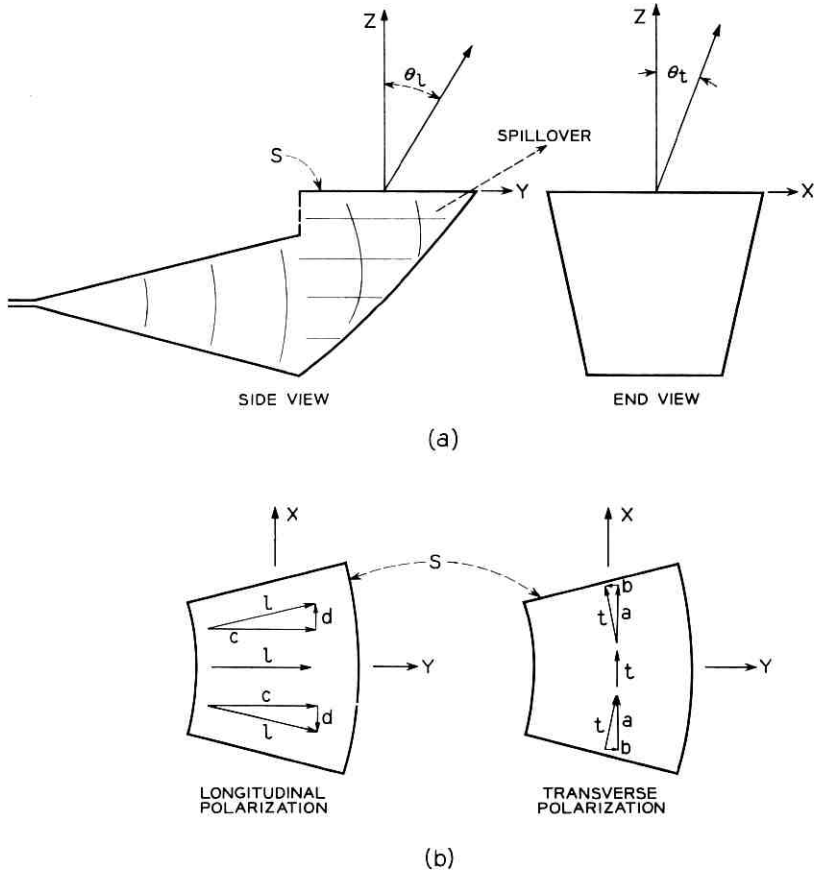


Fig. 3 — Sectional views in the longitudinal (y - z) and transverse (x - z) planes and field components in the projected aperture.

part, maintains the characteristic amplitude distribution of the TE_{10} mode as it proceeds along the horn; nevertheless, it is a spherical wave and undergoes inverse distance attenuation up to the point where it is rendered equiphase by the paraboloidal reflector. Thus, over the surface of the projected aperture, s in Fig. 3(a), the field has an unsymmetrical amplitude taper in the direction of the horn axis due to inverse distance attenuation in addition to the symmetrical characteristic of the TE_{10} mode.

In Fig. 3(b), two sets of vectors, t and l , representing transverse and longitudinal polarization in the projected aperture, are shown. On the bisector of the aperture, t is parallel to the x -axis and l to the y -axis; however, at points removed from the bisector, t and l preserve the polarization established in the pyramidal horn, and therefore are inclined with respect to the principal axes. At these points, t and l are broken down into components a, b and c, d respectively, as indicated in Fig. 3(b); note that there is asymmetry about the bisector in the cross components b and d .

The aperture field being known, one can calculate the field at a large distance R in the region near the axis of the beam to good approximation by

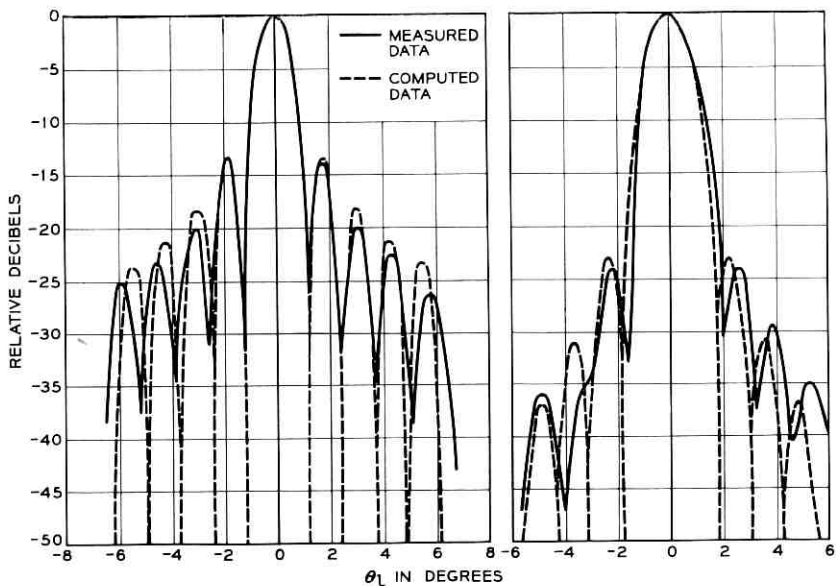
$$E = \frac{j}{\lambda R} \int_s E_i e^{-j\beta(y \sin \theta_t + x \sin \theta_l)} ds, \quad (1)$$

where E_i represents any one of the components a, b, c , or d , and θ_t and θ_l are angles in the principal plane, which either contains or is transverse to the axis of the pyramidal horn. The longitudinal plane contains the horn and beam axes; the transverse plane contains the beam axis and is normal to the axis of the horn. Thus, in Fig. 3, θ_t lies in the yz plane and θ_l in the xz plane. Both the principal and cross-polarized radiation patterns* may be computed using (1), provided the appropriate aperture field component E_i is chosen. The computed patterns are shown in Figs. 4, 5, and 6 as dashed curves†; the experimental data are shown as solid lines and will be discussed later. The two cross-polarization patterns in the longitudinal plane are zero for all angles since the aperture field components b and d are antisymmetrical with respect to that plane.

The radiation patterns for circular polarization may be calculated by combining the appropriate principal and cross-polarized components of the far field. An example of the method is given in Appendix B. The

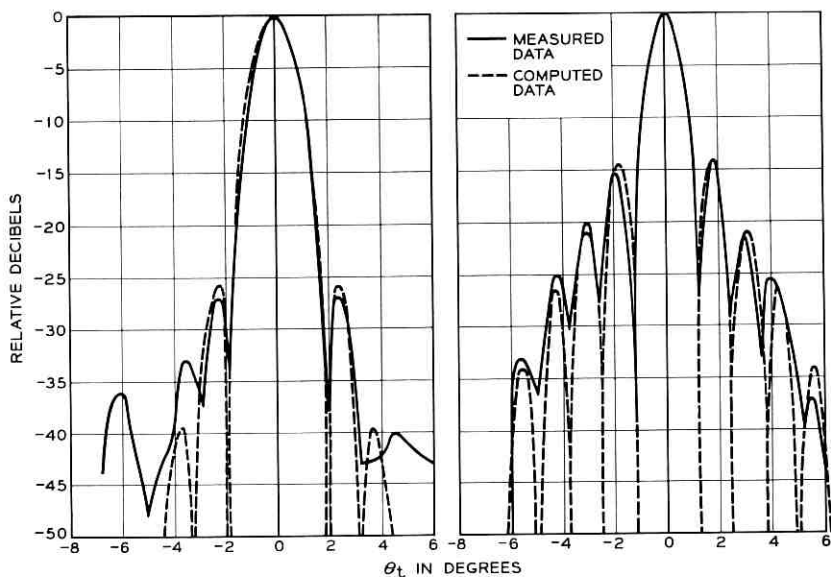
* Details are given in Appendix A.

† The computations were made for points separated 0.25° in θ ; thus, although the dashed curves extend to the -50 db level, they do not represent the depths of the nulls for the case of longitudinal plane patterns, but rather only their positions.



(a) LONGITUDINAL POLARIZATION (b) TRANSVERSE POLARIZATION

Fig. 4 — Principal radiation patterns in the longitudinal plane (2390 mc).



(a) LONGITUDINAL POLARIZATION (b) TRANSVERSE POLARIZATION

Fig. 5 — Principal radiation patterns in the transverse plane (2390 mc).

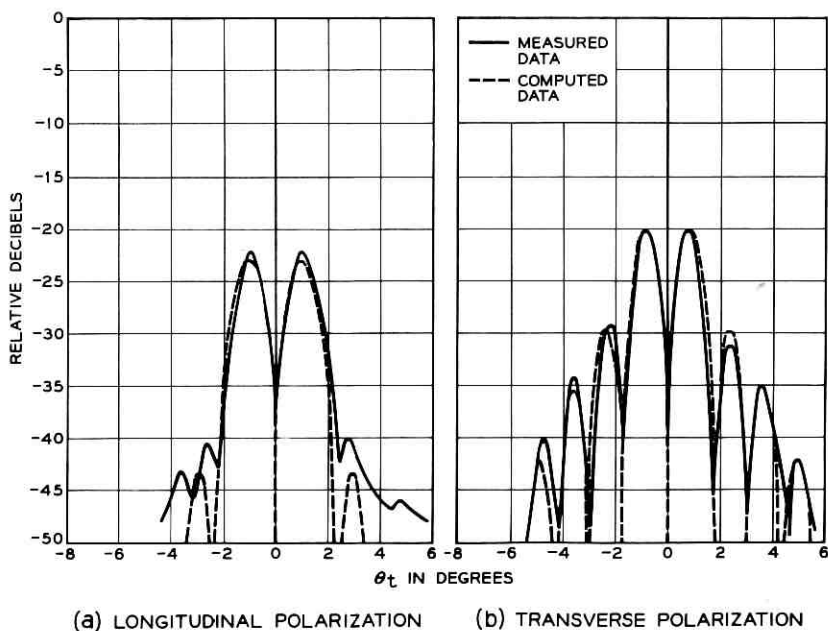


Fig. 6 — Cross-polarized radiation patterns in the transverse plane (2390 mc).

dashed lines of Figs. 7(a) and 8(a) show calculated radiation patterns where the antenna receives the desired (transmitted) sense of circular polarization, and Figs. 7(b) and 8(b) show the undesired sense. Note especially Figs. 8(a) and (b) for the transverse plane, in which the patterns are unsymmetrical with respect to the $\theta_t = 0$ axis; in Fig. 8(a), the maximum of the main beam is at $\theta_t = -0.1^\circ$. This effect is more clearly demonstrated by assuming that the antenna receives both clockwise and counter-clockwise senses simultaneously, as would be the case for a linearly polarized incident wave; the beam, for one sense, shifts to $\theta_t = +0.1^\circ$ and for the other to $\theta_t = -0.1^\circ$; this effect is shown in Fig. 9. The slight tilting of the beam in circular polarization is a consequence of asymmetry in the phase of the cross-polarized components of the far field.

Unfortunately, all the energy which proceeds along the horn does not illuminate the paraboloidal reflecting surface; some of it is diffracted at the edge of the horn aperture. As indicated by the dashed line in Fig. 3(a), the wave is again diffracted by the edge of the reflector and produces perturbations in the far-field pattern. The lobes thus produced are referred to as spillover lobes; in Appendix D a method of calculating

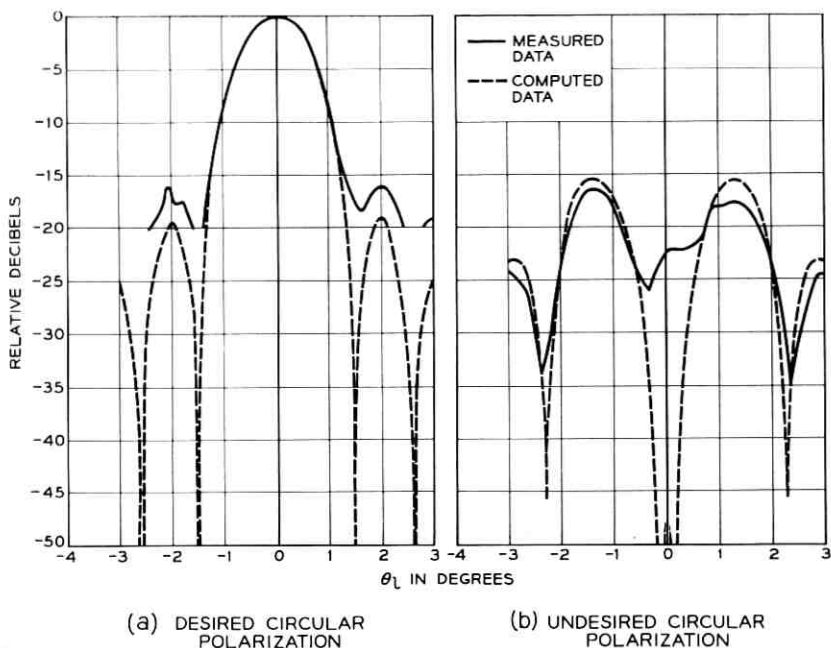


Fig. 7 — Circularly polarized radiation pattern in the longitudinal plane (2390 mc).

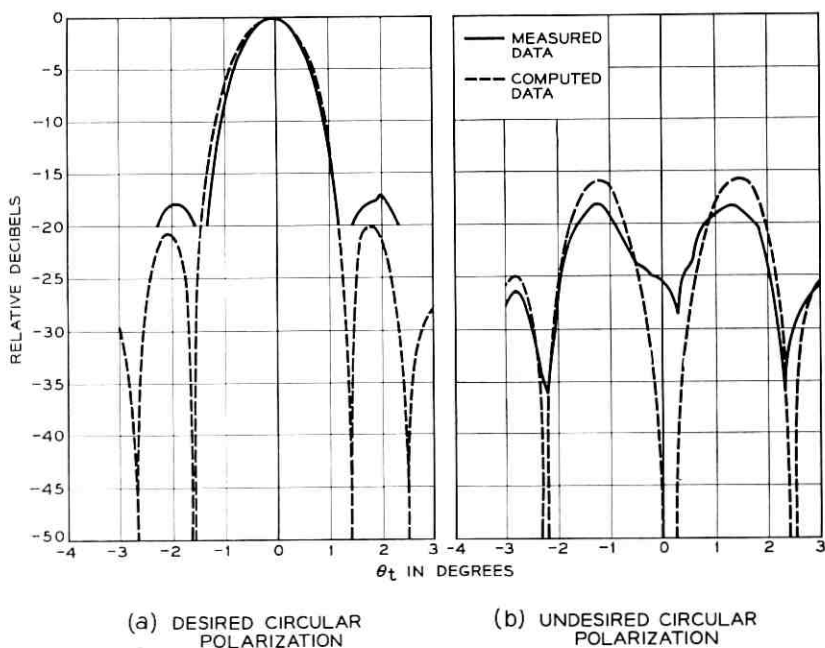


Fig. 8 — Circularly polarized radiation patterns in the transverse plane (2390 mc).

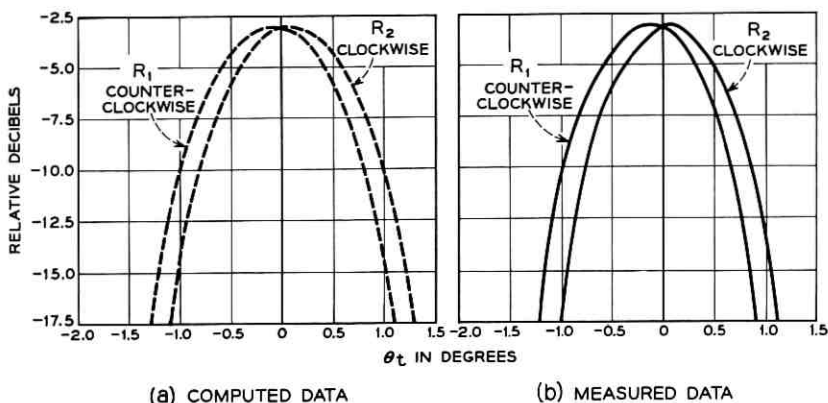


Fig. 9 — Circularly polarized radiation patterns in the transverse plane, showing dependence of beam displacement on sense of polarization.

them is discussed. The points in Fig. 10 show the spillover effect calculated for longitudinal polarization in the longitudinal plane. The maximum spillover energy is at an angle $\theta \simeq 70^\circ$; as indicated in the insert in Fig. 11, this differs by 7° from the direction determined by the flare angle of the horn, namely, 77° . For transverse polarization, the spillover effect is much reduced because of the cosine distribution in the z direction in the horn for that polarization.

IV. TECHNIQUE OF MEASUREMENTS

The important electrical properties of the antenna to be measured are its gain and radiation patterns at the frequency of interest, in this case 2390 mc. To make such measurements, it is necessary to provide a

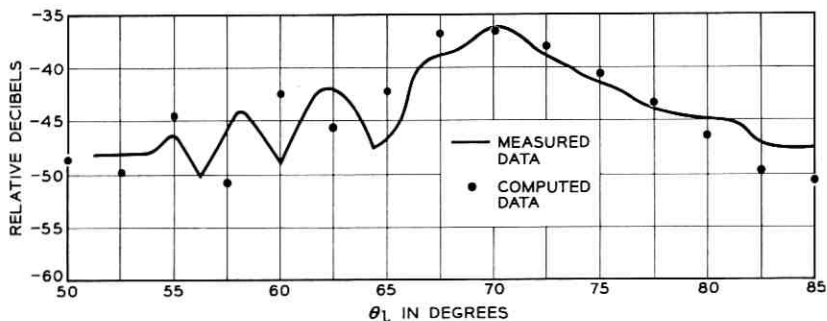


Fig. 10 — Calculated and measured spillover lobe; longitudinal plane, longitudinal polarization.

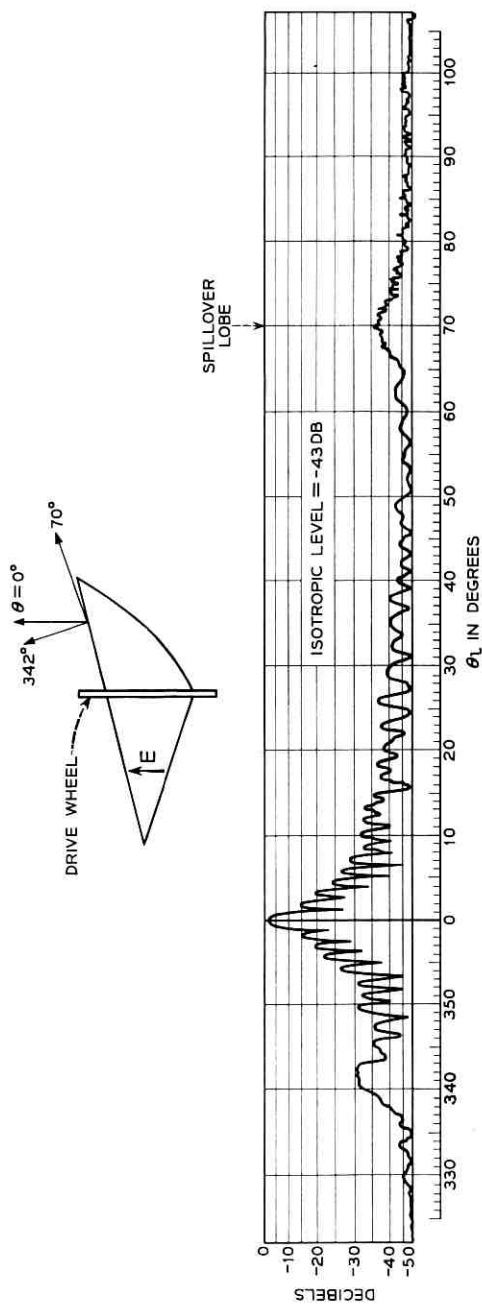


Fig. 11 — Extended radiation pattern; longitudinal plane, longitudinal polarization.

known incident field. In free space, ideally, the incident field would be uniform in amplitude and phase over the region occupied by the aperture of the antenna. In practice, this is accomplished by placing a source at a sufficient distance such that the wave incident at the antenna under test is essentially plane. The usual criterion is that the phase deviation over the aperture not exceed $\pi/8$. For the 20-foot aperture considered here, this criterion requires that a test transmitter operating at 2390 mc be at least one-third mile away; the distance used for these tests was about two miles. The antenna is not in free space, however, and environment such as trees and contours of the local terrain introduce reflections which distort the incident field. For these tests, nearby trees were removed and, both before and after the antenna was in place, the incident field was checked by exploring it with a probe consisting of a small horn. The horn was mounted on a motor-driven carriage that was drawn up and down a 55-foot vertical tower, the received output being continuously recorded. The tower was set at several horizontal positions so that the incident field over the area to be occupied by the antenna was mapped out. These height runs showed irregular variations in the incident field, but these did not exceed ± 1 db, and therefore were considered small enough to permit meaningful measurements. An analysis of the height runs indicated that, in addition to the direct space wave, a second wave, reflected from the intervening ground, was also present. The analysis fixed the reflection point at about midpath at an elevation corresponding to the tree-top level with an amplitude reflection coefficient of about 0.07.

V. GAIN MEASUREMENTS

The gain of the horn-reflector antenna was measured by comparing the strength of its received signal with that of a standard horn.* The latter was located in the plane of the aperture of the horn-reflector, but off to one side. The field at this particular location of the standard horn was equal to the average intensity of the field illuminating the horn reflector, as obtained from the height run data.

The measurement procedure consisted first of aiming the horn-reflector for optimum received signal strength and continuously recording the output. Because of scintillation of the signal, it was necessary to integrate for several seconds to obtain a dependable signal level. The coaxial line which fed the receiver was then shifted from the horn-reflector to the standard horn and the results recorded for a like period. A number of

* A pyramidal horn whose gain at 2390 mc, calculated from its physical dimensions, was 20.1 db.

such comparisons were made. The gain of the horn-reflector, referred to an isotropic radiator, was then obtained by adding the db difference between those two signal strengths to the db gain of the standard horn.

A double detection receiver was used in all the measurements. Signal-level differences were established by an attenuator in the intermediate frequency (65 mc) channel which was calibrated to an accuracy of ± 0.05 db. The gain was measured using both longitudinal and transverse polarizations and the results averaged:

Calculated gain of standard horn:	20.1 db,
Measured gain of horn-reflector over standard horn:	23.2 db,
Gain of horn-reflector:	43.3 db.

The rms scatter of the gain measurements was 0.16 db, due principally to scintillation of the signal.

The theoretical value for the horn-reflector gain is calculated by the method discussed in Appendix C. Due to the asymmetrical geometry of the aperture, the gain depends slightly on polarization, namely 43.43 db for longitudinal and 43.35 db for transverse. The average theoretical gain is therefore 43.39 db, which is 1.12 db below full area gain (44.51 db).

If we compare the measured and calculated values, the gain is 0.09 db less than expected.* Part of this discrepancy is due to the irregularities in the incident field discussed above in connection with the height run data. If one assumes that the variations in the phase of the incident field are random over the aperture, the deviation of the phase variation being derived from the 0.07 db reflection coefficient discussed above, one can estimate the decrease in received signal† due to this effect; this turns out to be 0.02 db, so that the discrepancy between calculated and measured values is reduced slightly. The remainder is most likely due to spillover.

VI. PATTERN MEASUREMENTS

Radiation patterns were obtained by continuously recording the receiver output as the horn-reflector was rotated at a constant speed.

There are several directional patterns of interest; these include the principal and cross-polarized patterns for the two linear polarizations in the two principal planes, and patterns in circular polarization for the

* In other words, the measured effective area is 1.2 db below actual area, or the measured efficiency, 76 per cent.

† For a small random fluctuation, the decrease in signal is $e^{-\delta^2}$ where δ is the standard deviation of the fluctuations in phase.⁵

two planes. As discussed in Section II, the two cross-polarized patterns in the longitudinal plane are expected to be zero, due to the odd symmetry of the cross-polarized components of the aperture field.

Detailed patterns for the principal polarizations in the region of the main beam are shown in Figs. 4 and 5 for longitudinal and transverse planes respectively. Measured data are shown by full lines and theoretical data by dashed lines. In general, the measurements agree very well with the calculated patterns except for some relatively small departures which are considered to be due to reflections from the environment and to scintillation. The salient factors obtained from the principal linear polarization patterns are shown in Table I.

The cross-polarization patterns in the transverse plane are shown in Fig. 6; here also the agreement between experiment and theory is considered to be good. The levels of cross-polarization in the longitudinal plane which are theoretically zero were lower than -30 db in the region near $\theta_i = 0$ and fell rapidly to less than -45 db for other angles.

The response of the antenna to circularly polarized waves is shown by the patterns of Figs. 7 through 9. In general, the agreement between measurement and theory is not as satisfactory as for the linear polarization patterns; this disagreement is believed due in part to lack of sufficient measuring range in the receivers used for the two circular senses. When both the transmitting test antenna and the horn-reflector were adjusted for the same sense of polarization, the first side lobes in both the longitudinal and transverse planes, as seen in Figs. 7(a) and 8(a), measured about 3 db higher than predicted by theory; the main beamwidths, however, agreed well with calculations. When the horn-reflector was adjusted to receive the sense opposite to that transmitted, the response on the first side lobes, as shown in Figs. 7(b) and 8(b), was about 2 db lower than predicted, while the response in the direction of the principal axis was about -27 db. The discrepancy between this value and that predicted by theory is believed due partly to depolarization by

TABLE I

Plane	Polarization	Beamwidths (3-db points)		Level of first minor lobes	
		Measured	Calculated	Measured	Calculated
transverse	longitudinal	1.35°	1.30°	-27.0db	-26.5 db
longitudinal	longitudinal	1.10°	1.10°	-13.5	-13.5
transverse	transverse	1.00°	1.00°	-14.5	-14.5
longitudinal	transverse	1.55°	1.55°	-24.0	-23.0

the ground and partly to imperfect circular polarization from the transmitter.*

A test was made in which the horn-reflector received simultaneously both senses of circular polarization which were generated by a wave from the test transmitter that was linearly polarized. The results appear in Fig. 9; the slight beam tilt, as evidenced by the displacement in opposite directions from $\theta = 0$ depending on the sense of polarization, agrees well with theoretical values. A similar displacement between the two senses was observed while receiving noise from the moon and sun.

Fig. 11 shows an extended radiation pattern measured in the longitudinal plane using longitudinal polarization. Let us refer to this region as the spillover sector; it is shown here in preference to any other sector because the level of the far-side lobes is of the order of the isotropic level rather than 10 to 30 db or so below isotropic, as is the case for the other sectors.^{2,4} The most prominent spurious lobe is the so-called spillover lobe at an angle of 70° from the main beam. A more detailed plot of the spillover lobe is shown in Fig. 10, the points being values calculated in Appendix D. The agreement in level and shape of the measured and calculated curves is fairly good; however, the calculated data appear to be translated about two degrees toward smaller values of θ_l . Pattern measurements using transverse polarization showed much lower levels for the far lobes in the spillover sector.

Also apparent in Fig. 11 is a prominent lobe at angle 342° . This lobe is apparently associated with the 30-foot-diameter drive wheel, which, as may be seen in the insert in Fig. 11, tends to shadow the aperture in that direction. Diffraction over the rim of the wheel might be the cause of this spurious lobe.

VII. CONCLUDING REMARKS

The performance characteristics of a relatively large horn-reflector type of antenna, measured at a frequency of 2390 mc, agree satisfactorily with calculated performance. The measured radiation patterns are readily identified with those calculated to at least the third side lobes, the antenna gain being about one-tenth decibel less than expected. This good performance, in conjunction with the low-noise properties of this type of antenna, place it in a favorable position, not only for use in space communications, but also for use as a standard for absolute flux measurements in radio astronomy. Of some concern is a small amount of spill-

* The circular polarization was produced by a quarter-wave plate placed in front of the transmitting horn; the axial ratio, measured by rotating a 20-db horn antenna at the receiving site, was about 0.8 db.

over which degrades the performance in one sector of the radiation pattern; fortunately, in the above applications, the spillover sector is directed skyward and therefore the noise contribution is small in the microwave band.

Assistance in the assembly and adjustment of electrical components and in the measurement of the electrical properties of the antenna was given by R. A. Semplak, H. A. Gorenflo, and R. A. Desmond. Computation of the theoretical data was made by Mrs. C. L. Beattie.

APPENDIX A

Calculation of Patterns for Linear Polarization

The radiation patterns for linear polarization in the region of the main beam of the antenna are calculated using

$$E = \frac{j}{\lambda R} \int_S E_i e^{-j\beta(y \sin \theta_t + x \sin \theta_l)} ds, \quad (2)$$

where E_i is a component of the aperture field and x, y are coordinates in the projected aperture, S ; R is the distance from the antenna to the

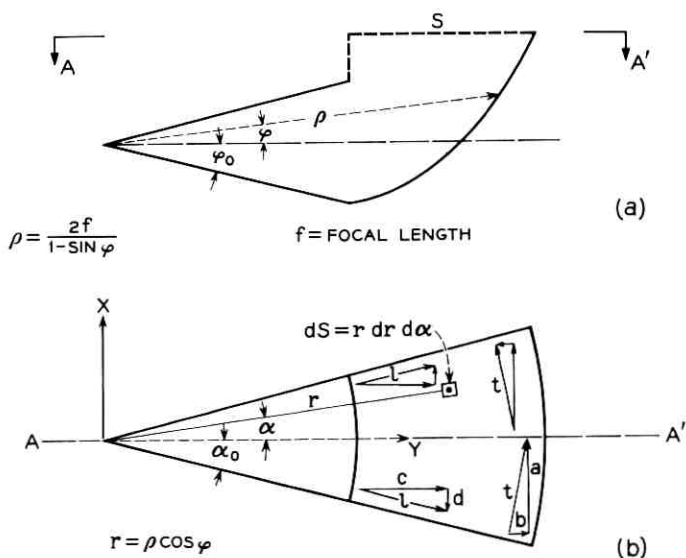


Fig. 12 — Coordinate system and projected aperture, S .

distant field point; θ_l and θ_t are angles in the principal planes; $\beta = 2\pi/\lambda$.

Since energy proceeds down the square horn in essentially a dominant waveguide mode, the field is constant along one coordinate and has a cosine distribution along the orthogonal coordinate. In addition, the field of the spherical wave decreases inversely with the distance ρ shown in Fig. 12(a), but, since the spherical phase front is corrected by the reflector, negligible attenuation occurs between the reflector and the projected aperture, S , in the plane AA' .

The total fields l and t , and the field components a , b , c , and d in the projected aperture, are shown in Fig. 12(b). Each of these can be expressed in terms of the symbols shown in the figure:

$$\begin{aligned} E_a &= E_0 \frac{\rho_0}{\rho} \cos \frac{\pi\varphi}{2\varphi_0} \cos \alpha, \\ E_b &= E_0 \frac{\rho_0}{\rho} \cos \frac{\pi\varphi}{2\varphi_0} \sin \alpha, \\ E_c &= E_0 \frac{\rho_0}{\rho} \cos \frac{\pi\alpha}{2\alpha_0} \cos \alpha, \\ E_d &= E_0 \frac{\rho_0}{\rho} \cos \frac{\pi\alpha}{2\alpha_0} \sin \alpha. \end{aligned} \tag{3}$$

The field has been normalized to the value E_0 at $\rho = \rho_0 = 2f$ (where $\varphi = \alpha = 0$), φ_0 and α_0 being the flare angles of the horn. Equation (3), substituted for E_i in (2), results in the far-field equations. However, for comparison with experimental data, one must specify the principal plane of interest as well as the polarization; therefore let us designate the far fields in the following way:

<i>Polarization of Antenna</i>	<i>Plane of Measurement</i>	<i>Polarization of Far Field</i>	<i>Designation of Far Field</i>
longitudinal	longitudinal	longitudinal	E_1
transverse	longitudinal	transverse	E_2
longitudinal	transverse	longitudinal	E_3
transverse	transverse	transverse	E_4
longitudinal	longitudinal	transverse	E_5
transverse	longitudinal	longitudinal	E_6
longitudinal	transverse	transverse	E_7
transverse	transverse	longitudinal	E_8

These designations are related to (2) and (3) as follows:

$$\begin{bmatrix} E_1 \\ E_2 \\ E_5 \\ E_6 \end{bmatrix} = j \frac{4f^2}{\lambda R} \int_{-\alpha_0}^{\alpha_0} d\alpha \int_{-\varphi_0}^{\varphi_0} d\varphi \begin{bmatrix} E_c \\ E_a \\ E_d \\ E_b \end{bmatrix} \frac{\rho}{\rho_0} \frac{\cos \varphi}{1 - \sin \varphi} e^{-j\beta\rho \cos \varphi \cos \alpha \sin \theta_t},$$

$$\begin{bmatrix} E_3 \\ E_4 \\ E_7 \\ E_8 \end{bmatrix} = j \frac{4f^2}{\lambda R} \int_{-\alpha_0}^{\alpha_0} d\alpha \int_{-\varphi_0}^{\varphi_0} d\varphi \begin{bmatrix} E_c \\ E_a \\ E_d \\ E_b \end{bmatrix} \frac{\rho}{\rho_0} \frac{\cos \varphi}{1 - \sin \varphi} e^{-j\beta\rho \cos \varphi \sin \alpha \sin \theta_t}.$$

Integration shows that E_5 and E_6 are zero. The remainder are computed by numerical integration, with $E_1, E_2, E_3, E_4, E_7,$ and E_8 corresponding to the patterns in Figs. 4(a), 4(b), 5(a), 5(b), 6(a), and 6(b) respectively.

APPENDIX B

Calculation of Patterns for Circular Polarization

The far-field patterns for circular polarization may now be calculated using the designations discussed in Appendix A. As an example, consider Fig. 13, in which the horn is assumed to be fed at the throat with a clockwise circularly polarized wave $-i_x - ji_z$, i_x and i_z being vectors

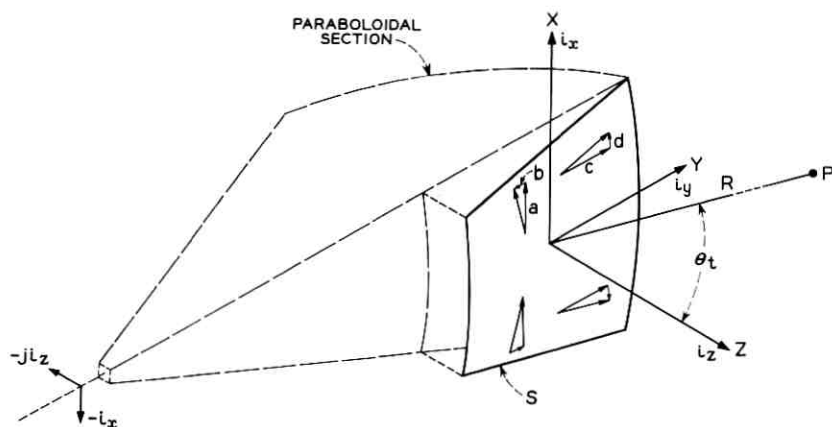


Fig. 13 — Aperture field components for calculation of circular polarization; distant point, P , is in the transverse plane.

in the x and z directions and $j = \sqrt{-1}$. Upon reflection by the paraboloidal section, this wave produces an aperture field

$$E_s = (i_x E_a - i_y E_b) + j(i_y E_c + i_x E_d), \quad (4)$$

i_y being in the y direction.* If we restrict the discussion to the transverse plane, E_a , E_b , E_c , and E_d are the aperture field components which produce the far fields E_4 , E_8 , E_3 , and E_7 discussed above.† At a point P defined by a line r in the transverse plane making a small positive angle θ_t with respect to the z -axis, the field is

$$E_p = i_x E_4 - j i_y E_8 + j i_y E_3 - i_x E_7. \quad (5)$$

In (5), account has been taken of the fact that the phase of the cross-polarized fields, E_7 and E_8 , differs from that of the principal fields by 90° . Gathering together the x and y components, (5) becomes

$$E_p = i_x (E_4 - E_7) + j i_y (E_3 - E_8),$$

which can be broken down into two circularly polarized waves

$$E_{p_{ccw}} = \frac{i_x}{2} (E_3 + E_4 - E_7 - E_8) + j \frac{i_y}{2} (E_3 + E_4 - E_7 - E_8), \quad (6)$$

and

$$E_{p_{cw}} = \frac{i_x}{2} (E_3 - E_4 + E_7 - E_8) - j \frac{i_y}{2} (E_3 - E_4 + E_7 - E_8), \quad (7)$$

with (6) being the desired and (7) the undesired sense of rotation.

If the point P in Fig. 13 is below the z -axis such that θ_t is negative, the signs of the cross-polarized components E_7 and E_8 are reversed and the fields are

$$E_{p_{ccw}} = \frac{i_x}{2} (E_3 + E_4 + E_7 + E_8) + j \frac{i_y}{2} (E_3 + E_4 + E_7 + E_8) \quad (8)$$

and

$$E_{p_{cw}} = \frac{i_x}{2} (E_3 - E_4 - E_7 + E_8) - j \frac{i_y}{2} (E_3 - E_4 - E_7 + E_8). \quad (9)$$

Comparison of (6) with (8) and (7) with (9) shows that the radiation patterns in circular polarization will be somewhat unsymmetrical about the $\theta_t = 0$ axis.

* Note reversal in sense of polarization on reflection.

† Here, $E_a, E_b, \dots, E_4, E_8, \dots$ etc., are the amplitudes of the aperture and far fields.

In the longitudinal plane, since the cross-polarized fields are zero, the radiation patterns for circular polarization are symmetrical about $\theta_l = 0$.

APPENDIX C

Gain

The antenna gain may be calculated using

$$G = 4\pi R^2 \frac{F(0)}{P_s}, \quad (10)$$

where $F(0) = (1/\eta) |E(0)|^2$ is the density of power flow in the direction $\theta_l = \theta_t = 0$ as obtained from (2) by numerical integration ($\eta = 120\pi$); P_s , the total power radiated by the aperture is obtained by integration of either of the components l or t of Fig. 12. For example, since

$$E_l = E_0 \frac{\rho_0}{\rho} \cos \frac{\pi\varphi}{2\varphi_0}$$

and

$$ds = r dr d\theta = 4f^2 \frac{\cos \varphi}{(1 - \sin \phi)^2} d\varphi d\alpha,$$

$$P_s = \frac{E_0^2}{\eta} 4f^2 \int_{-\alpha_0}^{\alpha_0} d\alpha \int_{-\varphi_0}^{\varphi_0} d\varphi \cos^2 \frac{\pi\alpha}{2\alpha_0} \cos \varphi = \frac{E_0^2}{\eta} 8f^2 \alpha_0 \sin \varphi_0.$$

The efficiency of the antenna is given by A_e/S , where $A_e = \lambda^2 G/4\pi$ is the effective area and

$$S = \int_s r dr d\alpha = 16f^2 \alpha_0 \frac{\sin \varphi_0}{\cos^2 \varphi_0}$$

is the actual area of the projected aperture.

APPENDIX D

The Spillover Lobe

The spherical wave in the horn (shown in Fig. 14) is diffracted at edge A and part of the energy proceeds beyond the rim of the reflector, c. For the purpose of calculating the spillover lobe, the antenna configuration is idealized by replacing the curved reflector, shown dashed in Fig. 14, with a plane semi-infinite sheet, the edge of which is $c/2$ above the axis of the horn. The distant field of this horn-sheet combination can

then be calculated by use of Fourier transforms, as discussed by Wootton.⁶ Restricting the discussion to the plane of Fig. 14, one obtains for the distant field at a point R , θ not too far removed from the axis of the horn:

$$E' = \left(\frac{j}{2\pi\lambda R} \right)^{\frac{1}{2}} E_0 e^{j(\pi-1)\gamma^2 b \lambda} \left\{ \sqrt{\lambda l} e^{j\pi\gamma^2 \lambda l} [C(v_2) - C(v_1) - jS(v_2) + jS(v_1)] - (1+j) \sqrt{\pi} \int_{-a/2}^{a/2} e^{-j\pi(h^2/\lambda l - 2\gamma h)} [C(v_0) - jS(v_0)] dh \right\}, \quad (11)$$

where E_0 is the field at the center of the horn aperture,

$$v_0 = \frac{1}{\sqrt{2b\lambda}} [c - 2(h - \gamma b \lambda)],$$

$$v_1 = \sqrt{\frac{2}{l\lambda}} [\gamma l \lambda - a/2],$$

$$v_2 = \sqrt{\frac{2}{l\lambda}} [\gamma l \lambda + a/2];$$

and $\gamma = -(1/\lambda) \sin(\pi/2 - \theta)$; a is the width of the horn aperture along the h coordinate; and b, c, l are the dimensions shown in Fig. 14, C and S being Fresnel integrals.

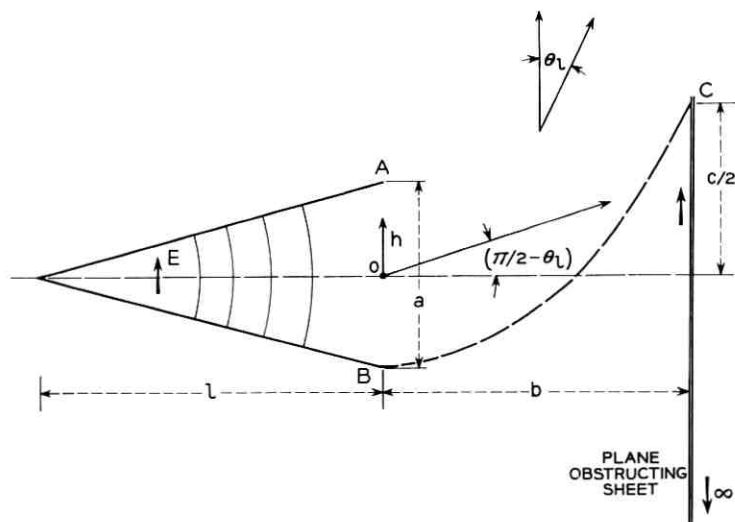


Fig. 14 — Two-dimensional geometry used for calculating the spillover lobe.

The two-dimensional solution, (11), predicts quite accurately the value of θ_l at which maximum spillover occurs, but it is in error in absolute value because in reality the diffracting edges *A* and *c* are of finite length and are curved. One can account approximately for the curvature of edge *c* by assuming that the diffraction effect in the plane of Fig. 14 and the effect in the plane *AC*, normal to the figure, are separable. In that case, (11) is multiplied by a factor

$$K = \frac{\int_{-d}^d e^{-j\pi(x^2/\lambda r)} \cos \frac{\pi x}{2d} dx}{\int_{-d}^d \cos \frac{\pi x}{2d} dx},$$

where x is the coordinate normal to the plane of Fig. 14 at *c*, $2d$ the extent of the edge along the x -axis, and r its radius of curvature.

The values plotted in Fig. 10 are KE' ; K amounts to -10.5 db for the case under consideration.

REFERENCES

1. Friis, H. T., and Beck, A. C., U. S. Patent 2,236,393.
2. Friis, R. W., and May, A. S., A New Broad-Band Microwave Antenna System, A.I.E.E. Trans., Pt. I, **77**, 1958, p. 97.
3. Hogg, D. C., Problems in Low Noise Reception of Microwaves, I.R.E. Trans., Nat. Symp. on Space Electronics and Telemetry, 1960, p. 8-2.
4. DeGrasse, R. W., Hogg, D. C., Ohm, E. A., and Scovil, H. E. D., Ultra-Low-Noise Antenna and Receiver Combination for Satellite or Space Communication, Proc. Nat. Elect. Conf., **15**, 1959, p. 370.
5. Ruze, J., Nuovo Cimento, **9**, supp. 3, 1952, p. 364.
6. Woonton, G. A., The Effect of an Obstacle in the Fresnel Field on the Distant Field of a Linear Radiator, J. Appl. Phys., **21**, 1950, p. 577.

PROJECT ECHO

The Dual Channel 2390-mc Traveling-Wave Maser

By R. W. DE GRASSE, J. J. KOSTELNICK, and
H. E. D. SCOVIL

(Manuscript received April 26, 1961)

Reflected 2390-mc signals from the Echo I satellite were received by a horn-reflector antenna and amplified by solid state traveling-wave masers. This paper describes the design of the dual channel maser amplifiers for this experiment. Each maser has sufficient gain (> 33 db) to override the noise of the following stage. Unconditional stability is obtained by the use of distributed ferrimagnetic isolator elements. Their instantaneous bandwidth is 13 mc, centered at 2390 mc. The effective input noise temperature is 8°K.*

I. INTRODUCTION

This paper discusses the design of an S-band traveling-wave maser for the Project Echo satellite communication experiment.¹ The masers described here were used at Bell Telephone Laboratories, Holmdel, New Jersey, receiving terminal to amplify the 2390-mc signals reflected from the passive Echo I satellite and received by the 20-foot horn-reflector antenna.²

The 2390-mc signal was transmitted with circular polarization. Imperfections in the transmission path such as a not perfectly spherical satellite could lead to deviations from the originally circular polarization. Such effects would show up in terms of a signal having the opposite sense of circular polarization. A quarter-wave plate in the antenna feed converted both senses of circular into orthogonal senses of linear polarization, which were then fed separately to the inputs of two masers. Thus one maser received the polarization as transmitted and served as pre-

* Although this equipment was designed by the Bell System as part of its research and development program, it was operated in connection with Project Echo under Contract NASW-110 for the National Aeronautics and Space Administration.

amplifier for the signal channel. The other maser served as a preamplifier for a monitoring channel which received data on the imperfections of the transmission path.

The system used frequency modulation. It required a receiving bandwidth of approximately 1 mc centered at 2390 mc for the signal. A slightly wider bandwidth was required, however, since continuous sky-noise monitoring was desired at 2388 mc; this frequency was outside but close to the signal channel. Further receiving system details are given in the accompanying paper by Ohm.³

II. SIGNAL REQUIREMENTS

The system objective called for masers with the following requirements:

1. two identical amplifiers for duplex operation;
2. lowest possible noise temperature;
3. bandwidth greater than 3 mc;
4. long-term gain stability;
5. at least 33 db gain;
6. dynamic range greater than 60 db;
7. sufficient running time between helium transfers to permit operation for a full sequence of neighboring satellite passes;
8. center frequency 2390 mc.

Because of items 2, 4, and 6, it was decided that traveling-wave masers would be the most desirable. It was shown previously⁴ that these general objectives could be met at 6 kmc. Apart from the frequency, the main differences were the requirement for a higher gain and no electronic tuning. This suggested the use of the 6-kmc traveling-wave maser as a basis for design, the main departure being a much narrower-bandwidth slow-wave structure with greater slowing.

Item 7 suggested a batch helium system using a stainless steel dewar with sufficient liquid storage capacity to give the required running time.

The two amplifiers were located in the same dewar and magnetic field, in order to obtain duplex operation.

III. THE ACTIVE MATERIAL (RUBY)

Chromium-doped aluminum oxide (ruby) was the one material which was proved to have the requisite properties. Fortunately, essentially complete information was available on the maser properties of this material at 2390 mc from the work of Geusic.⁵ In particular it was known that 0.05 per cent chromium was optimum and that the $\theta = 90^\circ$, high-field, single-pump operation was best.

The value of χ''_{\pm} for circular polarization is given by Equation (12) of Ref. 4. Geusic obtained the inverted state densities ($\bar{\rho}_n - \bar{\rho}_{n'}$) directly from a measurement of the inversion ratio, $\chi''_{\text{pump on}}/\chi''_{\text{pump off}}$. From the inversion ratio of 3.6 at 4.2°K he computed $-\chi''_{+}$ and $-\chi''_{-}$, the inverted susceptibilities, for the two senses of circular polarization defined with respect to the applied dc magnetic field. He gives $\chi''_{+} = -0.018$ and $\chi''_{-} = -0.0021$ when the material is pumped to saturation, the principal axis of the susceptibility tensor being along the *C*-axis of the crystal.

IV. THE INTERACTION BETWEEN THE ACTIVE MATERIAL AND THE SLOW-WAVE STRUCTURE

The gain in a length of structure, l , is given by Equation (5) of Ref. 4 as

$$G = e^{-\chi''_{\max} F(\omega v_g) l},$$

where χ''_{\max} is the magnitude of the diagonalized χ'' tensor, and the filling factor, F , is defined by

$$F = \frac{\int H \cdot \chi'' \cdot H^* ds}{\chi''_{\max} \int H^2 ds}.$$

Since χ''_{\max} is a property of the material and may be computed from Geusic's values for χ''_{\pm} , we find $\chi''_{\max} = 1.4 \chi''_{+}$. In order to obtain the largest gain, one should maximize F . This would occur if the structure were completely filled with ruby and if the RF fields everywhere had the correct ellipticity. In practice, however, this cannot be done. The comb structure cannot be conveniently filled with active material between the fingers, and some air dielectric has to be left near the tips in order to control the frequency and bandwidth. Further, the RF field configuration is controlled by the structure, and the ellipticity is different in different regions. In principle, the *C*-axis of the crystal can be oriented to give the best value for F . Unfortunately, at the time this device was built, large boules could not be obtained with the optimum orientation. It was necessary, therefore, to use the *C*-axis at 60° to the axis of the comb.

The 6-kmc maser was loaded with ruby on only one side, and the ratio of the db gains in the opposite directions of propagation was 3.5. A ratio of about 2 was expected at 2.4 kmc, because of the increased ellipticity of the susceptibility tensor. It was decided, therefore, that a

design would be attempted in which both sides of the slow-wave structure would be loaded with ruby in order to obtain maximum gain. In obtaining this increase in gain, we paid the penalty of reciprocal electronic gain. This led to a rather difficult job for the isolator, since short-circuit stability required the isolator reverse loss to now exceed twice the ruby gain.

The RF magnetic field patterns of the comb are not known exactly; nevertheless it was possible to make a reasonable estimate of the product $\chi''_{\max}F$, and hence obtain the magnetic Q_m at 4.2°K. This approximate computation gave

$$Q_m = \frac{1}{\chi''_{\max}F} \approx 190.$$

The electronic gain may be rewritten [Equation (22) of Ref. 4] as

$$G = 27.3 \left(\frac{SN}{Q_m} \right),$$

where S is the slowing factor and N the number of free space wavelengths in the length of the structure. Assuming an amplifier length of 5 inches and a $Q_m = 190$,

$$G \approx 1.4(10^{-1}S).$$

If the structure and isolator forward loss is assumed to be about 12 db, we see that a slowing factor of about 340 is required for operation at 4.2°K. As this was considered somewhat excessive, it was decided to operate at a pumped helium temperature of about 1.6°K. At this temperature cross-relaxation reduces the inversion ratio to about 2.5. Taking this into account, we obtain a required slowing of 190.

It is now possible to estimate the number of sections required in the slow-wave structure and the structure bandwidth from Equation (38) of Ref. 4,

$$SN = N_s \frac{f_0}{2\pi} \frac{d\varphi}{df},$$

where f_0 is the frequency at which the circuit fingers have an electrical length of one-quarter wavelength, N_s is the total number of sections in the structure, and $d\varphi/df$ is the rate of change of phase shift per section with frequency. Using an empirical relationship between structure bandwidth B_s and $d\varphi/df$, which is

$$\frac{d\varphi}{df} \approx \frac{k\pi}{B_s},$$

where $k \sim 0.6$, then

$$SN = 0.3N_s \frac{f_0}{B_s},$$

and putting in values we obtain

$$\frac{B_s}{N_s} \approx 3.8,$$

where B_s is in megacycles. In the final design, 25 sections were used, which indicates an approximate structure bandwidth of 95 mc, i.e., about 4 per cent. Previous experience showed that fabrication difficulties were often encountered with smaller percentage bandwidths.

V. THE SLOW-WAVE STRUCTURE

One difficulty with the use of the comb structure at low frequencies is the increase in size if the structure is simply scaled in dimensions. The nominal finger length is $\lambda/4$. This dimension is along the direction of the applied dc magnetic field; consequently, it will be a determining factor in the magnet gap size. The actual finger length required can be reduced by capacitive loading at the finger tips and by utilizing the dielectric constant of the ruby maser material.

The 6-kmc traveling-wave maser employed a finger length of $0.87 \lambda/4$. In order to keep the magnet size down, the Echo maser was designed to use a length of $0.64 \lambda/4$. The outer walls of the comb structure, which form the pump frequency waveguide, are 0.400 by 0.850 inches, which is close to X-band waveguide inside dimension. These dimensions give a 0.050-inch gap between the finger tips and the waveguide wall and increase the fringe capacity considerably. The final structure employed an array of 25 fingers having a diameter of 0.070 inch and a pitch of 0.214 inch. The unloaded phase shift per section, φ , versus frequency, f , curve for this structure is shown in Fig. 1 as curve A. The effects of dielectric loading are illustrated by curves B and C. The length of the loading along the fingers determines, to a good approximation, the upper cutoff frequency of the structure. The position of the lower cutoff frequency is then determined by the height of the loading perpendicular to the fingers. Full-height loading, without essentially changing the bandwidth, as in B, lowers the pass band.

In order to obtain maximum gain, full-height loading of the ruby is indicated near the base of the fingers where the RF magnetic fields are strongest. Consequently, the final amplifier design was based on the loading shown in Fig. 1. Under this condition the lower cutoff is deter-

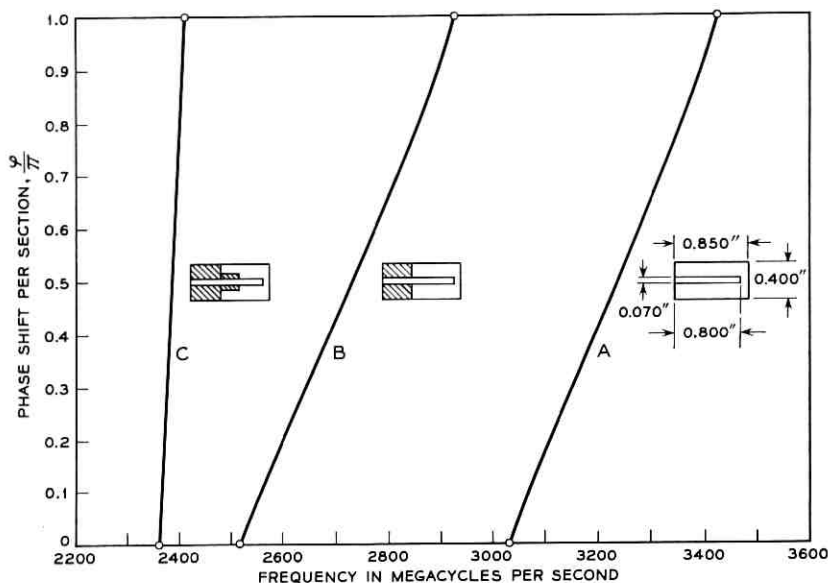


Fig. 1 — Unloaded phase shift per section vs. frequency.

mined primarily by the length of the full-height ruby loading, and is little effected by the partial-height loading. The high-frequency cutoff is determined primarily by the length of ruby directly in contact with the fingers.

VI. THE ISOLATOR

Development of a satisfactory isolator was essential to the design, since the ruby gain was reciprocal. An important aspect of the isolator design was the adjustment of geometry in order to obtain ferrimagnetic resonance at the ruby paramagnetic resonance field. A geometry approaching a thin disk was required, and polycrystalline iron garnet disks with an aspect ratio of 8:1 were used.

Isolator tests were carried out in a crossed-wire strip-line structure in order to determine the performance of the material. Ref. 6 shows typical curves.

The actual volume of yttrium iron garnet which could be used to obtain sufficient reverse loss was determined by the aspect ratio and the physical limitations imposed by the structure dimensions. The remaining parameter was the location of the disks in the signal RF magnetic field. The high field near the base called for placement of the disks in a plane

near the base; they were, however, spaced a small distance away to avoid interaction with the wall and simplify fabrication. The disks were located equidistant between fingers because the RF fields are most circular in this region. Finally, a compromise was made between high reverse loss and high reverse-to-forward loss ratio in choosing the transverse position of the disks between the fingers and the waveguide wall. The isolator has a reverse loss > 120 db and a forward loss of ~ 10 db.

VII. THE AMPLIFIER PACKAGE

The final maser cross section is shown in Fig. 2 along with the method used to hold the isolator disks, which are mounted in a composite alumina sandwich. An equivalent piece of alumina is used on the other side of the comb to symmetrize the loading. Details of the coaxial-to-comb matching arrangement are shown in Fig. 3. By using successive adjustment of the spacing, d , the bend in the wire, and the adjustable short, an adequate match could be obtained.

The dual maser package is shown in Fig. 4. The signal input and output coaxials were connected to low-heat-conductivity air-dielectric coaxial cables. The input cables have a diameter of 0.750 inch and an impedance of 70 ohms. Low electrical loss is important in these cables, since they have a higher noise contribution than any other single part of the amplifier. The output cables are 0.50 inch in diameter with a 50-ohm impedance. The pump frequency waveguide is Ku-band, and a 3-db top-wall short-slot coupler is provided to divide the incoming pump power equally for the two maser amplifiers.

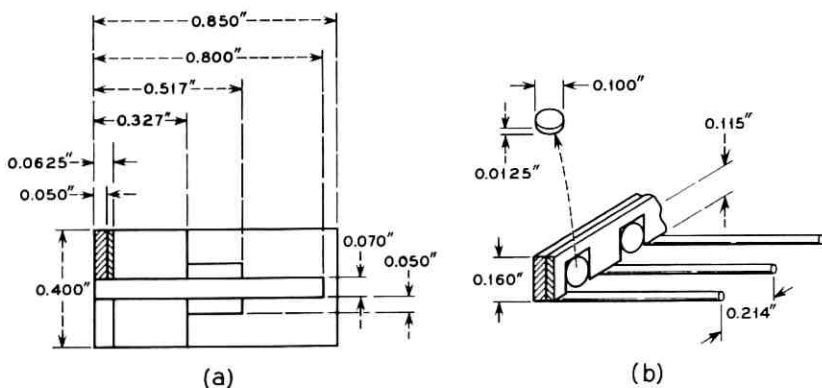


Fig. 2 — (a) Maser cross section including isolator; (b) placement of garnet disks relative to comb structure.

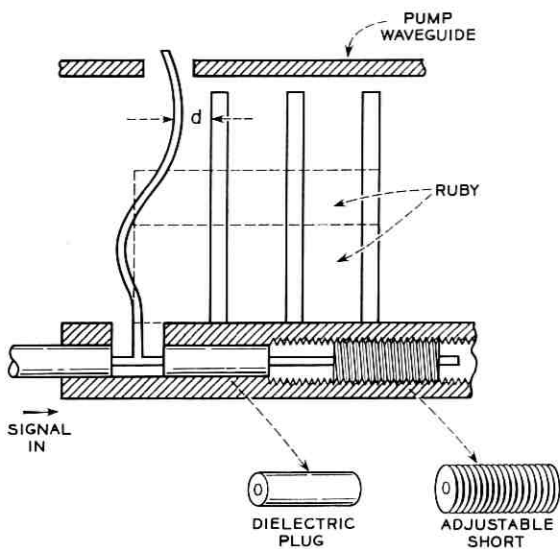


Fig. 3 — Coaxial-to-comb matching arrangement.

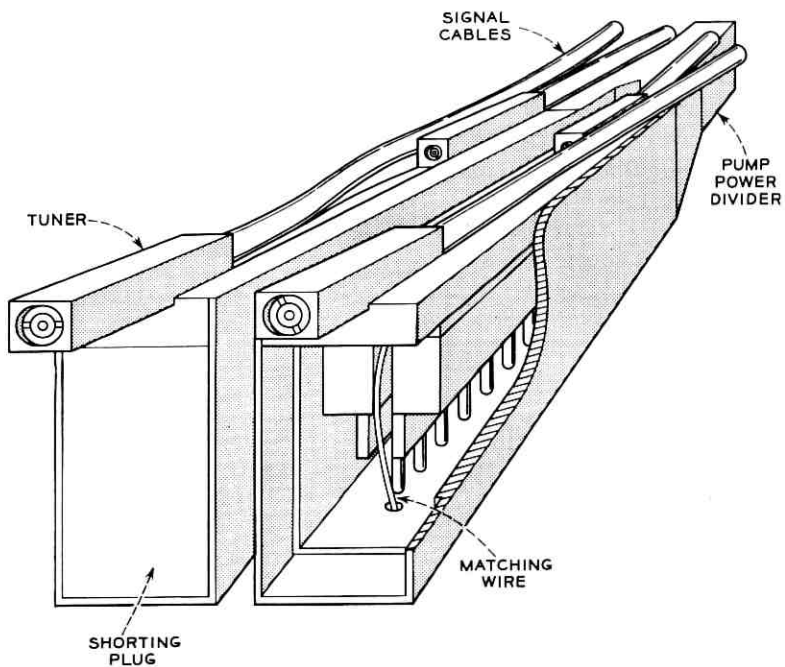


Fig. 4 — Two-maser package.

The cable assembly and traveling-wave maser structure are located in a stainless steel dewar with a 10-liter helium capacity. The tip of the dewar is between the poles of a permanent magnet whose field can be adjusted with movable shunts. The dewar and magnet are mounted in a frame which also contains the microwave pump klystron, the automatic frequency control discriminator and associated waveguide, the automatic nitrogen transfer controls, temperature and level monitoring meters, and the vacuum control valves and gauges.

The entire assembly is mounted just beneath the antenna feed in the cab at the back of the antenna, which also houses the remainder of the microwave receiver and the monitoring and calibration equipment. The vacuum pump is remotely located at the base of the antenna.

The dual maser amplifier characteristics are as follows:

Center frequency:	2390 mc
Instantaneous bandwidth:	13 mc
Tuning range:	± 10 mc
Gain, channel I:	36 db
Gain, channel II:	33 db
Pump frequency:	13 kmc
Pump power:	70 mw per channel
Magnetic field:	2530 oersteds
Noise temperature:	$8 \pm 1^\circ\text{K}$
Operating temperature:	1.8°K
Running time:	20 hours (approximately)
Helium capacity:	10 liters

The noise temperature is somewhat greater than the expected 5°K . This is believed due to excess loss in the input cables and mismatch, which together seem to contribute approximately 7°K , the maser proper contributing about 1°K . Using standard laboratory transfer procedures, about 12 liters of helium are needed to fill the dewar.

VIII. ACKNOWLEDGMENTS

We are indebted to P. P. Cioffi and D. C. Hogg, who supplied the variable shunt permanent magnet and stabilized pumping klystron respectively. We wish to thank J. E. Geusic and E. O. Schulz-DuBois for making measurements on the ruby and the isolator material, as well as for their many useful suggestions. We acknowledge the help of D. Halvorsen in the mechanical design.

The device was installed in the antenna in collaboration with E. A.

Ohm, who was responsible for the cryogenic transfer system used in the field.

The use of this device in Project Echo was in connection with National Aeronautics and Space Administration Contract NASW-110.

APPENDIX

Some Remarks on a Double-Valued $\omega\beta$ Diagram

At one stage of the design considerable difficulty was experienced when the device persisted in being unstable. These oscillations were quite unexpected, since they occurred well within the passband of the amplifier and at a frequency where the isolator seemed to give excellent reverse loss. It had also been observed that the passband with the isolator magnetic field at resonance was much narrower than when it was off resonance, and that sometimes a minimum in transmission would appear in the passband. It is now believed that these effects can be explained by an anomolous mode of propagation.

As previously mentioned, the height of the loading primarily controls the lower cutoff, while the width primarily controls the upper cutoff. By the use of a small-height dielectric loading, the upper cutoff of the empty structure can be shifted below the lower cutoff. Under these conditions the structure is backward wave; i.e., the phase and group

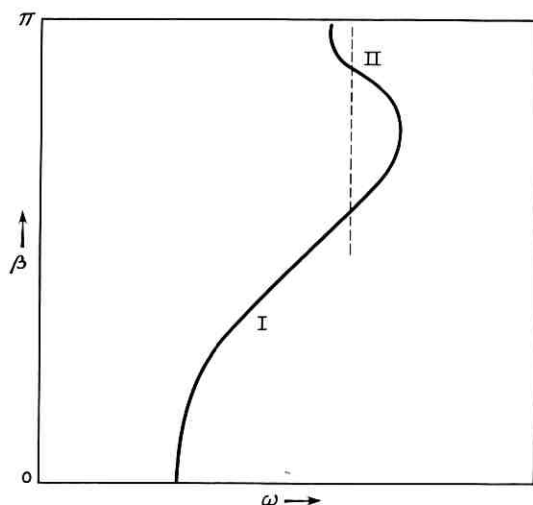


Fig. 5 — Double mode of propagation.

velocities have opposite directions. In our design we wished to use a narrow passband and consequently the loading was chosen such that small changes in the loading could shift the structure from forward to backward. Under these conditions curves such as shown in Fig. 5 can occur. Notice that the upper and lower cutoff frequencies are close together as indicated by the 0 and π phase-shift points. However, in the nominal passband of the structure the phase shift is double-valued.

This double mode has a particularly bad effect upon a traveling-wave maser. Consider operation at a frequency within the double mode region as indicated by the dotted line of Fig. 5. The mode labeled I has a forward phase velocity and a forward group velocity. With the correct direction of magnetic field and an isolator, we will obtain normal unilateral gain in the forward direction. However, under the same conditions, unilateral gain in mode II will be in the reverse direction because the group velocity is backward for the phase velocity which corresponds to low isolator loss. Oscillation can now occur—the wave travels forward in the structure on mode I, is reflected by any mismatch into mode II, and returns to the input of the amplifier on mode II. The result is a feedback path with potentially high gain.

These effects have since been encountered in masers at other frequencies when attempting to obtain very narrow bandwidths. Frequently a change of only a few mils in the dielectric loading is sufficient to cure the difficulty.

REFERENCES

1. Jakes, W. C., Jr., Participation of Bell Telephone Laboratories in Project Echo and Experimental Results, this issue, p. 975.
2. Crawford, A. B., Hogg, D. C., and Hunt, L. E., A Horn-Reflector Antenna for Space Communication, this issue, p. 1095.
3. Ohm, E. A., Receiving System, this issue, p. 1065.
4. DeGrasse, R. W., Schulz-DuBois, E. O., and Scovil, H. E. D., The Three-Level Solid State Traveling-Wave Maser, *B.S.T.J.*, **38**, 1959, p. 305.
5. Geusic, J. E., Microwave Solid-State Devices, U. S. Army Signal Corps Contract DA-36-039 sc-73224, Tenth Interim Report, August 1959.
6. Schulz-DuBois, E. O., Microwave Solid-State Devices, U. S. Army Signal Corps Contract DA-36-039 sc-73224, Eleventh Interim Report, November 1959.

PROJECT ECHO

Standby Receiver System

By L. U. KIBLER

(Manuscript received April 7, 1961)

The Echo I satellite receiving system at Holmdel, New Jersey, required a 2390-mc standby receiver system to maintain operation during possible failures of the primary maser receiver. This paper describes the details of the two matched parametric amplifiers that were used to provide the standby receiver. The use of this system in the initial Moonbounce experiments and in Project Echo is described. The details of an emergency operation at the beginning of a balloon pass are also presented.

I. INTRODUCTION

The Echo I 2390 mc receiving system* is shown in block diagram form in Fig. 1. The masers and parametric amplifiers are shown in parallel in the over-all system. Since the parametric amplifier system must provide performance similar to that portion of the primary system it parallels, it must have comparable gain and bandwidth, and must have an acceptable noise figure.

In addition to the general requirement that the parametric amplifier system be independent of the maser system, there were a number of specific requirements. The input frequency was 2390 mc and the output frequency was 70 mc. For system compatibility the parametric amplifier system, including the down-converter and IF amplifier, had to provide at least 60 db over-all gain. The minimum band width for the planned experiments was 5 mc. Considerations of the transmitter power and antenna gain at the Jet Propulsion Laboratory facility at Goldstone, California, the path loss, and the Holmdel antenna gain and noise temperature indicated that a noise temperature of 300°K would be acceptable for the standby system.

* Although this equipment was designed by the Bell System as part of its research and development program, it was operated in connection with Project Echo under Contract NASW-110 for the National Aeronautics and Space Administration.

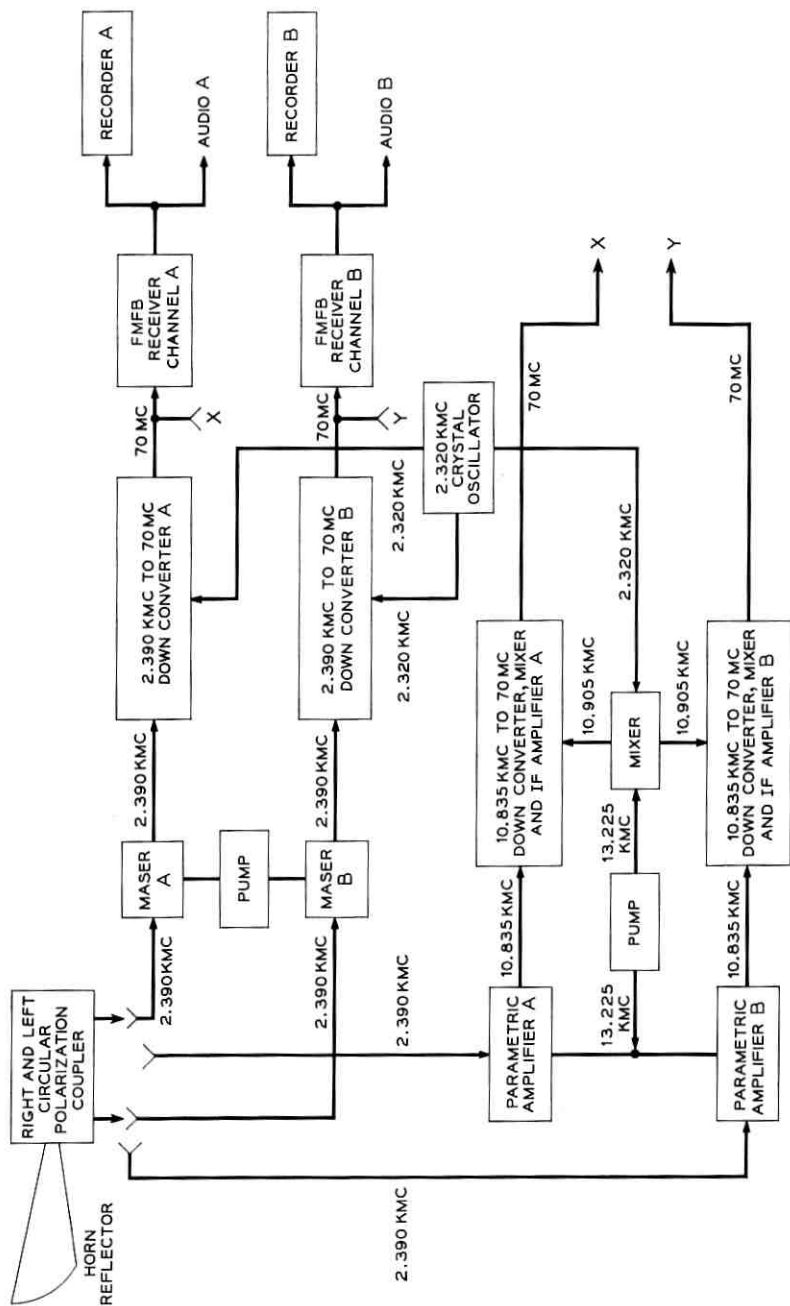


Fig. 1 — Over-all receiving system for Project Echo.

In addition to the electronic requirements, size and weight limitations were imposed. The parametric amplifiers (paramps) had to share a small antenna cab mounted on the horn antenna with the maser and the test equipment. The completed paramp system had to weigh less than 300 pounds and occupy a maximum space of 3 feet in width and length, 4 feet 8 inches in height.

The completed paramp system provided a total gain of 63 db in each channel with 3-db bandwidths of 15.5 mc and 21.5 mc respectively. The over-all system temperatures were 283°K and 297°K respectively. The gain of the system varied ± 0.5 db over the hour* of operation associated with a balloon pass.

II. PARAMETRIC AMPLIFIER SYSTEM

The parametric amplifier system consists of two identical negative-resistance up-converters using a common pump source, resistive down-converters, and a frequency-stabilizing circuit. The various parts of the complete system are detailed in the block diagram of Fig. 2.†

The choice of the negative-resistance up-converter mode of operation was dictated by gain-stability considerations and by the availability of low insertion loss isolators. Low-loss circulators were not available when this system was designed. It has been shown² that operation of a parametric amplifier with the idler frequency terminated in the varactor diode series resistance provides the lowest noise temperature. This mode of operation requires a reflection-type negative-resistance amplifier using a circulator. All the gain is achieved from the negative resistance. The negative-resistance up-converter achieves part of the gain from negative resistance and part from the frequency ratio of the up-conversion. Thus, for a given gain, the up-converter will generally have better gain stability than the reflection amplifier. The decrease in noise temperature associated with the reflection mode of operation was offset by the increased insertion loss of the available circulators. The promise of increased stability with only a slight increase in the over-all system noise temperature led to the choice of the negative-resistance up-converter mode of operation.

Silicon mesa varactor diodes with 1 kmc Q's of 60 to 70‡ were available. These diodes have zero bias capacitance of 1.8 to 2.1 $\mu\mu\text{f}$ including

* This hour includes the 12 to 20 minutes of the actual pass and the time for pre- and postcalibration of the system.

† The single parametric amplifier is similar in mode of operation to that described by Uenohara and Seidel.¹

‡ The Q of the wafer without encapsulation, measured at zero bias.

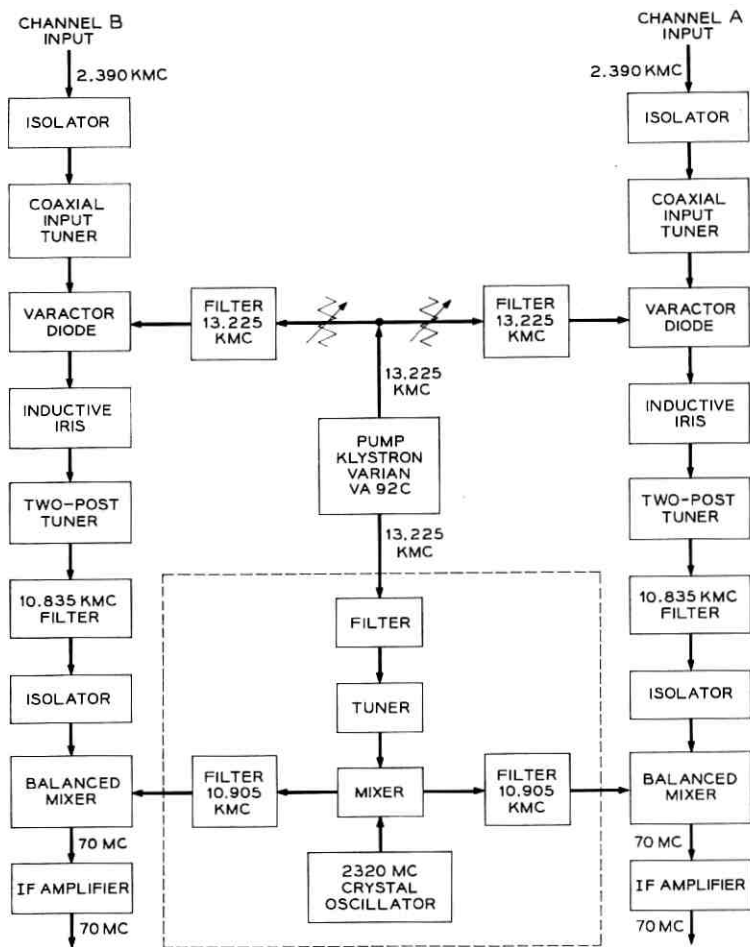


Fig. 2 — Block diagram of parametric amplifier system.

the cartridge. The series resistance typically lies between 1.7 and 2.4 ohms. A typical capacitance-voltage characteristic for these diodes is shown in Fig. 3; the double-ended ceramic cartridge is shown in Fig. 4.

The choice of the pump frequency was a compromise of several requirements: The availability of a stable klystron with sufficient power output to operate the two amplifiers and the frequency-stabilizing circuit; the gain-stability of the amplifier as represented by the proportion of negative-resistance gain and up-conversion gain required for the total paramp gain; and the optimum idler frequency for minimum noise figure

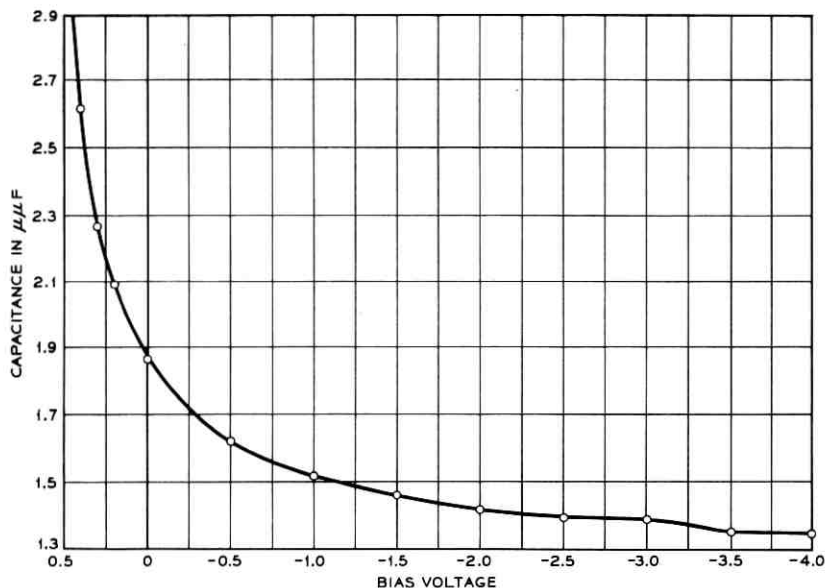


Fig. 3 — Capacitance vs. voltage for the silicon mesa varactor diode.

had all to be considered. The division of the required 60 db total gain between the parametric amplifier and the down-converter IF amplifier also entered into these considerations.

After study of the interaction of these various factors it was decided that the experimental system should operate under the following condi-

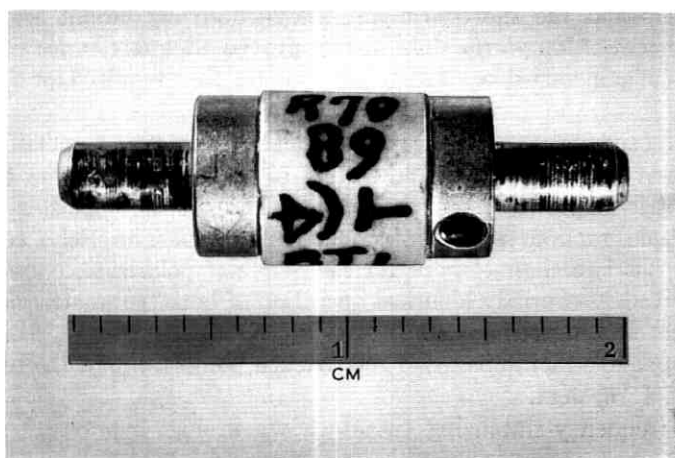


Fig. 4 — Typical encapsulated varactor diode.

tions. The pump frequency would be 13.225 kmc. The required pump power could be met with a 3-db margin by using the Varian VA-92-C reflex klystron. For the 2390-mc input frequency the idler or output frequency of the paramp became 10.835 kmc, with the paramp being assigned 23 db of the total 60 db required gain. The up-conversion gain for the idler frequency chosen was 6.5 db. Thus 16.5 db of negative-resistance gain was required. The Sylvania coaxial isolator* provided 0.4 db insertion loss with 24 db isolation over the required bandwidth at 2390 mc. The reflection coefficient (power) at the isolator input was 0.17 under these conditions. The antenna system return loss was greater than 30 db. The variation of antenna match resulted in an amplifier gain variation of less than 0.03 db.

The remaining 37 db of gain had to be supplied by the down-converter mixer and IF amplifier. The down-converter mixer was allowed a 12-db noise figure in the consideration of system operation; it was felt that the noise figure would not be greater than this value.

The parametric amplifier gain is sensitive not only to the antenna load variation, but also to the pump amplitude and frequency variation. The klystron chosen was a stable one; it was mounted in a heavy brass box with forced-air cooling from a blower that was shock-mounted, so that no vibration was transmitted to the tube. The cooling air was obtained from the antenna cab interior, which was kept within 5°F of a nominal 76°F by two large heater-airconditioning units. A stabilizing cavity with its feedback circuit was not used to stabilize the klystron, since such a system requires the expenditure of additional pump power, and there was insufficient power available after the requirements of the two amplifiers and the short-term frequency-stabilizing circuit were met. This system of long-term stabilization proved adequate, since the overall system gain varied less than 0.5 db over the time required for a balloon pass.

The receivers that follow the output of the parametric amplifier system operate over a narrow band centered at 70 mc. It was necessary that the parametric amplifier system output be held at 70 mc regardless of possible rapid random pump frequency variations. The Echo receiving system has two channels, one for each circular polarization that might be received. Essentially identical operation of both parametric amplifier channels was insured by use of the common pump source, which also makes possible maintenance of relative RF phase through the complete RF and IF system.

The frequency-stabilizing circuit shown in Fig. 2 prevents a rapid

* This isolator was a modified form of Sylvania model FD135P.

frequency variation in the output of both channels. The pump power was divided equally between the two parametric amplifiers and the local oscillator mixer by a 3-db directional coupler. A second signal at 2320 mc was supplied to the mixer by a modified crystal-controlled microwave radio transmitter† (100 mw of power available). The 5-mw output of this mixer at 10.905 kmc was used to supply the local oscillator power for the two balanced mixer down-converters. The local oscillator mixer was a gallium arsenide diode supplied by Bell Telephone Laboratories, Allentown, Pennsylvania.

The stabilization of the 70-mc output frequency against rapid pump frequency variation was accomplished in the following manner. Considered at some instant, the pump frequency becomes $f_p = (13.225 + \delta)$ kmc. The output of the local oscillator mixer then becomes $f_{LO} = (13.225 + \delta - 2.320)$ kmc = $(10.905 + \delta)$ kmc. The output of the paramp for a 2.390 kmc input signal under the effect of the pump shift is $f_o = 13.225 + \delta - 2.390 = (10.835 + \delta)$ kmc. The resulting frequencies were mixed in the down-converter mixer and the difference frequency applied to the 70-mc IF amplifier. This difference frequency becomes $f_{LO} - f_o = 10.905 + \delta - 10.835 - \delta = 70$ mc. A similar result is obtained for a negative δ shift in pump frequency. Thus for small shifts in pump frequency the output of the system was maintained at 70 mc. It is true that the frequency of the paramp idler output, 10.835 kmc, varies with δ as shown, but the 10.835-kmc circuits are relative wide-band and little or no signal impairment results.

III. PARAMETRIC AMPLIFIER DESIGN

The design of the parametric amplifier was based on a combination of mathematical analysis and experimental design. The gain of a lower-sideband up-converter can be expressed in terms of a reflection coefficient at a suitably chosen point in the input transmission line as:

$$PG = \frac{\omega_{-1}}{\omega_0} (1 - \rho\rho^*),$$

where ρ is the reflection coefficient, ω_{-1} is the idler or output frequency, and ω_0 is the signal or input frequency. The magnitude of the reflection coefficient can be determined for a given power gain. Seidel has shown³ that the Smith chart may also be used to plot the reflection coefficient,

† A Western Electric TDE microwave transmitter, Model SD-59409-02, was modified by retuning and elimination of the last doubler stage.

and hence impedances, when this coefficient is greater than one. With the paramp operating at low gain (relatively narrow bandwidth), the reflection coefficient was experimentally measured at both the signal and idler frequencies. These reflection coefficients were plotted on a Smith chart, and from this plot the impedance elements necessary to increase the gain and bandwidth were determined.

The initial paramp gain was obtained in the following manner. The capacitance-voltage characteristic of the varactor diode (Fig. 3 is typical) was measured at 100 kc; C_1 and C_0 were determined⁴ from this characteristic. Since these diodes were operated in a self-bias condition, the forward limit of capacitance variation was arbitrarily taken at a diode voltage corresponding to 1 microampere of direct current. This then located the limit of reverse bias capacitance for sine wave pumping. The change in capacitance between these two values was taken as C_1 , and the average of these two capacitance limits was taken as C_0 .

Microwave circuit elements were designed to resonate C_0 in the waveguide at the idler frequency and in the coaxial circuit at the signal frequency. These elements also transformed the waveguide impedance, considered on a voltage-power basis,⁵ to impedance levels at the diode that were comparable to the diode reactance. Provision for tuning was incorporated in the microwave elements.

The noise figure of the paramp was measured continuously while the circuit impedances were changed to increase the gain and bandwidth. The noise figure was minimized as the gain and bandwidth were increased.

The details of the completed parametric amplifier are shown in Fig. 5. The 2390-mc input circuit consists of coaxial elements. The 10.835-kmc idler output circuit is constructed in 0.4- by 0.9-inch X-band waveguide. The pump circuit consists of 0.311- by 0.622-inch Ku-band and 0.4- by 0.9-inch X-band waveguide.

The varactor diode is placed across the center of the X-band waveguide with one end supported by the center conductor of the 23-ohm input line. This section of line also contains the pump and idler choke sections. The other end of the varactor is grounded to the waveguide wall. The 23-ohm coaxial line is connected in series with an 11-ohm coaxial line slightly less than $\lambda/4$ in length at 2390 mc. This 11-ohm line is in series with a length of 50-ohm line, followed by a 50-ohm shunt-shortened stub. The isolator is connected in series at this point through a length of 50-ohm coaxial line.

The choke in the center conductor of the 23-ohm coaxial line connected to the diode terminal prevents both the idler and pump signals from

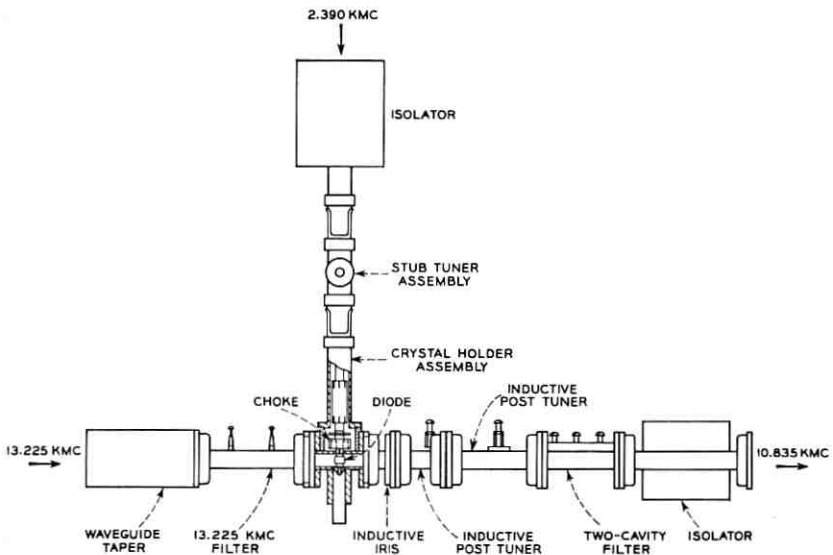


Fig. 5 — Assembly diagram of a single parametric amplifier.

entering the coaxial input circuit. The radial line portion of this choke is resonant at 10.835 kmc. This distance between this radial line section and the diode terminal at the waveguide wall is a quarter wavelength at the idler frequency. The high impedance at the radial line terminals becomes a short circuit at the guide wall. The high-impedance coaxial line formed on the inside of the choke is resonant at the pump frequency, and thus provides an open circuit for the pump at the guide wall. The choke provides 26 db idler rejection and 30 db pump rejection.

The pump signal is fed from the Ku-band waveguide through a linear-tapered section to the X-band guide containing the diode. Following the taper in the X-band guide is a two-cavity pump filter, which has a 60-mc bandwidth at 13.225 kmc. The pump filter is placed with respect to the diode terminals so as to provide an inductive circuit element required by the idler circuit.

The output circuit at the idler frequency contains an inductive iris followed by two post tuners. By properly positioning these microwave elements, the remaining idler circuit elements are provided. The idler output passes through a three-cavity filter with 50-mc bandwidth and an isolator.*

* Raytheon model 1HE4.

The coaxial stub tuner and the idler output post tuners are adjustable, so that amplifier response can be adjusted in the event that wide ambient temperature changes occurred or in the event of diode replacement. The spare diodes are not identical with the characteristics of the in-service diodes.

The frequency response of the two parametric amplifiers constructed for the system is shown in Fig. 6 for a gain of 23 db. The 3-db bandwidth is 15.5 mc for the channel A amplifier and 21.5 mc for the channel B amplifier. The noise figures are 2.69 db (250°K) and 2.79 db (261°K) respectively, including the 0.4-db insertion loss associated with the coaxial input isolators. It is possible to achieve gains of 40 db by increasing the pump power. The band shape remains, but the bandwidth narrows to 2 mc, and the gain stability is extremely poor. A broad minimum noise figure exists for gains between 20 db and 26 db, but above 26 db the increased pump level causes the dc short-circuited diode to draw current. A shorted dc diode mounting was chosen to simplify the diode mounting and to eliminate the need for separate stable bias supplies.

The down-converter mixer and the IF amplifier are of conventional design. The balanced mixer uses a "magic T" with a pair of 1N78MR diodes placed in broadband mountings in the conjugate arms. The mixer waveguide assembly is mounted directly on a five-tube 70-mc IF amplifier. This amplifier has a 1-db bandwidth of 20 mc and a gain of 51 db. The amplifier uses three WE 417A tubes, a WE 404A tube, and a WE 436A output tube. The down-converter mixer and the IF amplifier, when operated with a local oscillator drive sufficient to produce 0.5

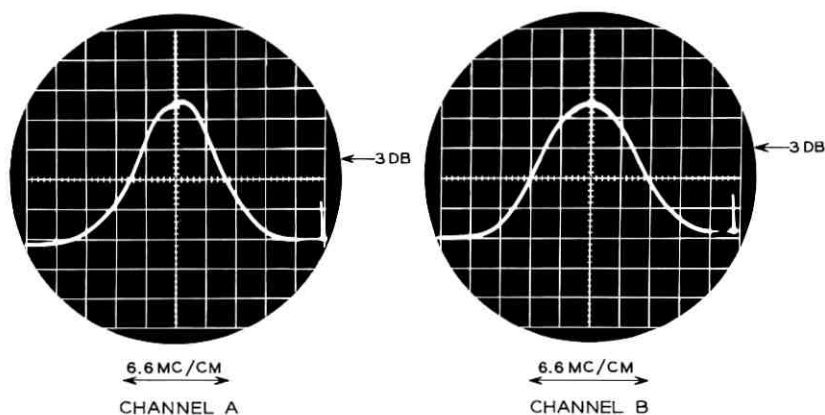


Fig. 6 — Parametric amplifier band-pass characteristic for channels A and B.

milliamperes diode current, have an over-all gain of 38 db, a 1-db bandwidth of 20 mc, and a noise figure of 12.5 db. The performance of the two units constructed was within 0.5 db of the above results.

The auxiliary mixer, which provides a frequency-stabilized local oscillator, employs a gallium arsenide diode supplied by the Allentown Laboratories. This diode is mounted across the center of a 0.4- by 0.9-inch X-band waveguide. One end of the diode is grounded to the guide wall, while the other end is held by the center conductor of the 23-ohm input coaxial line. The 2320-mc signal from the modified crystal-controlled transmitter is coupled to this 23-ohm line through a length of 50-ohm line and a shunt-shortened stub. The 23-ohm line contains a series choke of the type used in the parametric amplifier to block the pump frequency and the local oscillator output (10.905 kmc) from the coaxial input circuit. The pump power passes from the Ku-band waveguide through a linear taper to the X-band guide. A single-cavity filter is placed between the taper and the diode terminals, positioned so as to provide an open circuit across the diode at the local oscillator frequency (10.905 kmc). The tuning for the local oscillator circuit is provided by an inductive iris and a slide-screw tuner. The local oscillator output is taken through a narrow-band filter centered at 10.905 kmc and an isolator.* Sufficient output power was available to produce 1.2 milliamperes of current in each of the four 1N78 diodes in the two down-converter mixers.

IV. INSTALLATION AND SYSTEM OPERATION

The parametric amplifiers, with the mixers, pump klystron, and their associated components, were mounted on the aluminum and magnesium frame pictured in Figs. 7 and 8. The location of the various system parts are identified on these photographs.

In order to simplify the operation of the amplifiers in the small confines of the antenna cab, controls and meters were grouped functionally on both sides of the frame. The pump klystron, frequency monitor circuit, pump level attenuators, and parametric amplifiers were grouped on one side of the frame. The opposite side of the frame contains the controls and meters associated with the local oscillator, the down-converter mixer, and the IF amplifiers.

After extensive tests were conducted in an antenna cab mock-up in the laboratory, the assembled system was moved to the antenna cab and bolted to the floor between the maser and the racks of test equipment. Although initially provision had been made on the parametric amplifier

* An experimental Bell Telephone Laboratories isolator was used.

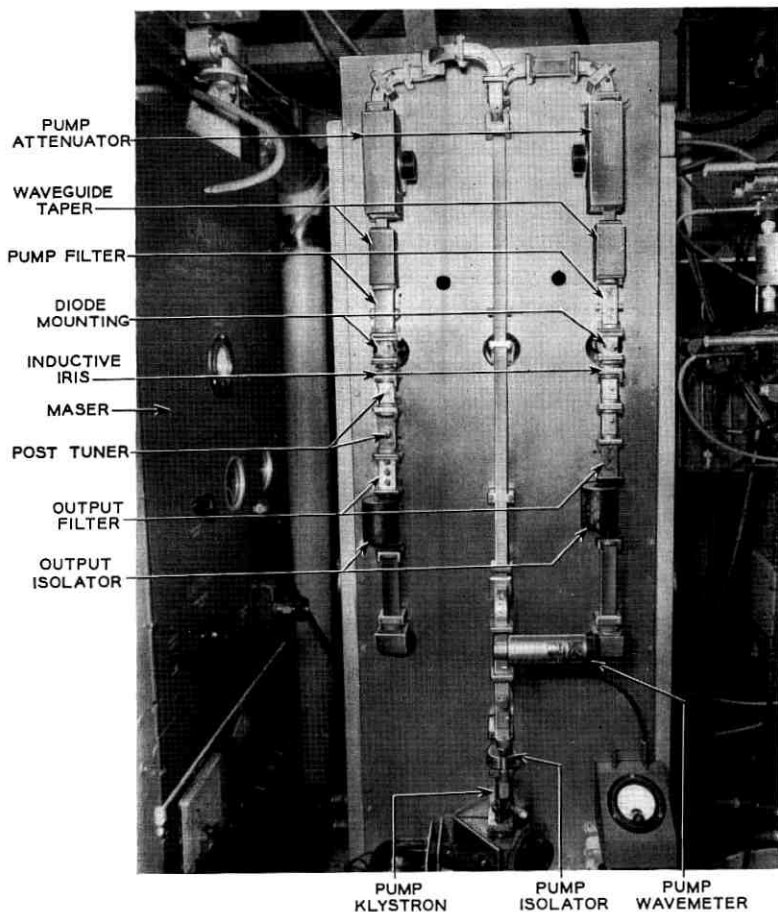


Fig. 7 — Dual parametric amplifiers mounted on support frame (side 1).

mounting frame for the power supplies, these components were mounted in a separate rack in the forward part of the cab with the 2320-mc transmitter. Figs. 9, 10, 11, and 12 indicate the position of the parts of the entire system within the antenna cab.

The inputs to the two channels of the parametric amplifier system were connected to waveguide-coaxial transducers at each polarization coupler with Styroflex semi-rigid coaxial line. The loss of each 6-foot coaxial cable run was 0.05 db. The transducers and coaxial cable runs were not permanently installed, since the maser was the primary receiving system. In the event of maser failure, the maser waveguide-coaxial

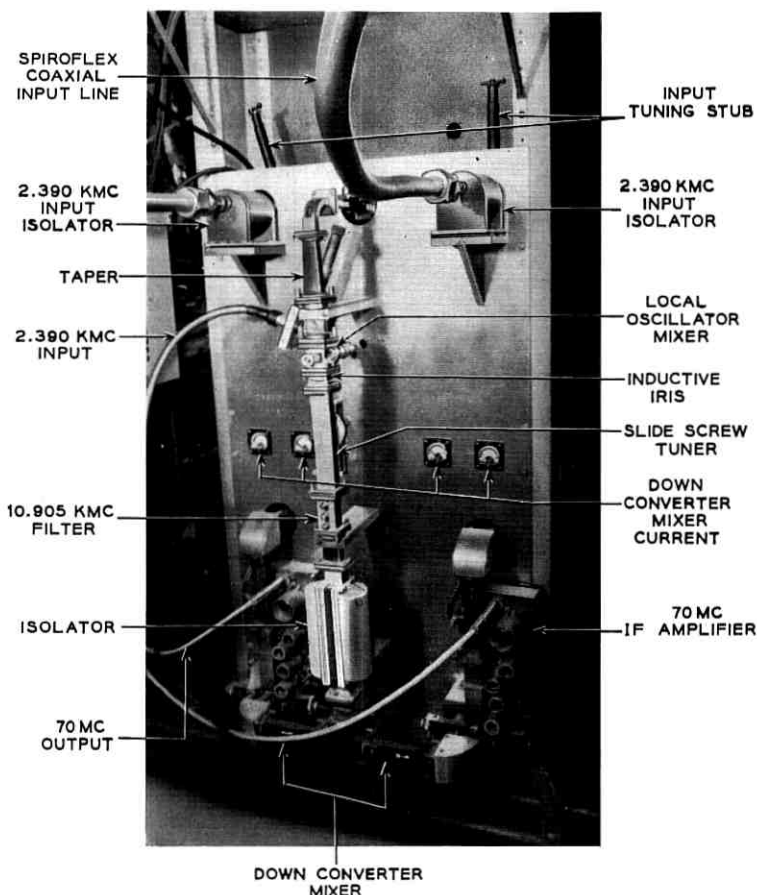


Fig. 8 — Dual parametric amplifiers mounted on support frame (side 2).

transducers were disconnected from the polarization couplers and the parametric amplifier system connected with its transducers and coaxial cable. The arrangements of the transducers and cable run can be seen in Figs. 8, 9, and 12.

Prior to the launching of the Echo I satellite the parametric amplifier system was tested using signals generated locally from a swept 2390-mc oscillator, a signal generator, and a precision attenuator or noise lamp. Gain, frequency response, and noise figure measurements were made with these signals. Tests on the installed parametric amplifier system at paramp gains of 23 db showed the same bandwidth as was measured

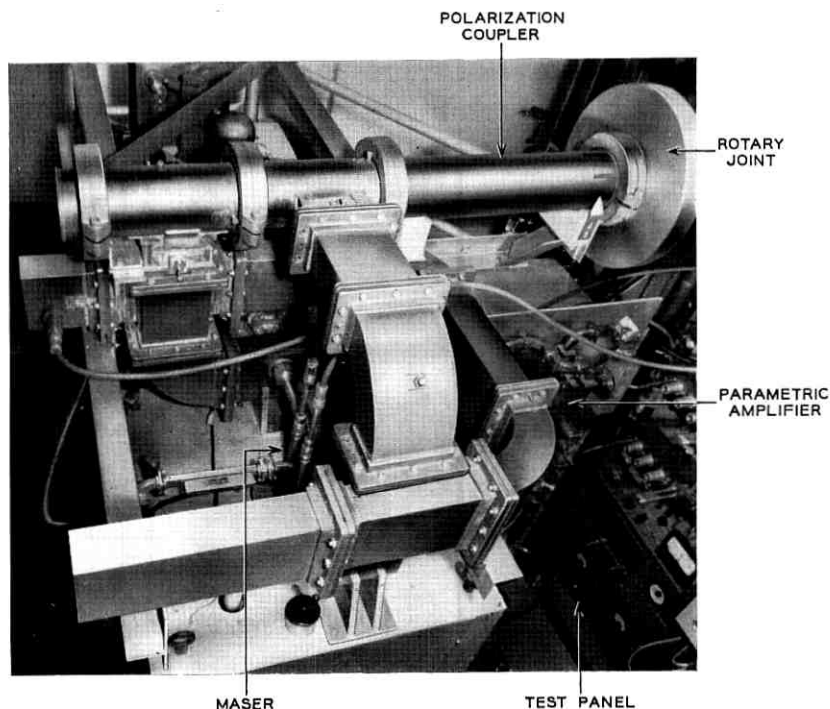


Fig. 9 — Relative position of parametric amplifier and maser in antenna cab.

for the separate paramps, but the noise figure had increased. The noise figure of the A channel was 2.97 db (283°K) and that of the B channel was 3.07 db (297°K). The increase in system noise figure over the individual amplifier noise figure was due to the effect of the down-converter mixers and the losses in the antenna lines and couplers.

These results were confirmed by on-air operating tests conducted with signals received from the Jet Propulsion Laboratory at Goldstone, California by moon bounce. Fig. 13 shows the noise received from the moon with the parametric amplifier system as the antenna was scanned across the moon. While the noise increase was not large, it is quite plainly observable. Further tests indicated that the over-all system using the parametric amplifiers had a minimum detectable signal level of -133 dbm over a 6-kc band.

The parametric amplifier system was put into use when the maser "iced up" 15 minutes prior to pass 93 of the satellite. The parametric amplifiers were not on standby, and hence the pump klystron and all

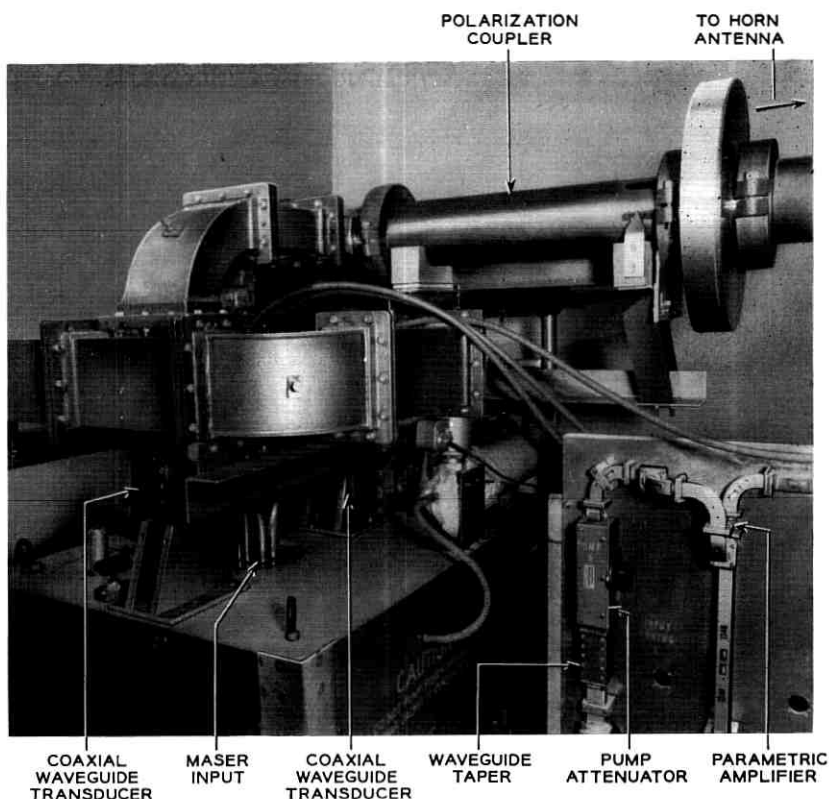


Fig. 10 — Position of parametric amplifiers and masers relative to the polarization coupler.

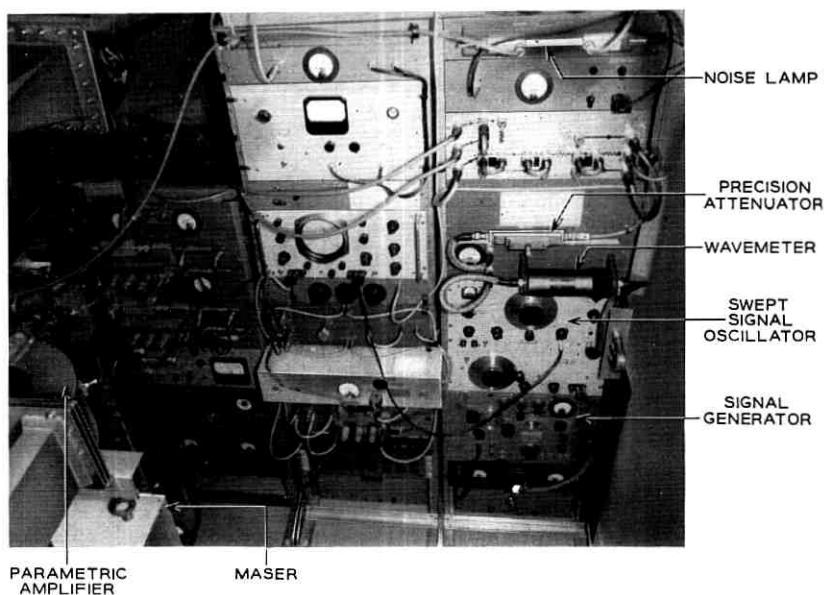


Fig. 11 — Test panel in the antenna cab.

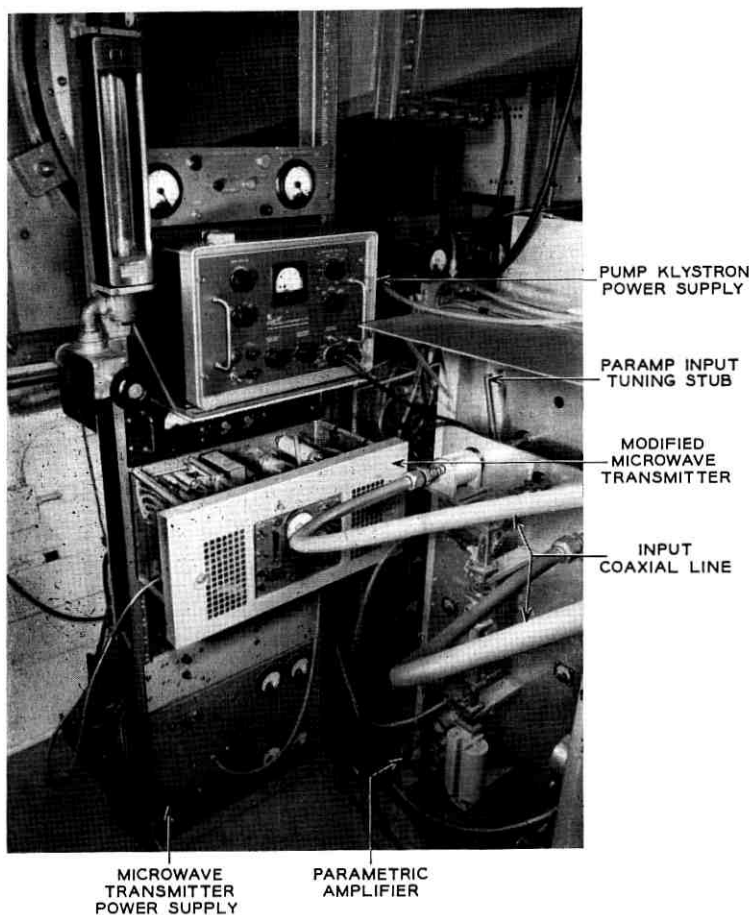


Fig. 12 — Parametric amplifier coaxial input lines, power supply mountings and microwave transmitter.

tube circuits were "cold." Eight minutes before the pass the parametric amplifier circuits were energized. Signals were received from JPL five minutes after the pass started, and the pass was completed satisfactorily. In the intervening 13 minutes, the maser was brought up to atmospheric pressure, vacuum seals were disconnected, and the parametric amplifier transducers and coaxial lines were installed in place of the maser units. The response of the parametric amplifier system was checked and minor tuning adjustments were made to compensate for the cold pump klystron. The parametric amplifiers continued in use during passes 93 and

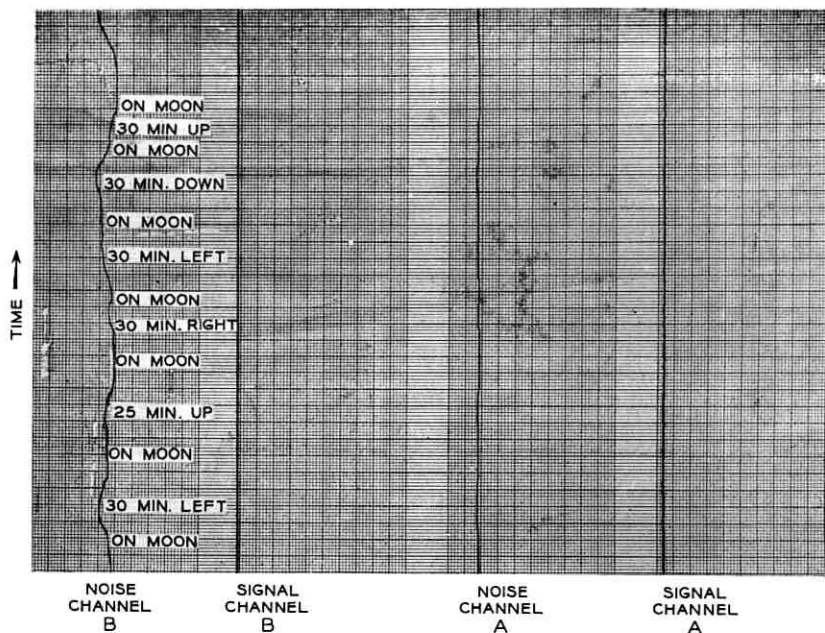


Fig. 13 — Noise signal received by the parametric amplifier system as the antenna scanned the moon.

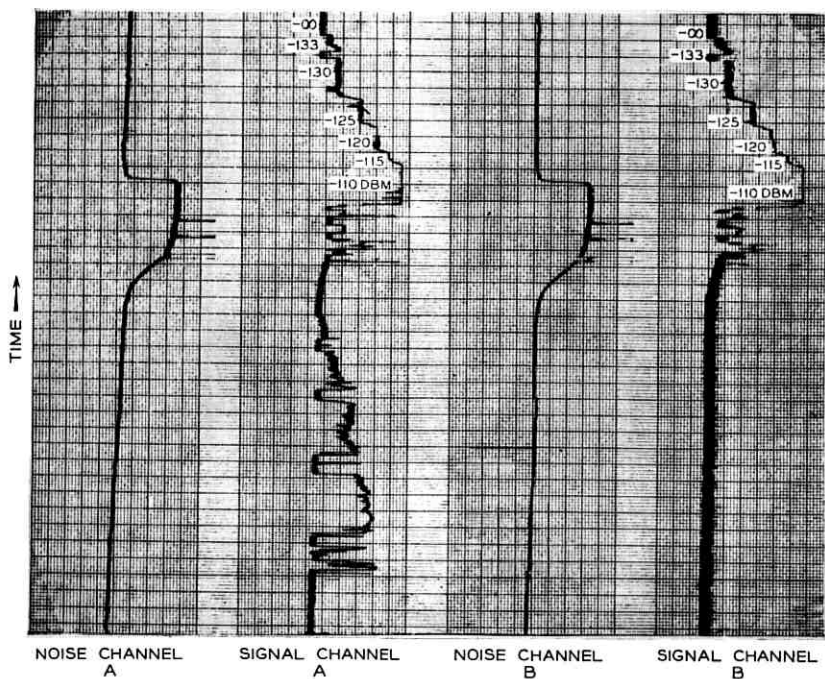


Fig. 14 — Recording of signal levels received by the parametric amplifier system from JPL, pass 93. Signal levels increase from left to right.

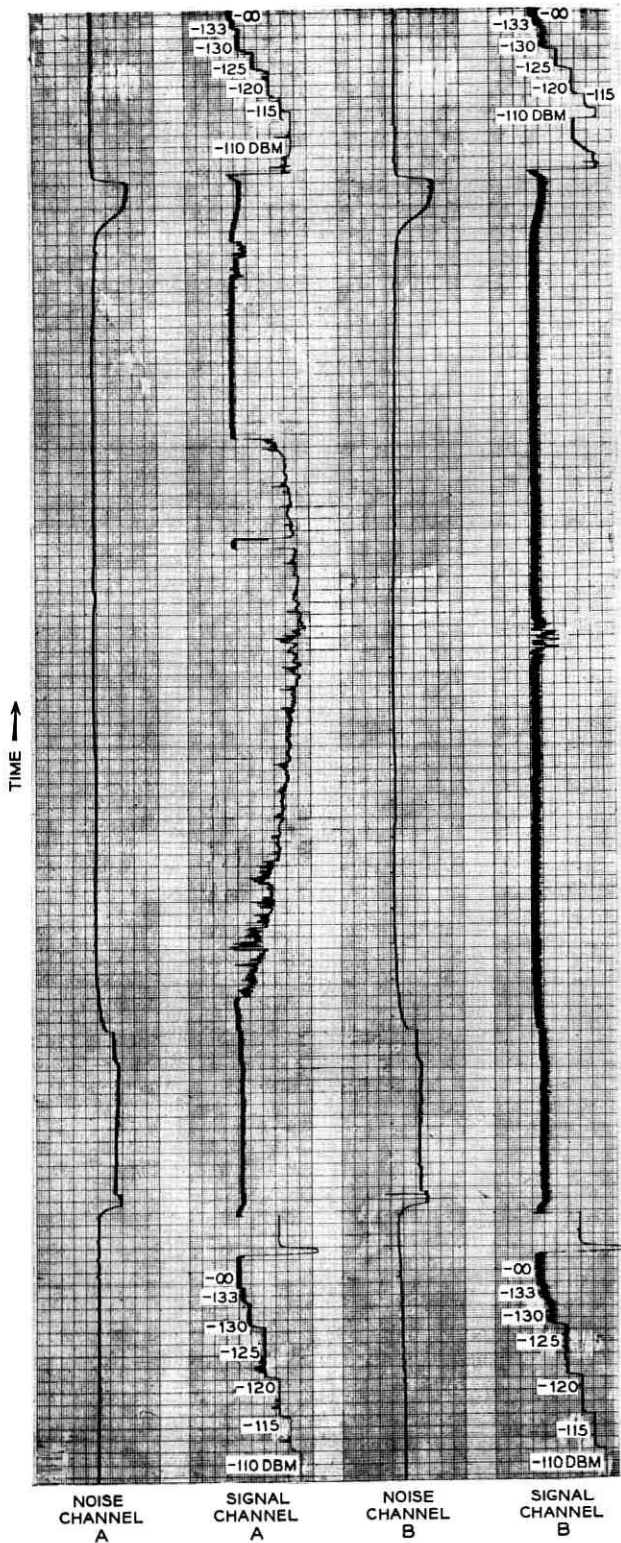


Fig. 15 — Recording of signal levels received by the parametric amplifier system from JPL, pass 94. Signal levels increase from left to right.

94. The recorded received signal levels and input noise temperature are shown in Figs. 14 and 15 for these passes.*

The parametric amplifier system was operated on several later passes when the maser helium supply was low. In all instances the parametric amplifiers have performed well and yielded the necessary information for the pass. The paramps are not generally able to detect the cross-polarized signals, since one polarization is 15 to 30 db below the main signal. The maser, with its lower noise temperature, was able to receive this component on almost all passes.

V. CONCLUSION

An experimental parametric amplifier receiving system has been shown to be adequate for communication experiments of the Echo type. The system is reliable and can be placed in operation in a short time. It is not subject to the vacuum failures, "freeze-ups," or the need for expensive coolants. This system, of course, does not have the extremely low noise temperature of the maser, although, if revised to provide liquid nitrogen cooling, it could have a noise temperature of as low as 40°K. In spite of the higher noise temperature, the parametric amplifier has been adequate for communication via balloon-type satellites.

VI. ACKNOWLEDGMENTS

I wish to express my appreciation to A. E. Bakanowski for supplying the varactor diodes, to W. M. Goodall and E. A. Ohm for their helpful criticism, and to J. E. LaVerne for assistance in the system assembly.

REFERENCES

1. Uenohara, M., and Seidel, H., 961-mc Lower-Sideband Up-Converter for Satellite-Tracking Radar, this issue, p. 1183.
2. Kurokawa, K., and Uenohara, M., Minimum Noise Figure of the Variable-Capacitance Amplifier, B.S.T.J., **40**, 1961, p. 695.
3. Seidel, H., unpublished manuscript.
4. Manley, J. M., and Rowe, H. E., Some General Properties of Nonlinear Elements, Proc. I.R.E., **44**, 1956, p. 904.
5. Southworth, G. C., *Principles and Applications of Waveguide Transmission*, D. Van Nostrand Co., New York, 1950, p. 104.

* This operation was part of the NASA-sponsored program under Contract NASW-110.

PROJECT ECHO

FM Demodulators with Negative Feedback

By CLYDE L. RUTHROFF

(Manuscript received March 22, 1961)

The FM receiving demodulators used in the Echo experiment are described in this paper. These receivers have negative feedback applied to the local oscillator to reduce the FM modulation index in the receiver intermediate frequency amplifiers. This technique results in a threshold performance which is superior to that of a conventional FM receiver.

I. GENERAL

In the Project Echo communications experiment the path loss from the transmitter to the receiver via the satellite was very large. Even with reasonably large antennas, high power outputs, and low-noise receivers, the received signal was so small that a modulation technique was required that traded bandwidth for signal-to-noise ratio (S/N).

For this experiment, wide-band frequency modulation was used, with receiving demodulators that were FM receivers with negative feedback (FMFB). The negative feedback results in an improved FM threshold and a resulting output S/N better than in other well-known techniques, such as single-sideband.*

II. SIGNAL-TO-NOISE RATIO AND THRESHOLD IN FMFB

A simplified block diagram of the FMFB demodulator^{1,2} is shown in Fig. 1. As indicated in the figure, a part of the baseband (audio) output is used to frequency modulate the local voltage-controlled oscillator (VCO). The audio signal is phased in such a manner that the VCO frequency tends to follow the frequency variations of the RF input signal. The result is a reduction of the modulation index of the IF signal relative

* Although this equipment was designed by the Bell System as part of its research and development program, it was operated in connection with Project Echo under Contract NASW-110 for the National Aeronautics and Space Administration.

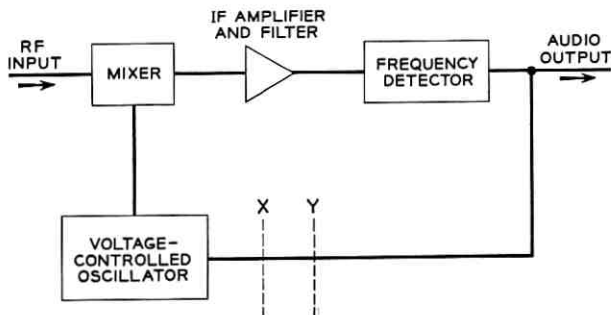


Fig. 1 — Simplified block diagram of FMFB system.

to the index of the RF signal and is, of course, negative feedback. If the RF index is M , the IF index is M/F , where F is the feedback factor. Since the IF index is small, the IF noise bandwidth can be made smaller than the RF bandwidth and an improvement in threshold can be expected relative to the threshold obtained using conventional FM in the same RF bandwidth.

There are two limitations on the IF filter. By a well-known approximation in FM work, the bandwidth required to transmit a baseband spectrum extending from 0 to f_b cycles per second is

$$B = 2f_b(1 + M), \quad (1)$$

where $M = \Delta f/f_b$ is the FM index and Δf is the peak frequency deviation in cycles per second. It is clear that the minimum required bandwidth is $2f_b$; hence the bandwidth of the IF filter in an FMFB receiver must be at least this wide. The second limitation on the IF filter has to do with the stability of the feedback loop.

For greatest threshold improvement the noise bandwidth of the filter should be small. This argues for steep skirts. Bode's stability criterion, on the other hand, limits the steepness of the skirts to a value not exceeding about 10 db per octave for practical receivers.³ This criterion is necessary but not sufficient to insure stability when modulation is present.

A complete theoretical analysis of the threshold effects in the receiver has not been made as yet. However, there is strong theoretical and experimental evidence⁴ that the C/N at which the threshold occurs is a function of the closed-loop bandwidth, the threshold occurring when the C/N in the integrated closed-loop bandwidth is about 6 db.

With reference to Fig. 1, the open-loop bandwidth can be measured by opening the loop between x and y and measuring the gain-frequency

response between x and y . The closed-loop bandwidth can be measured by measuring the gain-frequency response from the transmitter to the receiver output with the loop closed. For both of these measurements, low-level signals should be used. Fig. 2 indicates the type of results to be expected. The baseband analogs are shown, the actual IF characteristics being symmetrical about the IF carrier frequency.

The peak in the closed-loop response increases the noise bandwidth and is therefore undesirable. The height of the peak is dependent upon the steepness of the open-loop response and upon the phase shift in the circuit. Optimizing the threshold of this FMFB receiver is equivalent to designing the feedback network for minimum closed-loop noise bandwidth.

The performance of the FMFB receiver above the threshold can be understood with the aid of Fig. 1. When the feedback loop is opened at x the receiver is an ordinary FM receiver. Above the threshold the output signal-to-noise power ratio is

$$S_0/N_0 = 3 M^2(C/N), \quad (2)$$

where M is the modulation index and C/N is the carrier-to-noise power ratio at the input of the frequency detector, i.e., the noise power measured in a bandwidth of $2f_b$. The threshold for this case is described by Rice.⁵

When the loop is closed, the FM index in the IF is reduced by the

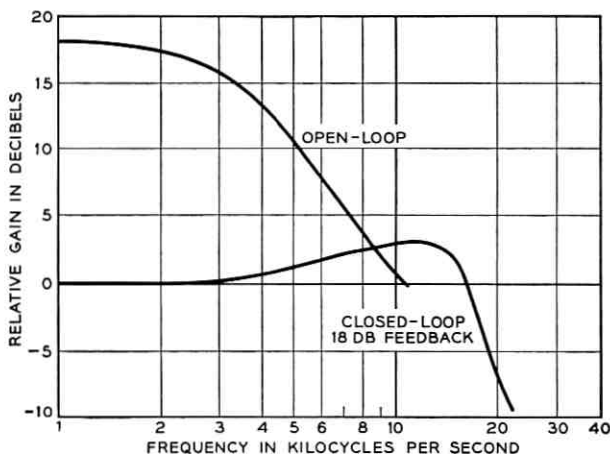


Fig. 2 — Open-loop and closed-loop response.

feedback factor F . This is true for both signal and noise, so that S_0/N_0 remains unchanged. The index at the transmitter can now be increased by F to restore the original FM index in the IF; this increases the output S_0/N_0 by the factor F^2 .

It is evident then that at operation above the threshold the output S_0/N_0 is given by (2), where M is the FM index at the transmitter. This is true for both FM and FMFB.

In summary, the signal-to-noise performance in FMFB is given by (2) above the threshold, and the threshold occurs at a C/N which depends upon the closed-loop bandwidth.

A word of caution is needed here. The foregoing statements have been made on the assumption that the feedback is large. For very small amounts of feedback, the threshold behavior approaches that of conventional FM.

III. PROJECT ECHO RECEIVER

A complete block diagram of the receiver is shown in Fig. 3. The main feedback loop includes the mixer, 1.2-mc IF filter, preamplifier, limiter, discriminator, baseband filter, attenuator, and voltage-controlled oscillator. Another feedback loop includes the RF amplifier, mixer, 1.2-mc IF filter, preamplifier, and AGC detector-amplifier.

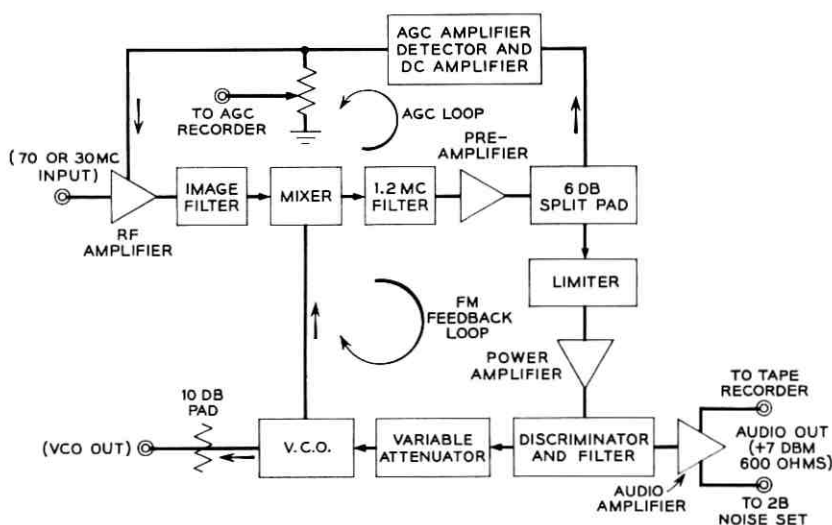


Fig. 3 — Block diagram of FMFB demodulator.

The purpose of the AGC is two-fold. The amount of FM feedback (i.e. loop gain) is proportional to the carrier level at the input of the discriminator. The AGC maintains this level constant and stabilizes the loop gain. Practical limiters are not good enough to do this, and, in fact, limiter input amplitude should be controlled for best limiting.⁶

The second purpose of the AGC is to provide a measure of the received carrier strength. The AGC voltage is calibrated in terms of known signal levels at the antenna input.⁷

Measurements of the performance of the receivers were made both in the laboratory and in the field. Fig. 4 is a measurement of audio S_0/N_0 versus input C/N and shows the threshold. The C/N is referred to a 6-kc noise bandwidth. An image-rejection filter precedes the mixer, and the RF C/N is measured ahead of this filter.

The exact C/N at which the threshold occurs is somewhat arbitrary, since the knee of the curve is not sharp. However, in this receiver with the C/N above the threshold the circuit is very quiet. At the point marked "threshold" in Fig. 4 a cracking or popping sound begins. Chaffee¹ noted this effect, which sounds remarkably like the popping of corn. In this work, the threshold is assumed to occur when the popping starts. This effect, to the ear, is much more drastic than is indicated by the measured rms S_0/N_0 . It is safe to say that at 1 db below this threshold the circuit is unusable in a realistic way, while just above the threshold the quality is excellent. A measurement of S_0/N_0 versus C/N for the case where the feedback is zero (loop open) is included in Fig. 4. In this

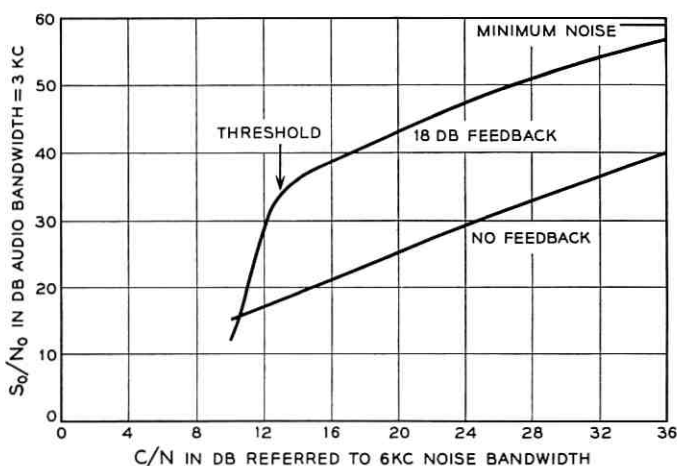


Fig. 4 — Threshold measurements.

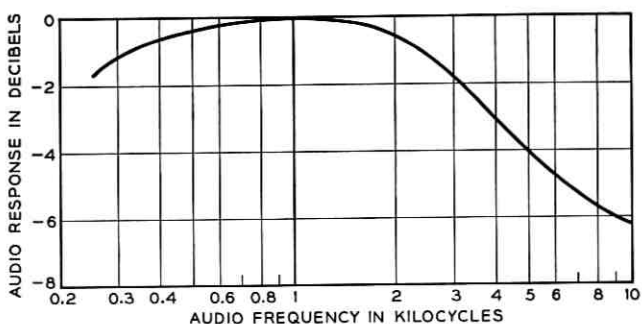


Fig. 5 — System audio response.

figure it is actually $1/N_0$ that is plotted and referred to the signal output S_0 obtained above the threshold. The threshold improvement of this receiver, compared to a conventional FM receiver using the same RF bandwidth, is about 9 db.

The audio frequency response of the receiver is given in Fig. 5, and is determined primarily by the filter in the audio amplifier.

During the operations,* the receiving systems were tested by inserting known signals into the antennas and plotting the output S_0/N_0 versus input carrier power. Fig. 6 is an example of such a calibration made at Goldstone. For this particular case the threshold occurred at -120 dbm, and the feedback is approximately 23 db.

When the whole receiving system is involved, the accuracy of the threshold measurement is a function of the accuracy of the RF input signal level and the gain and noise temperature stability of the RF receiver. The -120 dbm threshold quoted above, was often observed and is probably correct to within 2 db.

IV. CONSIDERATIONS IN FEEDBACK DESIGN

The minimum bandwidth required for a frequency-modulated signal is twice the bandwidth of the modulating signal. The IF filter in the FMFB receiver therefore has this bandwidth, i.e., $2f_b$. As discussed previously, the maximum threshold improvement is obtained when the closed-loop bandwidth is a minimum for a given feedback factor. Any excess phase shift will increase the closed-loop bandwidth and is therefore undesirable.

* These experiments were in connection with National Aeronautics and Space Administration Contract NASW-110.

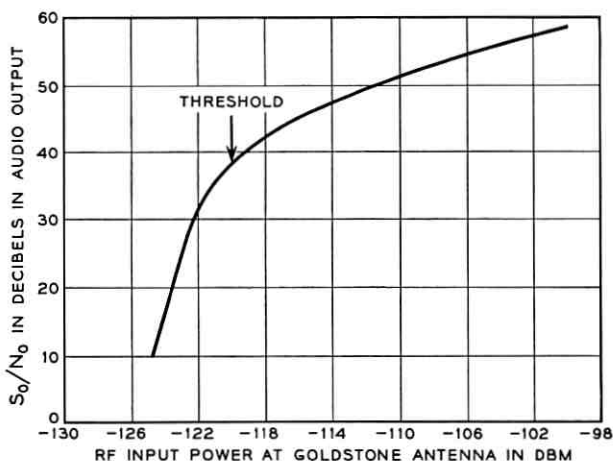


Fig. 6 — Demodulator calibration at Goldstone, August 11, 1960.

In the Echo receivers, all circuits were made extremely broad to minimize excess phase, and the shaping was done in the IF filter. There are several important factors which warrant discussion.

4.1 IF Frequency

The output of the broadband discriminator is largely carrier power. This cannot be allowed to reach the VCO so a filter is required to reduce the carrier and its harmonics and allow the baseband through with the least possible phase shift. Therefore the IF frequency should be as high as possible. The upper limit is determined by the circuit Q obtainable for the IF filter. Coil Q 's in the megacycle region are limited to 400 to 500, so an IF frequency of 1.2 mc was chosen requiring loaded Q 's of approximately $1200 \text{ kc}/6 \text{ kc} = 200$. The corresponding baseband filter is M -derived with a cutoff frequency of 1 mc.

4.2 Discriminator

This is a balanced circuit with a single-ended output. No filtering is used on the output side of the diodes other than the baseband filter. The usual filtering with capacitors would increase the output but would introduce excess phase shift. The balanced property provides some limiting in the absence of modulation.

4.3 Limiter

Limiters contain reactive elements and therefore add to the excess phase. For this reason, multistage limiters were avoided and a single-stage limiter was used. For best results, this limiter requires a controlled input level;⁶ hence the AGC operates to fix the level at the limiter input.

V. ACKNOWLEDGMENTS

The author is indebted to W. F. Bodtmann, Jr., for much of the equipment design, testing, and operation of the receivers. Noteworthy contributions were also made by J. P. Schafer, H. E. Keller, F. A. Dunn, and L. H. Enloe.

REFERENCES

1. Chaffee, J. G., Application of Negative Feedback to Frequency Modulation Systems, B.S.T.J., **18**, 1939, p. 404.
2. Carson, J. R., Frequency Modulation—Theory of the Feedback Receiving Circuit, B.S.T.J., **18**, 1939, p. 395.
3. Bode, H. W., *Network Analysis and Feedback Amplifier Design*, D. Van Nostrand Co., New York, 1945.
4. Enloe, L. H., to be published.
5. Rice, S. O., Properties of a Sine Wave Plus Random Noise, B.S.T.J., **27**, 1948, p. 109.
6. Ruthroff, C. L., Amplitude Modulation Suppression in FM Systems, B.S.T.J., **38**, 1958, p. 1023.
7. Ohm, E. A., Receiving System, this issue, p. 1065.

PROJECT ECHO

Satellite-Tracking Radar

By O. E. DE LANGE

(Manuscript received April 6, 1961)

This paper is concerned with the radar employed at Bell Telephone Laboratories, Holmdel, New Jersey, site for tracking the Echo I satellite. The radar was originally designed for the sole purpose of antenna pointing. Recently, however, it has also been employed to measure earth-balloon-earth path loss at regular intervals of time in order to keep track of the condition of the balloon.

The performance of the system and some of the data obtained are discussed. There is a general description of the system followed by more detailed descriptions of the various components.

I. INTRODUCTION

The operational plan of the Project Echo experiment provided for pointing of the transmitting and receiving antennas from calculated orbital data. The angle-tracking radar was intended as a "back up" to this system.* In operation the radar has been found to provide appreciably better pointing accuracy than is obtained from the computed data. As a result, the orbital data are employed only to keep the antennas pointed approximately on target, with the radar (or optical telescope during periods of visibility) providing for more exact alignment.

According to the original concept the radar was intended to serve only the purpose of keeping the antennas positioned during communications experiments. In recent months these experiments have practically ceased, which leaves us with only the radar as a regular source of signal for studying transmission effects. Under the present plan of operation the balloon is tracked approximately once per week and its cross section determined from the strength of the reflected radar signal.

* Although this equipment was designed by the Bell System as part of its research and development program, it was operated in connection with Project Echo under Contract NASW-110 for the National Aeronautics and Space Administration.

II. GENERAL

2.1 *Antenna-Positioning Plan*

The antenna-positioning plan for the complete Holmdel terminal* is shown on Fig. 1. Orbital information is taken off paper tape by the tape reader and is converted from digital to analog form by the digital-to-analog converter. This unit's synchro generators control the positions of the transmitting dish and the receiving horn, as well as the optical telescope in the M33 gun director. The readout synchros on the transmitting antenna control the position of the radar receiving antenna. The pointing-error information derived from the radar is displayed before an operator at the M33 director who applies corrections by means of a device which puts in controlled amount of offsets in azimuth and elevation until the indicated errors are reduced to zero. During periods of visibility the optical telescope can also be employed to determine pointing information. It is evident that, once a signal is acquired, pointing could be carried out entirely with information from the radar or optical system. However, the control provided by the digital-to-analog converter makes acquisition much easier and provides an excellent tracking aid, with the radar or optical system simply indicating the corrections which are needed.

Up to the present time there have been no attempts at auto-tracking the satellite. Some limited experiments on automatic following of the moon are described in a later section.

2.2 *Design Objectives*

The radar was designed to meet the following requirements:

1. It had to be capable of tracking the 100-foot balloon to a range of 3000 miles.
2. A pointing accuracy of about $\pm 0.1^\circ$ was desired.
3. Accurate range information was not required.
4. It had to be compatible with the communications system, although both shared a common transmitter and transmitting antenna.

2.3 *Radar Performance*

Except for some initial operating difficulties, the performance of the radar has been satisfactory. More than 100 successful tracking runs have been made up to the time this was written. It has almost always

* For a complete description of the Holmdel terminal see a companion paper.¹

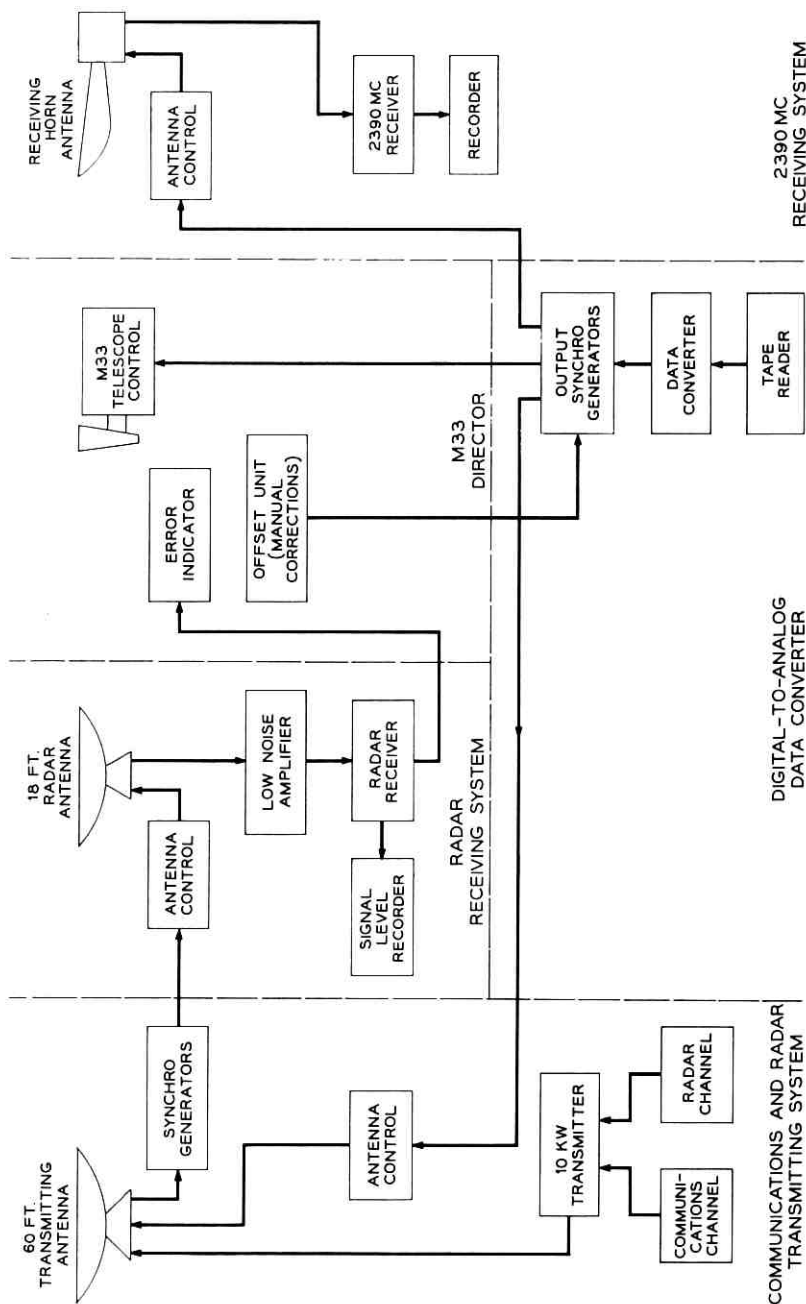


Fig. 1 — Antenna positioning plan.

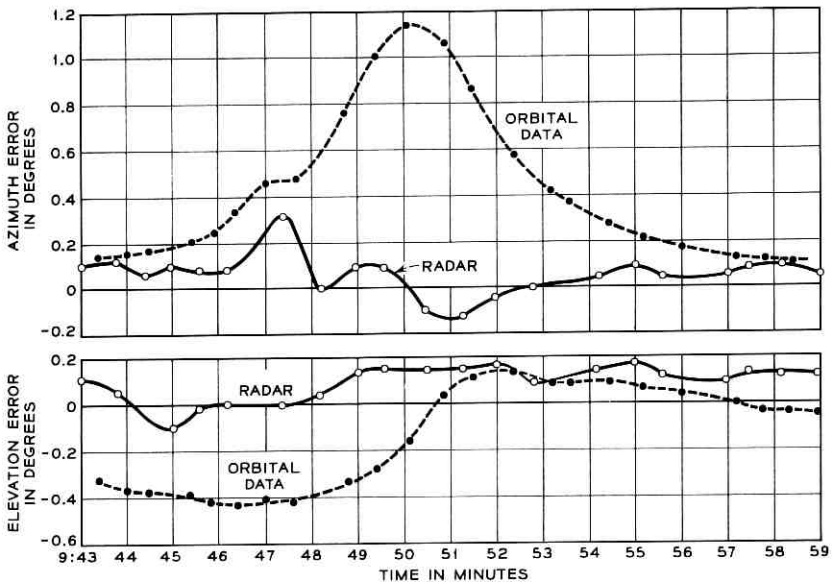


Fig. 2 — Radar vs. optical pointing.

been possible to acquire a signal from the balloon as soon as it has risen a few degrees above the horizon and to maintain contact until it has dropped to within a few degrees of the opposite horizon.

The low-noise parametric amplifier has been very stable with respect to both noise figure and gain. Over a period of months the sensitivity of the receiver has remained at -150 dbm in a 100-cycle band; i.e. the minimum detectable signal is near this level. This is consistent with the receiver noise power output as calculated in Appendix A.

During periods of visibility it has been possible to compare the radar pointing information with the more accurate information obtained by optical means. This is accomplished by alternating between the offset required to make the indicated optical error zero and the offset required to make the indicated radar error zero. The radar and optical data usually agree to within one to two tenths of a degree, except for short periods on some adverse passes. Fig. 2 is a plot of one set of data obtained in this manner, with the optical data being used as a standard of comparison.*

The abscissa on this plot represents time, with each division equal to one minute; the ordinates are angular errors in degrees. The dashed

* The experiments described herein were performed in connection with National Aeronautics and Space Administration Contract NASW-110.

curves represent the errors in the orbital data, the solid curves the radar errors. Between 0950 and 0951 GMT the balloon was passing through its point of nearest approach. As is usually the case, the error in the computed orbital azimuth data reached a maximum at this time, being nearly 1.2° . It is evident that the radar data are considerably better than the computed data, especially in azimuth.

The system is subject to errors due to parallax between the transmitting and the receiving antennas, to antenna lag at the higher rates of rotations, and to lack of exact alignment between the various axes in the receiving antenna. Although each of these errors is small, they can add up enough to become significant for parts of some adverse passes. Fortunately, the enhanced error does not last long and is maximum at the point of nearest approach of the balloon, where the signal level is great enough to allow for some discrepancy in pointing. The radar data have been found to be more accurate than the orbital data, even on these adverse passes.

Fig. 3 represents the received signal, as indicated by the AGC voltage, for part of pass 2407, which was recorded on February 24, 1961. The smooth curve is a plot of the theoretical value of signal strength. Over the period of time shown, the actual signal is not very different from the calculated value except during periods of deep fades. The fades shown on this chart are typical, except for the one at the right-hand side which is somewhat deeper than usual. Scintillations are usually considerably greater at the beginning and at the end of a pass than at the midpoint, probably due to atmospheric effects when the balloon is near the horizon.

Charts similar to the one shown on Fig. 3 have been prepared for 40 passes of the satellite. From these charts the average difference between the actual signal level and the theoretical value has been obtained for 33 passes between October 20, 1960, and March 2, 1961. These differ-

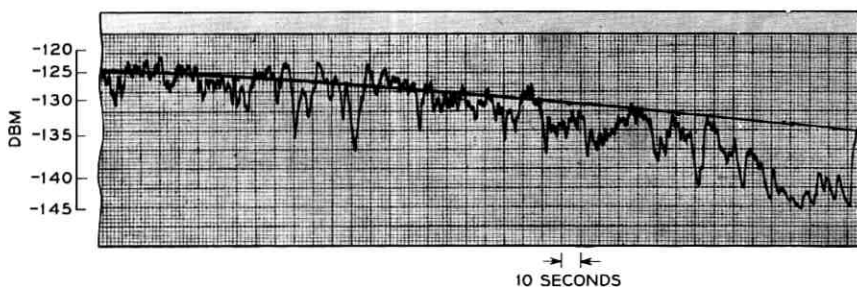


Fig. 3 — Return signal from the satellite, pass 2407 (February 24, 1961).

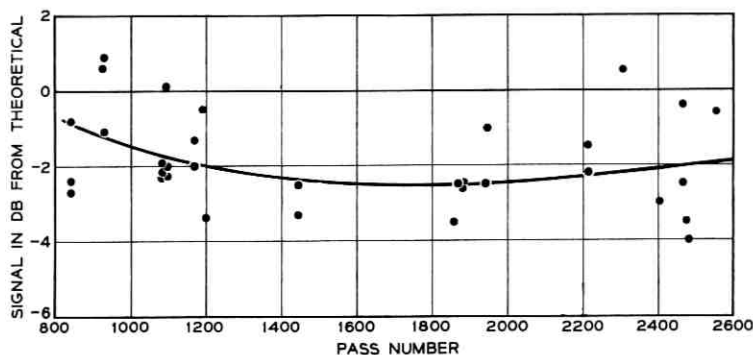


Fig. 4 — Received signals compared with theoretical values.

ences are shown plotted on Fig. 4. A smooth curve was drawn through an average of these points in an attempt to determine any long-time trend. The curve indicates that there has been some falling off in average signal strength since we started recording, though not more than about 1.5 db. This is less than the spread from one pass to the next, and may not be really significant. There has been no significant change in scintillations over the period for which we have records. It is evident that there has been no great change in the size or shape of the balloon up to the present time. Unfortunately, equipment was not set up to record accurate data before October 20.

On numerous occasions the radar has been used to track the moon. Fig. 5 is a recording of the received signal for part of one such operation. An outstanding feature of the record is the rapid and continuous fading of the signal. These fluctuations are known to be greater and more rapid than indicated on this chart, where the indications were limited by the time constant of the recording equipment. From the average signal level the earth-moon-earth path loss was calculated to be 268.7 db, compared to 268.1 db quoted by Trexler² for our frequency. (See Appendix B calculations.)

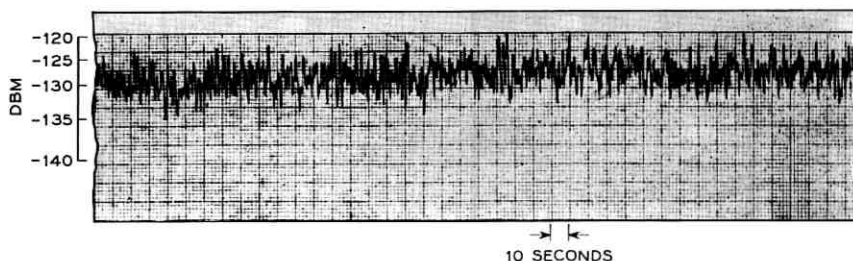


Fig. 5 — Return signal from the moon (February 8, 1961).

III. DESCRIPTION OF RADAR SYSTEM

3.1 *General Arrangements*

To provide a separate high-powered transmitter and large transmitting antenna for the radar would have been rather expensive and added considerably to the complexity of the systems. For these reasons it was decided that the transmitter and transmitting antenna employed for communications should be shared by the radar by means of frequency division. The 4-mc bandwidth of the transmitter would have allowed us a wide separation between the communications and radar frequencies; frequency assignment, however, limited this spacing to one megacycle, with the radar at the higher frequency. Although this spacing was sufficient to allow separation of the signals in the receivers, a somewhat greater spacing would have been advantageous.

The radar transmitter and receiver are each gated to be on one-half of the time and off one-half. In this way diplexing is accomplished by having the receiver on only during times when the transmitter is off. The gating rate is varied between 15 and 45 cycles depending upon the range to the balloon. To avoid overloading of the early stages of the radar receiver by the ungated communications transmitter, a radar receiving site was chosen at a distance of approximately one and one-half miles from the transmitter. The receiving antenna, which is provided with conical scan, is "slaved" to the transmitting antenna by means of synchro signals carried over telephone lines (see Fig. 1). There is no lobing of the transmitting antenna. Pointing-error signals are sent over telephone lines back to the antenna-control center, where the appropriate corrections in antenna pointing are made manually.

3.2 *Transmitter*

Since the transmitter is described in detail in a companion paper³ it will be discussed only very briefly here. From the block diagram of Fig. 6 we can see that the radar section of the exciter consists of a crystal-controlled oscillator, a gated harmonic generator, and an attenuator. The radar signal is combined with the 70-mc communications signal in a mixing amplifier. In the mixer and amplifier unit which follows the mixing amplifier the 70-mc signal is modulated up to 960.05 mc and the radar signal up to 961.05 mc. These two signals are amplified simultaneously by the klystron power amplifier which has a bandwidth of 4 mc.

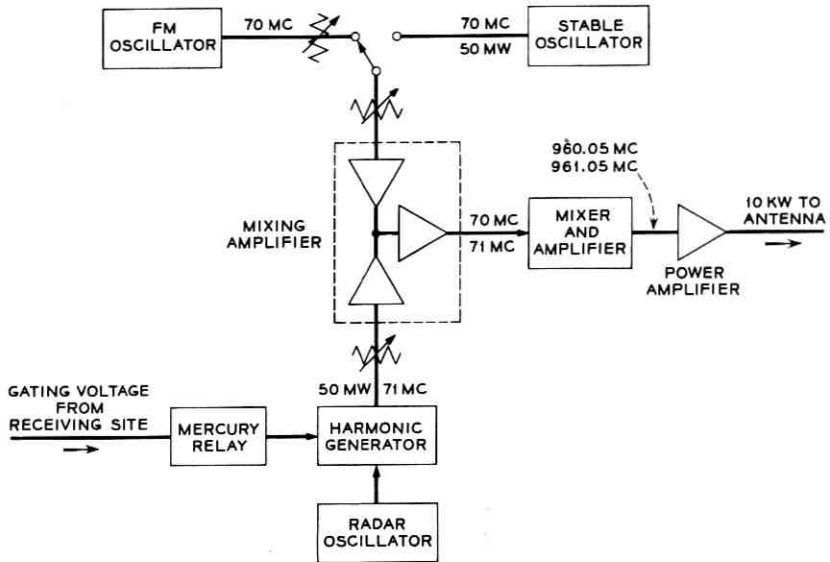


Fig. 6 — Block diagram of Echo I transmitter.

Because of the extremely high sensitivity of the receiver it is necessary to have the transmitter turned off at all times when the receiver is on. It was found by experience that intolerable interference at the receiver occurred whenever a 71-mc oscillator was on at the transmitting site, even though the oscillator was well filtered and shielded and disconnected from the exciter. This resulted from the high gain of the transmitter between the 71-mc input and the antenna. Because of this it was found necessary to employ an oscillator operating at a subharmonic of 71 mc and gate the harmonic generator that is required to obtain the desired frequency.

During simultaneous operation the transmitter power is shared, with 7.5 kw normally going to the communications channel and 2.5 kw to the radar. Because of amplitude nonlinearities in the transmitter, there is interaction between the two signals. In the first case, pulsing of the radar signal produces amplitude modulation of the communications signal at the pulse-repetition rate. It has been possible to reduce this crosstalk to a tolerable value, largely because the pulse-repetition frequency is very low. Secondly, the radar signal is compressed by a significant amount when the communications signal is present simultaneously. For this reason it is necessary to adjust the two signals to the desired values with

both present rather than adjusting each individually. This is discussed more fully in Ref. 3.

The transmitting antenna is the same one that is used for communications, i.e. the 60-foot Kennedy dish.

3.3 *Receiving System*

3.3.1 *General*

Fig. 7 is a block diagram of the complete radar receiving system. The 961.05-mc signal received by the conically scanned antenna is amplified by a low-noise parametric amplifier and heterodyned down to 30 mc. To avoid the need for rotary joints, this amplifier and a section of the 30-mc IF amplifier are mounted directly on the antenna and move with it both in azimuth and elevation. The 30-mc output is conducted to the radar shack through a length of flexible coaxial cable. This IF signal is passed through a crystal filter having a bandwidth of 200 kc, which is sufficient to take care of Doppler shift but is also narrow enough to remove the interference picked up from the communications transmitter. After filtering, the 30-mc signal is amplified by the main IF amplifier, which has a bandwidth of about one megacycle.

At the second converter the signal frequency is reduced to 199.1 kc by mixing the 30 mc with the 29.8009-mc output of the voltage-controlled local oscillator. The AFC control voltages are applied to this oscillator.

At the output of the 199.1-kc IF amplifier, which has a bandwidth of approximately 4 kc, the signal divides into two paths. One path contains a filter with a 100-cycle bandwidth; the other includes a filter with a 500-cycle band. The dc output of the detector supplied by the 100-cycle filter is used both to indicate the presence of a signal and as the AGC control voltage for the main 30-mc amplifier. From another detector, which is energized through the 500-cycle filter, we derive the four-cycle lobing frequency. This lobing frequency is filtered, amplified, and applied to the lobing detectors. At these detectors the lobing voltage is compared with the reference voltages derived from the antenna lobing unit. The resultant signals, which represent errors in azimuth and elevation, are indicated on meters at the receiving site and also on error indicating devices at the antenna-control position on Crawford Hill.

Because of Doppler shift, the received-signal frequency may differ from that of the transmitted signal by as much as ± 35 kc. Automatic frequency control circuits are provided to keep the receiver in tune. To

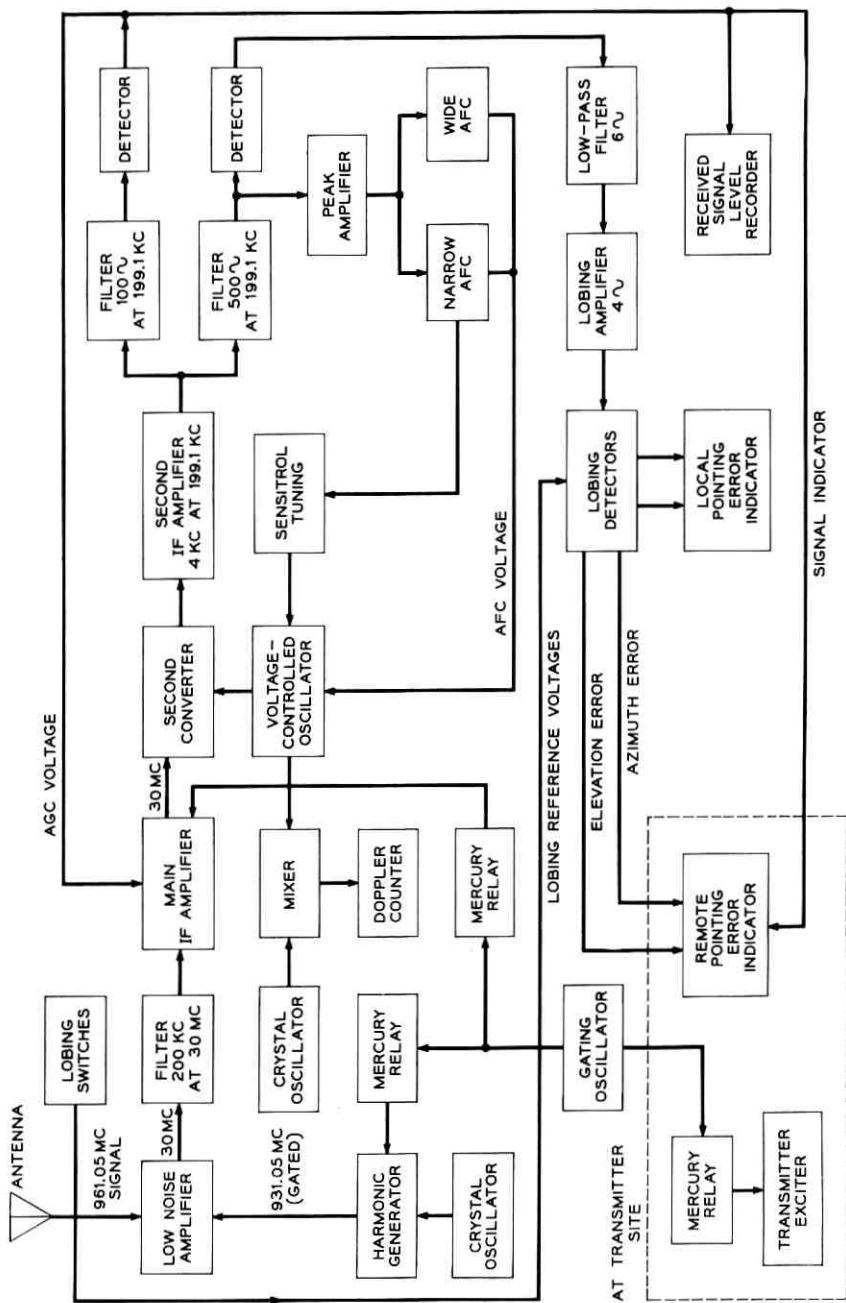


Fig. 7 — Block diagram of radar receiving system.

aid in acquisition, a sample of the voltage-controlled oscillator output is mixed with the output of a crystal-controlled oscillator operating at the nominal beating-oscillator frequency of 29.8009 mc. The frequency difference between these two oscillators is counted on an electronic counter. To tune in a signal, the voltage-controlled oscillator is adjusted to make the measured difference frequency equal to the expected Doppler shift.

With the satellite at its maximum range of 3000 miles and with the transmitter and receiver each gated to be on for one-half of the time, the optimum gating frequency is about 15 cycles per second. At a minimum range of 1000 miles the optimum pulse-repetition frequency increases to 45 cycles. Gating voltages are provided by an AF oscillator driving mercury relays. To prevent overload, it is desirable to gate the receiver at a point where the signal level is low. The most practical such point appeared to be the circuit of the local oscillator supplying the low-noise amplifier. Gating is done in a harmonic generator supplying this beating-oscillator voltage, and additional gating is applied to the main IF amplifier.

The lobing frequency of four cycles was chosen as being consistent with a 15-cycle pulse-repetition frequency and a one-second integrating time for the lobing-detector outputs.

With the exception of the parametric amplifier and the early stages of the 30-mc IF amplifier, all the electronic components of the receiver are mounted in a standard relay rack 7 feet high. This bay of equipment is shown on the left-hand side of Fig. 8. The cabinet on the right-hand side of the figure contains the antenna-control equipment.

3.3.2 *Parametric Amplifier*

Although the lobes from the back and sides of our antenna are not small enough in magnitude to warrant use of a maser amplifier, we are able to profit from the low noise figure provided by a parametric amplifier. Such an amplifier does not require cooling and is, therefore, considerably simpler than a maser. Our amplifier was designed and constructed under the direction of H. Seidel of the Murray Hill Laboratory of Bell Telephone Laboratories and is described in detail in a companion paper.⁴

The design of this amplifier provides for approximately 8 db of gain by frequency up-conversion by means of a nonlinear capacitance. Additional gain is derived from the negative resistance obtained by pumping such a capacitance (see Fig. 9). The amplifier is coupled to the

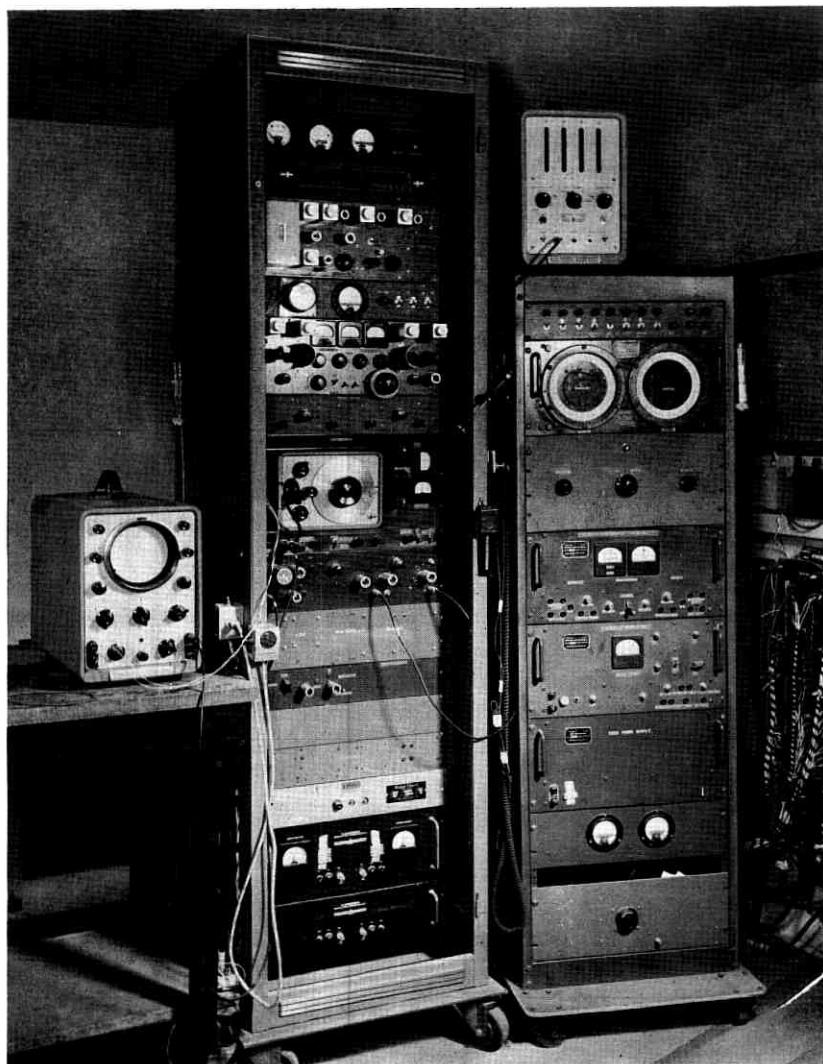


Fig. 8 — Receiver and antenna controls.

antenna by means of a circulator which is enclosed in a heat-insulated container and maintained at 120°F by means of heating tapes and a thermostat. In this way it is stabilized against variations in ambient temperature. An isolator could have been used in this position if one having the required degree of ruggedness and stability had been available.

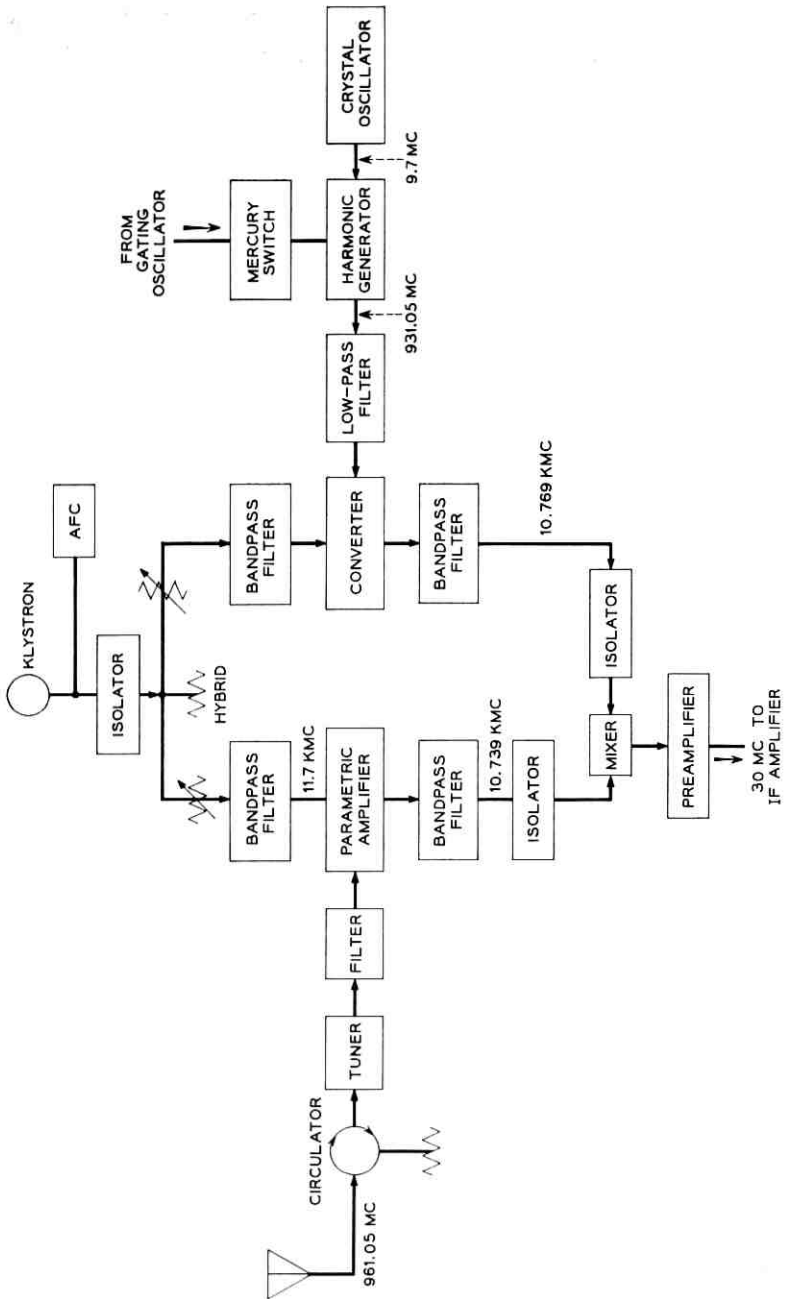


Fig. 9 — Block diagram of radar parametric amplifier.

The pump power is supplied by a Western Electric 445A klystron, operating at a frequency near 11.7 kmc. This frequency is maintained by a mechanical AFC circuit controlled by a Sensitrol* relay which is energized by the signal from a reference cavity. The lower sideband at 10.739 kmc is taken as the output of the amplifier. To obtain the 30-mc intermediate frequency a beating oscillator frequency of 10.769 kmc is combined with the 10.739-kmc signal in a nonlinear-resistance mixer.

Since the final predetection bandwidth of the receiver is only 100 cycles, it is obvious that the short-term stability of the 30-mc intermediate frequency must be exceptionally high. This frequency must, therefore, be made independent of the pump frequency, which is only roughly stabilized. The required independence of intermediate frequency is achieved by employing the klystron frequency in the process of heterodyning down as well as in heterodyning up. Changes of klystron frequency therefore cancel out in the process of going up in frequency and then back down. The beating-oscillator signal for the down-converter is obtained as follows: The output of a crystal-controlled oscillator operating at approximately 9.7 mc is multiplied up to 931.05 mc by means of a harmonic generator. (Gating of the receiver is accomplished by applying a gating voltage to the grid of one of the harmonic generator tubes.) By subtracting the 931.05 mc from the klystron output, the 10.769 kmc beating-oscillator frequency is obtained.

The bandwidth of the microwave section of the parametric amplifier is 20 mc. This is reduced to approximately one megacycle by a band-pass filter at the input to the first stage of the 30-mc IF amplifier. The gain of the microwave section is 22 db; the over-all gain 46.5 db. Over-all noise figures in the neighborhood of 1.6 db have been measured.

One db of compression takes place in this amplifier for an input signal of approximately -26 dbm. If the receiving site had been located near the transmitting antenna, interference at the communications frequency would have exceeded this overload value.

3.3.3 *Main IF Amplifier*

The crystal filter at the input to this amplifier has a total bandwidth of 200 kc. Its characteristic has extremely steep sides, so that the loss at the communications frequency, which falls one megacycle from the center of the band, is probably limited only by leakage around the filter. The amplifier itself has a total bandwidth of approximately one mega-

* Trade name owned by Weston Instruments Division of Daystrom, Inc., Newark, New Jersey.

cycle, and therefore provides some additional discrimination against the interfering communications signal. The design of this amplifier is conventional. Its gain is controlled by the AGC and gating voltages applied to the grids of its tubes.

3.3.4 *Voltage-Controlled Oscillator Unit*

This unit consists of an oscillator and a buffer amplifier. A pair of variable-capacitance diodes shunted across the oscillator tank circuit provides electronic tuning. Two separate circuits supply control bias to the diodes, one for AFC, the other for manual tuning. A one-volt change of bias is sufficient to produce a frequency change of nearly one megacycle, which makes it a fairly simple matter to obtain a very stiff AFC action. This high sensitivity does make it difficult to keep undesired frequency modulation of the oscillator down to acceptable levels. With a receiver bandwidth of only 100 cycles it is desirable to keep this modulation to 10 cycles or less. The modulation which was most difficult to eliminate was that produced by 60-cycle voltages and currents. Operating the heaters of the oscillator and all units near it on dc, and very careful filtering of all circuits reduced this modulation to a tolerable value.

3.3.5 *Second Converter and IF Amplifier*

A simplified schematic of this unit is shown in Fig. 10. The 30-mc signal comes in at an impedance of 50 ohms. A tuned transformer steps up this level on the grid of the Western Electric 6AK5 tube used as the converter. The 199.1-kc output of this mixer is amplified through a single tuned stage, then divided into two paths with an untuned single-stage amplifier in each path. One of these amplifiers supplies the input to a three-section, tuned filter with a total bandwidth of 500 cycles. The output of this filter is coupled to the AFC unit and the pointing detector through a cathode follower and 50-ohm cables. The crystal filter at the output of the second untuned amplifier has a total bandwidth of 100 cycles and a characteristic with very steep sides. The filtered output drives two detectors in parallel. One of these provides the AGC voltage and is back-biased to produce the desired threshold effect. The AGC voltage is amplified through a one-stage dc amplifier before being applied to the first IF amplifier. A time constant of approximately ten seconds is provided at the output of this amplifier to prevent the AGC circuit from affecting the four-cycle lobing modulation carried by the incoming signal. A second output from this dc amplifier has a much shorter time constant and goes to a Sanborn recorder on which a record of the strength

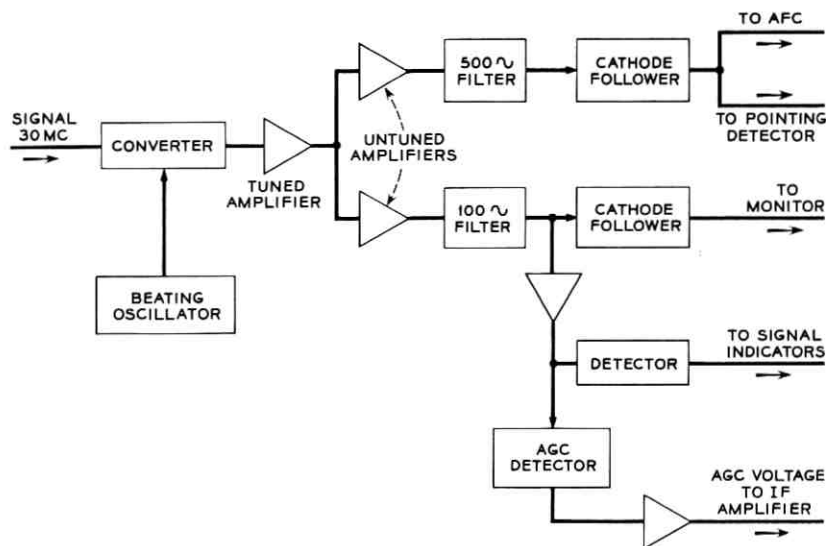


Fig. 10 — Block diagram of radar second converter and second IF amplifier.

of the received signal is provided. The other detector at the output of the narrow filter operates a meter used as a signal indicator.

3.3.6 *Lobing Amplifier and Detectors*

Before being applied to the lobing amplifier, the output of the detector with the 500-cycle bandwidth is filtered by a low-pass filter having a six-cycle cutoff frequency (refer to Fig. 7). The purpose of this filter is to prevent the pulse-repetition frequency from getting into the lobing amplifier. The input to the amplifier is provided with an adjustable phase-shifting network which makes it possible to maintain correct phase with respect to the lobing reference voltages. The lobing amplifier, which is untuned, employs simple RC circuits for coupling the various stages.

Each lobing detector consists of a Western Electric 276D mercury relay operated by one of the lobing reference voltages. These voltages, which are in quadrature, are derived from a pair of microswitches operated by cams on the antenna scanning unit. The simplicity of the lobing detection system is made evident by Fig. 11, which is a schematic of this system. It can be seen from this figure that the grids of a pair of phase-splitting triode tubes are supplied in parallel with the four-cycle lobing voltage. The plate of one triode is coupled to one input terminal of the

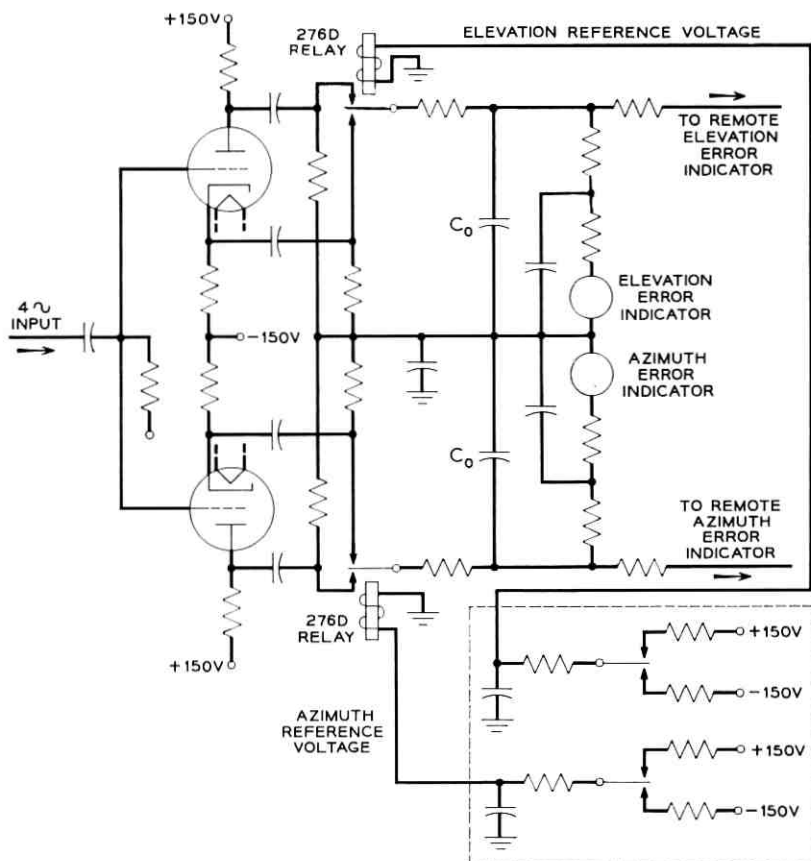


Fig. 11 — Schematic of radar lobing detectors.

elevation relay; the cathode of the triode is connected to the other input terminal of the same relay. The elevation error voltage is taken from the output terminal. If the four-cycle voltage has a component in phase with the reference voltage applied to that particular relay, there is a charge built up on the capacitor C_0 across the output terminal. A voltage component in quadrature with the reference voltage causes no change in the average charge on the capacitor; in this way, azimuth and elevation errors are separated. The voltage across C_0 indicates both the sense and magnitude of the pointing error.

The azimuth and elevation error voltages are displayed before operators in the form of meter readings and also as spot positions on a cathode

ray oscilloscope. The time constants of these display circuits are adjustable. For satellite tracking a time constant of 3 seconds appears to be about optimum; for moon tracking the optimum time constant increases to about 7.5 seconds.

3.3.7 Automatic Frequency Control

At the 961-mc operating frequency the Doppler shift at the radar receiver can be as much as ± 35 kc. To keep the signal within the 100-cycle band of the receiver requires a rather "stiff" AFC circuit. To meet the simultaneous requirements on sensitivity and stability a quartz crystal discriminator is employed; its characteristic is shown in Fig. 12. With the output of this discriminator connected to the voltage-controlled oscillator, nearly 60 db of negative feedback is obtained and the average frequency of the received signal is held to within a few cycles of the midband of the 100-cycle filter. To keep up with the change of Doppler frequency as a pass progresses, a motor-driven tuning control is also provided. The motor is controlled by a Sensitrol relay, which in turn is

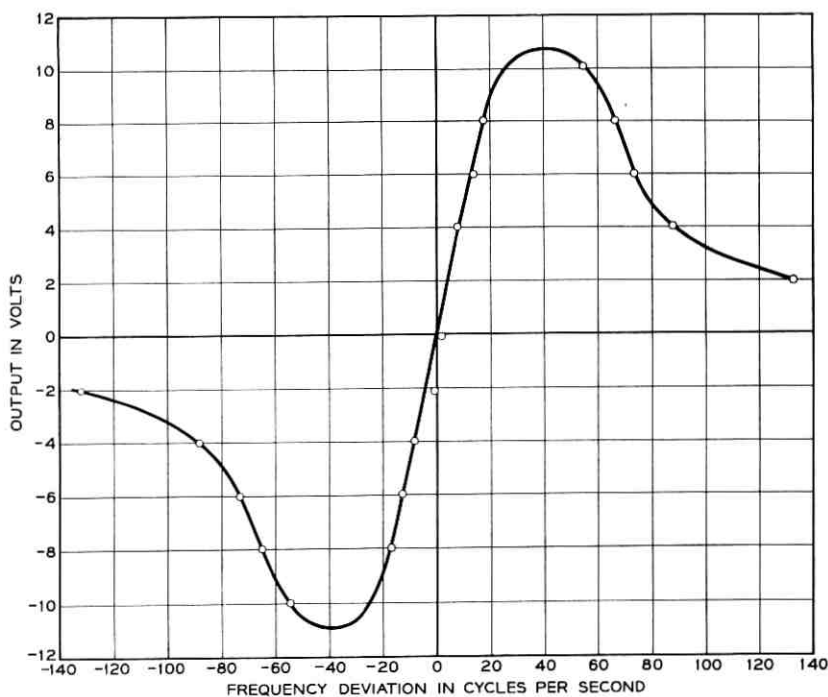


Fig. 12 — Frequency characteristic of frequency discriminator.

activated by the output of the crystal discriminator. This mechanical control keeps the receiver approximately tuned at all times and thereby takes much of the burden off the electronic AFC circuit.

As an aid in acquiring the signal, a wider-band discriminator is also provided. This circuit, which provides 30 db of feedback, brings the signal to within the pull-in range of the crystal discriminator, after which the latter takes control. The pull-in range of the wider circuit is about ± 500 cycles.

It is obvious that there is a tuning problem in acquiring the signal when one considers the narrow bandwidth of the receiver, the constantly changing Doppler shift, and the short time available for acquisition. The difficulties are reduced considerably by the availability of data on the rate-of-change of range to the balloon at all times during the pass. From these data it is possible to calculate the corresponding Doppler shifts. Usually the only data required are those at the start of the pass. Referring to Fig. 7, we can see that one output of the voltage-controlled oscillator is combined in a mixer with the output of a crystal-controlled oscillator. The frequency of the crystal oscillator is equal to the nominal frequency of the voltage-controlled oscillator, i.e., the frequency at which it should be set to bring in a signal with zero Doppler shift. Any difference between the two frequencies applied to the mixer is read on the counter connected to its output.

With the above arrangement the procedure in tuning the receiver is as follows: From orbital data the Doppler shift at the time in question is calculated. The frequency of the voltage-controlled oscillator is adjusted to cause the counter to indicate a frequency equal to the Doppler shift. If the calculated Doppler were exact and if the various oscillators were perfectly stable, this procedure would result in perfect tuning. To make up for discrepancies, however, a small amount of manual tuning about the calculated frequency is usually required.

3.3.8 Receiver Calibration and Testing

Two reference-signal sources are available on Crawford Hill for the purpose of testing and calibrating the receiving system. By employing these sources it is possible to determine the gain and noise power output of the receiver as well as to check pointing accuracy. Checks and calibrations are usually made before each pass.

3.3.9 Antenna

The radar receiving antenna consists of crossed dipoles mounted in front of a reflecting disk in such a way as to accept circularly polarized

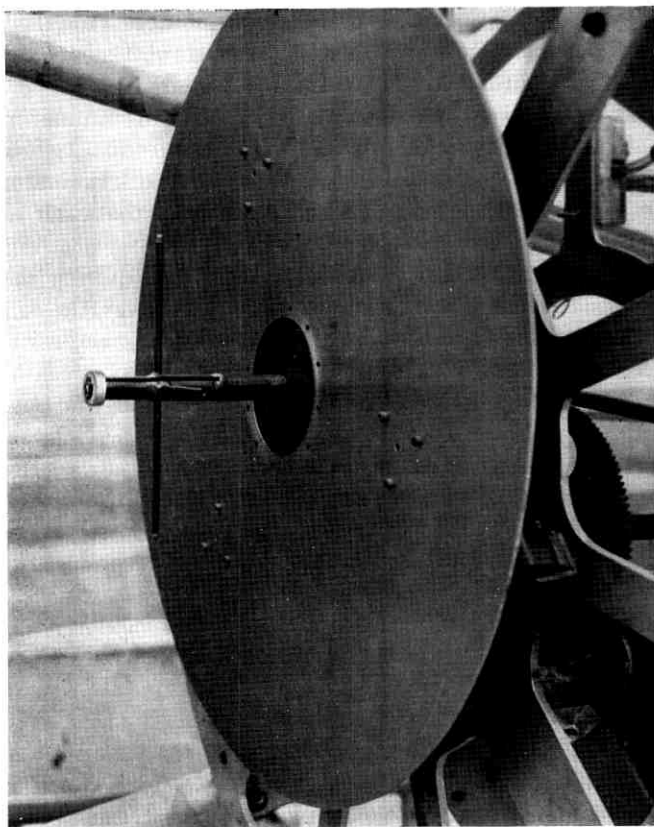


Fig. 13 — Antenna feed.

waves.* This feed, which is shown on Fig. 13, is mounted at the focus of an 18-foot parabolic reflector by means of a quadrupod consisting of four sections of aluminum tubing. The fiber glass cover which normally protects this feed from the weather was removed for the photograph. The parabolic reflector was fabricated of aluminum tubing and mesh by Prodeline, Inc.; it was chosen because it was lighter in weight than other available reflectors of the same diameter.

Fig. 14 shows the complete antenna, mounted on its supporting tower. The small building at the right of the picture houses the receiving equipment.

* The design of this dipole assembly was based on suggestions by personnel of the Jet Propulsion Laboratory of the California Institute of Technology.

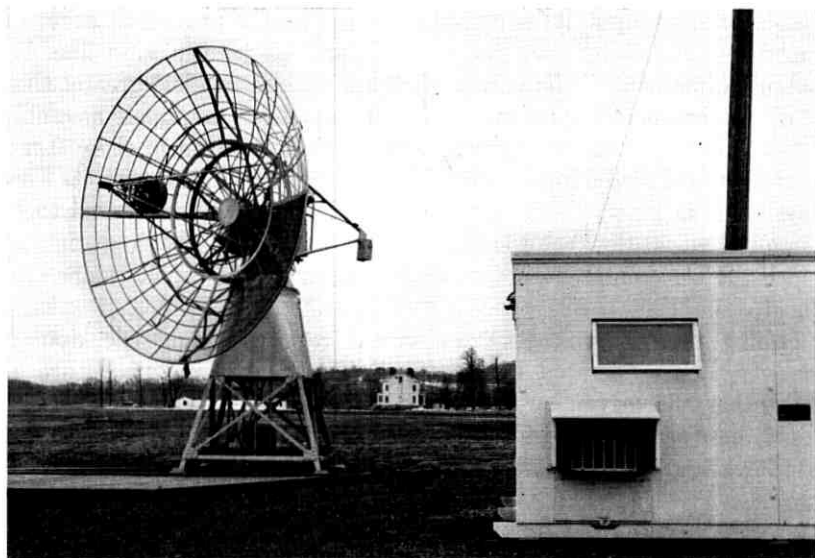


Fig. 14 — Echo I radar receiving antenna.

Since our received signal is circularly polarized it was not feasible to obtain conical scan by simple rotation of the feed. Rather, the feed was caused to rotate about the axis of the antenna in such a way that the radiators always remain parallel to themselves; i.e., the vertical dipole remains truly vertical and the horizontal dipole horizontal. The radiators are mounted at the center of the reflecting disk. This center point is caused to move in a circle about the antenna axis without any corresponding rotation of the disk about its own axis. The desired motion is obtained by supporting the disk on three motor-driven cranks.

To minimize losses, the coaxial line from the antenna feed to the low-noise amplifier has a diameter of $1\frac{5}{8}$ -inches. This rigid line, which is pressurized, is connected to the rigid line supporting the dipoles by a short length of flexible cable. The flexibility of this section of line allows scanning of the feed. No rotary joint is required.

The antenna has a gain of 32.6 db and a beam width of 3.9° . Because of the conical-scan feature, the antenna feed is always displaced from the centerline of the reflector by two inches. This results in a beam shift of 1.2° with a resultant loss of approximately 1.5 db of gain along the antenna axis.

In spite of the fact that the parametric amplifier is equipped with a

circulator at its input, it was considered important to provide an accurate impedance match between the antenna and its transmission line. By careful adjustment of the various dimensions, a return loss greater than 50 db at the operating frequency was obtained for the dipole assembly alone. This loss remained greater than 20 db over a range of ± 50 mc. With this feed at the focal point of the mesh reflector and with its fiber glass cover in place, the minimum return loss was still measured to be greater than 20 db over the 100-mc band, although the frequency at which the best match occurs is different than for the dipoles alone (see Fig. 15).

Lobing reference voltages are obtained from two single-pole, double-throw switches operated by a pair of cams placed in quadrature to each other and driven by the lobing motor. It was found necessary to shield these switches and filter the leads going to them in order to avoid interference in the receiver.

IV. ANTENNA MOUNT AND DRIVES

The receiving antenna is supported on, and driven by, a war surplus SCR-584 radar antenna mount. The mount is supported, in turn, on a steel tower fabricated for the purpose. The center of the reflector is approximately 15 feet above the ground (see Fig. 14).

This mount had originally carried an antenna only 6 feet in diameter,

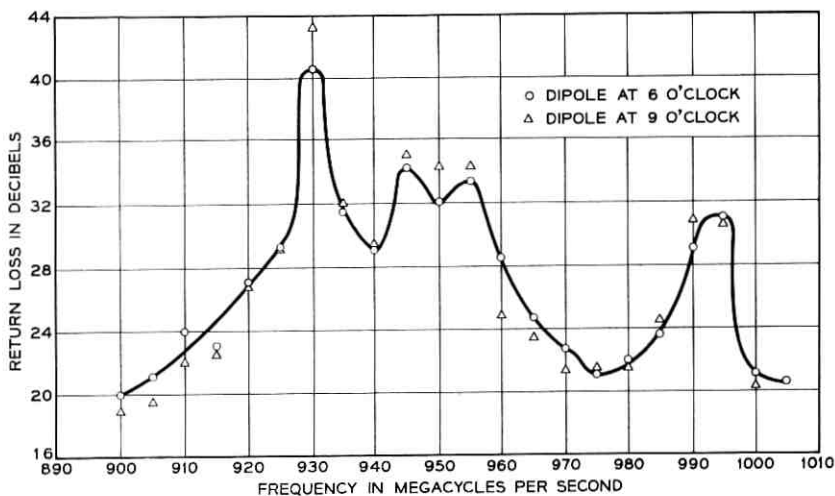


Fig. 15 — Antenna match. Feed with reflector.

and the much greater weight and inertia of our antenna increased the drive problems very considerably. As a result of corrosion and wear of gearing, the antenna drive was found to be very rough — a difficulty which was aggravated by substitution of the larger antenna. Furthermore, the increased inertia upset the characteristics of the feedback loop included in the positioning control system. The greater torque obtained by applying a 10:1 speed reduction to both the azimuth and elevation drive motors smoothed out the drive to a satisfactory degree. In spite of the speed reduction the antenna is still capable of a maximum rate of 4.5° per second in azimuth and 2.4° per second in elevation, which is sufficient for tracking the balloon.

Fig. 16 is a plot of azimuth lag error versus angular rate. Except for rare orbits that pass directly overhead, the maximum rate is 0.5° per second. The corresponding lag error is seen to be 0.04° or less.

The SCR 584 antenna mount was originally equipped with only one-speed control transformers. In order to improve positioning accuracy and operate with the synchro generators on the transmitting antenna, the system was converted to 1-and-36 speed in both azimuth and elevation. The 1-and-16-speed position-read-out synchros were also converted to 1-and-36 speed in order to be consistent with the rest of the Echo system. These speed changes were accomplished by adding gear trains constructed in our local shop.

In one experiment it was found to be a simple matter to set up the system to provide auto-tracking of the moon by the receiving antenna only. In this case the transmitting antenna was positioned manually. Because of the low angular rates involved it should not be difficult to

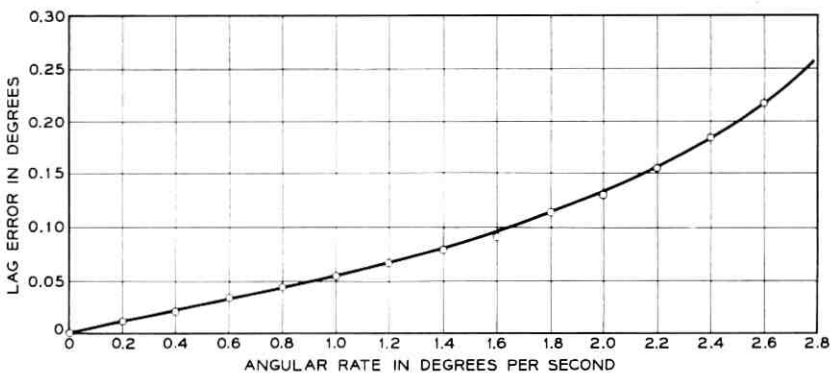


Fig. 16 — Azimuth lag error.

obtain completely automatic tracking of the natural satellite. But up to the present time we have not felt that it is worth expending the effort required to obtain automatic tracking of the balloon.

V. CONCLUSIONS

Although the performance of the radar as designed is adequate, it could be bettered in several ways. There is considerable improvement when the transmitter is employed exclusively for radar, not only because of the 6-db increase in power but because of the absence of extraneous signals which result from some forms of modulation of the communications channel. A further reduction in the amount of residual frequency modulation of the beating oscillator supplying the second converter is also desirable.

Automatic adjustment of the pulse-repetition frequency to the optimum value at all times would also be a worth-while improvement. The present method — making these adjustments manually — is satisfactory when the radar is employed only for antenna pointing. When the system is engaged to make measurements of the path loss to the balloon and return, misadjustments of the pulse-repetition frequency reduce the accuracy of these measurements. Automatic control of the pulse rate should, therefore, provide more accurate results.

VI. ACKNOWLEDGMENTS

Although it is not possible to give credit to everyone who contributed to the success of this project I do wish to acknowledge the many contributions of W. M. Goodall. I also wish to thank C. P. Frazee, F. E. Guilfoyle, and J. T. Ruscio of Bell Telephone Laboratories and L. G. Hegsted of Western Electric Company for the many long hours which they devoted to this radar.

APPENDIX A

Calculation of Received Signal Level

Let

$$P_R = \frac{P_T}{L},$$

where P_R is received power, P_T is transmitted power, and L is path loss. For isotropic transmitting and receiving antennas and a spherical reflector,

$$L = \frac{2524.2R^4}{\lambda^2 D^2},$$

where R is the distance to the reflector, D is its diameter, and λ the wavelength. At 961.05 mc, $\lambda = 1.025$ feet. For our case, $D = 100$ feet. Then

$$L = 0.2404 R^4,$$

with R in feet. For a range of 1000 miles $L = 0.2404 (5.28 \times 10^6)^4$:

$$L = 1.87 \times 10^{26} = 262.7 \text{ db.}$$

Taking into account the transmitting antenna gain of 43.1 db and receiving antenna gain of 32.6 db, with a lobing loss of 1.5 db and total transmission line loss of 0.5 db, we have

$$L' = 262.7 - 43.1 - 32.6 + 1.5 + 0.5 = 189.0 \text{ db.}$$

For a transmitted power of 1 kw,

$$P_T = +30 \text{ dbw} = +60 \text{ dbm.}$$

For the 50 per cent duty factor employed the average power is 3 db less, or +57 dbm.

For a distance of 1000 miles and peak power of 1 kw,

$$P_R = +57 - 189 \text{ db} = -132 \text{ dbm.}$$

For other distances and powers we have

$$P_R = -132 \text{ dbm} - 40 \log R + 10 \log W,$$

where R is the range in thousands of miles and W is the transmitted power in kilowatts. For $R = 1000$ miles and $W = 2.5$ kw, $P_R = -128$ dbm. For $R = 3000$ miles and $W = 2.5$ kw, $P_R = -147.1$ dbm.

Noise Calculations

At a temperature of 300°K, the KT noise power is -174 dbm per cycle of bandwidth. For a 100-cycle band and a noise figure of 1.8 db the noise power is

$$W_N = -174 + 20 + 1.8 = -152.2 \text{ dbm.}^*$$

At the maximum range of 3000 miles the predetection signal-to-noise ratio in the 100-cycle band is $152.2 - 147.1 = 5.1$ db. For the 500-cycle

* This value of noise power is to be expected during measurements of system sensitivity, since the signal-generating equipment has a noise temperature of approximately 300°K. It is also to be expected when the antenna is at zero elevation as it is at acquisition. In this position there are trees, ground, etc., in the beam. It has been found experimentally that the noise power decreases about 2 db below this value when the antenna is pointed at the zenith.

band the noise power is 7 db greater and the predetection signal-to-noise ratio is -1.9 db.

For a considerable number of the passes which were tracked, the full 10-kw output of the transmitter was given over to the radar. This 6-db increase in transmitted power brings the calculated signal-to-noise ratio at the maximum range of 3000 miles up to 11.1 db at the output of the 100-cycle filter and 4.1 db at the output of the 500-cycle filter. At the minimum range of 1000 miles the ratios are 30.2 and 23.2 db respectively.

Postdetection filtering provides a very considerable improvement in the pointing signal-to-noise ratio. For example, a one-second time constant at the output of a phase detector is equivalent to a bandwidth of 0.16 cycle. This provides a reduction of 34.9 db in noise power when compared to a 500-cycle bandwidth. This improvement, however, cannot be realized under all conditions.

APPENDIX B

Earth-Moon-Earth Path Loss

The following values apply:

$$\begin{aligned}
 \text{Peak transmitted power} &= 10 \text{ kw} = +70 \text{ dbm}, \\
 \text{Average transmitted power} &= 5 \text{ kw} = +67 \text{ dbm}, \\
 \text{Transmitting antenna gain} &= 43.1 \text{ db}, \\
 \text{Receiving antenna gain} &= 32.6 \text{ db}, \\
 \text{Lobing loss} &= 1.5 \text{ db}, \\
 \text{Total line loss} &= 0.5 \text{ db}, \\
 \text{Received power} &= -128 \text{ dbm}, \\
 \text{Path loss, } L &= 128 + 67 + 43.1 + 32.6 - 1.5 - 0.5 \\
 &= 268.7 \text{ db}.
 \end{aligned}$$

According to Trexler² the path loss is 258 db at 300 mc and increases at the rate of 6 db per octave. At 961.05 mc,

$$\begin{aligned}
 L &= 258 + 10 \log (961.05/300) \\
 &= 258 + 10.1 \\
 &= 268.1 \text{ db}.
 \end{aligned}$$

REFERENCES

1. Jakes, W. C., Jr., Participation of Bell Telephone Laboratories in Project Echo and Experimental Results, this issue, p. 975.
2. Trexler, J. H., Lunar Radio Echoes, Proc. I.R.E., **46**, 1958, p. 29.
3. Schafer, J. P., and Brandt, R. H., 960-mc, 10-kw Transmitter, this issue, p. 1041.
4. Uenohara, M., and Seidel, H., 961-mc Lower-Sideband Up-Converter for Satellite-Tracking Radar, this issue, p. 1183.

PROJECT ECHO

961-mc Lower-Sideband Up-Converter for Satellite-Tracking Radar

By M. UENOHARA and H. SEIDEL

(Manuscript received April 4, 1961)

A 961-mc lower-sideband up-converter has been specially designed to serve as preamplifier for the satellite-tracking radar used in Project Echo. The amplifier and its power supply are separately boxed and are installed directly behind the tracking antenna. The amplifier has been functioning most satisfactorily and has been used in routine manner to track the Echo satellite from horizon to horizon.*

This paper describes the design considerations, and details the special steps taken to ensure that the amplifier meets the particular system needs of low noise, absolute stability, insensitivity to temperature fluctuations, and high input-power level before onset of gain compression.

The satisfactory operation of this amplifier confirms the great potentiality of parametric amplifiers for stable, low-noise, high-frequency receivers.†

I. INTRODUCTION

The satellite-tracking radar amplifier operates at a center-band frequency of 961 mc in a lower-sideband mode and is pumped at 11.7 kmc; the output frequency of the amplifier is 10.739 kmc. The amplifier is unconditionally stable and its gain remains constant over long periods. The over-all noise figure of the amplifier, including the following mixer and IF stage, is less than 1.6 db; the gain at center band is 22 db and the bandwidth is 20 mc. The input power level that reduces the amplifier gain by 1 db is -26 dbm.

Since lower-sideband operation is employed, we are dealing with a regenerative amplifier, which is basically very sensitive to any changes

* Although this equipment was designed and constructed by the Bell System as part of its research and development program, it was operated in connection with Project Echo under Contract NASW-110 for the National Aeronautics and Space Administration.

† L. U. Kibler has come to similar conclusions in his paper¹ in this issue.

in circuit impedance and to fluctuations in the power supply. This feature has often been considered to be a disadvantage of parametric amplifiers in systems applications. To allay such fears, special precautions have been taken to stabilize the parametric amplifier. In particular, good isolators are provided to isolate the amplifier from any impedance fluctuations produced by antenna mismatches. Any fluctuation in the pump frequency is continuously corrected by an automatic frequency control, and all components, especially those near the diode, are made extremely rigid, thereby eliminating the possibility of impedance variations caused by mechanical vibrations. It is only through such careful design and engineering that the regenerative device can be, and indeed has been, made into a stable and reliable amplifier.

The system requirements of Project Echo made it necessary to pay special attention to the following two points:

(a) The amplifier had to be insensitive to large environmental changes; this was necessary because the amplifier was installed directly behind the antenna in order to reduce cabling losses. Otherwise, the insertion loss of the input circuit would degrade the noise performance of the system.

(b) The gain-compression characteristics had to be sufficiently good that, with an input power level of -26 dbm, the gain would be still within 1 db of the small-signal gain; at the same time, the over-all system noise figure had to be less than 1.8 db. This compression specification arose because the maximum possible leakage power from the 960-mc satellite communications transmitter was about -26 dbm at the radar receiver station.

It is difficult to construct a filter which has low insertion loss at 961 mc while suppressing a frequency only 1 mc away. If the gain compression were severe, with an input level of -26 dbm, the amplifier would be saturated by the leakage signal and the radar signal could not be detected. The power level at which compression sets in can be increased simply by decreasing the gain of the amplifier.* However, one must pay a penalty for decreasing the amplifier gain, since the over-all system noise figure increases through the increased noise contribution of the mixer and IF stages. The compression problem is thus not optimally solved simply by decreasing the amplifier gain; it requires a careful evaluation of the circuit design parameters.

The purpose of this paper is to describe the design consideration and the performance of the 961-mc amplifier with special emphasis on the

* For this particular amplifier the gain is almost constant until the output power reaches about -3 dbm. For example, for a gain of 22 db, the level at which compression sets in is about -25 dbm.

precautions taken to ensure that this amplifier met all the system requirements.

II. SPECIFICATIONS

The following were the specifications for the 961-mc preamplifier to be used with the Project Echo satellite-tracking radar:

Center-band frequency:	961 mc,
Over-all system noise figure:	<1.8 db,
Input power level at 960 mc for a gain compression of 1 db:	> -26 dbm.

The amplifier had to be unconditionally stable, providing constant gain over minimum periods of an hour. The amplifier also had to be installed as close as possible to the antenna to reduce the cabling loss from the antenna to the amplifier.

According to these specifications the amplifier was to be packed in a small box which would be mounted on the back of the parabolic dish. It was expected that the temperature of the environment of the amplifier would vary over a span of 80°F between midsummer and midwinter, and the performance of the amplifier had to be insensitive to such large environmental change. The amplifier had also to be insensitive to mechanical vibrations.

III. SELECTION OF MODE OF OPERATION

There are three presently accepted practical modes of operation of variable reactance communication amplifiers. They are all nondegenerate and are, respectively, the upper-sideband, the lower-sideband, and the reflection types. If ω_s is the signal frequency and ω_x is either the upper- or lower-sideband frequency, corresponding to either a positive or negative resistance device, then the minimum achievable system noise figures for uncooled systems are

$$F = 1 + \frac{\omega_s}{\omega_x} \frac{T_L}{290} \text{ (upper-sideband),}$$

$$F = 1 + \frac{\omega_s}{\omega_x} \text{ (lower-sideband or reflection),}$$

where T_L is the effective temperature of the load; that is, a fiction representing second-stage noise through the relationship

$$T_L = (F_2 - 1) 290,$$

where F_2 is the noise figure of the second stage.

The formulae above assume the varactors to be totally noise-free and, further, that the negative-resistance modes may be operated at infinite gain. While neither assumption is to be taken too seriously, they permit, nevertheless, elimination of the upper-sideband device from major consideration. The load temperature T_L may be estimated by an optimistic assumption of 7 db for a mixer IF combination. Assuming a probable value of ω_s/ω_z of order one-tenth, then with no other consideration of noise sources, this term would account for about $1\frac{1}{2}$ db in its own right.

Both the lower-sideband and the reflection types of amplifier system have minimum excess temperatures operating at infinite gain condition. They provide identical noise figures and, at this gain, only the diode noise terms enter into account. This condition of infinite gain is evidently a singular one and corresponds, in principle, to the situation in which the diode regenerates its own losses as well as those of the idler-frequency cavity. Viewing the amplifier back from the idler port, it corresponds to a zero impedance source, and the idler load must correspondingly be decoupled infinitely if power is to be drawn from that source. It is little wonder, in the case of infinite gain, that the regeneration requirements of the lower-sideband amplifier require a higher order of infinity of regeneration than does the reflection type of device, and that it is by far the more unstable of the two.

As we drop down from the infinite gain condition, the negative source impedance rises from zero and the coupling coefficient to the load likewise rises from zero. The details of the noise sources within the load then become increasingly significant in determining over-all performance. The stability situation is ultimately reversed, in that the frequency-ratio gain available in the lower-sideband converter, in accounting for the second-stage noise, diminishes the need for regenerative gain over the reflection device, and the lower-sideband amplifier becomes more suitable for operation.

There were four reasons why a moderate gain was desired, in contrast to a very high gain, and which eventually made the lower-sideband converter the desired choice in system considerations for the Echo radar:

1. A reasonably wide bandwidth was desired to avoid frequency stability problems;
2. Too high a gain leads to compression problems;
3. Very large gain leads to pump stability problems;
4. Antenna mismatches require excessive isolation at high regenerative gain and noise is introduced through isolator forward loss.

In the selection of either the reflection or lower-sideband amplifier, the choice resided in the penalty paid to system noise performance for finite gain operation. The total system temperature is

$$T_{\text{sys}} = T_{\text{amp}}(G) + \frac{T_L}{G}.$$

In either amplifier type, T_L is typically of the order of 1200°K , and a gain of 20 db is thoroughly adequate to reduce second-stage noise. It may be shown that T_{amp} is well behaved as G decreases from infinity, and that the increase in system noise temperature from its minimum value is very nominal.

Assuming a 20-db amplifier gain, Fig. 1 shows (see Appendix A) that a choice of $R_L/R_S = 0.8$ (that actually employed) demands a regenera-

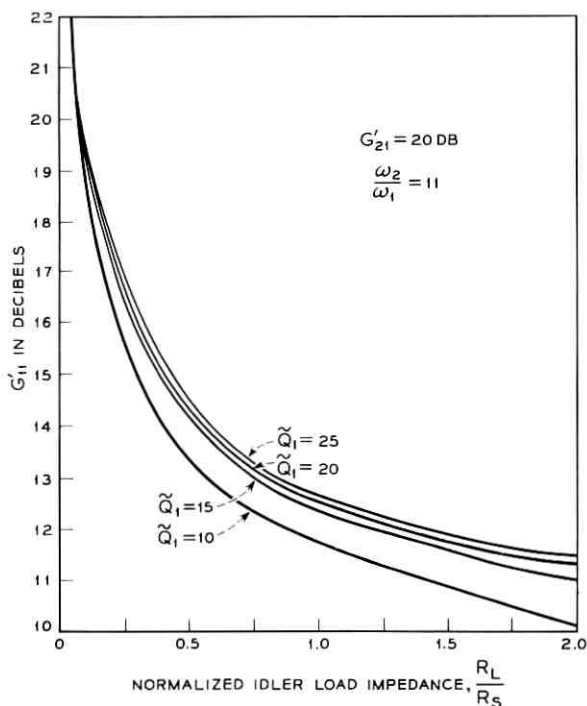


Fig. 1 — Regenerative gain G_{11}' of lower-sideband up-converter, which is needed to achieve a total gain G_{21}' of 20 db, vs. normalized idler load impedance R_L/R_S . The regenerative gains are shown for four different dynamic quality factors Q_1 , with $Q_1 = 25, 20, 15,$ and 10 .

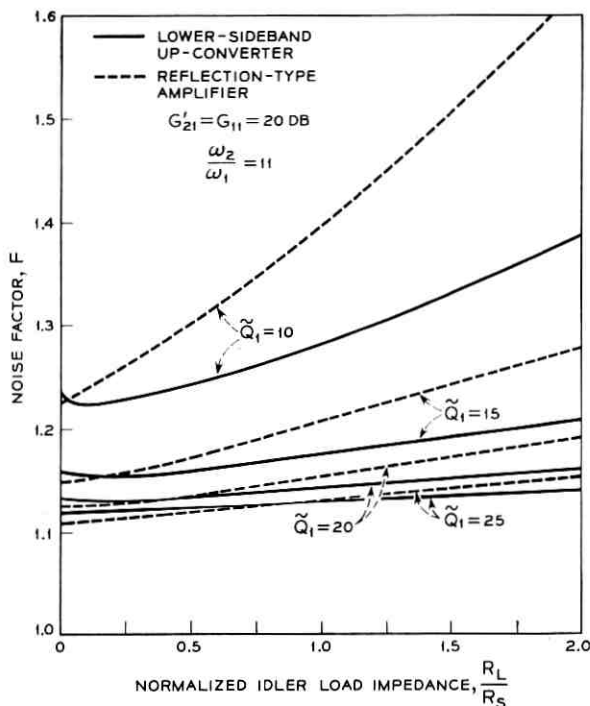


Fig. 2 — Noise figures of lower-sideband up-converter and reflection-type amplifier vs. normalized idler load resistance R_L/R_S . The curves for the lower-sideband up-converter are shown by solid lines, those for the reflection type amplifier dashed lines. Gains are assumed to be the same at 20 db for both amplifiers.

tive gain of about 13 db for the lower-sideband amplifier, almost independently of \tilde{Q}_1 ,* in contrast to the 20 db for the reflection type. Further, as shown in Fig. 2, the lower-sideband noise figure (see Appendix B) at $R_L/R_S = 0.8$, at which it is trivially different from its minimum value, is significantly less than that for the reflection amplifier for $\tilde{Q}_1 < 25$. The parameters chosen in evaluating the curves of Figs. 1 and 2 are somewhat arbitrary, but are, nevertheless, typical for amplifiers of the type under consideration.

It was under the force of the above arguments, considering both stability and noise, that the lower-sideband amplifier was chosen in preference to the reflection type.

* The quality Q is defined in the next section and is a quality factor modified by the dynamic capacity ratio; R_L is the load impedance; and R_S is the diode-spreading resistance.

IV. VARACTOR DIODE SELECTION

There are two major requirements in the choice of a varactor diode:

1. It has to have an impedance sensible in magnitude to that of the generator.

2. It should have a high Q relative to its variable capacity portion.

The first requirement follows from the desire both to achieve reasonable bandwidth and to avoid large tuning losses in obtaining adequate interaction with the diode. The second follows from the fact that a static capacitor, however excellent its Q , cannot provide a basis for amplification, and its variability must be taken into account. A more realistic definition is given by²

$$\tilde{Q} = \frac{Q}{\frac{2C_0}{C_1} - \frac{C_1}{2C_0}},$$

where C_0 is the static capacitance at the operating point and C_1 is the capacitance associated with first dynamic term of the Fourier expansion of the time variable charge. The quantity Q is that value conventionally defined for the static capacitance, and is equal to

$$Q = \frac{1}{\omega C_0 R_s},$$

where R_s is the spreading resistance of the diode. This result assumes other loss mechanisms to be negligibly effective, which is given excellent confirmation experimentally.³

The choice of the value of C_0 is a most complex one if it is to be done correctly. Corresponding to a value of C_0 and its quality factor, there exist generator and load impedances which minimize noise. Transforming to these impedance levels requires tuning elements which are noise sources. Since the diode, as a waveguide scatterer, is an unknown from present analytic considerations, the computation of that value of C_0 which minimizes total system noise figure is not now achievable.

The actual selection of the static capacity value is intuitive and empirical. Since the capacitive impedance must be of the same order of magnitude as that of the generator, a first choice of C_0 is that in which

$$C_0 = \frac{1}{\omega_s R_g}.$$

This establishes the range of values of C_0 , and initial experiments are performed to range in on an apparently best value. Experience has

demonstrated the choice to be fairly broad once a proper region has been found, since the tuning elements contribute but little loss.

The final question in choosing a diode relates to the material of the varactor. Diode development at this time has gone in two distinct directions in terms of the gallium arsenide point-contact and the silicon junction varactor. As of this writing, the gallium arsenide junction diode has shown no superiority over silicon, although it may yet well do so, and the selection was just between the aforementioned two.

The gallium arsenide point-contact diode has, to date, shown the highest achieved Q in practice, but has two mitigating features:

1. Currently available capacities are of order $0.5 \mu\text{mf}$.
2. Its long-term reliability is not yet proven.

Under these circumstances it was deemed more advisable to choose a silicon junction varactor with a zero bias capacity of $3.5 \mu\text{mf}$ and a cutoff frequency of 70 kmc in contrast to double that frequency for the gallium arsenide diode. Measurement of the silicon varactor showed it to possess a value of \bar{Q} of 22 at 960 mc, which is quite adequate for good performance.

V. DESCRIPTION OF THE AMPLIFIER

At the time this project was started, no suitable circulator was available at 960 mc. Of necessity, the choice was then that of the lower-sideband up-converter. However, even if a circulator had been available, the lower-sideband up-converter would still have been chosen for this particular application since it provides better stability, less severe compression, and possibly even better over-all noise performance, as discussed in the previous section.

The main features of the amplifier are as follows:

Input frequency, f_s :	961 mc,
Output (idler) frequency, f_i :	10.739 kmc (see Appendix C),
Pump frequency, f_p :	11.7 kmc,
Pump power supply:	TJ klystron (WE 455A) with AFC unit,
Bias voltage:	0 volt
$\frac{R_L}{R_s}$:	≈ 0.8
$\frac{R_g}{R_s}$:	≈ 22

Varactor diode:	silicon p-n junction diode in standard coaxial cartridge
f_c :	≈ 70 kmc,
C_0 :	≈ 3.5 $\mu\mu\text{f}$,
Estimated noise figure, F :	$1.19 = 0.75$ db (amplifier alone).

The reason for operating the diode at zero bias was to simplify the amplifier cavity structure through the absence of choking section, thereby improving stability. By doing this, a small sacrifice was made in the noise figure, since the dynamic quality factor decreases about 20 per cent, from $\tilde{Q} = 22$ to $\tilde{Q} = 17$, but the specifications were still met without any difficulty. The output circuit was designed to be near critical coupling under the no-pump condition. This coupling condition was also selected to improve the stability of the amplifier and the effects of compression.

One potential difficulty in employing a lower-sideband up-converter is the output frequency modulation due to fluctuation in the pump frequency. A slow frequency shift can, of course, be corrected by an AFC system. However, fluctuations which are fast and small cannot be corrected satisfactorily. This difficulty is solved by pumping the up-converter of the local frequency generator with the same pump supply as is used for the amplifier. The local oscillator consists of a lower-sideband up-converter and a 931-mc crystal-controlled modulator. The fluctuation of the 30-mc intermediate frequency is, therefore, exactly the same as that of the crystal oscillator.

A block diagram and photograph of the amplifier are shown in Figs. 3 and 4.

VI. CIRCUIT DESIGN

The first-order model of the parametric amplifier is well understood and accounts for the major portion of design. The parameters of this model may be found conveniently from a systematic static or "cold test" procedure,³ which defines the central operating point and the pump swing. It determines a tuning and impedance-level loading procedure by identifying a static susceptance together with the first-order imaging effects produced by the pumping coupling of signal and image circuits.

The first-order theory oversimplifies somewhat and assumes a sinusoidal pump voltage swing of the diode, and also does not adequately account for the curvature of the charge voltage characteristic of the depletion layer. This latter effect greatly accentuates the charge drawn

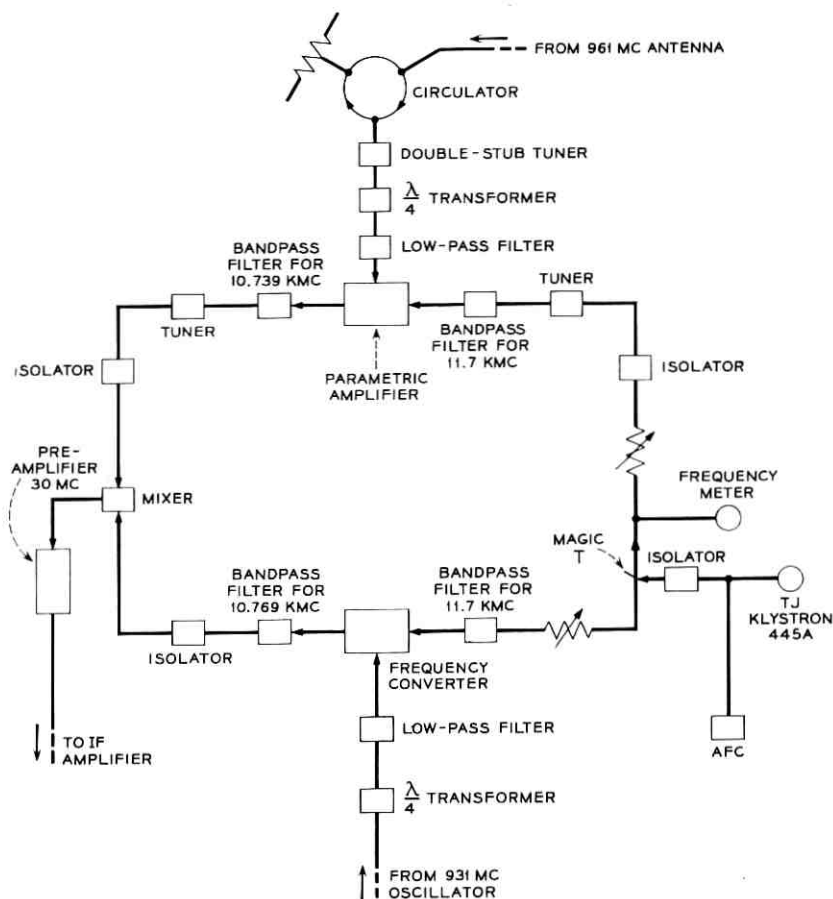


Fig. 3 — Block diagram of the 961-mc amplifier.

on the positive portions of the pump swing and increases the capacitive susceptance in viewing the system from either the signal or image port. The actual pump swing is defined in an equilibrium process of the pump, together with its complex network as a source, exciting the diode as a nonlinear element. Taking all things into account, the final tuning is completed by a dynamic or "hot" procedure.

The hot tuning may be accomplished adequately by a small bias increase to offset the effects of the pump excursion, and by a tuning touchup in the image circuit. This eliminates the need for variable tuning elements in the signal circuit where the effects of noise are major.

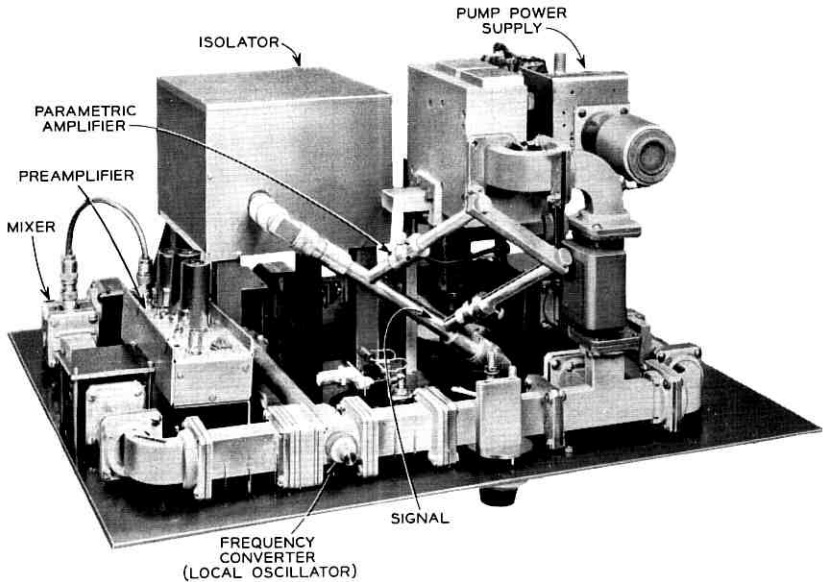


Fig. 4 — Photograph of the 961-mc amplifier.

The tuning procedure for minimum noise becomes increasingly difficult with high- Q elements, in that the spreading resistance of the diode is small and defies precise determination. Since the spreading resistance is the key to the impedance levels at signal and image frequencies, and since the effects of tuning losses become preponderant, the cold test procedure defers increasingly to the hot test with increasing Q . The demands on Q , however, are modest for most applications which do not demand ultimate noise performance, and the cold test procedure produces a good first design.

Tuning elements generally take the form of quarter-wave transformers, capacitive disks, and stubs. Final touchup is done by adjustable stub tuners in initial development. Figs. 3 and 4 show the early circuit for the Echo radar and still indicate the use of double stub tuners, but these were replaced by fixed elements in the final development.

The isolator is a most important unit in a stable parametric amplifier. It is desirable that the parametric amplifier system possess a large return loss. Since this number is typically 20 db, and since there is a return gain of the order of 13 db produced by regeneration, the isolator must possess a reverse loss of greater than 32 db, together with a minimal forward loss. The isolator must be stable to environmental cycling

so that its characteristics remain fixed. Small changes in the isolator are considerably amplified by the negative characteristics of the amplifier, and major consideration must be given both to mechanical and electrical stabilization.

VII. AMPLIFIER PERFORMANCE

The amplifier was designed as described in the previous sections. The general performance was satisfactory and closely approximated the design. The best measured over-all noise figure, including isolator, mixer, and IF amplifier, was 1.52 db with 22 db of gain and 20 mc of bandwidth; over-all noise figures of less than 1.6 db were obtainable without any difficulty. The noise figure of the amplifier portion itself was 1.33 db, of which 0.30 db was due to the insertion loss of the isolator, providing an inherent value of 1.03 db. This result is about 0.3 db above the theoretical value predicted for the diode, and suggests that the excess noise is probably caused by the tuner and the diode mount, and could be further reduced by careful engineering.

The stability of the amplifier was excellent. The gain varied by less than ± 1 db when the input impedance was varied from open-circuit to short-circuit. Under constant-temperature conditions, fluctuations in gain were mainly due to fluctuation in both pump frequency and pump power. The frequency problem was solved by using the electromechanical AFC, which was originally designed for the TJ radio relay system,⁴ while the TJ klystron itself was already designed for extreme power stability. The electromechanical feature of the AFC tunes the klystron cavity without changing the output power, so that the combination of AFC system and TJ klystron greatly improves the stability of the amplifier.

VIII. TEMPERATURE DEPENDENCE OF AMPLIFIER GAIN

Experiment yielded relatively large irreversible temperature sensitivity in the initially constructed amplifier. This difficulty was ultimately traced to a resonance isolator at the amplifier input. It was found that the temperature variation

(a) varied the ferrite magnetization, shifting the resonant frequency slightly, and

(b) created a minor hysteresis loop in the magnetic structure, not returning the isolator to its initial state.

A circulator* was found to be somewhat less critically affected by temperature since, by its essential construction, it is not constrained to operate in the region of a narrow line width.

* Raytheon circulator CLL 8.

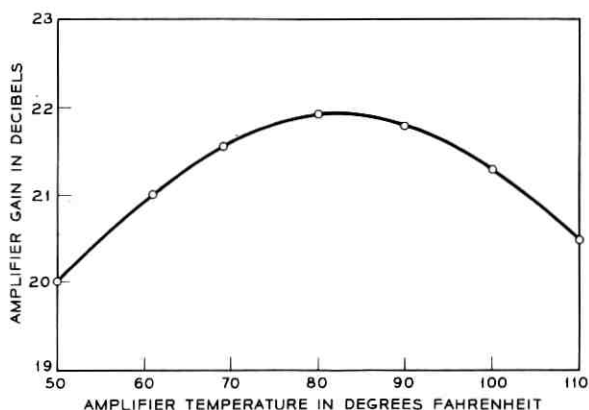


Fig. 5 — Amplifier gain vs. amplifier temperature.

Since the environmental variations seemed much beyond passive compensation, it was decided to thermostat the entire amplifier system at $110 \pm 5^\circ\text{F}$ and the circulator at $120 \pm 2^\circ\text{F}$. The system incorporating this thermostating has demonstrated constant performance over a temperature range of 80°F .

Aside from the temperature sensitivity of the circulator, it was of interest to measure the temperature sensitivity of the amplifier section itself. Fig. 5 shows a 2-db variation at 20-db gain for ambient temperatures varying between 50 and 110°F . There is little sensitivity to be ascribed to the diode itself, and it must be presumed that this variation is due to expansion of circuit elements in critically tuned regions of the amplifiers.

Fig. 6 shows the noise figure of the amplifier section to be an exceedingly insensitive function of temperature over the range examined. In the measurements there was an initially deceptive appearance that the

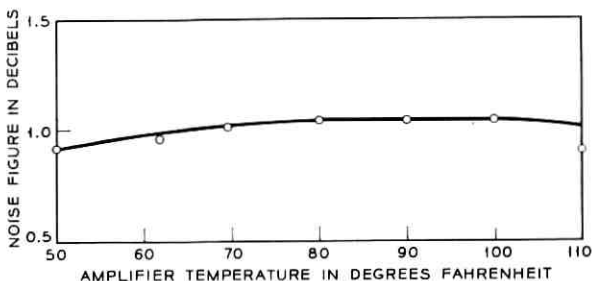


Fig. 6 — Noise figures vs. amplifier temperature.

noise figure increased much more rapidly than that in Fig. 6. This was shown, however, to be caused by the increased noise emission at higher temperature of the standard attenuators employed in conjunction with the measurements.

From the point of view of consistency, with the circulator thermostating, the use of a 110°F ambient temperature for the amplifier to maintain gain stability provided no substantial noise-figure deterioration of the amplifier system.

IX. GAIN COMPRESSION

The Echo radar system was inherently complicated by the proximity of the 960-mc transmitter, just one megacycle away from the 961-mc radar frequency, which hit the amplifier at a level of -26 dbm. Engineering the amplifier to avoid compression was a major design requirement in the construction of the Echo radar system.

Compression occurs in a parametric amplifier system for any or all of the following reasons:

1. The circuit is detuned by the shift of the average capacity of the diode produced by the large signal swing;
2. Current is drawn on the positive swing in the forward direction and avalanche current exists on the negative swing;
3. The higher mixing products become significant compared to those of the small signal theory.

The source of compression is generally to be identified with the image circuit for two reasons:

1. The diode swing at image frequency exceeds that of the signal by virtue of the frequency ratio gain;
2. Minimum-noise operation implies high- Q image operation, where regeneration almost completely cancels cavity losses. This implies high-energy storage in the diode, with consequent large diode swing.

Compression may be mitigated at some slight expense to noise by increasing the image-circuit loading and consequently decreasing the image-cavity Q . The dynamic range may be further increased by reducing gain.

Naturally, there are limits, to which gain may be decreased or image loading increased, provided by the ultimately tolerable degradation of system noise figure. Employing the above considerations, the final amplifier design furnished a 22-db small-signal gain amplifier having a 1-db compression at an input of -26 dbm.

Another consideration in the presence of a high-level signal is the possibility of its inducing parasitic oscillations in the amplifier system.

Such parasitics were indeed noted and their presence was marked by very early onsets of compression. For want of any meaningful theory, these effects were eliminated empirically by small shifts of adjustment, which were apparently entirely successful in accomplishing this purpose.

X. LONG-TIME STABILITY

The gain of the amplifier was monitored over a period of 24 hours. A part of such a trace is shown in Fig. 7. The horizontal scale indicates time; the vertical scale gain. One vertical section corresponds to 0.5 db of gain variation. The gain shift over 24 hours was not more than ± 0.5 db out of 22 db. It is believed that these small fluctuations were caused primarily by power-line variation which affected an insufficiently regulated pump regulator supply used in the test.

XI. CONCLUSION

The design considerations and performance of the 961-mc lower-sideband up-converter have been discussed, and it has been emphasized that careful design and good engineering are necessary to obtain a stable low noise amplifier. An over-all system noise figure of less than 1.6 db has been obtained with a center-band gain of 22 db and a bandwidth of 20 mc. The amplifier is very stable, and the gain varies by less than ± 1 db as the input impedance is varied from open-circuit to short-circuit. With an input power of -26 dbm, the gain was 1 db less than the small signal gain of 22 db.

XII. ACKNOWLEDGMENTS

The design of this amplifier is very similar to that of an 860-mc amplifier designed at Bell Telephone Laboratories for a tropospheric communication system. The authors are greatly indebted to its various members who participated in this 860-mc project for transmitting to them their valuable experience, which added to the success of the present design.

P. J. Pantano did much of the mechanical design and the measurements. His ability and productive efforts during the entire period of this project are greatly appreciated. L. E. Cheesman helped this project during its early period. E. G. Spencer and W. A. Dean supplied the isolators and spent much effort to solve the temperature instability of the isolator characteristics. The author wishes to acknowledge their major contributions.

Acknowledgment is also made to K. D. Bowers for his stimulating

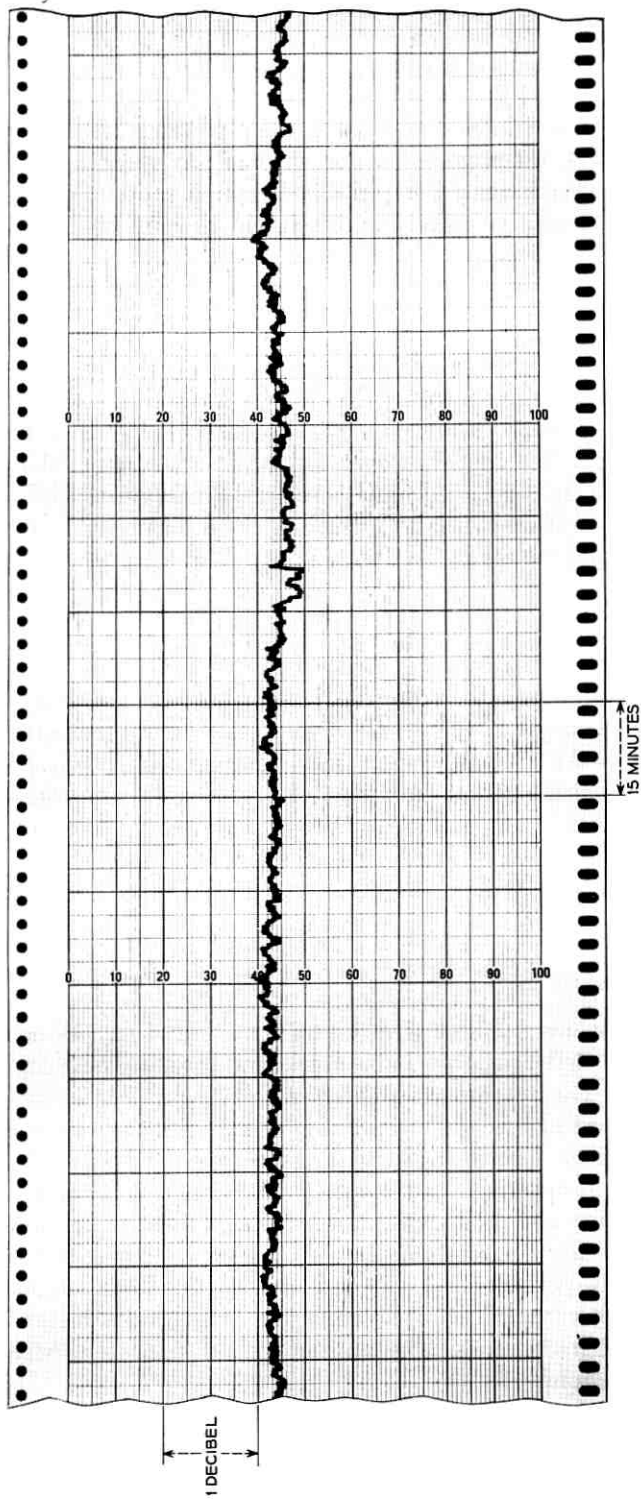


Fig. 7 — A part of a trace of the amplifier gain over a period of 24 hours. The gain shift over 24 hours was not more than ± 0.5 db.

discussions and helpful criticism and encouragement in the study of this project.

APPENDIX A

Normalized Generator Impedance for Given Gain and Diode

The gain G_{11} of the reflection-type amplifier is given by the square of the voltage reflection coefficient⁵ at the signal port, and is equal to

$$G_{11} = \frac{\left| \frac{Z_{11}^*}{R_s} - 1 + \frac{\tilde{Q}_1 \tilde{Q}_2}{1 + \frac{Z_{22}^*}{R_s}} \right|^2}{\left| 1 + \frac{Z_{11}}{R_s} - \frac{\tilde{Q}_1 \tilde{Q}_2}{1 + \frac{Z_{22}^*}{R_s}} \right|^2}, \quad (1)$$

and the gain G_{21}' * of the lower-sideband up-converter² is

$$G_{21}' = \frac{4 \frac{R_g'}{R_s} \frac{R_L'}{R_s} \tilde{Q}_1^2}{\left| \left(1 + \frac{Z_{11}'^*}{R_s} \right) \left(1 + \frac{Z_{22}'}{R_s} \right) - \tilde{Q}_1 \tilde{Q}_2 \right|^2}. \quad (2)$$

Here Z_{11} and Z_{22} are the input circuit impedance and the idler circuit impedance, respectively, including the static capacitance of the diode; R_g , R_L , and R_s are the generator resistance, idler load resistance, and series resistance of the diode, respectively. At the center frequency, (1) and (2) can be simplified and become

$$G_{11} = \frac{\left[\left(\frac{R_g}{R_s} - 1 \right) \left(1 + \frac{R_L}{R_s} \right) + \tilde{Q}_1 \tilde{Q}_2 \right]^2}{\left[\left(\frac{R_g}{R_s} + 1 \right) \left(1 + \frac{R_L}{R_s} \right) - \tilde{Q}_1 \tilde{Q}_2 \right]^2}, \quad (3)$$

and

$$G_{21}' = \frac{4 \frac{R_g'}{R_s} \frac{R_L'}{R_s} \tilde{Q}_1 \tilde{Q}_2 \frac{\omega_2}{\omega_1}}{\left[\left(\frac{R_g'}{R_s} + 1 \right) \left(1 + \frac{R_L'}{R_s} \right) - \tilde{Q}_1 \tilde{Q}_2 \right]^2}, \quad (4)$$

* The notation associated with a lower-sideband up-converter will always be primed to indicate that the scattering properties of the network are not taken simultaneously with those of the reflection type, whose quantities will be left unprimed.

where ω_1 and ω_2 are the angular frequencies of the input and idler respectively, and the circuit losses are assumed to be negligible. Fluctuation in pump power alters \tilde{Q}_1 and \tilde{Q}_2 , and, if the gain is reasonably high, fluctuation in $\tilde{Q}_1\tilde{Q}_2$ is equivalent to fluctuation in the circuit impedances R_g and R_L . At the same time, any fluctuation in the pump frequency adds reactive components to the circuit impedances. If the bandwidth of the amplifier is reasonably broad, small fluctuation in the pump frequency does not affect the gain of the amplifier significantly. The gain-bandwidth product is a simple measure of the stability of the amplifier to fluctuation in the pump frequency.

The most relevant measure of the stability of a parametric amplifier is the sensitivity of its gain to fluctuations in the resistance of the circuits. We shall now examine a measure of this sensitivity with the amplifier gain set at 20 db, a value close to that used in practice. The value of R_s/R_g is no longer coincident for both amplifier types. The major gain instability due to an impedance variation is caused by the denominators of (3) and (4), which are proportional to the regenerative gains of the amplifiers. To compare relative stability, therefore, it is much easier to compare the gain G_{11} of the reflection-type amplifier with the regenerative part G_{11}' (or input circuit gain) of the lower-sideband up-converter, whose total gain G_{21}' is equal to G_{11} . If G_{11}' is lower than G_{11} , the lower-sideband up-converter is the more stable, and vice versa. The values of R_g/R_s which provide gains G_{11} and G_{21}' for a given \tilde{Q}_1 and \tilde{Q}_2 are calculated from the following equations:

$$\begin{aligned} \frac{R_g}{R_s} &= \left(\frac{\tilde{Q}_1\tilde{Q}_2}{1 + \frac{R_L}{R_s}} - 1 \right) \left[\frac{G_{11} + 1}{G_{11} - 1} + \sqrt{\left(\frac{G_{11} + 1}{G_{11} - 1} \right)^2 - 1} \right], \\ &= \left(\frac{\tilde{Q}_1\tilde{Q}_2}{1 + \frac{R_L}{R_s}} - 1 \right) \left[\frac{(\sqrt{G_{11}} + 1)^2}{G_{11} - 1} \right], \end{aligned} \quad (5)$$

for the reflection-type amplifier, and

$$\begin{aligned} \frac{R_g'}{R_s} &= \left[\frac{2 \frac{R_L'}{R_s} \tilde{Q}_1^2}{\left(1 + \frac{R_L'}{R_s}\right)^2 G_{21}'} + \frac{\tilde{Q}_1\tilde{Q}_2}{1 + \frac{R_L'}{R_s}} - 1 \right] \\ &+ \sqrt{\left[\frac{2 \frac{R_L'}{R_s} \tilde{Q}_1^2}{\left(1 + \frac{R_L'}{R_s}\right)^2 G_{21}'} + \frac{\tilde{Q}_1\tilde{Q}_2}{1 + \frac{R_L'}{R_s}} - 1 \right]^2 - \left(\frac{\tilde{Q}_1\tilde{Q}_2}{1 + \frac{R_L'}{R_s}} - 1 \right)^2} \end{aligned} \quad (6)$$

for the lower-sideband up-converter. The values of R_g/R_s which provide 20-db gain for given values of \tilde{Q}_1 and \tilde{Q}_2 are plotted as a function of R_L/R_s in Fig. 8. The dashed lines are those for the reflection-type amplifier and the solid lines are for the lower-sideband up-converter. Substituting the appropriate value of R_g/R_s for the lower-sideband up-converter into (4), one finds G_{11}' . The results are plotted in Fig. 2.

The load coupling factor for which G_{11} exceeds G_{21}' is determined by the condition

$$\left[\left(\frac{R_g'}{R_s} - 1 \right) \left(1 + \frac{R_L'}{R_s} \right) + \tilde{Q}_1 \tilde{Q}_2 \right]^2 = 4 \frac{R_g'}{R_s} \frac{R_L'}{R_s} \tilde{Q}_1 \tilde{Q}_2 \frac{\omega_2}{\omega_1}. \quad (7)$$

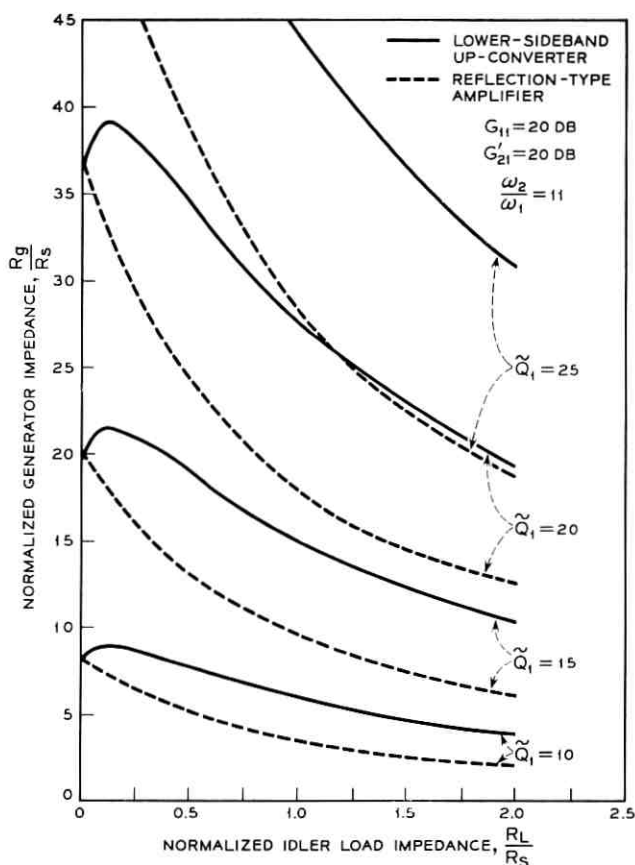


Fig. 8 — Normalized generator impedance R_g/R_s needed to obtain the gain of 20 db vs. normalized idler load impedance R_L/R_s . The curves for the lower-sideband up-converter are shown by solid lines; those for the reflection-type amplifier are shown by dashed lines.

A high-gain approximation leads to the simpler equation

$$\left(1 + \frac{R_L'}{R_S}\right) \frac{R_g'}{R_S} = \frac{R_L'}{R_S} \left(\frac{R_g'}{R_S} + 1\right) \frac{\omega_2}{\omega_1}, \quad (8)$$

from which R_L'/R_S is found to be

$$\begin{aligned} \frac{R_L'}{R_S} &= \frac{\omega_1}{\omega_2 \left(1 + \frac{R_S}{R_g'}\right) - \omega_1} \\ &\approx \frac{\omega_1}{\omega_2 - \omega_1} \quad \text{if} \quad \frac{R_g'}{R_S} \gg 1. \end{aligned} \quad (9)$$

APPENDIX B

Noise Figure at Arbitrary Gain for Reflection-Type Amplifier and Lower-Sideband Up-Converter

The noise output of the reflection-type amplifier is

$$N_{\text{out}} = N_{11} + N_{12}, \quad (10)$$

where N_{11} is the noise output due to the noise sources in the signal circuit and N_{12} is the noise output due to those in the idler frequency circuit. The noise N_{11} contains two sources: one is the noise generated within the amplifier²

$$N = \frac{4 KT B \frac{R_g}{R_S}}{\left[\left(\frac{R_g}{R_S} + 1\right) - \frac{\tilde{Q}_1 \tilde{Q}_2}{1 + \frac{R_L}{R_S}}\right]^2}, \quad (11)$$

and the other is the input noise that is amplified

$$N = KT BG_{11}. \quad (12)$$

The noise N_{12} is given by²

$$N_{12} = \frac{4 KT B \frac{R_g}{R_S} \frac{\tilde{Q}_1 \tilde{Q}_2}{\left(\frac{R_L}{R_S} + 1\right)} \frac{\omega_1}{\omega_2}}{\left[\left(\frac{R_g}{R_S} + 1\right) - \frac{\tilde{Q}_1 \tilde{Q}_2}{1 + \frac{R_L}{R_S}}\right]^2}. \quad (13)$$

From (10) through (13), the noise figure of the reflection-type amplifier is found to be

$$\begin{aligned}
 F &= \frac{N_{11} + N_{12}}{KT BG_{11}} \\
 &= 1 + \frac{4 \frac{R_g}{R_s}}{\left[\left(\frac{R_g}{R_s} - 1 \right) + \frac{\tilde{Q}_1 \tilde{Q}_2}{1 + \frac{R_L}{R_s}} \right]^2} + \frac{4 \frac{R_g}{R_s} \frac{\omega_1}{\omega_2} \frac{\tilde{Q}_1 \tilde{Q}_2}{1 + \frac{R_L}{R_s}}}{\left[\left(\frac{R_g}{R_s} - 1 \right) + \frac{\tilde{Q}_1 \tilde{Q}_2}{1 + \frac{R_L}{R_s}} \right]^2} \\
 &= 1 + \left(1 - \frac{1}{G_{11}} \right) \frac{1 + \frac{\omega_1}{\omega_2} \frac{\tilde{Q}_1 \tilde{Q}_2}{1 + \frac{R_L}{R_s}}}{\frac{\tilde{Q}_1 \tilde{Q}_2}{1 + \frac{R_L}{R_s}} - 1}.
 \end{aligned} \tag{14}$$

Similarly, for the lower-sideband up-converter, the noise output is

$$\begin{aligned}
 N_{\text{out}} &= N_{21} + N_{22} \\
 &= \frac{4 KT B \left(\frac{R_g}{R_s} + 1 \right) \frac{R_L}{R_s} \frac{\omega_2}{\omega_1} \frac{\tilde{Q}_1 \tilde{Q}_2}{\left(\frac{R_g}{R_s} + 1 \right)^2}}{\left[\left(\frac{R_L}{R_s} + 1 \right) - \frac{\tilde{Q}_1 \tilde{Q}_2}{\frac{R_g}{R_s} + 1} \right]^2} \\
 &\quad + \frac{4 KT B \frac{R_L}{R_s}}{\left[\left(\frac{R_L}{R_s} + 1 \right) - \frac{\tilde{Q}_1 \tilde{Q}_2}{\frac{R_g}{R_s} + 1} \right]^2} + KT BG_{22},
 \end{aligned} \tag{15}$$

where G_{22} is the reflection power gain of the idler circuit:

$$G_{22} = \frac{\left[\left(\frac{R_L}{R_s} - 1 \right) + \frac{\tilde{Q}_1 \tilde{Q}_2}{\frac{R_g}{R_s} + 1} \right]^2}{\left[\left(\frac{R_L}{R_s} + 1 \right) - \frac{\tilde{Q}_1 \tilde{Q}_2}{\frac{R_g}{R_s} + 1} \right]^2}. \tag{16}$$

Therefore, the noise figure of the lower-sideband up-converter is

$$\begin{aligned}
 F &= 1 + \frac{R_s}{R_g} + \frac{1}{\frac{R_g \omega_2}{R_s \omega_1} \frac{\tilde{Q}_1 \tilde{Q}_2}{\left(\frac{R_g}{R_s} + 1\right)^2}} + \frac{\left[\left(\frac{R_L}{R_s} - 1\right) + \frac{\tilde{Q}_1 \tilde{Q}_2}{\frac{R_g}{R_s} + 1}\right]^2}{4 \frac{R_g R_L \omega_2}{R_s R_s \omega_1} \frac{\tilde{Q}_1 \tilde{Q}_2}{\left(\frac{R_g}{R_s} + 1\right)^2}} \quad (17) \\
 &= 1 + \frac{R_s}{R_g} + \frac{\omega_1}{\omega_2} \left(\frac{1}{\omega_1 G_{21}} + 1 + \frac{R_s}{R_g} \right) \\
 &= \left(1 + \frac{R_s}{R_g} \right) \left(1 + \frac{\omega_1}{\omega_2} \right) + \frac{1}{G_{21}}.
 \end{aligned}$$

APPENDIX C

Optimum Idler Frequency for Arbitrary Idler Load

For high-gain and minimum-noise operation, the ratio of signal frequency to idler frequency is given by Equation (31) of Ref. 2. However, when R_L is not zero, the optimum idler frequency is different from that obtained using this equation, and it is instead determined by finding the value of ω_2 which minimizes the noise figure given by the following equation:

$$\begin{aligned}
 F &= 1 + \frac{R_s}{R_g} + \frac{\left(\frac{R_L}{R_s} + 1\right) R_s \omega_1 \left(1 + \frac{R_g}{R_s}\right)^2}{R_g \omega_2 \tilde{Q}_1 \tilde{Q}_2} \quad (18) \\
 &= \left(1 + \frac{R_s}{R_g} \right) \left(1 + \frac{\omega_1}{\omega_2} \right) + \frac{1}{G_{21}}.
 \end{aligned}$$

Using the high-gain approximation of (6) for R_g/R_s as a function of frequency, we find

$$F = \left(1 + \frac{\omega_1}{\omega_2} \right) \left[1 + \frac{1}{\frac{\tilde{Q}_1^2 \omega_1}{\omega_2} \left[1 + \frac{R_L}{R_s} \right]} \right] + \frac{1}{G_{21}}. \quad (19)$$

Equation (19) leads readily to the result that

$$\frac{\omega_2}{\omega_1} = \frac{\tilde{Q}_1^2}{\left(1 + \frac{R_L}{R_s} \right) \left(1 + \sqrt{1 + \frac{\tilde{Q}_1^2}{1 + \frac{R_L}{R_s}}} \right)}. \quad (20)$$

The error in approximating the value of R_g/R_s at high gain is usually small, and provides negligible error in determining noise figure. Substituting the parameters given in Section V, ($R_L/R_s = 0.8$, $Q_1 = 17$), one finds that $\omega_2/\omega_1 = 11.7$. The optimum idler frequency is thus about 11.3 kmc. From this idler frequency the pump frequency is determined to be 12.261 kmc. Since the optimum frequency result leads to broad noise figure minima, it was decided to forego the exact pump frequency calculated in favor of one within the band of the Western Electric 445A klystron. This klystron, which has been designed for the TJ system, has a notably stable and long life. It was operated as a pump at the top of its range, at 11.7 kmc, producing an idler frequency of 10.739 kmc.

REFERENCES

1. Kibler, L. U., Standby Receiver System, this issue, p. 1129.
2. Kurokawa, K., and Uenohara, M., Minimum Noise Figure of the Variable-Capacitance Amplifier, B.S.T.J., **40**, 1961, p. 695.
3. Kurokawa, K., Theory of Cold Test of Variable-Capacitance Amplifier, to be published.
4. Gammie, J., and Hathaway, S. D., The TJ Radio Relay System, B.S.T.J., **39**, 1960, p. 821.
5. Uenohara, M., Noise Consideration of the Variable-Capacitance Parametric Amplifier, Proc. I.R.E., **48**, 1960, p. 169.

PROJECT ECHO

Antenna Steering System

By R. KLAHN, J. A. NORTON, and J. A. GITHENS

(Manuscript received April 6, 1961)

The Project Echo experiment employed large steerable communication antennas at the ground terminals. These are highly directional transmitting and receiving antennas which must be continuously and accurately pointed at the passing satellite. While the dynamic control of antennas has not been required in prior Bell System communications, it will play an important role in future systems utilizing many orbiting repeaters.

I. INTRODUCTION

Although communications antennas could be slaved to optical or radar trackers at each antenna site, the use of basic orbital information to generate antenna steering instructions is expected to be more economical when many antennas and sites are served. The latter method was used in Project Echo and employed the following steps:

1. determine satellite positions by accurate radio observations and, from these, calculate the basic satellite orbital elements;
2. use these elements to calculate future satellite positions;
3. from these positions, compute pointing angles for the antennas.

In the Echo experiment, these functions were performed by the Mini-track satellite tracking network and the Goddard Space Flight Computation Center, which are facilities of the National Aeronautics and Space Administration. The predicted angles were transmitted by teletypewriter from the computer at Washington to the Bell Telephone Laboratories antennas on Crawford Hill at Holmdel, New Jersey. The first portion of this paper discusses system design problems concerning the transmission of pointing information from computer to antenna site, and conversion of these data into servo-actuating signals that move the antennas to the predicted angles at the desired time. The second portion describes how

these problems were approached in the antenna pointing system provided for Project Echo.*

1.1 *System Considerations*

Several factors affect the design of a data processing system for antenna steering. Functions performed by the system include:

1. transmission of predicted pointing data from a computer location to the communication antenna site and temporary storage there prior to each satellite pass;
2. assembly of the data from storage and synchronization to real time;
3. error checking and rejection of erroneous quantities;
4. conversion of the digital orders into analog command signals to control the antenna drive mechanisms.

The most important factor affecting the transmission facility, storage medium, and data reconstruction equipment is the sampling interval of the discrete pointing information delivered by the computer.

We will use the term *data point* to denote one sample of this information, and the term *data-point interval* to denote the interval between successive points. A wide range of intervals is possible, and interesting trade-offs can be made between data transmission rate, storage requirements, complexity of the conversion equipment, and reliability of performance.

There is, at one extreme, the possibility of transmitting large numbers of data points with short data-point intervals. Advantages of this approach come from two considerations. First, the digital-to-analog conversion process involves straightforward conversion of each point into an equivalent analog command. This simplifies the conversion equipment and offers advantages in reliability. Second, the data interval is short; therefore errors that occur in transmission, storage, or assembly from storage cause only momentary effects. Disadvantages result from the large quantity of data required to describe each satellite pass. This places an excessive load on the computer, the transmission, and the storage facilities.

At the other end lies the possibility of transmitting fewer sets of pointing angles with their derivatives at data-point intervals of many seconds. Interpolation between data points using these derivatives provides reconstruction of continuous pointing information. Reduction of data for

* Although this equipment was designed by the Bell System as part of its research and development program, it was operated in connection with Project Echo under Contract NASW-110 for the National Aeronautics and Space Administration.

each pass is obtained at the expense of more extensive calculations by the computer and more complex conversion equipment at the antennas. There is a trade between the data rate of the transmission and capacity of terminal storage facilities on one hand, and the complexity of the data-conversion equipment at the antenna on the other.

When long data intervals are used, reliability considerations become more complicated. Discrete samples of position and higher derivatives become initial conditions in an integration process which extends over each data interval. Errors in transmitted data which are not detected and removed affect the system for the duration of the data interval. However, in this case redundancy for automatic error checking can be applied to the encoded quantities without requiring prohibitively large amounts of data.

To summarize, the optimum data interval is a function of several factors. These include the load imposed on the Goddard computer in the generation of error-correcting codes and higher-order derivatives, the cost and availability of transmission links, and the complexity of the data conversion equipment needed at each antenna.

Other design considerations include the method used for conversion of the transmitted digital data into antenna steering commands. There are two methods. The first employs electronic decoding of digital pointing commands to equivalent analog signals. These may then be used to direct a number of antennas at one site. A second method involves encoding of the antenna shaft positions in digital form and a subtraction between the encoded positions and the digital command signals. Here digital error signals are derived, which are more easily converted to analog signals to actuate the antenna servos. The latter method, preferred for precise antenna control, requires separate encoding mechanisms and digital subtractors with each antenna mount.

II. ANTENNA STEERING FOR ECHO I

This section describes the system which was designed to transmit pointing instructions from the Goddard computer to Holmdel and there convert them into antenna steering orders.

2.1 *System Philosophy*

In the design, many of the factors discussed in Section I were considered. Uncertainties regarding expected orbital perturbations of the balloon satellite placed emphasis on an approach that would provide updated pointing instructions after each satellite pass. The experimental

nature of the project dictated the use of inexpensive transmission and storage media, and a reasonably simple digital-to-analog converter.

Of primary importance are the dynamic range of the steering signals, the conversion precision needed, and the form of analog signals required by the antenna control systems.

The Echo satellites were to be placed in near-circular orbits at altitudes of 800 to 1000 miles. Maximum angular tracking velocities would be under 1.5° per second, and average velocities would be much lower than this.

To insure that data conversion errors would not affect radio transmission characteristics, design error tolerances were set at $\pm 0.05^\circ$.

Continuous three-wire ac synchro voltages were required as outputs of the converter, to command each antenna and optical mount control system. While direct conversion from digital form to ac signals is possible, an approach using small intermediate servos to position synchro transmitter units was more attractive.

Pulse-time-modulation techniques were used to position these servos. Digital input commands were converted into pulse-position-modulated (PPM) signals. At the same time, the servo output shaft positions were monitored by precision resolver angle transducers. Resolver outputs produce PPM signals of the same form. The two PPM signals were compared on a time basis to create error signals that position the servo units.

2.2 *Input Data Transmission*

A four-second data-point interval was chosen. This allows the description of a single satellite pass to be transmitted over a 60-word-per-minute teletypewriter channel in approximately the same amount of time taken by the pass. The choice of standard-speed teletypewriter was influenced by two factors. Conversion equipment was available at the Goddard computer center to produce punched-paper teletypewriter tape from the computer output. This tape could be transmitted and reproduced at the antenna site to provide economical data storage.

The pointing data furnished are the azimuth and elevation antenna angles computed for the geographic location at Holmdel. These are supplemented by the average rates of azimuth and elevation over the succeeding data interval to permit a linear interpolation between data points.

2.3 *Digital-to-Analog Converter Organization*

The data format, scale factors, and coding were chosen to minimize the digital-to-analog converter equipment. Teletypewriter code combina-

tions were used to denote decimal data in an 8-4-2-1 binary code, with the fifth level of the tape being used as a single redundant parity-check bit. This was possible because a total of only 14 characters was needed. Sequences of tape characters called *words* represent the data-point time, azimuth angle, elevation angle, azimuth rate, and elevation rate. Each word is identified on the tape with an identifying "tag" code which follows the word. In addition to identifying the words, these tags control the switching of the words to the proper destination within the conversion unit. The use of tags makes the operation less dependent on the sequence of words and makes the system more tolerant of errors introduced by transmission links.

The conversion unit assembles the data from tape, synchronizes it with real time, and switches it to counting decoders, which produce pulse-position-modulated signals proportional to the digital data. The following paragraphs describe logical features of the conversion unit. The operation of the counting decoders and conversion of the PPM signals to analog commands are described in later sections.

A block diagram of the digital-to-analog conversion unit is shown in Fig. 1. A photoelectric tape reader reads the tape characters in sequence

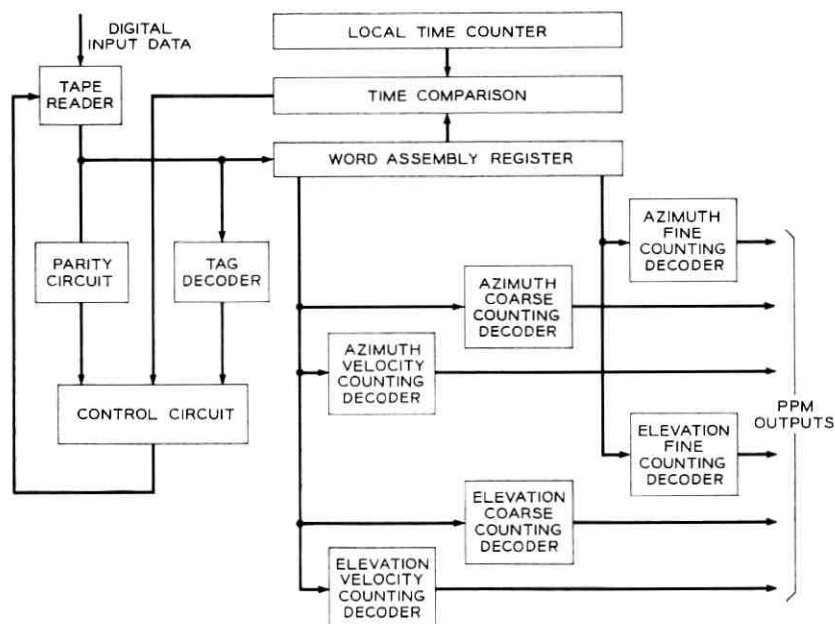


Fig. 1 — Block diagram of data conversion unit for Crawford Hill.

and converts the information to electrical signals. These are introduced to a shift register used to assemble the serial information from the tape into parallel words. The word-assembly register output feeds the counting decoders and the time-comparison circuit. The other input to the time-comparison circuit is the output of a local time counter. This circuit provides the conversion unit with real-time synchronization. Reader outputs are also applied to the tag decoder and the parity-check circuit. These actuate the control unit and determine the action taken by the conversion unit.

Consideration of events that occur while a block of information is read from the tape illustrates the operation of the conversion unit. Assume that the tape is stopped after the reader has read a time tag. This tag identifies the word in position in the word-assembly register as the time word corresponding to the time for the next data point. This time word is compared in the time-comparison circuit with the contents of the local-time counter. An affirmative indication from the time-comparison circuit causes a clock pulse to indicate that the next data point should be decoded. Tape reader action is initiated. As the tape moves, each character is examined by the tag decoder. If the tape character being read is not a tag, the contents of the word-assembly register are shifted one digit to the right and the new character is entered on the left.

This process continues until a tag is encountered — in this instance, the azimuth quantity. Detection of the azimuth tag indicates that the azimuth angle is in position in the word-assembly register and is ready for transmission to the azimuth-counting decoders. When a signal from the azimuth decoder indicates that it is ready to receive new data, it is cleared and the new azimuth word is gated from the word-assembly register. Reading of the tape continues, with examination of each character being introduced to the word-assembly register until the elevation tag is encountered. This causes the elevation word to be placed in the elevation decoder. The rate information is handled similarly. After the rate information has been transferred to the rate registers, reading of the tape continues until the next time tag is detected. This indicates that the time word for the next block of information is in the word-assembly register and is being compared with local time, to complete the cycle.

The logic of the time-comparison circuit is designed so that, for data blocks in the proper sequence, the comparison circuit will indicate comparison as soon as a time tag is detected in the reader. This comparison holds for the four-second interval. If, when a time tag is read, the contents of the word-assembly register and the local-time counter do not compare, the control circuit causes the tape to advance to the next time

tag and make another comparison. If these times compare, it then proceeds as normal; if not, it stops and gives an alarm. If the comparison should become good, it turns off the alarm and proceeds as usual. Thus, in the event of a time-comparison failure, the system makes a quick check to see that it has not somehow got behind, as may happen if an error makes a data character look like a time tag. If the comparison check still fails, the alarm alerts operating personnel. However, if, because of transmission drop-outs or errors, the system has got a few seconds ahead, it will automatically correct itself, probably before any manual maintenance routines can be initiated.

The redundant check bit with each character is checked as the character is read. If a parity error is detected, the control circuit causes the tape to advance to the next time tag. Thus, when an error is detected, the data block is discarded. As described in a later section, the counting decoders continuously decode azimuth and elevation angles, which are up-dated with the last-received rate information. This gives the system a coasting feature, so that erroneous blocks of information may be discarded without seriously affecting the system accuracy.

2.4 Counter Decoding

The conversion of digital pointing commands involves an intermediate conversion to PPM signals. This is performed in high-speed sequential counting circuits. The concept is very simple: the number to be converted is placed in a counter which is designed to count toward zero. At the occurrence of a start pulse, this number is reduced by one unit for each elapsed cycle of a stabilized clock pulse source. Zero-detection circuitry arranged on the counter output produces an output pulse when the counter reaches zero. The time interval t_{1d} between the start pulse and the output is related to the clock frequency f_c and the number being decoded θ , by

$$t_{1d} = \frac{\theta}{f_c}. \quad (1)$$

This time interval is clearly proportional to θ . Essential portions of the logical connections for a single counting decoder are seen in Fig. 2.

By arranging the counter to recycle after it reaches its zero content, successive zero-crossing output pulses are produced at time intervals equal to the product of the clock frequency and the total number of states in the counting sequence. Moreover, by arranging the repetition times of the start pulses t_s at

$$t_{ks} = \frac{kC}{f_c} \quad k = 0, 1, 2, \dots, \quad (2)$$

where C = total number of states in the counter, successive zero crossings times t_{kd} are always delayed from the start pulses by the same amount. That is,

$$t_{kd} = \frac{1}{f_c} (\theta + kC). \quad (3)$$

By subtracting (2) from (3), a repeated measure of θ is generated as

$$t_{kd} - t_{ks} = \frac{\theta}{f_c}. \quad (4)$$

Each pulse position is modulated by the digital quantity placed in the counter. The relationships between counter contents, start pulses, and outputs are usually shown as in Fig. 3.

Although a number placed in the counter is regularly being counted around, storage of that number is provided within the counter as the conversion process proceeds. This is a result of the unique relationship between counter contents and time that exists for each input.

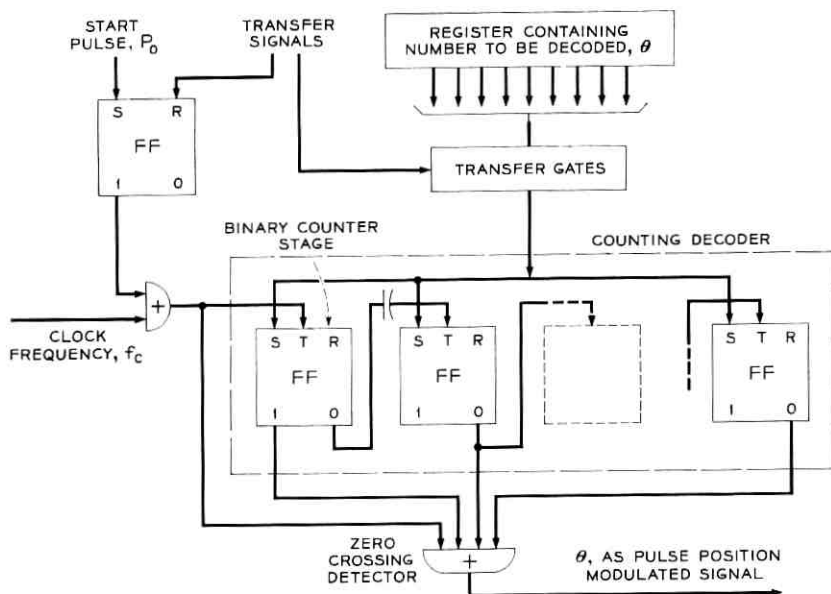


Fig. 2 — Counting decoder logic.

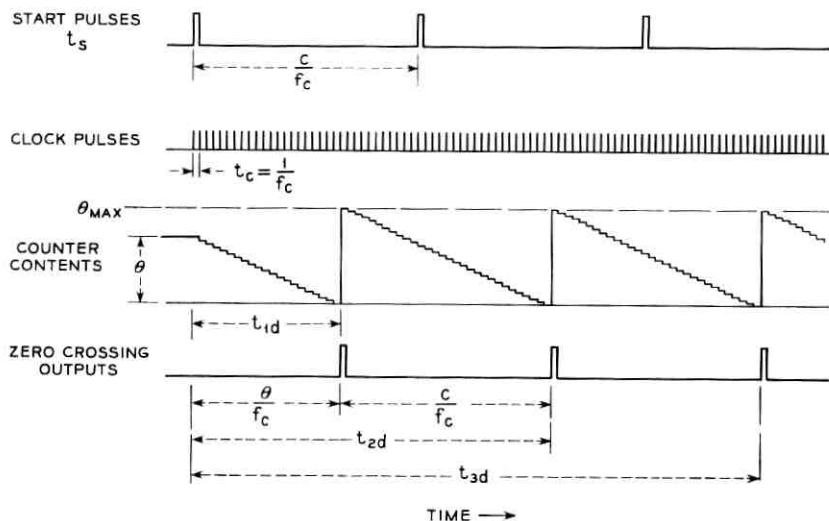


Fig. 3 — Counting decoder contents and waveforms.

In real-time control system applications, the repetition rate of the decoding process is important. This rate determines the bandwidth of signals that can be decoded. The decoding resolution is, of course, determined by the number of states in the counter. Counter stages operating at 5 mc allow sufficient range in resolution and repetition rate.

2.5 Interpolation

So far, counter decoding processes have been considered in which the counting rate remains constant and uninterrupted. The generated time interval is unchanged. However, by momentarily altering the counting rate, the arithmetic operations of addition and subtraction can be performed on the contents of the counter while the decoding process continues. For example, consider a down-counting sequential counter in which a number of clock input pulses are inhibited. The usual counting process is momentarily halted. The zero crossing occurs later than it ordinarily would have and a quantity equal to the number of inhibited clock pulses is effectively added to the counter. Similarly, if the clock input is shifted to the next most significant counting stage, the counting sequence is accelerated to twice its usual rate. A quantity equal to the number of shifted pulses is effectively subtracted from the counter contents.

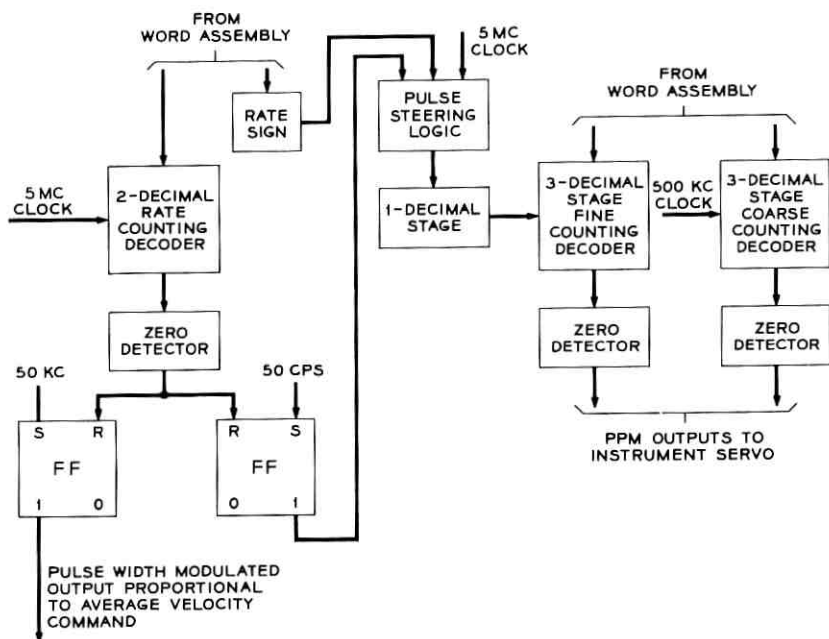


Fig. 4 — Interpolation logic.

The ability to modify the contents of the counter is used for interpolation of input data over each data interval. Angular position commands are placed in the counters at the beginning of each data-point interval. At the same time, angular velocity commands are placed in similar counters. Time intervals determined by the velocity counter decoders are extracted and used as gating signals to alter the number of clock pulses fed to the position counter decoders. Depending on the polarity of the velocity information, the inputs to the position counters are either inhibited or shifted one stage for the duration of this interval. In this manner increments of position proportional to average velocity are added to the position command several times over the data interval.

In the digital-to-analog converter, angle position commands are decoded to PPM signals to provide a modulo 360-degree, or coarse, command and a modulo 3.6-degree, or fine, command. Decoding is performed in a three-stage decimal counter, giving a decoding resolution of 0.0036° . A counter clock frequency of 500 kc provides outputs at a 500-cps rate.

Rate information is decoded with a clock frequency of 5 mc to PPM signals having a 50-kc repetition rate. One of these outputs is extracted 50 times per second, and controls the counting of a decimal pre-

ceding the fine position decoder. The logical connections for this control are shown in Fig. 4. This yields a quasi-linear interpolation in steps of $\frac{1}{50}$ -second duration, as shown in Fig. 5. The maximum deviation of this output from true linear interpolation is a sawtooth function with a 50-cps repetition rate and a maximum amplitude of 0.036° .

III. THE INSTRUMENT SERVO SYSTEM

The instrument servos convert the PPM signals produced by the counting decoders into analog command signals for the communications antennas. The control systems of these antennas use two-speed synchro control transformers as error detectors. The instrument servos position the two-speed synchro transmitters, which in turn command the antennas. Two instrument servos are required, one to command the azimuth and the other the elevation axes of the antennas. The two units are identical in design and construction and, in the following θ represents either the azimuth or elevation angle.

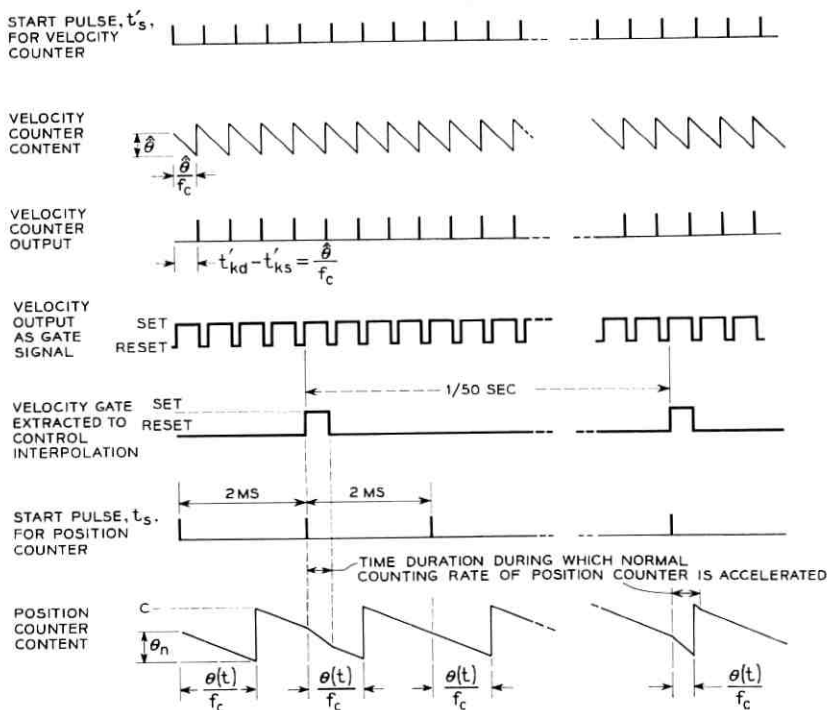


Fig. 5 — Quasi-linear interpolation.

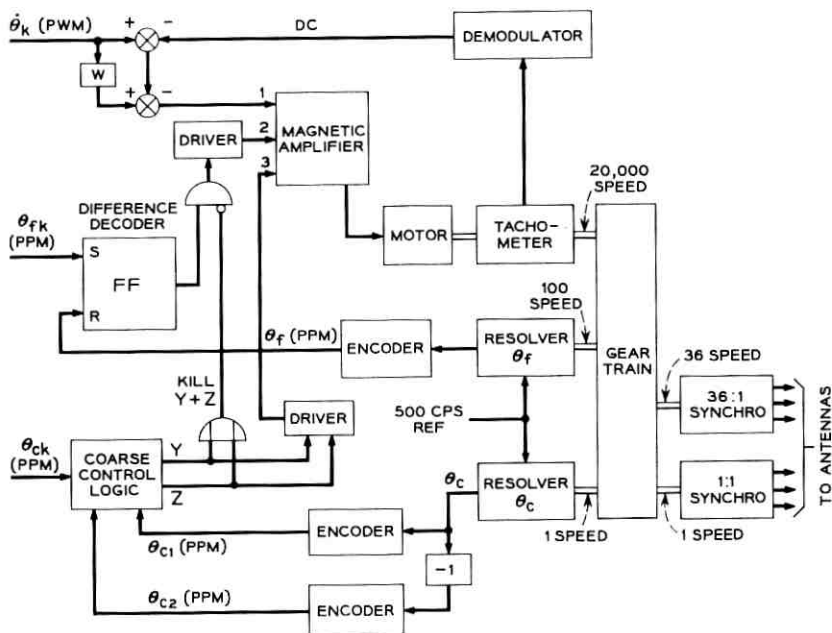


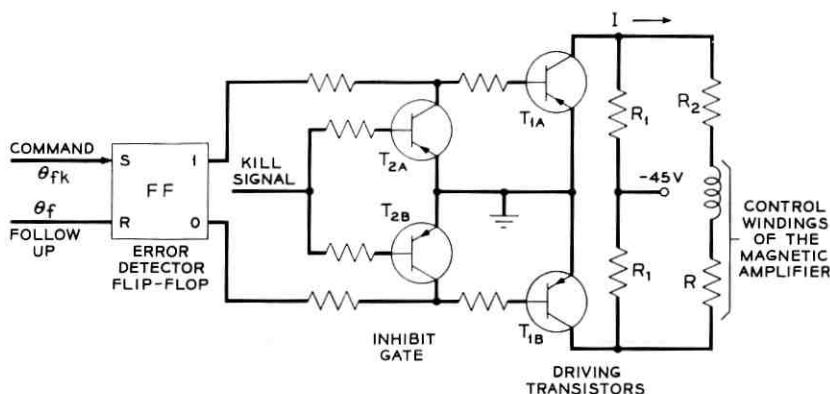
Fig. 6 — Block diagram of instrument servo.

3.1 System Mechanization

Inputs to the instrument servos are the PPM pulse trains derived from the counting decoders. Corresponding PPM follow-up signals are obtained from two angle-encoding resolvers connected to the 1:1 and 100:1 speed shaft on the servo gear trains. A description of the method of encoding shaft positions with these resolvers is given in Section 3.4. A block diagram of the instrument servo system, shown in Fig. 6, shows the derivation of the position and velocity follow-up signals, as well as the two-speed synchro transmitters which command the antenna control system. A high-speed two-phase servo motor is used to position the instrument servos. A magnetic amplifier provides the power for the controlled phase of the motor.

3.2 Tracking Control System

If the error between the angle θ called for by the counting decoders and the angle encoded from the resolvers is less than 1.8° , a system using θ_{fk} as a command and θ_f as a follow-up signal controls the servo. For errors larger than 1.8° a slewing mode of operation is employed, which is

Fig. 7 — Simplified θ_f circuit.

described in Section 3.3. The circuitry used in the tracking mode consists of the position feedback loop controlled by the fine position command θ_{fk} , the velocity loop controlled by the velocity command $\dot{\theta}_k$, and the feed-forward compensation represented by the block w in Fig. 6.

3.2.1 The Fine Position Loop

In this loop the follow-up pulse train θ_f is phased with respect to the decoded command pulse train θ_{fk} so that for zero error the pulses of one train occur half-way between the pulses of the other. The difference decoder is a flip-flop, with the θ_{fk} pulse train applied to the "set" input and θ_f to the "reset" input. For zero error the flip-flop spends equal time in the two states. For a nonzero error the duration of one of the states exceeds the other by an increment linearly proportional to the error. A current proportional to the difference of the dwell times of the two states is used to drive one of the control windings of the magnetic amplifier, which in turn controls the motor. Fig. 7 shows the simplified circuit between the output of the difference decoder and the magnetic amplifier. In absence of a "kill" signal, that is, with transistors T_{2A} and T_{2B} non-conducting, the flip-flop drives the magnetic amplifier through alternate switching of transistors T_{1A} and T_{1B} . The gain of this loop is set by the voltage applied to R_1 and R_2 and the resistance R of the control winding circuit. In order to provide the required tracking accuracy, the gain is adjusted so that an error of 0.01° gives ample drive to overcome sticking friction of the motor and gear train.

Due to the high gain of this loop it is necessary to disable it when the error is greater than 1.8° to prevent it from interfering with the slewing

mode of operation. The "kill" signal actuates the inhibiting gate composed of T_{2A} and T_{2B} , which disables the fine position loop. The generation of the "kill" signal is indicated in Fig. 6 and is described in Section 3.3.

3.2.2 The Velocity Loop

The velocity feedback loop is necessary to stabilize the system and improve its dynamic response. To prevent tachometric feedback from causing tracking errors proportional to motor velocity, a signal proportional to the difference between the actual and commanded motor speeds is used to drive the magnetic amplifier. The command signal is obtained from the rate-counting decoder. It is a pulse-width-modulated signal whose average value is proportional to $\dot{\theta}_k$. The follow-up consists of an ac tachometer followed by a demodulator producing a dc voltage proportional to motor speed.

3.2.3 The Feed-Forward Compensator

Ideally the feed-forward compensator (w) should provide a signal which is equal to that required by the motor to follow the commanded input. Tracking a satellite requires operation of the servo at almost constant speeds over periods of time which are long with respect to the characteristic time constants of the servo. Hence the feed-forward path provides the magnetic amplifier with a signal necessary to obtain the commanded velocity under steady-state operation. Since the relationship between the steady-state motor speed and the magnetic amplifier control winding current is almost linear over the range of speeds used in tracking, the required block w of Fig. 6 is a fixed attenuator. This is mechanized by increasing the voltage gain of the $\dot{\theta}_k$ decoder in the velocity loop, and therefore no additional circuitry is needed.

The instrument servo-tracking control system provides a static accuracy of $\pm 0.01^\circ$ and maximum errors in the tracking mode of $\pm 0.025^\circ$.

3.3 Slewing Control System

If the magnitude of the position error is greater than 1.8° the θ_f loop cannot bring the error to zero. This is because the θ_f loop operates on the error modulo 3.6° . If the position error, ϵ_s , as determined by the comparison of θ_{ek} and θ_c , exceeds an angle of δ degrees (where $\delta \leq 1.8^\circ$) the fine loop is disabled by the "kill" signal. A saturation torque is commanded

to decrease the error to a value less than δ degrees in minimum time. The actuating signal produced by the slewing control system assumes one of three values: zero, clockwise saturation torque, and counter-clockwise saturation torque. Fig. 8 illustrates the slewing strategy. The follow-up pulse trains θ_{c1} and θ_{c2} (see below) shown in Fig. 6 are used to obtain gate signals corresponding to the regions *A*, *B*, *C*, and *D* of Fig. 8. Since *A*, *B*, *C*, and *D* form a mutually exclusive complete set of time intervals over the $\frac{1}{\pi\dot{\theta}}$ -second command repetition time, the command pulse θ_{ck} will then occur during one of these gate pulses and determine the error region. Let the commands of the clockwise and counter-clockwise torque be represented by binary functions *Y* and *Z* respectively; for example, the counter-clockwise torque is commanded if and only if $Y = 1$.

From Fig. 8,

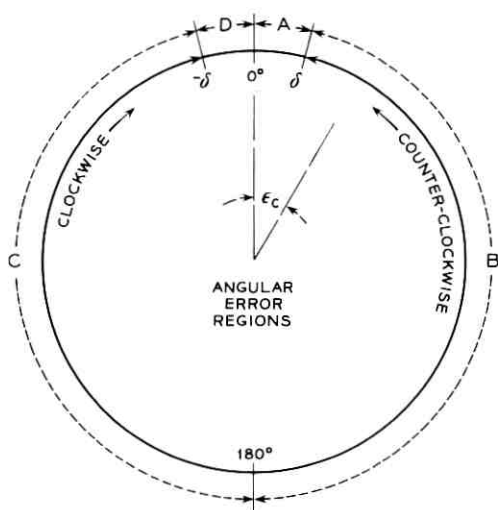
$$\text{counter-clockwise: } Y = \theta_{ck} \otimes B,$$

$$\text{clockwise: } Z = \theta_{ck} \otimes C,$$

$$\text{also the "kill" signal: } K = Y \oplus Z,$$

where \oplus = logical OR, \otimes = logical AND.

The timing pulses for the generation of the gate signals are obtained from θ_{c1} and θ_{c2} . The phase of the follow-up pulse train θ_{c1} is adjusted so that for zero error it coincides with θ_{ck} , the course command pulse train.



SLEWING CONTROL LOGIC

ERROR REGION	TORQUE COMMAND
A OR D	NONE
B	COUNTER-CLOCKWISE
C	CLOCKWISE

$$\epsilon_c = \theta_{ck} - \theta_{c1}$$

Fig. 8 — Slewing strategy in θ_c control logic.

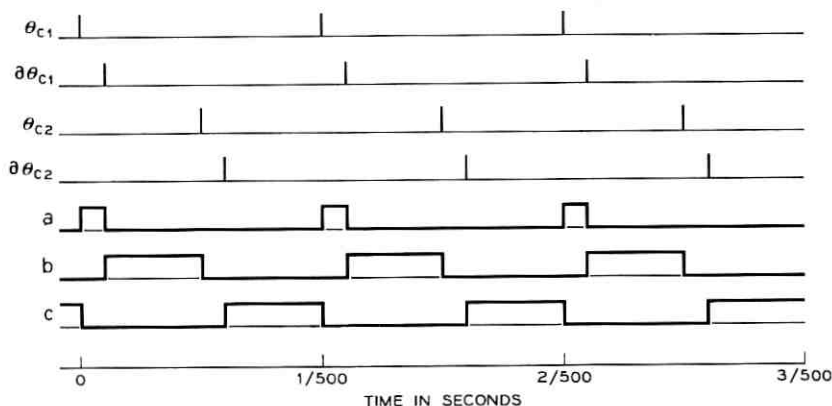


Fig. 9 — Generation of gates a , b , and c in θ_c control logic.

The θ_{c2} follow-up signal is 180 electrical degrees behind θ_{c2} . Circuits providing a time delay corresponding to δ degrees are used in the generation of the gate signals. Fig. 9 shows the generation of the gates a , b and c by a set of flip-flops operated by the follow-up signals. By comparing Fig. 8 and Fig. 9 it is evident that:

$$a = A = \partial D,$$

$$b = B,$$

$$c = \partial C,$$

where ∂ is a delay operator of δ degrees.

The determination of the error regions is done 500 times per second. Flip-flops Y and Z are set by the detection of error region B and C respectively; both are reset by the detection of region A or D . The required output to drive the motor is obtained from one of the two flip-flops. Therefore:

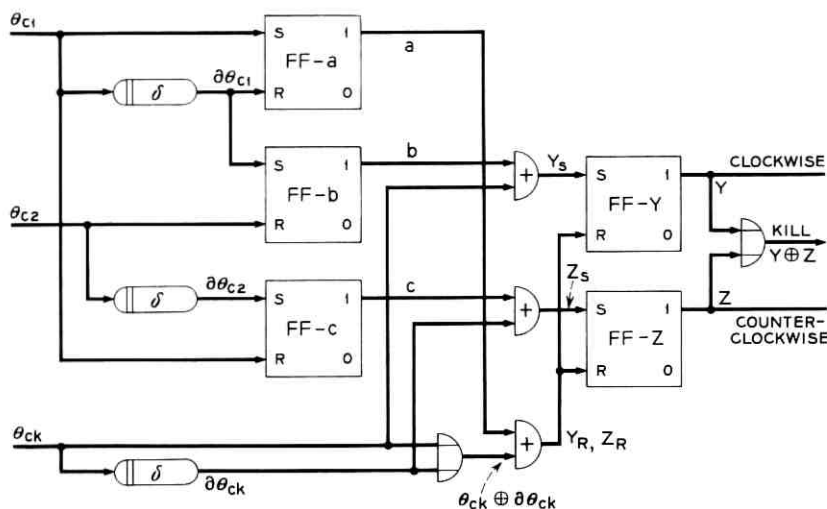
$$Y_s = \theta_{ck} \otimes B = \theta_{ck} \otimes b,$$

$$Z_s = \theta_{ck} \otimes C = \partial\theta_{ck} \otimes \partial C = \partial\theta_{ck} \otimes c,$$

$$\begin{aligned} Y_r = Z_r &= (\theta_{ck} \otimes A) \oplus (\theta_{ck} \otimes D) = (\theta_{ck} \otimes A) \oplus (\partial\theta_{ck} \otimes \partial D) \\ &= (\theta_{ck} \otimes a) \oplus (\partial\theta_{ck} \otimes a) = (\theta_{ck} \oplus \partial\theta_{ck}) \otimes a, \end{aligned}$$

$$K = Y \oplus Z,$$

where Y_s and Y_r are the set and reset inputs to the Y flip-flop respectively. Similarly for the Z flip-flop. A circuit diagram for the above logic is shown in Fig. 10.

Fig. 10 — Circuit diagram for θ_e control logic.

The signals Y and Z are applied to a pair of transistors driving the magnetic amplifier control winding No. 3 as shown in Fig. 11.

3.4 Resolver Encoding

Shaft positions of the instrument servos are encoded to PPM signals using resolver encoding techniques. Two precision resolvers are used with each instrument servo. The first of these rotates 1:1 with the servo output and gives a modulo 360-degree indication of the shaft angle. The second rotates 100:1 with respect to the output, to give the modulo 3.6-degree indication of the shaft angle. These ratios were chosen to match the coarse and fine outputs of the decimal counting decoders.

The method used to convert these resolver outputs to PPM signals

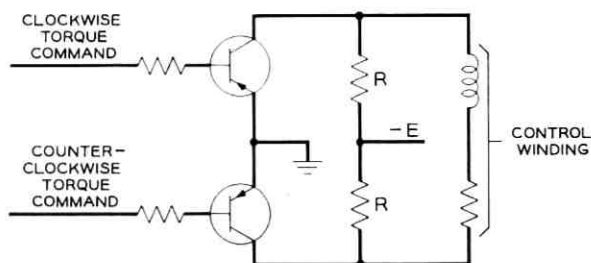


Fig. 11 — Coarse control circuit.

has been described in an earlier paper,¹ but will be reviewed here for completeness. Electrically, each resolver is a mechanically variable transformer with couplings between primary and secondary windings that are functions of the rotor angle θ_R . When excited by the ac signal

$$E_{in} = E_{max} \sin \omega t,$$

output voltages are the input voltage modulated by the sine and cosine of the rotor shaft angle θ_R . The resolver outputs are combined in phase-shifting networks which advance the phase of the sine voltage by $\pi/2$ degrees and add it to the cosine voltage. Thus a phase-modulated signal results according to:

$$E_{max} \sin \left(\omega t + \frac{\pi}{2} \right) \sin \theta_R + E_{max} \sin \omega t \cos \theta_R = E_m \sin (\omega t + \theta_R).$$

The positive-going zero crossing of this signal is the desired PPM signal representing the shaft position. Since the excitation voltage is 500 cps, a 0.18° movement in the output of the instrument servo causes a change of 1 microsecond in the PPM output of the coarse encoder. Similarly, a movement of 0.0018° causes a 1 microsecond change in the PPM output of the fine encoder.

Resolver excitation is derived from the digital-to-analog converter central timing by filtering and amplification of a 500-cps square wave. A zero-crossing detector, similar to the one used for encoding the phase-shifted resolver output, is connected to the resolver excitation. This output is the start pulse and is so phase-locked to the resolver excitation. It is used in the digital portion of the conversion equipment to time the start of the counter decoder sequence.

IV. SUMMARY

The above is a description of a new type of special purpose data converter for the direction of narrow beam communication antennas from predicted information. It is capable of converting digital input data into real-time analog voltage commands with a dynamic accuracy $\pm 0.05^\circ$, which is sufficiently accurate for the present antennas. It employs a moderate quantity of input data, and a reasonably simple digital-to-analog converter.

The single-parity-bit error detection provides moderate resistance to transmission errors. During the Echo I experiments the number of errors in transmissions from Goddard Space Flight Center were logged for 30 passes. Out of a total of 250 errors, the single-parity detection was effective in rejecting over 90 per cent of the erroneous data. During these

periods the coasting features designed into the converter provided adequate antenna commands.

The use of instrument servos as an intermediate step in the conversion process provides convenient generation of two-speed voltages for commanding more than one antenna or optical mount simultaneously. Separate synchro units can be placed on the gear trains for each antenna, and each synchro can be excited by the particular frequency required by that mount. Furthermore, choice of the ratios in the gear train provides outputs in the "two-speed" combination required by each mount.

The use of counter decoders is quite attractive. They provide the storage necessary to give continuous outputs to command the servos. Data interpolation makes possible an input data interval sufficiently long so that ordinary teletypewriter transmission can be used. The interpolation method outlined here makes additional use of the counter decoders, without the need for a conventional arithmetic unit. The interconnections between counters needed to perform interpolation require simple control logic. Since the decoders and many of the low-speed operations in the converter operate synchronously, the additional pulse rates needed for interpolation are already available from the timing section.

The resolver encoding technique converts instrument servo shaft positions into pulse-position-modulated signals of the same general form as the counter output. These signals are easily combined to form error signals to control the servos. In the same manner that gear ratios can be chosen to provide outputs at a desired "two-speed" ratio, the gearing between resolver encoders can be chosen to yield PPM signals in any desired speed ratio. This allows freedom of the number base in which the decoding process is performed.

V. ACKNOWLEDGMENTS

Of the many people who contributed to this system, we are particularly indebted to J. C. Lozier for the system concept employed, and to the efforts of F. C. Young and W. J. Spiegel for the electrical and mechanical design and fabrication of the instrument servos.

REFERENCE

1. Kronacher, G., Design, Performance, and Application of the Vernier Resolver, *B.S.T.J.*, **35**, 1957, p. 1487.

PROJECT ECHO

Boresight Cameras

By K. L. WARTHMAN

(Manuscript received April 7, 1961)

Motion picture cameras equipped with telephoto lenses were installed on the Project Echo transmitting and receiving antennas located at Holmdel, New Jersey. When the Echo satellite was visible, a camera obtained a photographic record of the pointing accuracy of the antenna. These data were then used to correlate variations of signal strength with deviations in antenna pointing angle.

I. INTRODUCTION

The conventional method of evaluating the tracking performance of radar antennas has been to provide a camera-lens system mounted on the antenna structure to provide an optical line-of-sight parallel to the radar beam. This permits the recording on motion picture film of the radar pointing error, whenever the object being tracked is capable of being photographed. Camera instrumentation of this type was provided for both Holmdel antennas, the 60-foot paraboloid transmitter and the 20-foot horn receiver.*

II. PHOTOGRAPHIC CONSIDERATIONS

The brightness of the Echo satellite was expected to be greater than that of a first-magnitude star. Experience in astronomical photography indicated that first-magnitude stars could be recorded on Tri-X negative film (Eastman Kodak No. 7233) with an exposure of $\frac{1}{30}$ second and a lens aperture of f3.5. Accordingly, it was decided to use a camera speed of four frames per second. This frame rate provides an exposure time of $\frac{1}{8}$ second and at the same time affords 16 minutes of continuous camera

* Although this equipment was designed by the Bell System as part of its research and development program, it was operated in connection with Project Echo under Contract NASW-110 for the National Aeronautics and Space Administration.

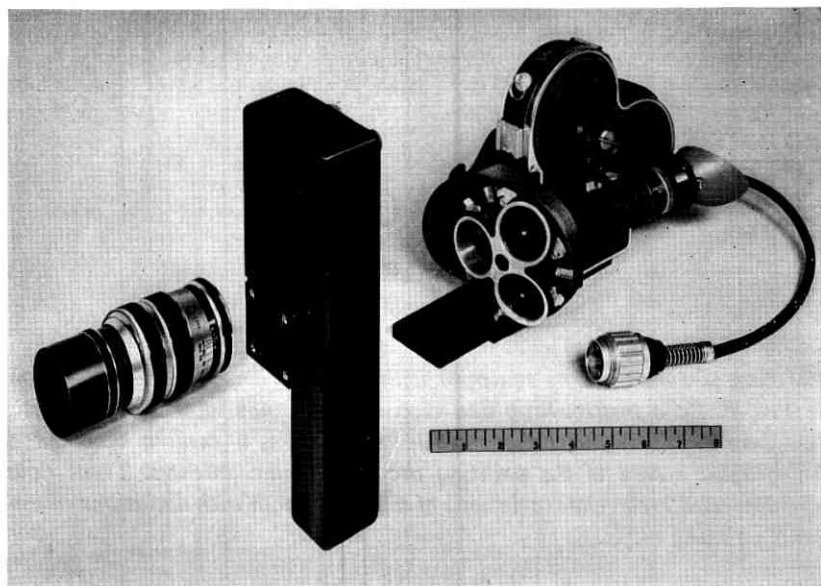


Fig. 1 — Tracking camera.

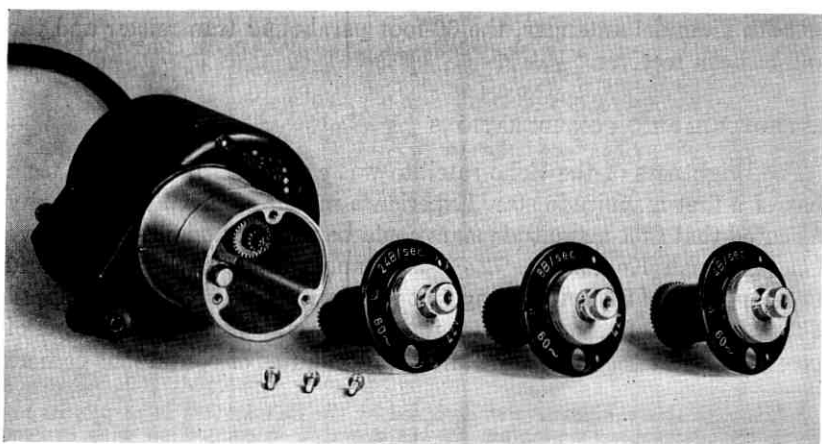


Fig. 2 — Synchronous motor with gear reductions for 24, 8, 4 frames per second.

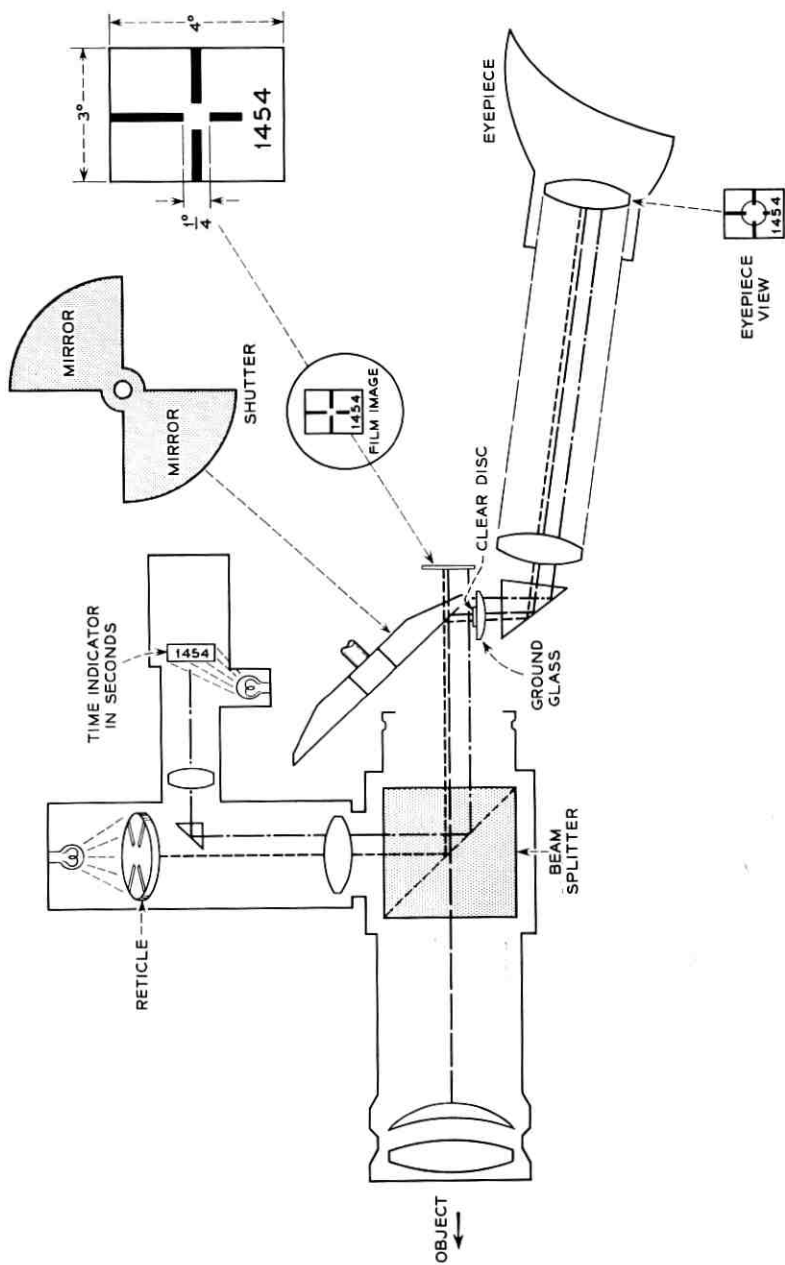


Fig. 3 — Optical schematic.

operation with the 100-foot film capacity of the camera. The 16-mm film was considered adequate for the photographic detail required and was selected in preference to 35-mm film in order to minimize film costs, processing charges, storage space, and equipment investment.

III. CAMERA

The Arriflex 16-mm camera (see Fig. 1) was selected for Project Echo because the feature of through-the-lens viewing was desired for alignment of the optical system with the transmitting and receiving antennas. Also, this camera could have been equipped with a 400-foot magazine if a faster frame rate or longer tracking time had been desired. A 24-frame-per-second synchronous motor was ordered with special gear reductions that could be easily interchanged to provide four or eight frames per second (see Fig. 2).

IV. LENS

The desired field of view of 3 degrees was obtained by using a 150-mm, f3.5 Kilfitt lens. This field of view was large enough to keep the satellite



Fig. 4 — Camera mounted on horn receiver.

image within the film frame during early tests when some tracking difficulties could be expected. The 150-mm lens gave enough magnification to permit reducing the data to the desired accuracy. The camera system was designed so that a 300-mm lens could be used without modification if desired in later tests.

V. RETICLE AND TIMING MARKS

A projected reticle was imaged on the film by using a beam splitter. The optical schematic is shown in Fig. 3. The time in seconds was recorded on the film by using a conventional telephone message register as a stepping counter. The reticle and message register were also visible through the eyepiece for optical alignment and time correlation. The necessary optics to project these images on the film were assembled in a housing which replaced the standard lens-to-camera adaptor.



Fig. 5 — Camera mounted on paraboloid transmitter.

VI. CAMERA MOUNTING

The cameras were mounted on the vertical center-line and just beyond the lower edge of the antenna apertures (Figs. 4 and 5). This location placed the cameras about 8 feet above ground level when the antennas were pointed at the horizon so that they could be loaded and checked for alignment from a small platform. A special dovetailed mount was pro-

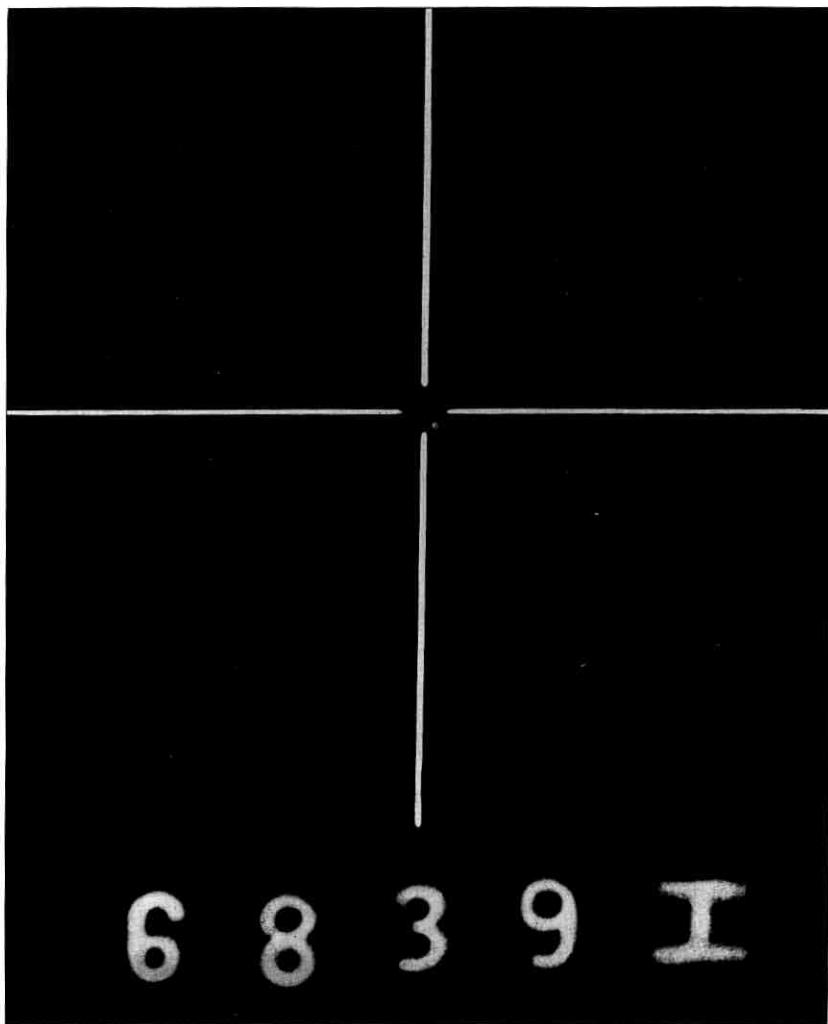


Fig. 6 — Typical single 16-mm frame (pass 70, August 18, 1960).

vided for the cameras to permit removal and replacement without disturbing the alignment. The base of this special mount was equipped with adjustments for alignment in elevation and azimuth. A weatherproof cover with a front opening was provided in the event that inclement weather was experienced during operation.

VII. POWER SUPPLY AND CAMERA CONTROL

Special 42-volt power supplies were used to operate the synchronous camera drive motors. These power supplies were mounted on the antennas adjacent to the cameras. The cameras could be operated at the antennas to facilitate loading of film and alignment, or could be operated remotely from the main control console.

VIII. RESULTS

The enlarged view of a single 16-mm frame of pass 70 shows the Echo satellite in the reticle opening (Fig. 6). The reticle opening is 0.15 degree, which is slightly less than the original design of $\frac{1}{4}$ degree. The letter H at the end of the message register number indicates that the film came from the camera mounted on the horn antenna. From August 12, 1960, to March 15, 1961, 6900 feet of film were exposed during 39 Echo satellite passes.

Contributors to This Issue

ROBERT H. BRANDT, Stevens Institute of Technology; Bell Telephone Laboratories, 1944—. His work in the radio research group has been concerned with components for microwave radio relay systems, antenna impedance measurements, multiplexing system for light route microwave relay, phase correction and pulse timing circuits and the Project Echo satellite communication experiments.

ARTHUR B. CRAWFORD, B.S. in E.E., 1928, Ohio State University; Bell Telephone Laboratories, 1928—. He has specialized in radio research, including work with measuring techniques, propagation, and antenna studies in the ultra-short wave and microwave areas. He designed the horn-reflector antenna used in the Project Echo satellite communication experiments. Fellow I.R.E.; member Eta Kappa Nu, Pi Mu Epsilon, Sigma Xi, Tau Beta Pi.

ROBERT W. DE GRASSE, B.S., 1951, California Institute of Technology; M.S., 1954, and Ph.D., 1958, Stanford University; Bell Telephone Laboratories, 1957-60; Microwave Electronics Corp., 1960—. Mr. DeGrasse's work at Bell Laboratories was in research and development of solid state masers. He took part in the development of the ruby maser used in the Bell Laboratories receiving system for the Project Echo satellite communication experiments. Member I.R.E., Sigma Xi.

OWEN E. DE LANGE, B.S., 1930, University of Utah; M.A., 1937, Columbia University; Bell Telephone Laboratories, 1930—. He has specialized in radio research, including development of high-frequency transmitters and receivers, and frequency modulation research. During World War II he was engaged in radar development, and later he worked on broadband and pulse systems. He was in charge of the design and construction of the radar used in tracking the artificial satellite in the Project Echo satellite communication experiments. Member I.R.E.

JOHN A. GITHENS, B.S.E.E., 1951, Drexel Institute of Technology; Bell Telephone Laboratories, 1951—. He has been engaged primarily in computer research, especially applied to military systems. This has included design of solid state circuits, computer systems and logical

design. He took part in the design and development of the Tradic and Leprechaun computers, early transistorized computers. He supervised work on the logical design of the data conversion unit used in the Project Echo satellite communication experiments. Member I.R.E., Eta Kappa Nu, Phi Kappa Phi, Tau Beta Pi.

D. C. HOGG, B.Sc., 1949, University of Western Ontario; M.Sc., 1950, and Ph.D. 1953, McGill University; Bell Telephone Laboratories, 1953—. His work has included studies of artificial dielectrics for microwaves, diffraction of microwaves, and over-the-horizon and millimeter wave propagation. He was concerned with evaluation of sky noise and analysis of performance characteristics of microwave antennas most recently. Senior member I.R.E.; member Commission 2, U.R.S.I.; Sigma Xi.

LOYD E. HUNT, A.B., 1927, Reed College; M.S., 1949, Stevens Institute of Technology; Bell Telephone Laboratories, 1929—. He has concentrated on radio research, including propagation and antenna studies and design of antennas. During the war he was engaged in preliminary work on the proximity fuse and in work on countermeasures and some jamming devices. After the war he worked on microwave relay projects, some involving studies of frequency measurements. More recently he did antenna work connected with the early warning system and he is presently engaged in research on low-noise antennas. Senior member I.R.E.

WILLIAM C. JAKES, B.S. in E.E., 1944; M.S. in E.E., 1947, and Ph.D., 1949, Northwestern University; Bell Telephone Laboratories, 1949—. He has been engaged in research in microwave radio antennas and microwave propagation. He was project engineer in charge of the Bell Laboratories team participating in the Project Echo satellite communication experiments. He is presently working on the planning of other experiments in satellite communications and radio astronomy. Member I.R.E., Eta Kappa Nu, Pi Mu Epsilon, Sigma Xi.

LYNDEN U. KIBLER, B.S., 1950, U.S. Coast Guard Academy; M.S. in E.E., 1956, Massachusetts Institute of Technology; Bell Telephone Laboratories, 1956—. His first work was concerned with microwave diode studies and with microwave logic design. He was engaged in visual systems work for a short time before returning to radio research and parametric amplifier studies. He was concerned with the design and construction of parametric amplifiers which were used in the Holmdel receiver and the Goldstone tracking radar for the Project Echo experiments.

RICHARD KLAHN, B.S.E.E., 1957, University of Buffalo; M.S. in E.E., 1959, New York University; American Telephone and Telegraph Company, 1948-55; Bell Telephone Laboratories, 1956—. With A.T.&T. in Buffalo, New York, he was a transmission test man, concerned with testing and locating troubles on long distance circuits. Since joining Bell Laboratories he has been engaged in studies of digital systems, with emphasis on digital-to-analog conversion techniques. He took part in the development of a data conversion unit used by Bell Laboratories in the Project Echo experiments. Member I.R.E.

JOSEPH J. KOSTELNICK, Bell Telephone Laboratories, 1955—. His first work was in development of microwave ferrite devices. Since 1959 he has been engaged in work on maser development.

J. A. NORTON, B.A.Sc., 1957, University of Toronto; A.M., 1959, Princeton University; Bell Telephone Laboratories, 1960—. He has been engaged in design of a high-accuracy instrument servo used in the digital-to-analog conversion unit developed for Bell Laboratories work in Project Echo. He is also engaged in research in adaptive control systems and process identification. Member I.R.E., Sigma Xi.

EDWARD A. OHM, B.S., 1950; M.S., 1951, and Ph.D., 1953, University of Wisconsin; Bell Telephone Laboratories, 1953—. He has been concerned with fundamental studies in guided-wave techniques, which has resulted in the design of high-quality microwave circulators, isolators, and waveguide filter networks. He was alternate general coordinator and was responsible for the receiving operation at Bell Laboratories during the Project Echo satellite communication experiments. Member I.R.E., Sigma Xi, Tau Beta Pi.

C. L. RUTHROFF, B.S. in E.E., 1950, and M.A., 1952, University of Nebraska; American Telephone and Telegraph Company, Long Lines, 1946-52; Bell Telephone Laboratories, 1952—. Since transferring from Long Lines in Lincoln, Nebraska, where he was a central office maintenance man, Mr. Ruthroff has concentrated on radio research with emphasis on FM problems and transistor circuits for microwave components and systems. He took part in the design and construction of the receivers used at Bell Laboratories and Jet Propulsion Laboratories at Goldstone, California, for the Project Echo experiments. He supervised the operation of the receiving equipment at Goldstone. Member I.R.E.

J. PETER SCHAFER, B.S.E.E., 1921, and E.E., 1925, Cooper Union; Western Electric Co., 1915-25; Bell Telephone Laboratories, 1925—. His

first work was in vacuum tube development. Since 1918 he has specialized in radio research, taking part in the installation, testing, and operation of the first long-wave transatlantic radio telephone circuit. He studied radio transmission characteristics of the upper atmosphere, high-power transmitter and antenna problems of radar during the war, and for a number of years has been engaged in work on microwave repeater components. He was in charge of the installation and operation of the Bell Laboratories Project Echo transmitter. Senior member I.R.E.

H. E. D. SCOVIL, B.A., 1948, and M.A., 1949, University of British Columbia; D. Phil., 1951, Oxford University; Nuffield Research Fellow, Oxford, 1951-52; faculty, University of British Columbia, 1952-55; Bell Telephone Laboratories, 1955—. He has been engaged in development of solid state devices at microwave frequencies. He took part in designing the maser amplifier used in the Project Echo receiving equipment at Holmdel.

HAROLD SEIDEL, B.E.E., 1943, College of the City of New York; M.E.E., 1947, and D.E.E., 1954, Polytechnic Institute of Brooklyn; Federal Telecommunications Laboratories, 1948-53; Bell Telephone Laboratories, 1953—. His work has related particularly to microwave solid state interactions and has ranged from the study of ferrite propagation phenomena to semiconductor parametric amplification. Member I.R.E., Sigma Xi.

MICHIYUKI UENOHARA, B.E., 1949, Nihon University (Japan); M.S., 1953, and Ph.D., 1956, Ohio State University; D.E., Tohoku University (Japan), 1958; Bell Telephone Laboratories, 1957—. He has been engaged in exploratory studies of microwave variable reactance amplifiers and microwave tubes. He was also engaged in microwave tube research at Nihon University from 1949 to 1952, and taught there in 1957. Member American Physical Society, I.R.E., Institute of Electrical Communication Engineers (Japan), Eta Kappa Nu, Pi Mu Epsilon, Sigma Xi, R.E.S.A.

K. L. WARTHMAN, B.M.E., 1939, Ohio State University; Bell Telephone Laboratories, 1939—. Mr. Warthman was engaged in design of maintenance tools and gauges for a number of years. Since 1951 his work has been in military electronics, and he has been especially concerned with design of camera equipment for Nike and Titan missile projects. He worked on the tracking cameras for the radars associated with the receiving and transmitting antennas used by Bell Laboratories in the Project Echo experiments.